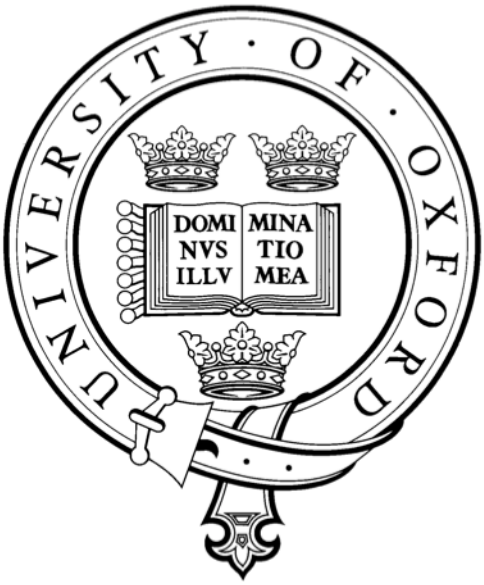
Diffusion Kinetics in Radiation Chemistry

An Investigation of Competition and Correlation Effects



A thesis submitted for the degree of Doctor of Philosophy

Eyad H. Al-Samra

Trinity Term 2015

University of Oxford

Physical & Theoretical Chemistry Laboratory

and

Kellogg College

Diffusion Kinetics in Radiation Chemistry

An Investigation of Competition and Correlation Effects

Eyad H. Al-Samra, Kellogg College, Trinity Term 2015

A thesis submitted in partial fulfilment of the requirements for
the degree of Doctor of Philosophy of the University of Oxford

Abstract

The study of radiation chemistry is very important because of the wide range of applications. Many of the processes in radiation chemistry evolve randomly and can be modeled using the theory of stochastic process.

The main aim of this thesis is to study correlation effects in model systems of the type found in radiation chemistry, i.e. clusters of reactive particles.

Studies of this type involve a substantial amount of computer simulation. The first work described in the thesis shows how the Message Passing Interface can be incorporated in the algorithms used to simulate radiation chemical kinetics and how that can improve the performance of the programs.

The reaction probability for two diffusing particles is well known, and current theories are based on this, making the approximation that pair distances evolve independently. This work analyses some correlation effects that appear in a system of three particles, with some new results, notably in the distribution of the joint distribution of the distances and the underlying 3-body backward diffusion equation, but it has not yet been possible to use these results to introduce corrections in the working simulations.

The competition between scavenging and recombination is investigated in detail in chapters 4-6. A correction to the Smoluchowski theory for a fully-diffusion controlled reaction is proposed, and it is shown how the Independent Reaction Times method can be used to simulate this competition. The approximation is justified both by comparison to simulation results and theoretically, and is shown to apply to all the ordered scavenging reactions in a multi-particle system.

Finally, the problem of modeling a reversible reaction is briefly investigated in chapter 7. The main result of this chapter is a generalization of previous work on the

distance between a pair conditional on its future reaction time, generalized to a radiation boundary condition.

Acknowledgments

I would like to thank my supervisor, Dr Nicholas Green, for his help over the past years. This work would not have been possible without his continuous support.

I would like also to thank my family, particularly my parents.

Table of Contents

Abstract.....i

Acknowledgments..... iii

Table of contents.....iv

Table of abbreviations.....vii

Chapter 1..... 1

Introduction..... 1

1.1. Thesis overview.....1

1.2. Radiation chemistry.....3

1.2.1. History and introduction.....3

1.2.2. Radiation track.....5

1.2.3. The physics of radiation-matter interaction.....7

1.2.3.1. Charged particles interaction with matter.....10

1.2.3.1.1. Elastic scattering.....10

1.2.3.1.2. Inelastic scattering.....12

1.2.3.2. Photon interaction with matter.....16

1.2.3.3. Energy straggling.....18

1.2.4. Radiolysis of liquid water.....19

1.2.5. Deterministic and stochastic chemical kinetics.....24

Chapter 2..... 29

Monte Carlo Random Flights..... 29

2.1. General background.....30

2.2. RF simulations.....35

2.3. Parallel computing and MPI.....38

2.4. Geminate recombination and testing.....40

2.5. Conclusion.....42

Chapter 3..... 43

Three-Body Correlation..... 43

3.1. The IRT method.....44

3.2. Correlation effects.....47

3.2.1. Simulations.....50

3.2.2. The backward diffusion equation....55
3.2.2.1. The infinitesimal mean....56
3.2.2.2. The infinitesimal variance....58
3.2.2.3. The infinitesimal covariance....58
3.2.2.4. Possible approximations....59
3.2.2.4.1. Perturbation....60
3.2.2.4.2. Equilateral triangle....69
3.2.3. Further simulations....74
3.3. Summary and conclusions....78
Chapter 4....80
Scavenging and Recombination Kinetics I: Smoluchowski Theory....80
4.1. Smoluchowski theory....81
4.2. Details of the simulations....84
4.3. Results....86
4.4. Correction....91
4.5. More tests....97
4.5.1. Different distributions....97
4.5.2. The S3 scheme....100
4.5.3. Different concentrations....102
4.6. Conclusions and future work....104
4.7. Appendix....105
Chapter 5....107
Scavenging and Recombination Kinetics II: IRT Theory....107
5.1. The Smoluchowski rate constant....108
5.2. The predicted correction....110
5.3. General case....111
5.4. The simulation method....117
5.4.1. Scavenging probability with the continuum....118
5.4.2. Details of the simulations....123
5.4.3. Results....124
5.4.4. Other coefficients....128
5.5. Conclusions....133
Chapter 6....135

Scavenging and Recombination Kinetics III 135
6.1. Prescribed diffusion 136
6.2. Scavenging rate constant 142
6.3. Successive (ordered) scavenging events 144
6.3.1. The S2 scheme (scavenging only) 144
6.3.2. The S1 scheme 148
6.3.3. Statistical errors 152
6.4. Summary and conclusions 153
Chapter 7 155
Reversible reaction 155
7.1. Radiation boundary condition (RBC) 156
7.2. RF simulations with RBC 158
7.3. IRT simulations with RBC 162
7.4. The IRT method and a reversible reaction 165
7.4.1. Bessel process with RBC 166
7.4.1.1. The backward and forward diffusion equations 166
7.4.1.2. The survival probability 171
7.4.1.3. The reaction probability 172
7.4.1.4. Interpolation conditional on a reaction time 172
7.4.2. Practical considerations 173
7.5. Summary and future work 181
7.6. Appendix 182
Chapter 8 192
Summary and Conclusions 192
Bibliography 195

Table of abbreviations

Abbreviation	Definition
C. P2	Hybrid Simulations with the added correction
IRT	Independent Reaction Times
LET	Linear Energy Transfer
MPI	Message Passing Interface
P1	Monte Carlo Random Flight with a periodic boundary condition
P2	Hybrid Simulations
P3	Independent Reaction Times Simulation with a spherical symmetry
RBC	Radiation Boundary Condition
RF	Monte Carlo Random Flight
S1	Scavenging and recombination scheme
S2	Scavenging only scheme

Chapter 1

Introduction

"The most important questions of life are indeed, for the most part, really only problems of probability." ***Pierre-Simon Laplace***

1.1. Thesis overview

Radiation chemistry studies the interaction of energetic charged particles and high-energy photons or neutrons (ionizing radiation) with matter. The study of radiation chemistry is of great importance due to its applications in industry and medicine.[1,2,3]

Stochastic processes can be defined as processes that concern sequences of events governed by probabilistic laws. Their applications occur in many disciplines including Physics, Chemistry and Engineering.[4,5]

Many of the processes in radiation chemistry are random in nature, for example the structure of the radiation track as it evolves event to event, the development of "spurs", regions of locally high concentration of radicals, and the subsequent diffusion of the reactive species formed in the spurs. Such processes can be modelled and analysed using the theory of stochastic processes.[1,6] In particular, the main aim of this work has been to develop stochastic methods for the purpose of modelling radiation chemical kinetics in liquids.

The Monte Carlo Random Flights (RF) simulation is the most common approach to model radiation chemical kinetics. It involves simulating the diffusive trajectories of all the reacting particles present in the sample and the reactions that may occur. The RF method has been well tested before and can be used as a reference when developing more approximate models.[6,7] The main challenge in using the RF method is that a large number of realizations is required for the data to be statistically representative and this makes the method very time consuming. However, as

discussed in chapter 2, the inclusion of the Message Passing Interface (MPI) technique in the simulation was found to successfully overcome this issue.[8,9] The use of MPI has also made it practical to write multi-method simulation programs, as in chapters 4-7.

Modelling a problem using the theory of stochastic processes typically involves, at the initial stages, formulating the stochastic equation of motion describing the problem. Then a suitable method must be constructed either to solve for the underlying probability distribution or to simulate the process with an appropriate sampling method. For example, the Independent Reaction Time (IRT) method is widely used to simulate chemical kinetics when the conventional (or deterministic) treatment is inadequate, but in some cases it can also give analytic solutions. As discussed in more detail later, the starting point of the IRT method is to formulate the backward-diffusion equation for the relative motion of two diffusing particles and then finding its physically meaningful solution, the time-dependent reaction probability of the two particles. After that the solution is used to simulate the kinetics through independently generating a reaction time for each reactive pair present, as a sample from this underlying probability distribution.[6,10,11] Following a similar route, chapter 3 of this work presents the formulation of the backward-diffusion equation for three diffusing particles and is meant to see if the independence assumption of the IRT method can be relaxed by the analysis of the correlations among the diffusing distances.

When trying to experimentally study the radiolysis of a sample (the radiolysis of hydrocarbons for example), it is common to use a relatively high concentration of a substance, scavenger, which quickly reacts with the radiation-generated radicals and hence it competes with their recombination reactions.[12,13] To compete successfully with the fast spur reactions, the radical-scavenger reaction must be fully diffusion-controlled (or close to fully diffusion-controlled).[6] Fully diffusion-controlled reactions also occur in many areas.[14,15] Interestingly, the rate constant of such reactions is a time-dependent quantity and follows a formula derived by M. Smoluchowski early last century.[16] One of the assumptions of the Smoluchowski theory is that the reactive particles are far apart, but in such a case the scavenging will always out-compete recombination and the experiment will give no information about the recombination kinetics. In chapter 4, the Smoluchowski theory is examined using a specifically built computer simulation, where the RF model is used for the purpose of comparison. An

empirical correction to the Smoluchowski rate constant is suggested for systems in which radical recombination takes place on the same timescale as the transient in the Smoluchowski rate constant. As discussed later, this simple correction seems to be remarkably successful.

The Smoluchowski rate constant can be derived using the IRT theory. Furthermore, a previous IRT theory study, on the competition between scavenging and recombination reactions, predicted a correction for the Smoluchowski rate constant.[17] The value of this correction is almost the same as the value calculated in chapter 4. As such, it was interesting to build IRT simulations parallel to those of chapter 4; this will be the subject of chapter 5.

Chapter 6 continues the investigation of the radical-scavenger reaction and it holds a comparison of the results of chapters 4 and 5. It presents the deterministic, prescribed diffusion treatment of the problem. It also presents the use of the master equation analyses and simulations for the rates of the successive (ordered) scavenging events when more than one radical is present in the spur.

Modelling the reversible association-dissociation reaction using the IRT method poses a number of challenges. For example, the association reaction has to follow the radiation boundary condition, which is more challenging to model.[18] Also, it is difficult to determine the distances separating the newly formed reactants from the other reactants present in the sample, after a dissociation occurs, which is essential in order to generate the new reaction times.[19] Chapter 7 discusses these issues in more detail and presents the progress made in modelling this type of reaction.

Chapter 8 summarizes the conclusions of this work. The current chapter is meant to provide an overview of this thesis and also includes a general background on radiation chemistry.

1.2. Radiation chemistry

1.2.1. History and introduction

The history of the discovery of radioactivity and radiation has been described in many places.[1,20,21,22] Shortly after the discovery of the radioactivity of uranium by H. Becquerel in 1896 and the discovery of polonium and radium by the Curies in 1898, it became evident that the radiation emitted by the radioactive elements induces

chemical effects in matter.[23] W. Roentgen noticed that these chemical effects were similar to those induced by the X-ray light.[24,25] In 1901 P. Curie and A-L. Debierne observed the evolution of hydrogen and oxygen from solutions of radium salts.[26] The paper published by W. Ramsay in 1907 on what is known now as the radiolysis of water is widely considered the start of the field of radiation chemistry, which was first called so by M. Burton in 1942.[27,28] Due to the wide range of potential applications, the field has substantially grown since its early days and currently its studies are utilized in many areas such as food preservation, medicine and energy production.[1,20]

Ionizing radiation possesses enough energy to result in the complete removal of electrons from the molecules (or atoms) of the targeted medium. Its interaction with the medium results in the formation of a track, a series of geometrically correlated, discrete energy-loss events. As will be discussed later, each individual event may not necessarily lead to ionization; instead an excited molecule may be formed. The initial products of the energy-deposition events (ions, low energy electrons and excited molecules) rapidly undergo further processes including thermalization, fragmentation and ion-molecule reactions, all in the vicinity of the initial event, which lead to the formation of spurs, regions of locally high concentration of radicals and ions (this is the case for high-speed electrons or X-rays). The radicals and ions of the spurs then diffuse and undergo fully (or partly) diffusion-controlled combination reactions. It is common to organize the above radiolytic processes, based on their nature and time-scale of occurrence, into groups as shown in Figure 1.1.[1,6,29-31] The radiation-molecule interaction and the early processes that follow, such as the thermalization and fragmentation of the resulting species, lie in the physical domain of the processes whereas the biological domain contains processes that happen much later on, such as mitosis. The timescales of spur reactions, which are the primary interest of this work, cover the range from a few ps to a μs, and thus span the end of the physicochemical stage and the start of the chemical domain (it should be noted that in some systems (radioactive wastes in particular) it is necessary to investigate the chemistry at much longer times (many years etc.). However, the kinetics in this case is homogenous and can be studied using the normal methods).[32,33]

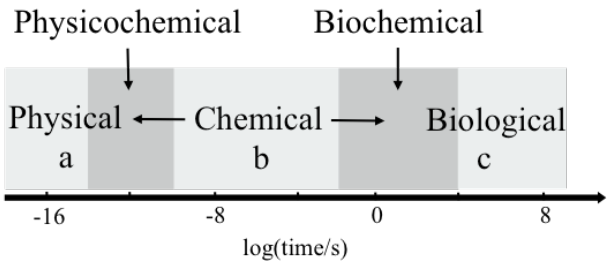


Figure 1.1. Time scales and examples of the processes of radiolysis. The dark grey indicates an overlap between two types of processes. Examples: a) Energy loss events. b) Spur, diffusion controlled reactions. c) Mitosis.

1.2.2. Radiation track

It is possible to use track detectors to visualize the trail of the radiation particles in matter. Techniques such as cloud chambers, autoradiograph and solid-state detectors are used for this purpose in nuclear physical studies.[34-36]

The radiolysis of liquids is a complicated, multidisciplinary problem and a better understanding of it requires two stages of simulation.[37] The reason for this is that because the fast chemistry is diffusion-controlled (or close to it), it depends critically on the initial distribution of the reactive particles, which comes from the structure of the radiation track. The first stage, therefore, involves simulating the physical radiation-matter interaction (or in other words simulating the radiation track).[6,30,38] The typical results of a track simulation are the space coordinates of the energy-loss events and the nature of the resulting species (excited molecules or ions etc.). The second stage uses the results of the first stage to simulate the radiation chemical kinetics, using RF simulations for example.[6] The physical aspects of radiation-matter interaction will be discussed generally in this chapter. In this section, the track structure (or entities) is discussed.

The discrete energy-loss events forming the trail (or track) of radiation mainly involve the interaction of radiation with the electrons of the targeted medium rather than with its nuclei. (Effects such as bremsstrahlung emission in the case of charged particle-matter interaction and pair production in the case of photon-matter interaction are not discussed here. This is because they become significant only for very high-energy radiation; for example exposing water to ~100 MeV electrons, and this range of energy is not commonly used in the field of radiation chemistry. Neutrons are an exception to this general observation as they interact preferentially with nuclei by a completely different mechanism.)[2,39]

If we consider the interaction of energetic charged particles with matter, as an example, it is helpful to use the concept of the impact parameter *b*, the perpendicular distance of the closest approach between the energetic charged particle's trajectory and targeted molecule (or atom) of the medium. From the earliest days of relativistic quantum mechanics there has been an alternative formulation of the theory of energy loss, derived in terms of the impact parameter.[40] As schematically shown in Figure 1.2, when the impact parameter is large compared to the radius of the target, the amount of energy lost by the projectile (the incident charged particle) is small and this kind of interaction is referred to as a soft collision and typically results in an excited-state molecule. However, it may result in the ionization of the target and in this case the liberated electron (or secondary electron) will have a small kinetic energy. On the other hand, when *b* is small, the interaction is referred to as a hard (or knock on) collision where the projectile loses a substantial amount of its energy and this leads to the ionization of the targeted molecule. In this case the secondary electron will have a relatively high kinetic energy and form its own track.[1,2,41]

Consequently, the secondary electrons liberated in the primary energy deposition events have widely varying kinetic energies. If the energy of a secondary electron is relatively low, then it will not travel very far (specially in a condensed phase) and the ionizations and excitations that it may cause will be very close to the location of the original energy deposition event; this leads to the formation of a spur (corresponding to a primary energy deposition event of up to 100 eV in the case of water for example).[1,2,42,43] When the kinetic energy of the secondary electron is higher, the spur contains more secondary events, has a larger size and is called a blob (for example, energy deposition of 100 – 500 eV in water will lead to the formation of a blob). Finally, when the secondary electron has a very high kinetic energy, it is called δ-ray and it will be able to travel far from the location of the energy deposition event. In this case it will lead to the formation of a short track, a column of excited and ionized species, (energy deposition of 500 – 5000 eV in water for example). Spurs, blobs and short tracks form the set that is known as the entities (or structure) of the radiation track.[1,2,42,43]

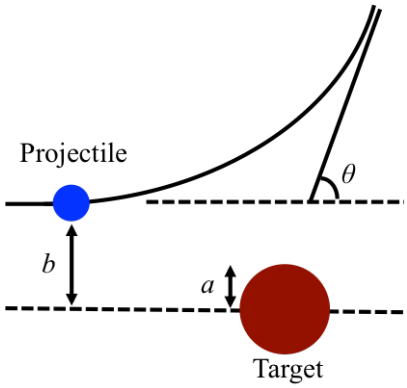


Figure 1.2. The concept of impact parameter. The target (molecule or atom) is assumed spherical with a radius a. When the impact parameter *b* is large compared to *a*, the interaction is called a "soft collision". When *b* is larger but comparable to *a*, the interaction is called a "hard collision". As the projectile interacts with the target it gets deflected with an angle θ.

1.2.3. The physics of radiation-matter interaction

The current section will generally discuss the physical aspects of the radiation matter-interaction. It starts from the interaction of energetic charged particles with matter and then it moves to discuss the photon interaction with matter. As mentioned before, neutrons interact preferentially with nuclei by a completely different mechanism and this will not be discussed here.

The first step in describing the physical radiation-matter reaction is to define the cross-section of the radiation-matter reaction. The cross- section is a quantitative measure of the likelihood of a given interaction occurring between the incident radiation and the targeted medium. The language comes from collision theory: the probability of interaction of the radiation with a particular molecule is the same as the probability of a collision between the radiation and a hard sphere whose cross-sectional area is given by the total cross-section. As shown in Figure 1.3, the ratio of the relative reduction in the flux dI/I over a path length dx is related to the number of targeted molecules through the integral cross-section σ as follows[34,44]

$$\frac{dI}{I} = -\sigma\, N\, dx \tag{1.1}$$

where N is the number density of molecules in the target, or if we use the differential cross-section

$$\frac{dI}{I} = -N\, dx \int \frac{d\sigma(\theta,\varphi)}{d\Omega}\, d\Omega \tag{1.2}$$

where $d\Omega$ is the solid angle element along the deflected wave direction and given by

$$d\Omega = \sin\theta \, d\theta \, d\varphi \tag{1.3}$$

where θ and φ are the angles of the spherical coordinates. Normally, the coordinates are chosen in such a way that the differential cross-section is independent of φ and so we can write

$$d\sigma(\theta,\varphi) = d\sigma(\theta) \tag{1.4}.$$

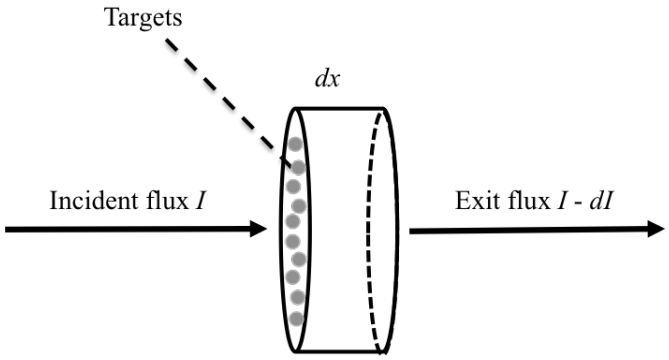


Figure 1.3. The cross-section. The total number of targets in the volume is *Ndx*.

There are two methods to obtain the expression for the cross- section of the target-projectile reaction. The first one is the use of Fermi's golden rule No. 2 to measure the rate of the radiation-induced transition as follows

$$\lambda = \frac{2\pi}{\hbar} \left| M_{\text{long}} \right|^2 \rho \tag{1.5}$$

where λ is the rate of the transition between the initial state and the final state. ρ is the density of final states. M_{long} is the matrix element given by

$$M_{\text{long}} = \left\langle \Psi' \middle| H_p \middle| \Psi \right\rangle \tag{1.6}$$

where Ψ' and Ψ are respectively the final and initial time-independent wavefunctions for the projectile-target system, and H_p is the perturbation part of the Hamiltonian. The reasoning behind the term 'long' will be discussed later. The differential cross-section defined in equation (1.2) is equal to the rate λ normalized to the incident particle flux ($\beta c/V$ where β is the speed of the incident particle divided by the speed of light c and V is the volume of a cube, used to normalize the wavefunctions for the plane-wave)[41,44]

$$d\sigma = \frac{V}{c\beta}\lambda \tag{1.7}.$$

The second method to derive the expression of the cross-section comes from scattering theory. Briefly, if we assume the incident wave to be a plane-wave (PW), then the overall wavefunction will asymptotically be a sum of two parts[41,44,45]

$$\psi = e^{i\mathbf{k}.\mathbf{r}} + f\left(\theta,\varphi\right)\frac{e^{ikr}}{r} \tag{1.8}$$

where the first term is the PW contribution and the second term is the contribution from scattering. It should be noted that the last equation is valid for both elastic and inelastic scattering where f is the scattering amplitude and $\mathbf{k}$ is the wavevector of the incident radiation. r, θ and φ are the spherical coordinates. It is possible to choose the coordinates in such way that the scattering amplitude is independent of φ and then equation (1.8) becomes

$$\psi = e^{i\mathbf{k}.\mathbf{r}} + f\left(\theta\right)\frac{e^{ikr}}{r} \tag{1.9}.$$

This is equivalent to applying the first Born approximation to the Lippmann-Schwinger equation.[44] The scattering amplitude determines the scattering probability and is directly related to the differential cross-section as follows

$$\frac{d\sigma}{d\Omega} = \left| f(\theta) \right|^2 \tag{1.10}$$

where

$$f\left(\theta\right) = -\frac{m}{2\pi\hbar^2}\int U\left(r'\right) e^{i\mathbf{q}.\mathbf{r}'/\hbar} d^3r' \tag{1.11}$$

where U is the potential energy of the target-projectile system, m is the mass of the projectile and

$$\mathbf{q} = \mathbf{p} - \mathbf{p}' = \hbar\left(\mathbf{k} - \mathbf{k}'\right) \quad , \quad \theta = \left(\hat{\mathbf{p}}, \mathbf{p}'\right) \tag{1.12}$$

where $\mathbf{p}$ and $\mathbf{p}'$ are respectively the momentum of the projectile pre- and post scattering so $\mathbf{q}$ is the momentum transferred to the target. $\mathbf{k}'$ is the wavevector post-scattering. The use of either equation (1.5) or equation (1.10) along with the PW to obtain the cross-section is known in the literature as the plane wave Born approximation theory (PWBA).[44,46-48]

1.2.3.1. Charged particles interaction with matter

The Coulomb scattering of energetic charged particles, when interacting with matter, is discussed here. This interaction is normally categorized in terms of elasticity, i.e. whether or not the kinetic energy of the target-projectile system is conserved.[41,44]

1.2.3.1.1. Elastic scattering

An example of elastic Coulomb scattering is the scattering of a charged particle by infinitely massive target where the projectile is considered to retain its kinetic energy and only changes its direction. Another example is Møller scattering; the scattering of an electron by a free electron, where the amount of kinetic energy lost by the projectile is equal to the kinetic energy gained by the targeted free electron.

Obtaining the expression for the cross-section for this kind of interaction is straightforward using equation (1.5). For example, if we consider the Coulomb scattering of a spin-0 projectile with a charge z and speed v by a heavy Z-electron atom, the wavefunction of the projectile-target system pre-collision is of the form[41,44,47]

$$\Psi = N\, e^{i\mathbf{p}\cdot\mathbf{r}/\hbar}\, \psi_0\left(r_1, r_2, ..., r_Z\right) \qquad : \; N = \left(V\right)^{-1/2} \tag{1.13}$$

where N is a normalization factor, V is the volume of a cube (equation (1.7)),[44] $\mathbf{r}$ is the position of the projectile relative to the centre of the atom and $\mathbf{p}$ is its pre-collision (or pre-scattering) momentum. r_j is the position of the j^{th} electron. ψ_0 is the ground state wavefunction for the atom. After the collision, we have

$$\Psi' = N\, e^{i\mathbf{p}'\cdot\mathbf{r}/\hbar}\, \psi_0\left(r_1, r_2, ..., r_Z\right) \tag{1.14}$$

where $\mathbf{p}'$ is the projectile post-collision momentum. It should be noted that the atom is considered to remain in its ground state. The perturbation in equation (1.6) is the total potential energy for the projectile-target Coulomb interaction and is given by

$$H_p = U = z\alpha\hbar c\left[\frac{Z}{r} - \sum_{j=1}^{Z}\frac{1}{\left|\mathbf{r}-\mathbf{r}_j\right|}\right] \tag{1.15}$$

where α is the fine structure constant.* Inserting the last three equations in equation (1.6) and then the result into equation (1.5) along with the following expression for ρ (where V is the confining volume which is used for normalizing the wavefunctions)

$$\rho = \frac{V\,q}{4\pi^2 c\beta\,\hbar^3}dq \quad : \quad \beta = v/c \quad , \quad q = \left|\mathbf{q}\right| \tag{1.16}$$

gives the following formula for the differential cross-section, after using equation (1.7),

$$\frac{d\sigma}{dq} = \frac{8\pi}{q^3}\left(\frac{z\alpha\hbar}{\beta}\right)^2 \left|Z - F_0\left(q,Z\right)\right|^2 \tag{1.17}$$

where **q** is defined in equation (1.12) and

$$q = 2p\sin\frac{\theta}{2} \tag{1.18}$$

and $F_0\left(q,Z\right)$ is the elastic scattering form factor, which will be discussed later, and is given by

$$F_0\left(q,Z\right) = \left\langle \psi_0 \right| \sum_{j=1}^{Z} e^{i\mathbf{q}.\mathbf{r}_j/\hbar} \left| \psi_0 \right\rangle \tag{1.19}.$$

When the projectile spin is not zero (or if relativistic effects need to be included), the derivation proceeds using the following relativistic version of equations (1.5) and (1.6)[49,50]

$$\lambda = \left|\kappa\right|^2 \rho \tag{1.20}$$

where ρ is the density of final states and

$$\kappa = -\frac{i\,e}{\hbar}\int \bar{\Psi}'\,\mathbb{A}\,\Psi\,dt\,d^3r \tag{1.21}$$

where Ψ' and Ψ are the time-dependent spinors for the final and initial states respectively, $\bar{\Psi}'$ is the transpose of Ψ' and

$$\mathbb{A} = \gamma^0 A_0 - \boldsymbol{\gamma}.\mathbf{A} \tag{1.22}$$

---

* The fine structure constant is defined as follows:

$$\alpha = \frac{1}{4\pi\varepsilon_0}\frac{e^2}{\hbar c}$$

where ε_0 is the permittivity of free space, c is the speed of light, e is the elementary charge and $\hbar$ is the reduced Planck constant.

where A_0 and **A** are the scalar and vector potentials respectively. γ^0 and $\boldsymbol{\gamma}$ are four-matrices of the Dirac's equation of the problem ($\boldsymbol{\gamma}$ is a set of three matrices).† The rest of the derivation remains fairly similar to the example above.[44,47]

1.2.3.1.2. Inelastic scattering

Inelastic Coulomb scattering is the more important form of interaction and always results in transferring part of the kinetic energy of the penetrating projectile through to the medium. To discuss this, it is useful to introduce the concept of the Linear Energy Transfer (LET), the rate of energy loss of a charged particle per unit path length, or similarly the mass stopping power *S*, which is LET normalized to the density of the medium. The mass stopping power is a sum of two quantities. The first one is the collision stopping power S_{col} and results from the inelastic Coulomb scattering. The second one is the radiative stopping power S_{rad} and is due to the emission of bremsstrahlung (X-ray) when the penetrating projectile is violently deflected by a nucleus's electric field. The radiative stopping power becomes important only when the projectile has a very high kinetic energy. As mentioned in section 2.2, this case is not common in radiation chemistry and thus the radiative stopping power will not be discussed here. Mathematically, the stopping power is related directly to the integral cross-sections as follows[41,43,44,51]

$$S \approx S_{\text{col}} = N_e \sum_f E_f \sigma_{f0} \tag{1.23}$$

where the sum can become an integral if needed, N_e is the electron density of the medium and σ_{f0} is the cross-section of the transition from the ground state to the state *f* whose energy is E_f.

† As mentioned above, $\boldsymbol{\gamma}$ is a set of three 4×4 matrices γ^1, $\gamma^2$and γ^3. Using the Pauli representation, we have:

$$\gamma^1 = \begin{bmatrix} 0 & 0 & 0 & 1 \\ 0 & 0 & 1 & 0 \\ 0 & -1 & 0 & 0 \\ -1 & 0 & 0 & 0 \end{bmatrix}, \quad \gamma^2 = \begin{bmatrix} 0 & 0 & 0 & -i \\ 0 & 0 & i & 0 \\ 0 & i & 0 & 0 \\ -i & 0 & 0 & 0 \end{bmatrix}, \quad \gamma^3 = \begin{bmatrix} 0 & 0 & 1 & 0 \\ 0 & 0 & 0 & -1 \\ -1 & 0 & 0 & 0 \\ 0 & 1 & 0 & 0 \end{bmatrix}$$

For the fourth matrix (γ^0), we have

$$\gamma^0 = \begin{bmatrix} 1 & 0 & 0 & 0 \\ 0 & 1 & 0 & 0 \\ 0 & 0 & -1 & 0 \\ 0 & 0 & 0 & -1 \end{bmatrix}.$$

While the foundations of quantum mechanics and relativistic mechanics were still being built, N. Bohr used what is known now as classical physics to obtain the first mathematical formula for LET in 1913.[52,53] Briefly, he considered the case when the projectile is moving with a speed v that is very small compared to the speed of light but very large compared to the speed of the electrons in the targeted atom. Under this condition, the motion is perfectly described by Newton's laws and thus it is possible to classically calculate the value of the momentum transfer (or the energy transfer) of the interaction. He used the concept of the impact parameter introduced in section 2.2 and defined the cross-section of the process. He then assumed that the impact parameter is confined between two values $b_{\min}$ and $b_{\max}$ so that the projectile retains a straight trajectory throughout the interaction. The value of $b_{\min}$ is obtained through the impulse approximation (assuming the targeted electron stationary) while the value of $b_{\max}$ is directly related to the mean ionization energy $\bar{I}$. The final result of his analysis is as follows

$$S \approx S_{\text{col}} = 2\pi N_e \left(\frac{e^2}{4\pi\varepsilon_0} \right)^2 \frac{z^2}{m_e v^2} \ln\left(\frac{2mv^2}{\bar{I}} \right) \tag{1.24}$$

where N_e is the electron density of the medium, the number of electrons per mass, and z is the charge of the projectile and m is its mass. This equation can be generalized to molecules using Bragg's rule of additivity.[1,2,43] While historically very important, Bohr's formula does not always give a good agreement with the experimental data simply because it ignores the effects of relativistic quantum mechanics.

The first to propose a modern treatment for the problem of stopping power, based on the PWBA theory mentioned above, was H. Bethe in 1930.[54-56] The theory was analyzed and reviewed later on by U. Fano and M. Inokuti.[51,57] The kinematics of the problem is as follows:[41,44,58]

Using equation (1.12), we can write the momentum transfer q as follows

$$q = \sqrt{p^2 + p'^2 - 2pp'\cos\theta} \tag{1.25}.$$

If we denote the kinetic energy of the projectile T pre-scattering and T' after scattering, then the energy loss W is

$$W = T - T' \tag{1.26}.$$

The momentum transfer and the recoil energy Q are related by the following relativistic relation

$$Q\left(1+\frac{Q}{2m_e c^2}\right)=\frac{q^2}{2m_e} \qquad (1.27).$$

The non-relativistic relation can be obtained from the last equation as follows

$$Q=\frac{q^2}{2m_e} \quad : \quad Q<<2m_e c^2 \qquad (1.28).$$

The transition energy W_t is introduced to distinguish between two types of collisions: soft collisions ($W < W_t$) and hard collisions ($W > W_t$). The value of W_t itself does not need to be specified, as it does not eventually appear in the final expression for the stopping power. As a result of this, there will be two forms of collision stopping power, the soft collision stopping power and the hard collision stopping power; the overall stopping power is the sum of the two. For the soft collision stopping power, the projectile interacts with the atom as a whole rather than with one specific electron. If we assume the atom to be in its ground state pre-collision and then it moves to the state ψ_f as a result of the collision, then the pre-collision wavefunction will be the same as equation (1.13) while post collision we have[44]

$$\Psi' = N\, e^{i\mathbf{p}'.\mathbf{r}/\hbar}\, \psi_f\left(r_1, r_2, ..., r_Z\right) \qquad (1.29)$$

where the notations are similar to those of equations (1.13) and (1.14). Fano pointed out that in general there are two forms of the 0 - *f* transition. The first is the direct (or longitudinal) transition represented by the matrix element of equation (1.6). The second is the indirect (or transverse) transition where the transition occurs through an intermediate state Ψ_n (Fermi's golden rule No. 1). The matrix elements for these transitions are[44,47,51]

$$M_{\text{trans}} = \sum_n \frac{\left\langle \Psi' \middle| H_p \middle| \Psi_n \right\rangle \left\langle \Psi_n \middle| H_p \middle| \Psi \right\rangle}{E_0 - E_n} \qquad (1.30)$$

where the sum is taken over all the possible intermediate states where E_0 is the energy of the ground state (typically chosen to be 0) and E_n is the energy of the intermediate state *n* and

$$\Psi_n = N\, e^{i\mathbf{p}_n.\mathbf{r}/\hbar}\, \psi_n\left(r_1, r_2, ..., r_Z\right) \qquad (1.31).$$

In this case the following general expression

$$M_{\text{tot}} = M_{\text{long}} + M_{\text{trans}} \qquad (1.32)$$

should be used in equation (1.5) instead of M_{long} only. Now inserting equations (1.13), (1.29) and (1.31) into equations (1.6) and (1.30) and then the sum of the results into equation (1.5) we get, using equation (1.7),[44,47,51,58]

$$\frac{d\sigma_f}{dQ} = \frac{2\pi z^2 e^4}{m_e v^2} Z \left(1 + \frac{Q}{m_e c^2} \right) (h + l) \left| F_f(q,Z) \right|^2 \tag{1.33}$$

where the following expression for ρ was used

$$\rho = \frac{m_e V}{4\pi^2 c \beta \hbar^3} \left(1 + \frac{Q}{m_e c^2} \right) dQ \tag{1.34}$$

and

$$h = \frac{1}{\left[Q\left(1 + Q/2m_e c^2\right) \right]^2} \tag{1.35}$$

$$l = \frac{\beta^2 \sin^2 \theta_r}{\left[Q\left(1 + Q/2m_e c^2\right) - E_f^2/2m_e c^2 \right]^2} \quad : \ \theta_r = (\mathbf{p}, \hat{\mathbf{q}}) \ , \beta = \frac{v}{c} \tag{1.36}.$$

$F_f(q,Z)$ is the inelastic scattering form factor and is given by

$$F_f(q,Z) = \left\langle \psi_f \left| \sum_{j=1}^{Z} e^{i\mathbf{q}.\mathbf{r}_j/\hbar} \right| \psi_0 \right\rangle \tag{1.37}.$$

The inelastic scattering form factor is related to $f_f(q,Z)$, the generalized oscillator strength (GOS), as follows[44]

$$\frac{df_f(q,Z)}{dE_f} = \frac{\left| F_f(q,Z) \right|^2}{Q} \tag{1.38}.$$

Inserting the last equation into equation (1.33) we get

$$\frac{d\sigma_f}{dQ} = \frac{2\pi z^2 e^4}{m_e v^2} Z \left(1 + \frac{Q}{m_e c^2} \right) (h + l) Q \frac{df_f(q,Z)}{dE_f} \tag{1.39}.$$

It should be noted that equation (1.33) becomes very simple in the non-relativistic limit as follows[44,51]

$$\frac{d\sigma_f}{dQ} = \frac{2\pi z^2 e^4}{m_e v^2} Z \frac{\left| F_f(q,Z) \right|^2}{Q^2} \tag{1.40}.$$

In any case, obtaining the formula for the stopping power requires the integral cross-section, which according to the above requires information about the GOS. The GOS depends on the studied material and its three-dimensional plot over the energy E_f, and the momentum transfer q plane is known as the Bethe surface. The Bethe surface depends on the initial and final states (equations (1.37) and (1.38)) and generally is impossible to build from first-principles, except for the simple example of atomic hydrogen. The modern treatment of this nontrivial problem is based on semi-empirical models where the Bethe surface is built starting from experimental data. The inelastic X-ray scattering method (IXS) is used, as described in detail in the literature.[46,58-61]

With regard to the hard collision stopping power ($W > W_t$), the projectile is considered to interact with a specific electron of the targeted atom; the theory states that this collision can be approximated to be elastic. Elastic scattering depends on the nature of the projectile and has been briefly discussed above.[41,44,47]

Finally, combining both the soft collision stopping power $S_{\text{col}}^{\text{soft}}$ and the hard collision stopping power $S_{\text{col}}^{\text{hard}}$ gives the Bethe stopping power. The Bethe stopping power depends in general on both the projectile and the targeted medium, and as discussed above, it requires experimental data to be resolved. However, approximations are available in radiation physics and radiation chemistry literature, for example in the case of a heavy charged projectile, such as an α particle, we have[41,44,62]

$$S \approx S_{\text{col}} = S_{\text{col}}^{\text{soft}} + S_{\text{col}}^{\text{hard}} = C_0 N_e \frac{z^2}{\beta^2}\left(\ln\frac{2m_e c^2}{\bar{I}} + \ln\frac{\beta^2}{1-\beta^2} - \beta^2 \right) \tag{1.41}$$

where z is the charge of the projectile, β was defined in equation (1.36), $\bar{I}$ is the mean ionization/excitation energy and

$$C_0 = 4\pi\left(\frac{e^2}{4\pi\varepsilon_0}\right)^2 \frac{1}{m_e c^2} \tag{1.42}.$$

1.2.3.2. Photon interaction with matter

In this section, the photon-matter interaction will be briefly discussed as an example of the indirectly ionizing radiation interaction with matter. If the photon possesses

very high energy (more than a threshold of $2m_ec^2$ which results from the basics of Dirac's hole theory[49,50]), then the photon reacts with the nucleus (pair production). This case is not discussed here for the reason mentioned in section 2.2 and we will focus on the interaction of the photon with the electrons of the medium.

The photon may be conserved during the interaction and in this case it will be scattered from its original trajectory with or without energy loss. The relevant processes in this kind of interaction are Thomson, Rayleigh, and Compton scattering. Thomson scattering concerns the elastic scattering of a photon by a single free electron. It is perfectly described by combining Newton's mechanics and Maxwell's equations. The differential cross-section is given as[2,41,44]

$$\frac{d\sigma_{\text{Tho}}}{d\Omega} = \frac{r_0^2}{2}\left(1+\cos^2\theta\right) \tag{1.43}$$

where r_0 is the classical radius of the electron. Rayleigh scattering concerns the elastic scattering of a photon by an ensemble of electrons. The differential cross-section in this case is[44]

$$\frac{d\sigma_{\text{Ray}}}{d\Omega} = \left|F_0\left(q,Z\right)\right|^2 \frac{d\sigma_{\text{Tho}}}{d\Omega} \tag{1.44}$$

where $F_0\left(q,Z\right)$ was defined in equation (1.19). Both Thomson and Rayleigh scattering do not result in energy transfer to the target. On the other hand, Compton scattering, which is a quantum mechanical interaction, results in energy transfer to the targeted electron where the photon exits the interaction with reduced energy. The kinetics of Compton scattering is given by the following relativistic equation[44,62]

$$\Delta\lambda = \lambda' - \lambda = \frac{h}{m_e c}\left(1-\cos\theta\right) \tag{1.45}$$

where θ is the scattering angle. λ and λ' are the wavelength of the photon pre and post scattering respectively. The differential cross-section for Compton scattering, the Klein-Nishina cross-section, is given as[44,62]

$$\frac{d\sigma_{KN}}{d\Omega} = \frac{r_0^2}{2}\left(\frac{\varepsilon'}{\varepsilon}\right)\left(\frac{\varepsilon'}{\varepsilon}+\frac{\varepsilon}{\varepsilon'}-\sin^2\theta\right) \tag{1.46}$$

where ε and ε' are the energies of the photon pre- and post-scattering respectively and as before r_0 is the classical radius of the electron.

The photoelectric absorption is a photon non-conserving interaction. The photon disappears and its entire energy is transferred to the target. This could result in the ionization of the targeted molecule if the following condition is met

$$\varepsilon > E_b \tag{1.47}$$

where ε is the photon's energy and E_b is the electron's binding energy. The differential cross-section for the photoelectric effect can be obtained using equation (1.5) and it depends on which energy level the targeted electron occupies; for example an electron in a K-shell we have[44,62]

$$\frac{d\sigma_{pe}}{d\Omega} = 4\sqrt{2}\, r_0^2\, \alpha^4 Z^5 \left(\frac{m_e c^2}{\varepsilon}\right)^{7/2} \frac{\sin^2\theta \cos^2\varphi}{\left(1-\beta_e \cos\theta\right)^4} \tag{1.48}$$

where β_e is the speed of the electron divided by the speed of light.

Finally, the integral cross-sections can be easily obtained through integrating the above equations. The total cross-section is the sum of the cross-sections of the above effects as follows[41,62]

$$\sigma_{\text{tot}} = \sigma_{\text{Tho}} + \sigma_{\text{Ray}} + \sigma_{KN} + \sigma_{pe} \tag{1.49}.$$

1.2.3.3. Energy straggling

As a particle penetrates through the target medium, it loses energy through discrete interactions with molecular electrons and, as a result, the energy loss process is not continuous but stochastic in nature. This is known as the energy-loss straggling effect. Briefly, the theory describing this starts from writing the one-dimensional, integro-differential continuity equation as follows[44,63]

$$\frac{\partial f\left(x,\Delta E\right)}{\partial x} = -f\left(x,\Delta E\right)\int_0^{Q_{\max}} w\left(Q\right) dQ + \int_0^{\Delta E} w\left(Q\right) f\left(x,\Delta E - Q\right) dQ \tag{1.50}$$

where $f\left(x,\Delta E\right)$ is the fraction of the penetrating particles that have lost ΔE of their initial energy as they travelled a distance x in the medium. $Q_{\max}$ is the maximum energy loss over the length element dx. $w(Q)$ is called the probability of energy loss per path length and is obtained through multiplying the differential cross-section by the density of electrons in the medium. The function $f\left(x,\Delta E\right)$ can then be either

approximated to a Gaussian or more accurately considered asymmetrical, the Vavilov approach. The energy straggling parameter is defined as[44,64]

$$\Omega_{\text{col}}^2 = \frac{1}{\lambda_{\text{col}}} \int Q^2 \, w(Q) \, dQ \tag{1.51}$$

where λ_{col} is the mean free path. The asymmetrical solution of equation (1.50) is used to build up Monte Carlo radiation track simulations where several codes have been developed as described in the literature.[36,65-69]

1.2.4. Radiolysis of liquid water

The radiolysis of water has been extensively studied (both theoretically and experimentally) for decades for many reasons.[6,11,70-74] For example, water is the main component of our bodies, and a ubiquitous molecule on Earth. It has also been used as a cooling agent in nuclear reactors. In this section the radiolysis of liquid water is briefly discussed.

It is known that irradiation with fast heavy ions leads to different results compared to γ-rays, X-rays, and fast electrons, which are categorized as low-LET radiations. For example, some special cancers are radio resistant against low-LET radiations but not against heavy ions.[75] Heavy ions, which are categorized as high-LET radiations, deposit their energies much more densely than low-LET radiations. The spurs in their tracks will be close to one another and the neighbouring spurs overlap at all times, while for low-LET radiations the spurs can be treated independently from one another, as they are far apart. For the case of water, a value of LET above the limit of ~1.5 eV/nm is considered to be high-LET.[75] This estimate is calculated based on the diffusion coefficients of water and H_3O^+ and assuming that the mean energy required to generate a spur is ~60 eV. This gives a mean inter-spur distance of about 40 nm, and it takes of the order of 50 ns for a H_3O^+ ion to diffuse this distance; the spur recombination reactions are essentially complete by this time. Finally, it should be noted that high-LET studies are much fewer in number relative to low-LET studies. This is because the accessibility to ion accelerators is much more limited than to electron accelerators (or other low-LET sources), in fact only a few groups worldwide have access to such facilities.[75-77]

The primary species (or products) are the species present when the spur processes are complete (around 10^{-7}–10^{-6} s in Figure 1.1). In the case of water, the primary products are well known and represented by the following equation[30,71,78,79]

$$H_2O \xrightarrow{Rad} e_{aq}^- , H , OH , H_2 , H_2O_2 , H_3O^+, OH^-, HO_2/O_2^- \qquad (1.52)$$

where e_{aq}^- is the hydrated electron. The molecular yields of the primary products, the number of molecules formed or destroyed per 100 eV absorbed energy, depend on the value of LET and also on the ionizing particle. For neutral water irradiated by ^{60}Co γ-rays‡ (low-LET of 0.23 eV/nm) at room temperature, the yields are[3,71,79-81]

$$3.94\ H_2O \xrightarrow{100\ eV} 2.5\ e_{aq}^- , 0.56\ H , 2.5\ OH , 0.45\ H_2 , 0.7\ H_2O_2 , 3.2\ H_3O^+, 0.7\ OH^- \qquad (1.53).$$

The yield of the last species in equation (1.52) is very small and consequently have been ignored. As the value of LET increases, the yields (or the G-values) drift away from the values in equation (1.53): For example, the yields of the hydrated electron and the hydroxyl radical decrease with the increase of LET (in general the yields of radicals decrease with the increase of LET), while the yield of hydrogen peroxide increases as LET increases.[75,82-85] This can be explained by the spur-overlap effect mentioned above.[86] Under the same conditions as described above, the use of 5 MeV α (high-LET of 156 eV/nm) gives the following (although it becomes impossible to define a timescale at which the spur reactions are complete and so with high LET radiation the time should always be specified: the values below are for ~ 10^{-6} s.)[80]

$$2.48\ H_2O \xrightarrow{100\ eV} 0.26\ e_{aq}^- , 0.12\ H , 0.38\ OH , 1.12\ H_2 , 0.95\ H_2O_2 , 0.1\ HO_2 \qquad (1.54).$$

Interestingly, the pair HO_2/O_2^- represents an exception to the general observation mentioned above (the decrease in the radical yield with the increase of LET due to the spur-overlap), because of the relatively low reactivity of these species in pure water which is essentially due to the following slow dismutation reaction[75,82]

$$HO_2 + O_2^- \xrightarrow{H_2O} OH^- + H_2O_2 + O_2 \qquad (1.55)$$

‡ $^{60}_{27}Co \longrightarrow {}^{60}_{28}Ni + e^- + \overline{\nu_e} + \gamma$

which makes it easy for them to escape from the track recombination and persist for much longer times.

Scavengers have been used in almost all of the experimental studies on water radiolysis.[6,75,83,87,88] They have been used not only to convert the transient species, such as hydroxyl radical and hydrated electron, into stable and easily detectable species but also to prevent their reactions with other species present, such as hydrogen peroxide for example. This will be discussed in more detail later but briefly if we denote the scavenged radical R and the scavenger used S then[75]

$$\mathrm{R} + \mathrm{S} \xrightarrow{k_S} \mathrm{P} \tag{1.56}$$

where k_S ($M^{-1}.s^{-1}$) is the second-order scavenging rate constant. The scavenger concentration is typically very large compared to the bulk concentration of the radicals and so we have

$$\mathrm{R} \xrightarrow{k} \mathrm{P} \tag{1.57}$$

where k is the pseudo-first-order rate constant and is given by

$$k = C_S\, k_S \tag{1.58}.$$

The pseudo-first-order rate constant k is called the scavenging capacity, and its inverse gives an approximate timescale for the scavenging reaction.

The main processes thought to comprise the physical and physicochemical stages are listed in Table 1.1.[3,6,71,78,89] The first two processes represent respectively the ionization and excitation of H_2O due to energy deposition events. The ejected electron (reaction R1) may undergo geminate recombination (reaction R3); it may also escape and ionize or excite further water molecules (if it has sufficient energy). In the latter case the process continues until the energy of the electron is too low to induce an electronic excitation, and at that stage it is known as sub-excitation electron. The fate of the sub-excitation electrons is detailed in the R5 and R10 reactions. The recombination of H_2O^+ and e^- in the R3 reaction produces an excited state molecule H_2O^* which can be vibrationally or electronically excited (the other possible fate of H_2O^+ is the R4 reaction). The excited state H_2O^* has three possible dissociation channels (reactions R6, R8 and R9, of which the most likely (79%) is R9).[77] The reaction R6 gives H_2O_2 and H_2 and is thought to be the main source of H_2 in the physicochemical stage (this does not contribute significantly to the overall yield

of H_2 (the R7 reaction). The main sources of H_2 are the reactions that happen at later times).

Hence even for a simple molecule such as water, the reaction scheme for its radiolysis is very complicated. With regard to the reactions that occur at a later time (the spur reactions), Figure 1.4 schematically summarizes a recent scheme for the low-LET case.[3,6,11,78] It should be noted that the scheme is more complicated in the case of high-LET radiation, as more reactions should be added to account for the presence of the pair HO_2/O_2^- in equation (1.54).[77,81,90] A more complete set of reactions is listed in Table 1.2.

Table 1.1. The reactions of the physical and physicochemical stages of water radiolysis. The approximate time of occurrence ranges from ~10^{-16} to ~10^{-12} sec.[3,6,71,78]

Symbol	Reaction
R1	$H_2O \xrightarrow{Rad} H_2O^+ + e^-$
R2	$H_2O \xrightarrow{Rad} H_2O^*$
R3	$H_2O^+ + e^- \rightarrow H_2O^*$
R4	$H_2O^+ + H_2O \rightarrow OH + H_3O^+$
R5	$e^- + H_2O \rightarrow OH + H^- \xrightarrow{H_2O} OH + H_2 + OH^-$
R6	$H_2O^* \rightarrow H_2 + O(^1D)$
R7	$H_2O + O(^1D) \rightarrow H_2O_2 (\text{or } 2OH)$
R8	$H_2O^* \rightarrow 2H + O(^3P)$
R9	$H_2O^* \rightarrow H + OH$
R10	$e^- + nH_2O \rightarrow e^-_{aq}$

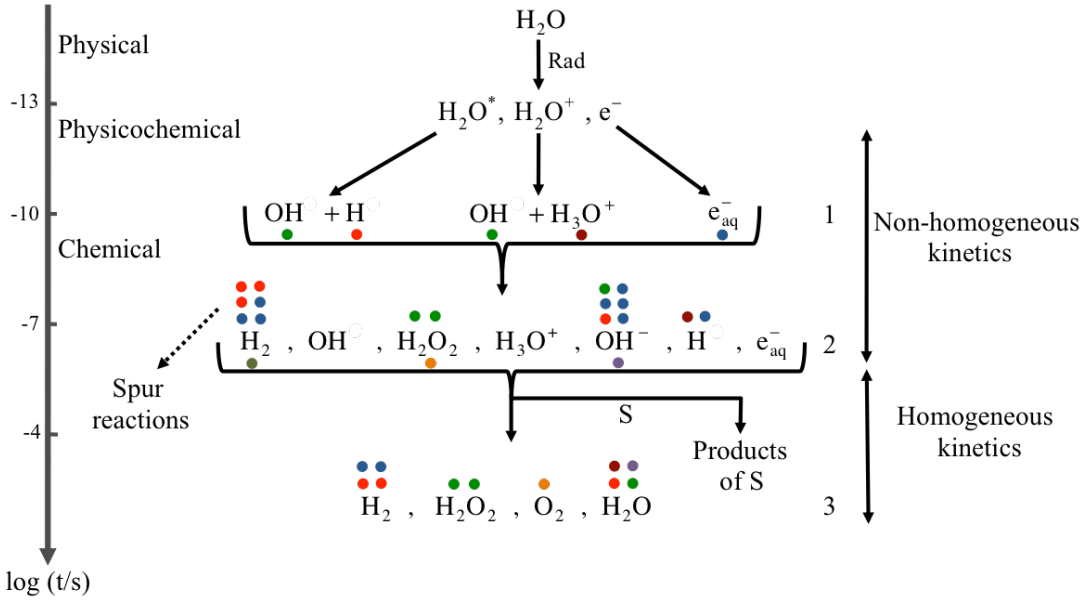


Figure 1.4. Water radiolysis. Each species (from the end of the physicochemical stage onwards) is assigned a colour (the one below it) and then the reactions are written using the colours (above the species). For example, the hydrogen atom corresponds to red and the hydrated electron to light blue, the H_2 can be generated from the reaction of two hydrated electrons (two light blue circles) or the reaction of a hydrated electron and a hydrogen atom (red circle and light blue one) etc. 1 refers to the products at the end of the physicochemical stage, 2 refers to the primary species (equation (1.52)) and 3 refers to the final products. S refers to scavenger. The full reactions are listed in Tables 1.1 and 1.2.[3,6,11,78]

Table 1.2. The reaction scheme for the radiolysis of water (from the end of the physicochemical stage). The rate constant for each reaction is also included.[3,6,11,75,78] More details can be found in references 71, 77, 81 and 90 for example.

Symbol	Reaction	$k \times 10^{-10}/\mathrm{M^{-1}s^{-1}}$
R1	$e_{aq}^- + e_{aq}^- \rightarrow H_2 + 2OH^-$	0.54
R2	$e_{aq}^- + H_3O^+ \rightarrow H + H_2O$	2.3
R3	$e_{aq}^- + H \rightarrow H_2 + OH^-$	2.5
R4	$e_{aq}^- + OH \rightarrow OH^-$	3.0
R5	$e_{aq}^- + H_2O_2 \rightarrow OH^- + OH$	1.1
R6	$e_{aq}^- + O_2 \rightarrow O_2^-$	1.9
R7	$H + H \rightarrow H_2$	0.78
R8	$H + OH \rightarrow H_2O$	2.0
R9	$H + H_2O_2 \rightarrow OH + H_2O$	0.009
R10	$H + O_2 \rightarrow HO_2$	2.1
R11	$H_3O^+ + OH^- \rightarrow 2H_2O$	14.3
R12	$H_3O^+ + O_2^- \leftrightarrows HO_2 + H_2O$	3.8
R13	$OH + OH \rightarrow H_2O_2$	0.55
R14	$OH + H_2O_2 \rightarrow H_2O + HO_2 \leftrightarrows O_2^- + H_3O^+$	2.7×10^{-3}
R15	$OH + HO_2 \rightarrow H_2O + O_2$	0.6
R16	$OH + O_2^- \rightarrow OH^- + O_2$	0.8
R17	$HO_2 + O_2^- \xrightarrow{H_2O} OH^- + H_2O_2 + O_2$	9.7×10^{-3}

1.2.5. Deterministic and stochastic chemical kinetics

Chemical kinetics concerns the rate of chemical reactions, or in other words, how the chemical reaction proceeds through time either towards completion or an equilibrium point. Formally, a rate law is an equation that expresses the rate of the reaction *R* as a function of the concentrations of all the species present in the overall chemical equation for the reaction as follows[91,92]

$$R = f\left(\left[\mathrm{A}\right],\left[\mathrm{B}\right],...\right) \tag{1.59}$$

where [F] is the concentration of F at time t. For example, if we consider the following simple, second order reaction

$$2\mathrm{A} \rightarrow \mathrm{M} \tag{1.60}$$

we write

$$R = -\frac{1}{2}\frac{d\left[\mathrm{A}\right]}{dt} = k_2\left[\mathrm{A}\right]^2 \tag{1.61}$$

where the rate is assumed independent of M, and k_2 is the rate constant which is considered here to be time independent and then we have

$$C = \frac{\left[\mathrm{A}\right]}{\left[\mathrm{A}\right]_0} = \frac{1}{1+D} \quad : \quad D = k\,t\left[\mathrm{A}\right]_0 \ , \ k = 2k_2 \tag{1.62}$$

where $[\mathrm{A}]_0$ is the concentration at the start of the reaction. This is known as the deterministic (or classical) treatment of chemical kinetics because equation (1.62) assumes the variable [A] to be a continuous, real-valued function of time and it does not consider any deviations from its value. It has been known since the middle of the last century that there are a number of examples where the above deterministic treatment is inadequate, particularly in systems containing a small number of reactant species. For example, reactions occurring in a biological cell or in a radiation-generated spur described in the previous sections; in this case, a stochastic approach was found necessary.[6,93-95] To demonstrate this, we briefly continue the analysis of the above example using a stochastic approach. If we assume the number of A particles at the start of the reaction is n_0, then the number of the remaining particles at a later time t, $N(t)$, is a random integer. The time evolution of the probability distribution function P is given by the following chemical master equation[6,93-97] (more detail and background on the master equation will be given later)

$$\begin{aligned}\frac{\partial}{\partial t}P\left\{N\left(t\right)=n\right\} = \frac{1}{2}k\left(n+2\right)\left(n+1\right)P\left\{N\left(t\right)=n+2\right\} - \\ \frac{1}{2}k\,n\left(n-1\right)P\left\{N\left(t\right)=n\right\}\end{aligned} \tag{1.63}.$$

If we use the probability generating function $g(s,t)$ defined as[4]

$$g\left(s,t\right) = \sum_n s^n P\left\{N(t)=n\right\} \tag{1.64}$$

equation (1.63) becomes[94,95]

$$\frac{\partial g}{\partial t} = \frac{k}{2}\left(1 - s^2\right)\frac{\partial^2 g}{\partial s^2} \tag{1.65}$$

which can be solved using the standard separation of variables technique.[98] If we then use the properties of the probability generating function, we can define the mean or the first moment $\overline{N}$ and then we can write the following equation[93-95]

$$C = \frac{\overline{N}}{N_0} = \frac{1}{N_0}\sum_{n=2}^{N_0} A_n T_n \quad : \quad n = 2,4,...,N_0 \tag{1.66}$$

where Γ is the gamma function in the following equation

$$A_n = \left(\frac{2n-1}{2^n}\right)\left\{\frac{\Gamma\left(N_0+1\right)\Gamma\left[\left(N_0-n+1\right)/2\right]}{\Gamma\left(N_0-n+1\right)\Gamma\left[\left(N_0+n+1\right)/2\right]}\right\} \tag{1.67}$$

and

$$T_n = e^{-k\,n(n-1)t/2} \tag{1.68}.$$

The gamma function is defined as follows

$$\Gamma\left(\alpha\right) = \int_0^\infty x^{\alpha-1}\,e^{-x}\,dx \tag{1.69}.$$

Equation (1.66) is the stochastic equivalent of equation (1.62). A comparison now can be made between the stochastic and deterministic approaches. In Figure 1.5 we see that equation (1.62) is a very good approximation to equation (1.66) when the number of reactant particles is large. However, as shown in Figure 1.6, when the number of reactants is small (this is a spur-like situation), then the deterministic equation no longer matches the stochastic one. This worsens even more as the number of reactants gets smaller (Figure 1.7). The basic reason for this problem is that the rate of reaction is proportional to the expectation value $E[N(N-1)]$, which is only close to the deterministic approximation $[E(N)]^2$ when both N is much larger than 1 (so that $N-1$ is approximately the same as N, the small number correction) and the standard deviation of N is much smaller than N so that the deterministic approximation ($E(N^2) = [E(N)]^2$ can be made.

It should be noted that the above example is not the only problem that can appear when using the deterministic treatment to study radiation chemical kinetics.[6,99,100] Consider the following simple reaction scheme[99]

$$\begin{aligned} A + A &\rightarrow A_2 \\ B + B &\rightarrow B_2 \\ A + B &\rightarrow AB \end{aligned} \tag{1.70}$$

in a spur of two reactants A and B. The particles are assumed to be identical in all aspects. Also the reaction distances are all assumed to be identical. According to the deterministic treatment, the ratio of the products A_2:B_2:AB is always 1:1:2 (regardless of the initial distribution of the reactants and also regardless of the initial number of reactants), as the formation of the first two products require the reaction of two A particles for the first and two B particles for the second.[99] However, the stochastic treatment indicates that the correct ratio is[6,99]

$$n_A\left(n_A - 1\right)/2 : n_B\left(n_B - 1\right)/2 : n_A n_B \tag{1.71}$$

where n_A and n_B is the initial number of A and B particles respectively. Hence, the correct ratio depends on the number of reactants. Note that in particular if there is only one A and one B the only possible product is AB, whereas the deterministic rate equation gives the unphysical AA and BB products as well. Thus it is essential to take the above effects into account when studying radiation chemical kinetics,[6,94,95,99,100] and this is what the next chapters are aiming to do.

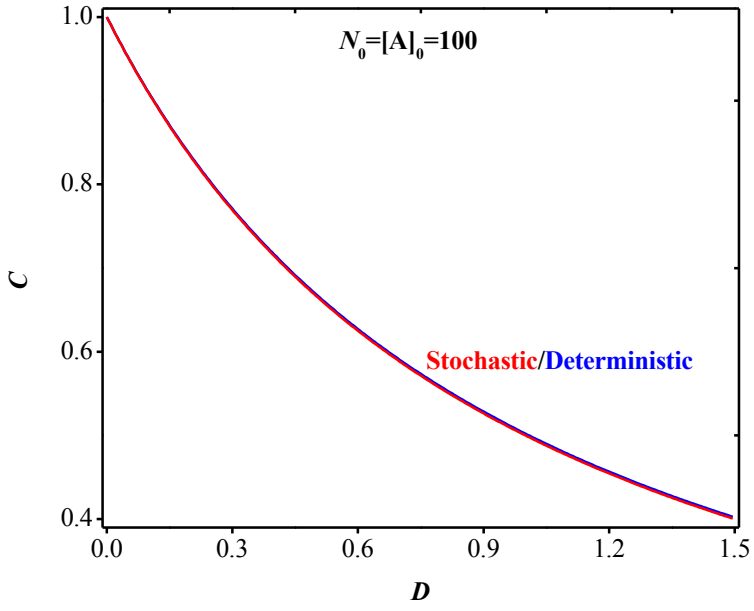


Figure 1.5. Comparison of stochastic and deterministic kinetics for a large number of reactants, redrawn from references 94 and 95. *D* is given in equation (1.62) and *C* is given in equations (1.62) and (1.66). The deterministic approach is in good agreement with the stochastic approach when the number of reactants is relatively large.

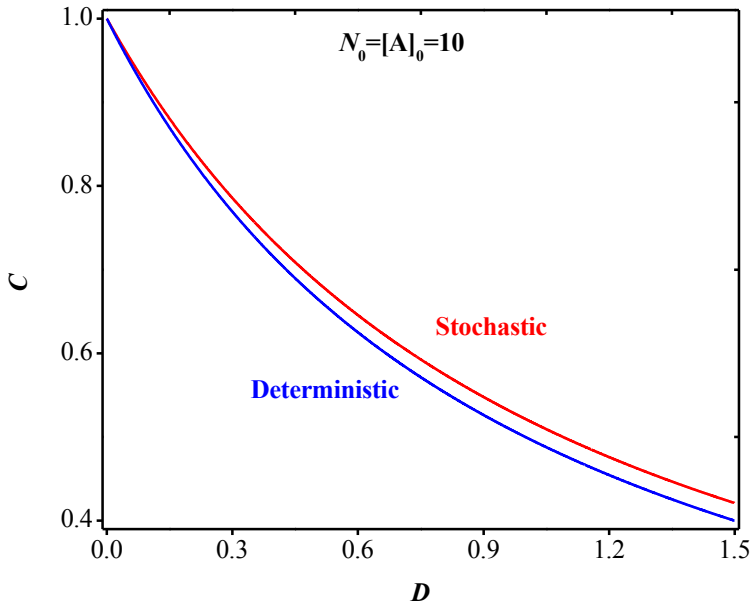


Figure 1.6. Comparison of stochastic and deterministic kinetics for a small number of reactants redrawn from references 94 and 95. *D* is given in equation (1.62) and *C* is given in equations (1.62) and (1.66). The agreement between the deterministic approach and the stochastic approach breaks down when the number of reactants is small (see also the next figure).

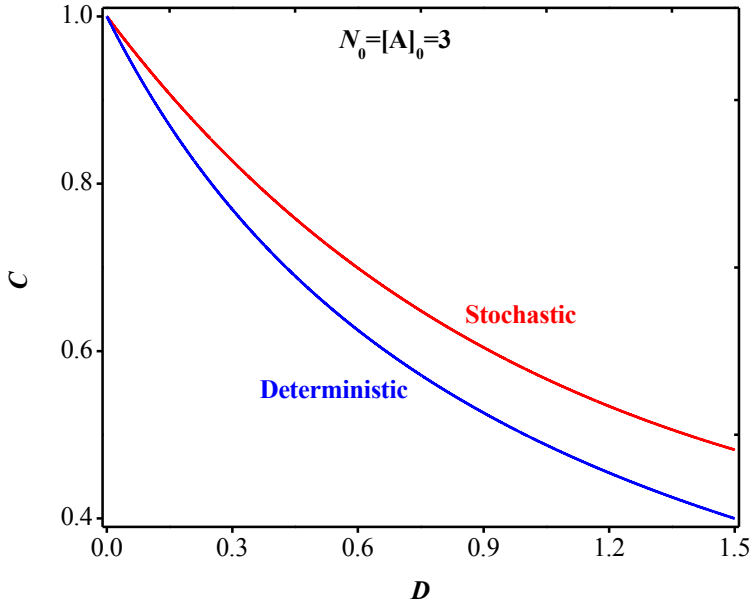


Figure 1.7. Comparison of stochastic and deterministic kinetics for a small number of reactants. *D* is given in equation (1.62) and *C* is given in equations (1.62) and (1.66).

Chapter 2

Monte Carlo Random Flights

"These motions were such as to satisfy me, after frequently repeated observation, that they arose neither from currents in the fluid, nor from its gradual evaporation, but belonged to the particle itself."
Robert Brown

As discussed in the last chapter, the deterministic approach is inadequate when considering the problem of chemical kinetics in the track of ionizing radiation. It was found necessary to take into account the stochastic nature of the problem.[95,101]

A theory (or model) is meant to account for certain experimental data. The theory's success is then measured by how well its results match the experimental data available. However, sometimes it is not possible to compare theoretical and experimental results together; for example when the experimental data are not yet fully complete or when establishing the theoretical results require a set of unknown parameters (such as diffusion coefficients and reaction distances etc.). In this case, the alternative is to use the results of an already known and tested model as a reference instead of experimental results. This brings about the subject of the current chapter, Monte Carlo Random Flights (RF). As mentioned before, the RF model has been well tested and successfully used in modelling problems in radiation chemical kinetics and also problems of biological importance.[6,7,10,102] In this work, the RF model has been used for the purpose of comparison when testing more approximate methods (chapters 3-7) and the current chapter will describe the RF model in general and provide some background about it. It also proposes a solution to overcome the time-consuming nature of the model through the use of the Message Passing Interface (MPI) in the program code.[8,9]

2.1. General background

Probability theory provides a mathematical description for random processes, i.e. processes involving uncertainty. The sample space Ω is a set containing all the possible outcomes of an experiment associated with the process. The following mapping function[98,103]

$$X:\ \Omega \to S \tag{2.1}$$

is a random variable associated with the probability space (Ω,Ξ,P) where Ξ is sigma-algebra on Ω and P is the probability function. The set S can be discrete (for example 0,1,2… in this case the random variable is discrete) or continuous (for example the real line. In this case the random variable is continuous). In that sense, a stochastic process is a collection of random variables as follows[4,5]

$$\left\{ X_t, t \in T \right\} \tag{2.2}$$

where t refers to time and the set T can be discrete (in this case we have a discrete time stochastic process) or continuous (in this case we have a continuous time stochastic process). If the random variables are discrete, the stochastic process is a discrete state process. If the random variables are continuous, the stochastic process is a continuous state process. If we consider, for simplicity, a discrete time and discrete state stochastic process where

$$T = \left\{ 0, 1, 2... \right\} \tag{2.3},$$

then at a given time $t > 0$, the probability of finding X_t in the state j_t depends in general on the entire history of the process i.e.

$$P\left(X_t = j_t\right) = \Pr\left\{ X_t = j_t \middle| X_{t-1} = j_{t-1}, X_{t-2} = j_{t-2}, ..., X_0 = j_0 \right\} \tag{2.4}.$$

However, a certain type of stochastic processes (Markov processes) possess the following property

$$P\left(X_t = j_t\right) = \Pr\left\{ X_t = j_t \middle| X_{t-1} = j_{t-1} \right\} \tag{2.5}$$

where the probability in this case depends only on the last value specified right before the time of concern t and not on the entire history. For a Markov process it is common to write this property in the form of a transition probability between two states i and j as follows

$$P_{ij}^{t-1,\,t} = \Pr\left\{ X_t = j \middle| X_{t-1} = i \right\} \tag{2.6}.$$

If the transition probability in the last equation is independent of time, the process is said to be a *stationary* Markov process.[4,104] The Markov property has many practical applications; for example the chemical master equation used in the last chapter (equation (1.63)) is a consequence of the Markov property described above.[97,105]

The random variable S (with values 0,1,2… for simplicity) is a Markov time (also called a stopping time or random variable independent of the future) with regard to the stochastic process $\left\{ X_t, t = 0, 1, 2... \right\}$ if at any time t, the event $S = t$ is determined by the history of the process up until the time t (hence it is independent of the future). This can be written in the following form[4,103]

$$I_{(S=t)} = I_{(S=t)}\left(X_{t-1}, X_{t-2}, ..., X_0\right) = \begin{cases} 0, & \text{if } S \neq t \\ 1, & \text{if } S = t \end{cases} \tag{2.7}$$

where I indicates if the event $S = t$ has occurred or not. This is an important concept as it introduces the strong Markov property. The Markov process possesses the strong Markov property if for any stopping time ξ the probability distribution of the following[106]

$$X\left(t_1 + \xi\right),\ X\left(t_2 + \xi\right), ..., X\left(t_k + \xi\right) \quad : t_1 < t_2 ... < t_k \tag{2.8},$$

given that $X\left(\xi\right) = x$, is identical with the probability distribution of

$$X\left(t_1\right),\ X\left(t_2\right), ..., X\left(t_k\right) \quad : t_1 < t_2 ... < t_k \tag{2.9}$$

given that $X\left(0\right) = x$.

A continuous time and state stochastic process $\left\{ X_t, t \geq 0 \right\}$ which possesses the strong Markov property, and for which the sample paths $X(t)$ are continuous functions of time is called a diffusion process. Diffusion processes satisfy the following Dynkin condition[106,107]

$$\lim_{h \downarrow 0} \frac{1}{h} \Pr\left[\left\{ \left| X\left(t+h\right) - X\left(t\right) \right| > \varepsilon \right\} \middle| X\left(t\right) = x \right] = 0 \quad : \varepsilon > 0 \tag{2.10}$$

which formalizes the continuity of the paths in the definition above. They also satisfy the following infinitesimal moment generator

$$\lim_{h \downarrow 0} \frac{1}{h} E\left[\left\{ \left| X\left(t+h\right) - X\left(t\right) \right|^p \right\} \middle| X\left(t\right) = x \right] = \beta_p\left(x, t\right) \tag{2.11}$$

where $p = 1, 2, ...$ and

$$\beta_p(x,t)=\begin{cases}\mu(x,t) & \text{for } p=1\\ \sigma^2(x,t) & \text{for } p=2\\ 0 & \text{for } p=3,4...\end{cases} \tag{2.12}$$

where the first moment $\mu(x,t)$ and the second moment $\sigma^2(x,t)$ are the infinitesimal mean and infinitesimal variance of the process respectively. Most of the cases of interest satisfy the additional constraint that the infinitesimal mean and infinitesimal variance of the process are time-independent, i.e.

$$\mu(x,t)=\mu(x) \quad , \quad \sigma^2(x,t)=\sigma^2(x) \tag{2.13}.$$

In this case the diffusion process is said to be time-homogenous. The probability distribution function is then given as follows[106,107]

$$P(t,x,y)=\Pr\left\{ X(t)\le y \middle| X(0)=x \right\} \tag{2.14}$$

which is a function of three variables: Time *t*, initial status (or configuration) *x* and current status (or configuration) *y*. Two partial differential equations for $P(t,x,y)$ can be written: The first one contains derivatives with regard to *t* and *x* and it is known as the backward diffusion equation (or Kolmogorov backward equation) and is written as follows (this will be discussed in more detail in chapter 3)

$$\frac{\partial}{\partial t}P(t,x,y)=\left[\frac{1}{2}\sigma^2(x)\frac{\partial^2}{\partial x^2}+\mu(x)\frac{\partial}{\partial x}\right]P(t,x,y) \tag{2.15}$$

or in terms of the probability density function *p*

$$\frac{\partial}{\partial t}p(t,x,y)=\left[\frac{1}{2}\sigma^2(x)\frac{\partial^2}{\partial x^2}+\mu(x)\frac{\partial}{\partial x}\right]p(t,x,y) \tag{2.16}$$

where

$$p(t,x,y)=\frac{\partial}{\partial y}P(t,x,y) \tag{2.17}.$$

The second differential equation contains derivatives with regard to *t* and *y* and it is known as the forward (or evolution) diffusion equation and is written as follows

$$\frac{\partial}{\partial t}p(t,x,y)=\left[\frac{1}{2}\frac{\partial^2}{\partial y^2}\sigma^2(y)-\frac{\partial}{\partial y}\mu(y)\right]p(t,x,y) \tag{2.18}.$$

It is common to write the above two equations in operator-like form; for example in the case of the backward diffusion equation we have

$$\frac{\partial}{\partial t}P\left(t,x,y\right)=L\,P\left(t,x,y\right) \tag{2.19}$$

where

$$L=\frac{1}{2}\sigma^{2}\left(x\right)\frac{\partial^{2}}{\partial x^{2}}+\mu\left(x\right)\frac{\partial}{\partial x} \tag{2.20}.$$

Historically, the botanist R. Brown discovered in 1828 that pollen suspended in fluids show, under the collisions with the molecules of the fluid, a completely irregular movement and this movement has since been named after him.[104,108] The first to propose an account for this phenomenon based on the laws of physics was A. Einstein around the beginning of last century. He considered the problem of a non-electrolyte molecule dissolved in liquid and used the basics of thermodynamics to derive an expression for the diffusion coefficient D as follows[109]

$$D=\frac{RT}{N}\frac{1}{6\pi\eta r} \tag{2.21}$$

where R is the ideal gas constant, T is the temperature, N is Avogadro's number, η is the viscosity of the liquid and r is the radius of the molecule which is assumed spherical. He then used the concepts of statistical mechanics to obtain the following known one-dimensional diffusion equation

$$\frac{\partial p}{\partial t}=D\frac{\partial^{2}p}{\partial y^{2}} \tag{2.22}.$$

Following that, studies continued to appear including works by M. Smoluchowski and P. Langevin.[16,110,111] Mathematically, a stochastic process $\left\{B_{t},t\geq 0\right\}$ is a Brownian motion (when $D=1/2$, it is known as a Wiener processes after N. Wiener and denoted W in that case[112]) if it satisfies the following conditions[4,5,113]

- The increments $B\left(h+t\right)-B\left(h\right)$ are normally distributed random variables with mean 0 and variance $2Dt$.
- The time-disjoint increments $B\left(t_{2}\right)-B\left(t_{1}\right)$ and $B\left(t_{4}\right)-B\left(t_{3}\right)$ are independent random variables.
- $B\left(0\right)=0$ and sample path $B\left(t\right)$ is a continuous function of t.

Equation (2.22), which is known as the Fokker-Planck equation, can be solved under the following conditions for the probability density function

$$\lim_{t\downarrow t_0} p\left(y,t\middle|x\right)=0 \quad : y\neq x \tag{2.23}$$

where

$$B\left(t\right)=y \quad \& \quad B\left(t_0\right)=x \tag{2.24}.$$

The solution is

$$p\left(y,t\middle|x\right)=\frac{1}{\sqrt{4\pi D\left(t-t_0\right)}}\,e^{-\left(y-x\right)^2/4D\left(t-t_0\right)} \tag{2.25}.$$

The probability distribution function is obtained through integrating the last equation. The Brownian motion satisfies the definition of the diffusion process given above; in fact several properties of the Brownian motion can be derived based on its property as a diffusion process.[106] If we consider the random vector defined as[4]

$$\mathbf{B}\left(t\right)=\left(B_1\left(t\right),B_2\left(t\right),B_3\left(t\right)\right) \tag{2.26}$$

where $\left\{B_i\left(t\right);t\geq 0\right\}$ is a Brownian motion, then the following Brownian stochastic process is called the radial Brownian motion or Bessel process with a parameter of (1/3)

$$R\left(t\right)=\left[\mathbf{B}\left(t\right).\mathbf{B}\left(t\right)\right]^{1/2} \tag{2.27}.$$

Finally, the above mathematical background is used to account for the trajectory of a moving particle in liquids through the concept of stochastic differential equation, a differential equation containing a stochastic process.[114] This is given by the following special case of the general Itô's equation (after K. Itô, the following equation is also called Langevin's equation as it contains a Brownian motion[115])[106,107]

$$dX\left(t\right)=\alpha\left(X_t,t\right)dt+dB\left(t\right) \tag{2.28}$$

where this equation describes the increment of a one-dimensional motion and $X(t)$ is the position of the particle. The first term in the last equation represents the drift experienced by the particle due to external forces (if any exists) while the second represents the contribution of the Brownian motion $B(t)$ to the movement. For example, when we consider a Bessel process with a relative diffusion coefficient D', we have

$$dR=\frac{2D'}{R}dt+dB \tag{2.29}.$$

2.2. RF simulations

Firstly, the case of a fully diffusion-controlled reaction is considered in this section. The partially diffusion-controlled reaction will be discussed later, in chapter 7.[6,18]

The chemical kinetics is simulated in the RF model through simulating the diffusive trajectories of the reactant particles.[6,116] As discussed above, simulating a diffusive trajectory involves solving the corresponding stochastic differential equation. If the particle i, whose diffusion coefficient is D_i, is at the position $\mathbf{R}_i$ and feels an average Coulomb force $\mathbf{F}_i$, then the equation describing the infinitesimal change in the particle's position in a time period dt is obtained from equation (2.28) which becomes[7,92,114]

$$d\mathbf{R}_i = \frac{D_i}{kT}\mathbf{F}_i\, dt + d\mathbf{B}(t) \tag{2.30}$$

where $\mathbf{B}(t)$ was given in equation (2.26), k is the Boltzmann constant and T is the temperature. The particle trajectory can then be obtained through solving the last equation. Obtaining the solution (or the trajectory) requires choosing a method to discretize the time variable and then working out how to sample the process over this discrete interval.[117, 118] The Euler-type discretization of stochastic differential equations was found convenient to use before and in this case the last equation can be written as[6,7,10,119]

$$\delta\mathbf{R}_i = \frac{D_i}{kT}\mathbf{F}_i\delta t + \left(2D_i\delta t\right)^{1/2}\mathbf{N}(0,1) \tag{2.31}$$

where $\delta\mathbf{R}_i$ is the change in the position during the small time increment δt and $\mathbf{N}(0,1)$ is a vector of independent, normally distributed random numbers of mean zero and unit variance. The second term on the right hand side of the above equation results directly from equation (2.25). If we assume that the only form of force $\mathbf{F}_i$ is the ion-ion Coulomb force when the particles carry electrical charges, then in the case of a neutral reactant particle we can write the following equation[6,7]

$$\delta\mathbf{R}_i = \left(2D_i\delta t\right)^{1/2}\mathbf{N}(0,1) \tag{2.32}.$$

Under these conditions, the discretized stochastic differential equation is exact and hence the trajectories can be sampled exactly. For charged particles, $\mathbf{F}_i$ is given as follows[6,119]

$$\mathbf{F}_i = -kT\sum_j \frac{z_i z_j r_c}{r_{ij}^3}\mathbf{r}_{ij} \tag{2.33}$$

where z_m is the charge of the ion m, $\mathbf{r}_{ij}$ is the i to j vector and r_c is the Onsager distance.[§] In this case, the discretization in equation (2.31) represents only an approximation. This approximation converges to the real stochastic differential equation when the time increment (or step) is sufficiently small that, during which, the force $\mathbf{F}_i$ can be considered constant.

The choice of the time step in the RF simulation is very important particularly when considering the case of non-neutral reactants. This is because it is essential that the drift (or in other words, the Coulomb forces in equation (2.31)) remain effectively unchanged.[6,7,10,119] Hence, the time step is selected in such a way that the drift varies by less than some prescribed proportion ε with some prescribed confidence C. The change in the drift is then formulated using the Itô transformation formula,[106] and a solution is then sought for the values ε and C. This has recently been described in the literature.[120]

In conclusion of the above discussion, the procedures of RF simulations can be summarized as follows: the simulation starts from a certain configuration, which in a real track will usually be modelled as a random distribution of some kind, but for the purposes of testing approximations could be a fixed geometry. Then the diffusive trajectory of each particle is simulated using time-discrete jumps (or flights) based on equation (2.32) for neutral particles, and based on equation (2.31) for electrically charged ones. At the end of each step, the distance between each pair of particles is evaluated and if it is less than or equal to the corresponding reaction distance, then a reaction will be counted and that pair will not be considered in the next step of the simulation.[6,7,19]

Because of the non-zero time-step, it is essential in this model to take into account the possibility that a reaction may happen between two particles during the course of the time step but that by the sample time the pair may have diffused apart again. This correction is made using what is called a bridging process.[19,121,122] Briefly,

[§] The Onsager distance r_c is defined as follows

$$r_c = \frac{e^2}{4\pi\varepsilon\varepsilon_0 kT}$$

where $\varepsilon\varepsilon_0$ is the dielectric permittivity of the medium, e is the electron charge, k is the Boltzmann constant and T is the temperature.

the problem of finding the bridging condition is reduced to the problem of finding the probability that one-dimensional Brownian motion (either a Brownian motion with a constant drift for equation (2.31) or a Bessel process for equation (2.32)) moves from a separation of x to a separation of y during time δt and passing through a separation of a (the reaction distance of the two particles here). The probability of passing through a conditional on starting at x and ending at y is given as follows[122]

$$W = 1 - \frac{p_a(x, y, \delta t)}{p(x, y, \delta t)} \tag{2.34}$$

where $p_a(x,y,\delta t)$ is the probability density of an absorbed motion (a motion that is killed when it first hits a separation of a) and $p(x,y,\delta t)$ is the probability density of reaching the separation y starting from x during δt in an unbounded diffusion. Both of the functions are known, and for a Brownian motion with a constant drift parameter μ we have the following[4,122]

$$p(x,y,\delta t) = \frac{1}{\sqrt{4\pi D'\delta t}} e^{-(y-x-\mu\delta t)^2/4D'\delta t} \tag{2.35}$$

$$p_a(x,y,\delta t) = p(x,y,\delta t)\left[1 - e^{-(x-a)(y-a)/D'\delta t}\right] \tag{2.36},$$

and for a Bessel process with a parameter of (1/3) we have

$$p(x,y,\delta t) = \frac{y}{x\sqrt{4\pi D'\delta t}}\left[e^{-(y-x)^2/4D'\delta t} - e^{-(y+x)^2/4D'\delta t}\right] \tag{2.37}$$

$$p_a(x,y,\delta t) = \frac{y}{x\sqrt{4\pi D'\delta t}}\left[e^{-(y-x)^2/4D'\delta t} - e^{-(y+x-2a)^2/4D'\delta t}\right] \tag{2.38}.$$

The use of the first two equations in equation (2.34) yields the bridging condition for a Brownian motion with a constant drift as follows

$$W_{\text{Drift}} = e^{-(x-a)(y-a)/D'\delta t} \tag{2.39}.$$

Similarly, the use of the other two equations in equation (2.34) yields the bridging condition for a Bessel process as follows

$$W_{\text{Bessel}} = \frac{e^{-(x-a)(y-a)/D'\delta t} - e^{-xy/D'\delta t}}{1 - e^{-xy/D'\delta t}} \tag{2.40}$$

where D' is the relative diffusion coefficient in the above equations. Equation (2.39), which is the reaction probability on a Brownian bridge from x to y, can be used for

both charged and neutral particles but the choice of the time step is very important when considering charged particles as it was derived under the assumption of a constant drift. Equation (2.40) can be used for neutral particles with any size of the time step.[6] The bridging condition can be included in the simulations as follows: if the distance between two particles is larger than their reaction distance at the end of the time step, then the probability of encounter on the appropriate bridging process is evaluated, and if it is found larger than a random number generated from a uniform distribution between 0 and 1, then a reaction is registered and the pair will be removed from the simulations.

Finally, it is known that the main disadvantage of the RF model is that it is very time consuming.[6] This is because in order for the simulations to be statistically representative, a large number of realizations (or repeats) are required and each realization requires the simulation of a new set of particle trajectories. As discussed next, the MPI is included in the simulations to overcome this and build parallel simulations.

2.3. Parallel computing and MPI

Historically, the so-called parallel computing started about thirty years ago and has progressed very quickly since. It has become particularly important because most of the manufacturers of microprocessor chips currently achieve the gain in performance through including multiple complete processors (also known as cores) on a single integrated circuit, while in the past (last century and the first few years at the beginning of this century) the gain in performance was obtained through developing the ever-faster monolithic processor. The problem for software developers and computational scientists is that simply adding more processors to the same integrated circuit will not magically improve the performance of the vast majority of serial (or sequential) programs, programs that were classically written to run on a single processor.[8,123] As such, it was important to take these effects into account and develop the algorithms used in simulating radiation chemical kinetics and make them parallel algorithms, in other words, algorithms that can make use of the multiple-core system.

In general, “parallelizing” a sequential program can be achieved through two techniques, data-parallelism and task-parallelism. In data-parallelism, the data used in solving the problem of the program are divided among the cores, and then each core

carries out more or less similar operations on its part of the data. In task-parallelism, the various tasks carried out in solving the problem are partitioned among the cores. Depending on the nature and the complexity of the program, its parallelization can use either or both techniques.[8,123] As discussed in more detail later, the method proposed here for parallelizing the radiation chemical kinetics simulation can mainly be considered as data-parallelism.

There are libraries (or languages or models) that can be used to convert a sequential program to a parallel one. This includes the Bulk Synchronous Parallel (BSP) and the Message-Passing Interface (MPI). As mentioned before, MPI was used in this work to achieve parallelism. MPI, which was first released in 1994, is a distributed-memory model where each core has its own, private memory, and the cores must communicate explicitly by doing something like sending messages across a network.[8,123,124] The steps taken to build parallel simulations using MPI are symbolically shown in Figure 2.1. At the start, each core involved in the work is assigned a number by MPI and this number will be kept unchanged until the end of the process. Then the amount of work to be done is divided equally among the cores involved. Once all the cores finish with their individual share of the work, the results are collected at the processor 0 (in principle, this could be done on any other core), which in its turn gives the results back in the appropriate output form. Finally, it should be noted that MPI has been recently applied for the same purpose in other areas.[125-127]

In conclusion, the MPI can be used in the RF simulations described above as follows: at the beginning of the simulations, the MPI commands are used so that each processor available to work is assigned a number. Each processor will then be given a different random number sequence to use during the simulations. Then the number of realizations is divided equally into the number of processors available. Each processor carries out its share of the work exactly as described in section 2.2 and once the work is complete the individual results are sent to the root processor which collects all the results and process them further to give them back in the desired output form. An example of this is on the enclosed CD.

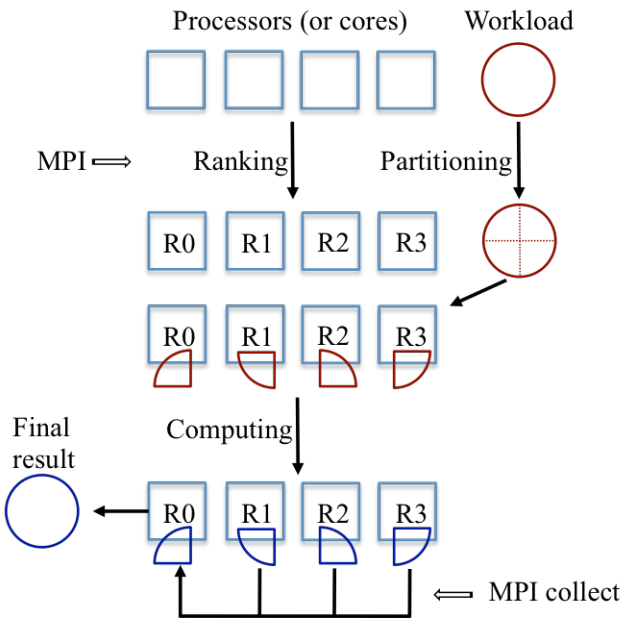


Figure 2.1. Parallel simulations using MPI. An example is included on the attached CD.

2.4. Geminate recombination and testing

It is known that the time-dependent geminate recombination probability of a pair of neutral particles is the solution of the following backward-diffusion equation[6,10]

$$\frac{\partial W}{\partial t} = D'\left(\frac{\partial^2}{\partial r^2} + \frac{2}{r}\frac{\partial}{\partial r}\right)W \tag{2.41}$$

where D' is the relative diffusion coefficient and it was assumed that W depends only on r (the initial distance between the two particles) of the spherical coordinates r, θ and φ. This equation is written for two neutral particles (this will be discussed in more detail in chapter 3). For a fully diffusion controlled reaction, the above equation can be easily solved and the solution is well known. Briefly, this can be summarized as follows: after taking the Laplace transform, the equation becomes an ordinary differential equation, which can be solved in the light of the following boundary conditions

$$\begin{gathered} t \to 0 \Rightarrow W \to 0 \quad , \quad r \to a \Rightarrow W \to 1 \\ r \to \infty \Rightarrow W \to 0 \end{gathered} \tag{2.42}$$

where a is the reaction distance. After taking the inverse Laplace transform of the final result, we have[6,10]

$$W\left(t,r;a\right)=\frac{a}{r}\operatorname{erfc}\left(\frac{r-a}{\sqrt{4D't}}\right) \tag{2.43}$$

where $\operatorname{erfc}\left(x\right)$ is the complementary error function and is given as follows

$$\operatorname{erfc}\left(x\right)=\frac{2}{\sqrt{\pi}}\int_{x}^{+\infty}e^{-u^2}\,du \tag{2.44}.$$

Since equation (2.43) is an exact solution, it can be used to test the RF simulation of the diffusion and reaction of a single pair.[6,122] As shown in Figure 2.2, the RF matches the analytical solution of equation (2.43) (the value for the RF simulation at 500 ps is 0.438(±0.002), where the number of realization is 10^5. The value for the analytic solution at 500 ps is 0.437). Also to signify the importance of the bridge condition, RF simulations without the bridge condition are also shown in Figure 2.2; this resembles the "old RF simulations" as in reference 128. The old RF simulations ignore the possibility that the particles may encounter during the course of the time step, but that by the sample time the pair may have diffused apart again, i.e. they only register a reaction if the particles are found in a reactive configuration at the end of a time-step, missing a substantial number of reactions. Hence, the reaction probability is smaller than it should be as shown in Figure 2.2.

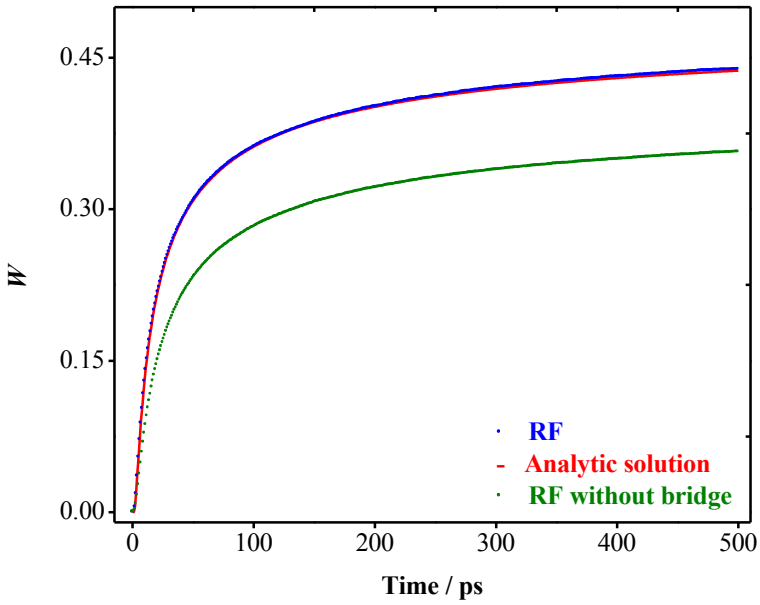


Figure 2.2. The reaction probability *W* based on RF simulations and the analytic solution (equation (2.43)). The simulations are for two identical particles whose diffusion coefficient is 5×10^{-9} m^2s^{-1}. The reaction distance is 5 Å and their initial separation is 10 Å. The time step is considered constant and equal 1 ps.

2.5. Conclusion

As discussed above, the RF simulation is the most common approach to model radiation chemical kinetics and it has been described and used before.[6,7,10] It is also known that the RF model is accurate (Figure 2.2) but it is very time consuming. The use of a bridging condition can help, as it enables reasonable timesteps to be used. The MPI is a known technique to make a sequential (or classical) program a parallel one,[9,123,124] and has been successfully used to build parallel RF simulations as described above. Because of the complications of including MPI, a new simulation program was written for this study. Most of the simulations run in this work were carried out on a node of 12 physical processors (24 virtual processors), which runs the recent Mac OS. Devoting 100% of the machine power to run simulations (as done in most of the simulations of this work) was found to speed up the simulations by a factor of ~24. This gain in performance has made it practical to build multi-method simulation programs as discussed in the next chapters (4-6).

Chapter 3

Three-Body Correlation**

"If you can not solve your problem, try to solve a simpler one." ***Erwin Kreyszig***

As discussed in the last chapter, the RF model simulates the diffusive trajectories of all the reactive particles involved, which, in its turn, leads to a set of reaction times and, after many realizations, the chemical kinetics. Another widely used method to simulate the radiation-induced chemical kinetics is the Independent Reaction Time (IRT) method.[6] This chapter starts from describing the IRT method in general. Then it moves on to see if the independence assumption of the IRT method can be relaxed by the analysis of the correlations among the diffusing distances. As discussed later, this is done through building and investigating the backward-diffusion equation for three diffusing particles, which are assumed to be identical and neutral here.

It is useful to introduce a practical example where the contents of this chapter will be relevant. Consider the reactions R2 and R4 of Table 1.2 of chapter 1 applied to a spur in which a single water molecule has been ionised. An e^-_{aq} can undergo a reaction with OH radical or react with H_3O^+. Hence, we have a system of three particles with three possible encounters, which is similar to the problem that this chapter is trying to investigate.

** **Acknowledgements and details**: N. Green showed how the Clifford-Green theorem (section 3.2) can be used. To avoid any mathematical error, the derivations of the infinitesimal mean, variance and covariance in sections 3.2.2.1-3.2.2.3 were obtained independently by N. Green and E. Al-Samra, and the results were then compared. N. Green suggested that equation (3.61) may be treated as a perturbation problem, and E. Al-Samra performed the mathematics in section 3.2.2.4.1. E. Al-Samra suggested and derived the mathematics in section 3.2.2.4.2. N. Green was very helpful in pointing out the useful references used in section 3.2.2.4.2.

3.1. The IRT method

The IRT method to simulate radiation chemical kinetics was first proposed in 1982.[19,101,129,130] Since the only necessary parameter to obtain the chemical kinetics is the reaction time, the IRT method is built to generate the reaction times without having to monitor the trajectories of the reactants. Briefly, if we consider a system of only two neutral particles separated initially by a distance r, the probability that they have reacted by time t is given by equation (2.43) where, as was discussed in section 2.4, the reaction is assumed to be fully diffusion-controlled (in other words it follows the Smoluchowski boundary condition given in equation (2.42)). Using equation (2.43) we can write the following equation[11]

$$t = \frac{1}{4D'}\left[\frac{r-a}{\mathrm{erfc}^{-1}\left(b\right)}\right]^2 \qquad : b = \frac{r}{a}W\left(t, r; a\right) \tag{3.1}$$

where $\mathrm{erfc}^{-1}\left(b\right)$ is the inverse of the complementary error function. This is very important because it indicates that if the initial separation of the two particles r is known, a reaction time for them can be generated when we replace W in the last equation by a uniformly distributed random number between 0 and 1 (provided the function erfc^{-1} can be computed). This is known as the inverse function method for generating non-uniform random numbers.[131] The IRT method employs the independent pairs approximation to obtain the reaction times in systems of more than two particles i.e. it generates a reaction time for each pair present as described above, ignoring the presence of any other particles.[6,10,132] It is worth noting that the reaction times generated are not completely independent. They are generated from a set of distances that belong to a realizable particle configuration (e.g. they obey triangle inequalities etc.) The reaction times are independent but conditional on the initial distances.

The Monte Carlo IRT simulations generally proceed as follows: it starts from an initial configuration, which in a model track will typically be a random distribution of some sort but for the purpose of testing can be of a specific geometry. The inter-particle separations are then used to generate random reaction times independently using equation (3.1). Following that, the minimum of the generated times is chosen to be the first reaction time. The next minimum time (limited to the surviving particles) is then chosen to be the next reaction time and so on. The processes terminate either

by the reaction of all particles involved or by reaching a maximum time limit used to stop the process. The process is repeated a large number of times (realizations) so that the data become statistically representative and this leads to the reaction rate (or similarly the survival probability).[6,10,11,19]

The last equation can only be used when the reactants are neutral and their reaction is fully diffusion-controlled. If this is not the case, then an alternative must be used to generate the reaction times. Deriving the alternative probability distribution has been described in detail before and will be summarized briefly here; the general form of the backward diffusion equation for the relative diffusion of two particles is needed rather than the special case of equation (2.41). This is given as follows[6,133]

$$\frac{\partial W}{\partial t} = D'\left[\frac{\partial^2}{\partial r^2} + \left(\frac{2}{r} - \frac{dU}{dr}\right)\frac{\partial}{\partial r}\right]W \qquad : W = W\left(t, r; a\right) \tag{3.2}$$

where U is the Coulomb potential energy measured in the units of kT (k is the Boltzmann constant and T is the temperature) and a is the reaction distance. In general, the last equation cannot be solved analytically but an approximation can be obtained when the potential U is weak. It becomes more convenient if it is written in a similar way to equation (2.19), where we use the so-called canonical representation of the infinitesimal operator, as follows[106,134]

$$\frac{\partial W}{\partial t} = LW \qquad : L = \frac{1}{2}\frac{\partial}{\partial M}\left(\frac{\partial}{\partial S}\right) \tag{3.3}$$

where S is the transformed distance scale and M is the speed measure and they are given as follows

$$S\left(r\right) = \int^{r} s\left(\varsigma\right) d\varsigma \qquad : s\left(r\right) = -r^2 e^{U\left(r\right)} \tag{3.4}$$

$$M\left(r\right) = \int^{r} m\left(\varsigma\right) d\varsigma \qquad : m\left(r\right) = \frac{1}{2D's\left(r\right)} \tag{3.5}$$

where m is called the speed density. The following Laplace transform of W

$$\tilde{W}\left(p, r; a\right) = \int_0^{\infty} W\left(t, r; a\right) e^{-pt}\, dt \tag{3.6}$$

was found to satisfy the following relationship[134,135]

$$\tilde{W}\left(p,r;a\right)=\frac{S\left(r\right)}{p\,S\left(a\right)}\,e^{-\Phi\left(p,r;a\right)} \tag{3.7}$$

where the function Φ satisfies the following

$$\Phi\left(0,r;a\right)=0\ ,\Phi\left(p,a;a\right)=0\ ,\ \partial\Phi=\phi\,\partial x \tag{3.8}.$$

The approximated solution to equation (3.3) (or the equivalent (3.2)) is obtained through making use of the function W^*, the reaction probability conditioned on the ultimate reaction, which satisfies its own backward diffusion equation and also has its own canonical representation of the infinitesimal operator (equations (3.4) and (3.5)).[134,136] This leads to a differential equation for Φ which is written as a power series in p, the Laplace transform variable. When the potential energy is small relative to kT, only the leading terms in the expansion need to be considered. Further analysis and applying the following radiation boundary condition (where the reaction happens with a finite rate on encounter)[134,137]

$$\left.\frac{\partial W}{\partial r}\right|_{r=a}=\frac{v}{D'}\left[1-W\left(t,r;a\right)\right] \tag{3.9}$$

where v is the reaction velocity, which is related to the observed rate constant k_{obs} as follows[18]

$$k_{\text{obs}}=\frac{4\pi D'a^2v}{v\,a+D'} \tag{3.10},$$

yields the following expression for the reaction probability[6,18,134]

$$W\left(t,r;a\right)\approx\frac{a}{r\left(1+\delta\right)}\left[\operatorname{erfc}\left(\alpha\right)-e^{\beta\left(2\alpha+\beta\right)}\operatorname{erfc}\left(\alpha+\beta\right)\right] \tag{3.11}$$

where

$$\alpha=\frac{r-a}{\sqrt{4D't}}\ \ ,\ \ \beta=\frac{\left(1+\delta^{-1}\right)}{a}\sqrt{D't}\ \ ,\ \ \delta=\frac{D'}{v\,a}e^{U\left(a\right)} \tag{3.12}.$$

It is important to invert equation (3.11) so that reaction times can be generated from it as it was done in equation (3.1). As is described in the literature, this is not simple and it will be discussed further in chapter 7.[138] Finally, there are no straightforward approximations when the potential cannot be considered small. As described in detail in the literature, the way to get around this problem is to seek a numerical solution to equation (3.2) and this will not be discussed here.[6,120,133]

3.2. Correlation effects

As discussed above, the IRT method applies the independent pairs approximation when generating the reaction times in systems of more than two reactive particles, but this imposes a number of questions. What does the backward diffusion equation look like for a system of more than two particles? And can this equation be actually solved, in order to obtain an expression for the reaction probability? In other words, what are the correlation effects due to the presence of more than two particles? Can these effects be somehow incorporated in the IRT simulation, and hence is there a way to improve the IRT method? Answering the above questions is technically very challenging.

In order to discuss this, we consider the case of three freely diffusing-identical-neutral particles with a diffusion coefficient of 0.5 $Å^2.ps^{-1}$. IRT simulations (along with RF simulations which was described in the last chapter) are first presented for the possible patterns of geometries that can be taken by the three particles. Following that, the formulation of the backward diffusion equation of the problem is presented along with some suggestions to relax the equation. Finally, further RF model simulations to investigate the correlations are presented.

Before we start the discussion outlined above, it should be noted that the subject of "diffusion of shapes"[139] (in our case, the three particles form either a straight line or, more importantly, a triangle, and as they diffuse a reaction may or may not occur) continued to attract attention over the years,[140] and related studies can be found in the literature.[141-143] In particular, the most relevant study to radiation chemistry is that of reference 144 (it is also referred to, in the literature, as the Clifford-Green theorem)[145] and the application of it will be summarized here. Briefly, the study considers the case of n points (or particles) in d dimensions. The coordinates for each point are sampled from a Gaussian distribution with mean 0 and variance σ^2. In this case we have $n(n-1)/2$ distances and if we denote the distance i as r_i, then the joint moment generating function of the squared distances r_i^2 is given as[144]

$$M_G(\omega) = E\left[e^{\sum_i r_i^2 \omega_i} \right] \tag{3.13}$$

where G is the undirected graph defined by the n points and the straight lines connecting them (the language is that of the graph theory in mathematics. The lines

connecting the points together form a graph and since these lines are not ordered (they do not carry arrows etc.), then the graph is undirected. More details on this can be found elsewhere).[146,147] The sum in the last equation is over all the possible distances in the graph G. ω_i is the variable associated with r_i^2, and ω is "the collection" of ω_i. The study then uses the following convention

$$\sum_{i\in\phi} = 0 \quad , \quad \prod_{i\in\phi} = 1 \tag{3.14}$$

where ϕ is the empty group, and proves that[144]

$$M_G(\omega) = \left[\sum_{g\in G} (-1)^{\#g} C_g \prod_{i\in g} 2\sigma^2 \omega_i \right]^{-d/2} \tag{3.15}$$

where g is a subgraph of G (again this is from the graph theory where the subgraph g is obtained from the original graph G through eliminating point(s) and (or) line(s)) and where the sum extends over all the possible subgraphs. #g refers to the cardinality of g (the number of distances in the graph g (also called the size of the graph g)[146]). The coefficient C_g is given as follows

$$C_g = \begin{cases} 1 & \text{if } g = \phi \\ C_{g_1} C_{g_2} & \text{if } g = g_1 \cup g_2 \quad \& \quad g_1 \cap g_2 = \phi \\ 0 & \text{if } g \text{ is a cycle} \\ \psi(g) & \text{if } g \text{ is a tree} \end{cases} \tag{3.16}$$

where g_1 and g_2 are subgraphs of g and $\psi(g)$ is the vertex degree of the graph g. The application of the above theorem to the case of three particles forming a triangle in three dimensions is straightforward and gives some interesting results. The subgraphs that we need to consider are the empty group (#g = 0), the triangle itself (a cycle graph with #g = 3), each one of the three distances (i.e. we remove a point with the two connecting distances and the resulting subgraph in each case is a tree. Hence in each case we have #g = 1 and C_g = 2) and finally the subgraphs formed when we remove just one distance (this gives three subgraphs and in each one we have #g = 2 and C_g = 3). Hence the moment generating function is

$$M_G(\omega) = \Big[1 - 4\sigma^2(\omega_1 + \omega_2 + \omega_3) + 12\sigma^2(\omega_1\omega_2 + \omega_1\omega_3 + \omega_2\omega_3) \Big]^{-3/2} \tag{3.17}$$

where ω_i is the variable associated with r_i^2. Now we can use the properties of the moment generating function to calculate the mean (the first moment) of the squared distances as follows

$$E\left(r_i^2\right) = \lim_{\omega \to 0} \frac{\partial M_G}{\partial \omega_i} = 6\sigma^2 \tag{3.18}.$$

The second moment is

$$E\left[\left(r_i^2\right)^2\right] = \lim_{\omega \to 0} \frac{\partial^2 M_G}{\partial \omega_i^2} = 60\sigma^4 \tag{3.19}.$$

Therefore, the variance of the squared distances is $24\sigma^4$. In order to calculate the covariance of two squared distances r_i^2 and r_j^2 we need the following

$$E\left(r_i^2 r_j^2\right) = \lim_{\omega \to 0} \frac{\partial^2 M_G}{\partial \omega_i \partial \omega_j} = 42\sigma^4 \tag{3.20}.$$

Hence, the covariance is $6\sigma^4$ resulting in a correlation coefficient of (1/4). It is also interesting to obtain the following triple moment

$$E\left(r_1^2 r_2^2 r_3^2\right) = \lim_{\omega \to 0} \frac{\partial^3 M_G}{\partial \omega_1 \partial \omega_2 \partial \omega_3} = 300\sigma^6 \tag{3.21}.$$

We can define the "triple" covariance as follows

$$T_{\text{cov}} = E\left[\left(r_1^2 - E\left(r_1^2\right)\right)\left(r_2^2 - E\left(r_2^2\right)\right)\left(r_3^2 - E\left(r_3^2\right)\right)\right] \tag{3.22}.$$

Using the results above we have $T_{\text{cov}} = -24\sigma^6$ and a "triple" correlation coefficient of $\left(-1/\sqrt{24}\right)$ which is clearly a result of the constraint that the three distances must form a triangle. The final point to make is that the above study also gives *f*, the joint probability density function of the squared distances, which for a three particles is as follows[144]

$$f\left(\rho_1, \rho_2, \rho_3\right) = C\, e^{-\left(\rho_1 + \rho_2 + \rho_3\right)/6\sigma^2} \tag{3.23}$$

where

$$C = \frac{1}{3^{3/2}\,\Gamma\left(3/2\right)\left(4\pi^{1/4}\,\sigma^3\right)^2} \tag{3.24}$$

where Γ is the gamma function (equation (1.69)). All initial configurations will approach this random Gaussian limit as time proceeds.

Now we will proceed with the discussion as was described at the beginning of this section.

3.2.1. Simulations

In all of the following simulations, the encounter distance (or the reaction distance) is considered to be $a = 5$ Å. Also the function P represents the probability that a reaction has taken place by time t. The number of realization is 10^5. The time step is chosen to be a constant of 1 ps used with the Bessel bridge (equation (2.40)).

The simulations for three particles whose initial coordinates are generated independently from a random distribution (spherical Gaussian with mean zero and a standard deviation of $2a$) are shown in Figure 3.1.

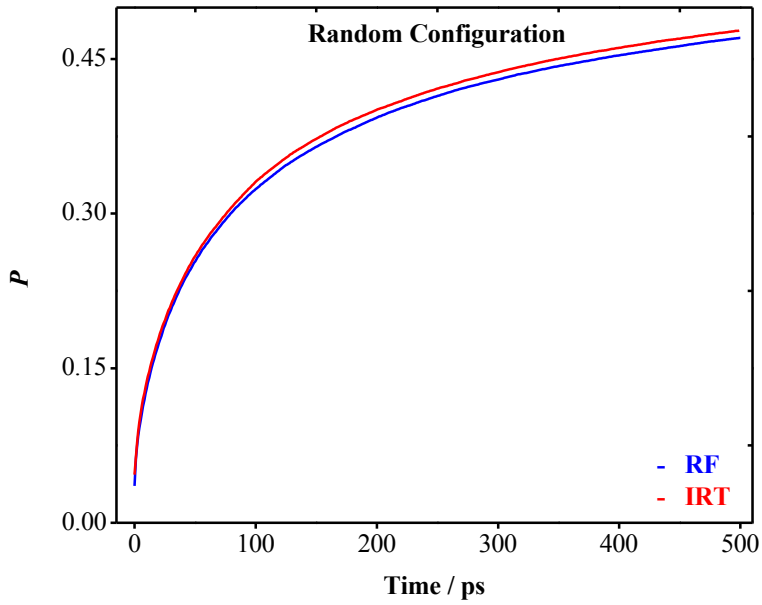


Figure 3.1. The Probability that a reaction has happened for three particles whose initial coordinates are randomly generated from a Gaussian distribution. The values at 500 ps are 0.478(±0.003) for the IRT and 0.471(±0.003) for the RF.

Similarly in Figure 3.2, we have the simulations for the case of three particles initially fixed on a straight line of length $20\sqrt{3}$ Å where two particles are located on the two ends and one is in the centre. It should be noted that the above length in this

set of simulations (and similarly the lengths used in the simulations that follow) was chosen in such a way that the inter-particle distance between the central particle and an outer one is comparable with the mean inter-particle distance in the random distribution above.

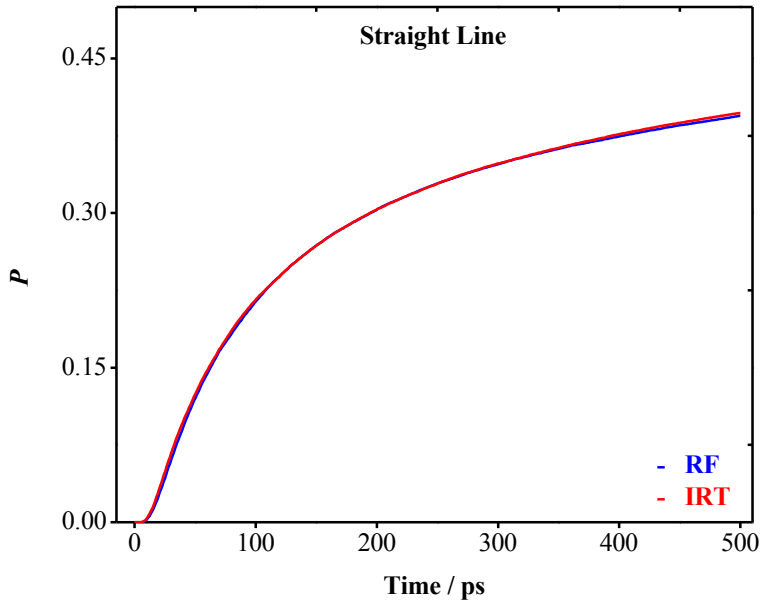


Figure 3.2. The Probability that a reaction has happened for three particles initially on a straight line. The values at 500 ps are 0.397(±0.003) for the IRT and 0.395(±0.003) for the RF.

The simulations when the particles are located initially on an equilateral triangle, where the length of its edge is $10\sqrt{2}$ Å, are shown in Figure 3.3. In Figure 3.4 the particles initially form an isosceles triangle where the length of the symmetrical sides is $10\sqrt{3}$ Å and the length of the different side is $20\sqrt{2}$ Å. When the particles form initially a right triangle whose edges are 10, $10\sqrt{2}$ and $10\sqrt{3}$ Å, the results are shown in Figure 3.5. The simulations also monitor the function *W*, the probability of encounter (or reaction) of a certain pair. For example, in the isosceles triangle case, the probability of encounter for the pair initially forming the different side of the triangle is shown in Figure 3.6; also for a pair forming one of the equal sides, the function *W* is shown in Figure 3.7.

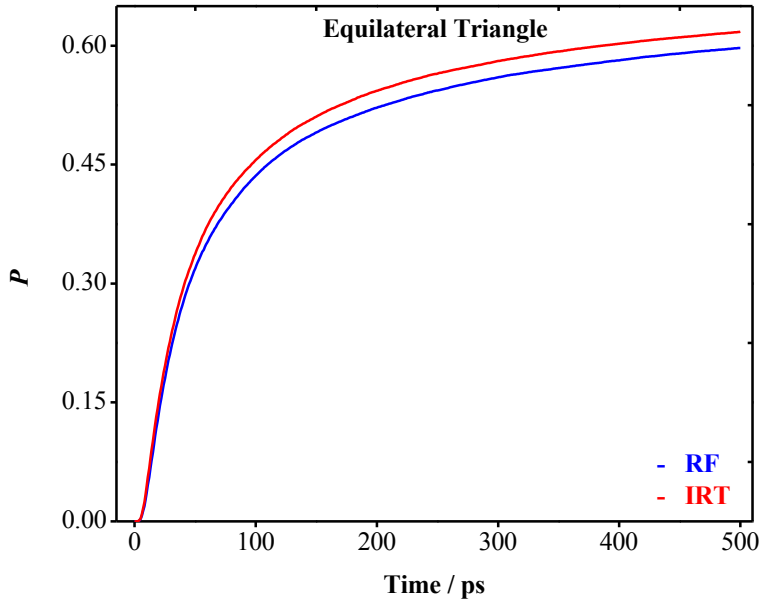


Figure 3.3. The Probability that a reaction has happened for three particles initially on an equilateral triangle. The values at 500 ps are 0.618(±0.003) for the IRT and 0.597(±0.003) for the RF.

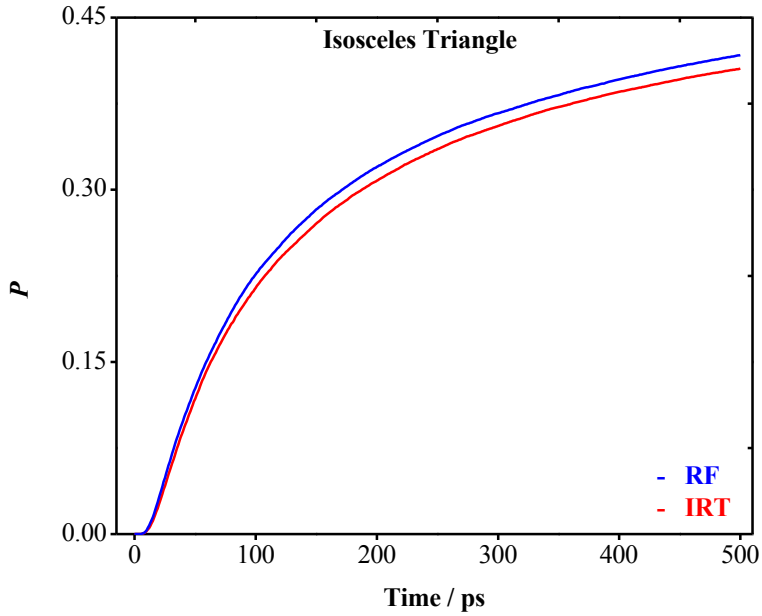


Figure 3.4. The Probability that a reaction has happened for three particles initially on an isosceles triangle. The values at 500 ps are 0.417(±0.003) for the IRT and 0.405(±0.003) for the RF.

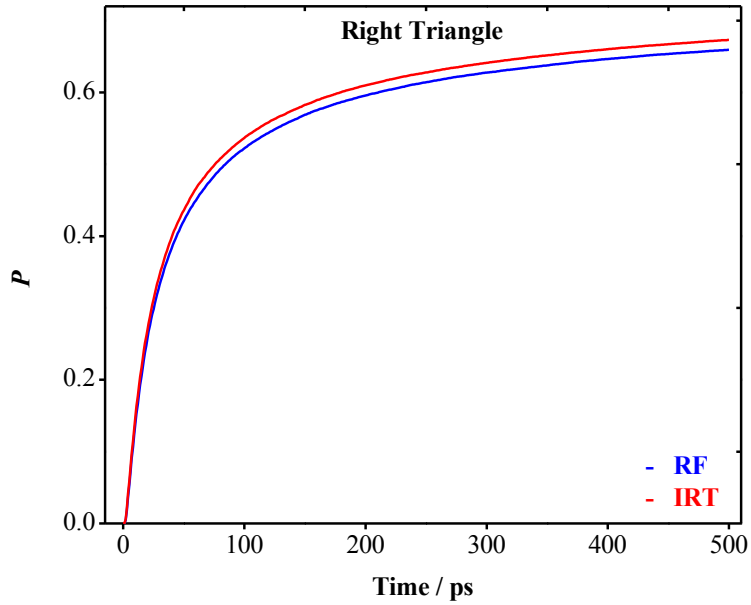


Figure 3.5. The Probability that a reaction has happened for three particles initially on a right triangle. The values at 500 ps are 0.673(±0.003) for the IRT and 0.659(±0.003) for the RF.

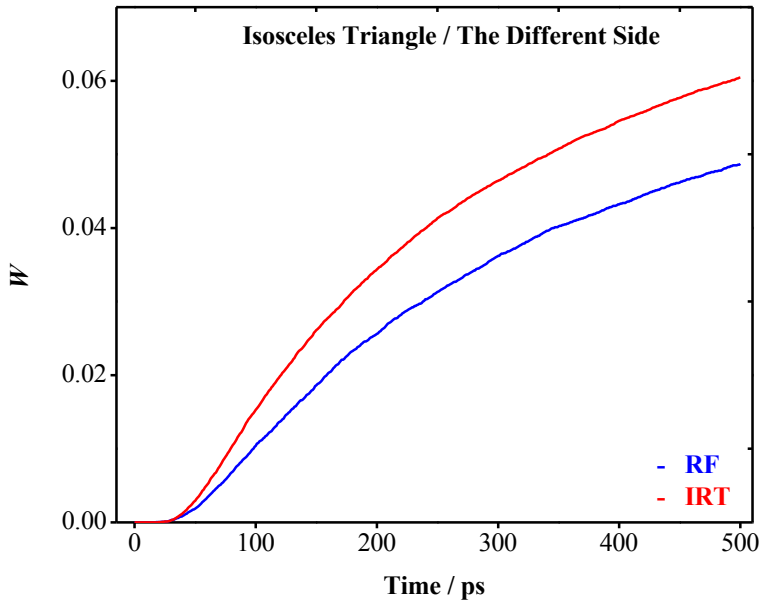


Figure 3.6. The Probability of reaction for a certain pair. The pair forms the different side of an isosceles triangle at the start. The values at 500 ps are 0.06(±0.002) for the IRT and 0.049(±0.002) for the RF.

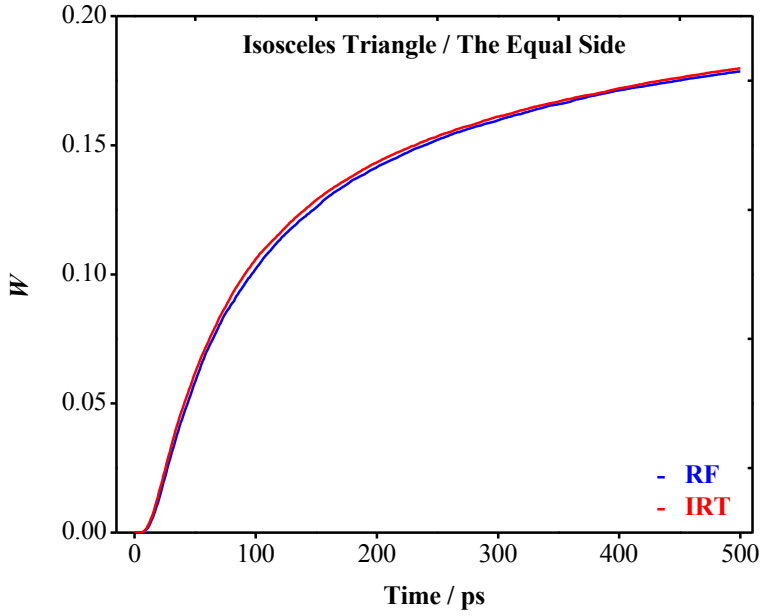


Figure 3.7. The Probability of reaction for a certain pair. The pair forms one of the equal sides of an isosceles triangle at the start. The values at 500 ps are 0.179(±0.003) for the IRT and 0.178(±0.003) for the RF.

The above simulations indicate that the discrepancy between the IRT method and the RF model is generally small specially when starting from a random configuration (Figure 3.1) and surprisingly for the case of three particles on a straight line (Figure 3.2). This agreement can be explained as follows: In the case of a straight line (Figure 3.2), the probability that a reaction has taken place by 500 ps is 0.395(±0.003) in the RF simulations and it is a sum of three reaction probabilities 0.186, 0.184 and 0.025 (one for each pair). Similarly, the probability that a reaction has taken place by 500 ps is 0.397(±0.003) in the IRT simulations and it is a sum of three reaction probabilities 0.179, 0.182 and 0.036 (one for each pair). Hence, although the overall reaction probability is well described by the IRT approximation (0.397 and 0.395), it is a result of cancelling discrepancies, as can be seen by distinguishing the individual reacting pairs.

Furthermore, the discrepancy is relatively large when the particles initially form a triangle, particularly the equilateral triangle case (Figure 3.3). Finally, it should be noted that, in all the cases, the discrepancy is in one direction; the IRT method overestimates the probability that a reaction has taken place relative to the RF model. This is a consequence of the independence approximation of the IRT method.

3.2.2. The backward diffusion equation

The backward diffusion equation, that has been referred to in the current chapter and also in the last chapter, is the special case for the relative diffusion of two particles. A more general form of the backward diffusion equation is needed when considering the diffusion motions in a system of more than two particles. This can be easily obtained by modifying the operator L given in equation (2.20) to have the following form[114]

$$L = \sum_{i=1}^{n} \mu\left(r_i\right) \frac{\partial}{\partial r_i} + \frac{1}{2} \sum_{i=1}^{n} \sum_{j=1}^{n} \sigma^2\left(r_i, r_j\right) \frac{\partial^2}{\partial r_i \partial r_j} \tag{3.25}$$

where n is the number of diffusing distances in the system. It should be noted that equation (2.13) has been taken into account when writing the last equation. We can write L in a more useful form as follows

$$L = \sum_{i=1}^{n} \left[\mu\left(r_i\right) \frac{\partial}{\partial r_i} + \frac{1}{2} \sigma^2\left(r_i\right) \frac{\partial^2}{\partial r_i^2} + \frac{1}{2} \sum_{j=1, j \neq i}^{n} \sigma^2\left(r_i, r_j\right) \frac{\partial^2}{\partial r_i \partial r_j} \right] \tag{3.26}$$

where $\mu\left(r_i\right)$ and $\sigma^2\left(r_i\right)$ are the infinitesimal mean and infinitesimal variance of the diffusing distance r_i and were defined in the last chapter (equations (2.11) and (2.12)). In the last equation, $\sigma^2\left(r_i, r_j\right)$, which will be discussed in more detail shortly, is the infinitesimal covariance of the diffusing distances r_i and r_j. The next step is to write L more specifically for the case of three particles. To avoid any confusion, the particles are labelled 1, 2 and 3 and hence their separation distances are r_{12}, r_{13} and r_{23}. The last equation then becomes

$$L^{(3)} = L_{12} + L_{13} + L_{23} + L_p \tag{3.27}$$

where

$$L_{ij} = \mu\left(r_{ij}\right) \frac{\partial}{\partial r_{ij}} + \frac{1}{2} \sigma^2\left(r_{ij}\right) \frac{\partial^2}{\partial r_{ij}^2} \tag{3.28}$$

and

$$\begin{aligned} L_p = & \frac{1}{2} \sigma^2\left(r_{12}, r_{13}\right) \frac{\partial^2}{\partial r_{12} \partial r_{13}} + \frac{1}{2} \sigma^2\left(r_{12}, r_{23}\right) \frac{\partial^2}{\partial r_{12} \partial r_{23}} \\ & + \frac{1}{2} \sigma^2\left(r_{13}, r_{23}\right) \frac{\partial^2}{\partial r_{13} \partial r_{23}} \end{aligned} \tag{3.29}.$$

The next step is to obtain the explicit expressions for the infinitesimal mean and variance of a diffusing distance and also for the infinitesimal covariance of two diffusing distances.

3.2.2.1. The infinitesimal mean

Firstly, the expression for the infinitesimal mean (and also the infinitesimal variance) can be easily obtained by comparing equation (2.41) with equation (2.19) (after replacing x with r). However, its stochastic derivation will be presented here and it is based on equations (2.11) and (2.12).[106,148] Let r_{ij} be the distance separating the two diffusing particles i and j at time t (it is any of the distances r_{12}, r_{13} and r_{23}). r_{ij} is the length of the vector $\mathbf{r}_{ij}$ given as

$$\mathbf{r}_{ij}(t) = \left(X_{ij}(t), Y_{ij}(t), Z_{ij}(t)\right) \tag{3.30}$$

where X_{ij}, Y_{ij} and Z_{ij} are independent Brownian motions along the x, y and z axes respectively and

$$U_{ij}(t) = U_j(t) - U_i(t) \tag{3.31}$$

where U_{ij} is X_{ij}, Y_{ij} or Z_{ij}. Since they are Brownian motions, their infinitesimal mean and variance are given as follows[106]

$$\mu_{U_{ij}} = \lim_{\delta t \downarrow 0} \frac{1}{\delta t} E\left[\left\{\left|\delta U_{ij}(t)\right|\right\} \middle| U_{ij}(t)\right] = 0 \tag{3.32}$$

$$\sigma^2_{U_{ij}} = \lim_{\delta t \downarrow 0} \frac{1}{\delta t} E\left[\left\{\left|\delta U_{ij}(t)\right|^2\right\} \middle| U_{ij}(t)\right] = 2\left(D_i + D_j\right) = 2D_{ij} \tag{3.33}$$

where D_l is the diffusion coefficient of the particle l, D_{ij} is the relative diffusion coefficient of the particles i and j, δt is an infinitesimal time increment, U_{ij} is again X_{ij}, Y_{ij} or Z_{ij} and

$$\delta U_{ij}(t) = U_{ij}(t + \delta t) - U_{ij}(t) \tag{3.34}.$$

The vector $\mathbf{r}$ changes infinitesimally during the time increment δt and becomes $\mathbf{r}+\delta\mathbf{r}$ where

$$\delta\mathbf{r}_{ij}(t) = \left(\delta X_{ij}(t), \delta Y_{ij}(t), \delta Z_{ij}(t)\right) \tag{3.35}.$$

Hence, the wanted expression for the infinitesimal mean μ is (equations (2.11) and (2.12))

$$\mu\left(r_{ij}\right)\delta t = E\left[\delta r_{ij} \,\middle|\, r_{ij}\right] = E\left[\left\{\left|\mathbf{r}_{ij} + \delta\mathbf{r}_{ij}\right| - r_{ij}\right\} \middle| r_{ij}\right] \tag{3.36}$$

and then

$$\mu\left(r_{ij}\right)\delta t = r_{ij}\, E\left[\left\{\sqrt{1 + \frac{2\mathbf{r}_{ij}\,.\,\delta\mathbf{r}_{ij}}{r_{ij}^2} + \frac{\delta\mathbf{r}_{ij}\,.\,\delta\mathbf{r}_{ij}}{r_{ij}^2}} - 1\right\} \middle| r_{ij}\right] \tag{3.37}$$

where the following property of the conditional expectation was used[4]

$$E\left[r_{ij} \,\middle|\, r_{ij}\right] = r_{ij} \tag{3.38}.$$

Expanding the square root as a series yields

$$\mu\left(r_{ij}\right)\delta t = r_{ij}\, E\left[\frac{\mathbf{r}_{ij}\,.\,\delta\mathbf{r}_{ij}}{r_{ij}^2} + \frac{1}{2}\frac{\delta\mathbf{r}_{ij}\,.\,\delta\mathbf{r}_{ij}}{r_{ij}^2} - \frac{1}{8}\left(\frac{2\mathbf{r}_{ij}\,.\,\delta\mathbf{r}_{ij}}{r_{ij}^2} + \frac{\delta\mathbf{r}_{ij}\,.\,\delta\mathbf{r}_{ij}}{r_{ij}^2}\right)^2 + O\left[\left(\delta\mathbf{r}_{ij}\right)^3\right]\right] \tag{3.39}$$

where we have dropped the indicator of conditional expectation (| r_{ij}) for convenience and O is a polynomial function of leading order $(\delta\mathbf{r}_{ij})^3$. The terms containing δr_{ij} of order 3 and higher have zero expectation (equation (2.11) and (2.12)) and so do the first-order terms because of (3.32). Hence

$$\mu\left(r_{ij}\right)\delta t = \frac{r_{ij}}{2} E\left[\frac{\delta\mathbf{r}_{ij}\,.\,\delta\mathbf{r}_{ij}}{r_{ij}^2} - \left(\frac{\mathbf{r}_{ij}\,.\,\delta\mathbf{r}_{ij}}{r_{ij}^2}\right)^2\right] \tag{3.40}.$$

Finally, if we use equations (3.30), (3.35), (3.32) and (3.33) and bearing in mind the property used in the last step we have

$$\mu\left(r_{ij}\right)\delta t = \frac{r_{ij}}{2}\left[\frac{3\times 2D_{ij}\delta t}{r_{ij}^2} - \frac{2D_{ij}\delta t}{r_{ij}^2}\right] = \frac{2D_{ij}\delta t}{r_{ij}} \tag{3.41}.$$

Hence, for equation (3.28) we have

$$\mu\left(r_{ij}\right) = \frac{2D_{ij}}{r_{ij}} \tag{3.42}.$$

3.2.2.2. The infinitesimal variance

The derivation for the infinitesimal variance proceeds similarly and will be briefly presented here. If we use the same notations above, we have

$$\sigma^2\left(r_{ij}\right)\delta t = E\left[\left(\delta r_{ij}\right)^2 \middle| r_{ij}\right] = E\left[\left(\left|\mathbf{r}_{ij}+\delta\mathbf{r}_{ij}\right|-r_{ij}\right)^2 \middle| r_{ij}\right] \tag{3.43}.$$

As before, we expand the square root as a power series and use equation (3.38)

$$\sigma^2\left(r_{ij}\right)\delta t = r_{ij}^2 E\left[\left(\frac{\mathbf{r}_{ij}\,.\,\delta\mathbf{r}_{ij}}{r_{ij}^2}+O\left[\left(\delta\mathbf{r}_{ij}\right)^2\right]\right)^2\right] \tag{3.44}$$

where we have also dropped the indicator (| r_{ij}) for convenience, and now we have

$$\sigma^2\left(r_{ij}\right)\delta t = r_{ij}^2 E\left[\left(\frac{\mathbf{r}_{ij}\,.\,\delta\mathbf{r}_{\mathbf{ij}}}{r_{ij}^2}\right)^2+O\left[\left(\delta\mathbf{r}_{ij}\right)^3\right]\right] \tag{3.45}.$$

Because the terms of order 3 and higher (as before) have expectation zero, we write

$$\sigma^2\left(r_{ij}\right)\delta t = r_{ij}^2 E\left[\left(\frac{\mathbf{r}_{ij}\,.\,\delta\mathbf{r}_{ij}}{r_{ij}^2}\right)^2\right] \tag{3.46}.$$

Finally, if we use equations (3.30), (3.35), (3.32) and (3.33), we have

$$\sigma^2\left(r_{ij}\right) = 2D_{ij} \tag{3.47}.$$

3.2.2.3. The infinitesimal covariance

Deriving the expression for the infinitesimal covariance of two distances r_{ij} and r_{jk} proceeds in the same way and again the same notations used above will be used here. We start from the following definition for the covariance

$$\sigma^2\left(r_{ij}, r_{jk}\right)\delta t = E\left[\left\{\left(\left|\mathbf{r}_{ij}+\delta\mathbf{r}_{ij}\right|-r_{ij}\right)\left(\left|\mathbf{r}_{jk}+\delta\mathbf{r}_{jk}\right|-r_{jk}\right)\right\} \middle| r_{ij}, r_{jk}\right] \tag{3.48}.$$

We will drop the conditional expectation indicator (| r_{ij}, r_{jk}), use equation (3.38) and expand the square root as before to obtain the following

$$\sigma^2\left(r_{ij}, r_{jk}\right)\delta t = r_{ij}\,r_{jk}E\left[\left(\frac{\mathbf{r}_{ij}\,.\,\delta\mathbf{r}_{ij}}{r_{ij}^2}+O\left[\left(\delta\mathbf{r}_{ij}\right)^2\right]\right)\left(\frac{\mathbf{r}_{jk}\,.\,\delta\mathbf{r}_{jk}}{r_{jk}^2}+O\left[\left(\delta\mathbf{r}_{jk}\right)^2\right]\right)\right] \tag{3.49}.$$

If we keep only the terms that have non-zero expectation, we have

$$\sigma^2\left(r_{ij}, r_{jk}\right)\delta t = r_{ij}\, r_{jk} E\left[\frac{\mathbf{r}_{ij}.\,\delta\mathbf{r}_{ij}}{r_{ij}^2}\,\frac{\mathbf{r}_{jk}.\,\delta\mathbf{r}_{jk}}{r_{jk}^2}\right] \tag{3.50}.$$

Evaluating the last expression and realizing that the only terms that will contribute to the expectation are the terms containing $(\delta U_j)^2$ where U_j is X_j, Y_j or Z_j and (this is similar to equation (3.33))

$$\sigma_{U_j}^2\,\delta t = E\left[\left|\delta U_j\left(t\right)\right|^2\right] = 2D_j\delta t \tag{3.51}$$

we have

$$\sigma^2\left(r_{ij}, r_{jk}\right)\delta t = \frac{\mathbf{r}_{ij}.\,\mathbf{r}_{jk}}{r_{ij}\, r_{jk}}\,2D_j\delta t \tag{3.52}$$

or

$$\sigma^2\left(r_{ij}, r_{jk}\right) = 2D_j\cos\left(\mathbf{r}_{ij}, \hat{\mathbf{r}}_{jk}\right) \tag{3.53}.$$

It should be noted that the diffusion coefficient in the last equation is that of the particle in common between the two distances and not the relative diffusion coefficient. Thus, if the particle in common between the two distances is stationary, then the two distances evolve independently because the particles are assumed to diffuse independently. It is also worth noting in passing that in a larger system with more than three particles, disjoint distances with no particle in common are independent, the proof of this follows exactly the same method.

3.2.2.4. Possible approximations

Now that we have the expressions for the infinitesimal mean and variance (equations (3.42) and (3.47)), we can write equation (3.28) as follows

$$L_{ij} = \frac{2D_{ij}}{r_{ij}}\frac{\partial}{\partial r_{ij}} + D_{ij}\frac{\partial^2}{\partial r_{ij}^2} \tag{3.54}$$

or

$$L_{ij} = \frac{D_{ij}}{r_{ij}}\frac{\partial^2}{\partial r_{ij}^2}\left(r_{ij}\right) = \frac{D'}{r_{ij}}\frac{\partial^2}{\partial r_{ij}^2}\left(r_{ij}\right) \tag{3.55}$$

where we have made use of the fact that we are looking at the case when the particles are identical and have the same diffusion coefficient. Similarly if we use equation (3.53) in equation (3.29) we have the following

$$L_p = 2D_1 \cos\left(\hat{\mathbf{r}}_{12}, \hat{\mathbf{r}}_{13}\right) \frac{\partial^2}{\partial r_{12}\partial r_{13}} + 2D_2 \cos\left(\hat{\mathbf{r}}_{12}, \hat{\mathbf{r}}_{23}\right) \frac{\partial^2}{\partial r_{12}\partial r_{23}} + 2D_3 \cos\left(\hat{\mathbf{r}}_{13}, \hat{\mathbf{r}}_{23}\right) \frac{\partial^2}{\partial r_{13}\partial r_{23}} \tag{3.56}$$

Since the particles are identical, we have

$$L_p = D'\left[\cos\left(\hat{\mathbf{r}}_{12}, \hat{\mathbf{r}}_{13}\right) \frac{\partial^2}{\partial r_{12}\partial r_{13}} + \cos\left(\hat{\mathbf{r}}_{12}, \hat{\mathbf{r}}_{23}\right) \frac{\partial^2}{\partial r_{12}\partial r_{23}} + \cos\left(\hat{\mathbf{r}}_{13}, \hat{\mathbf{r}}_{23}\right) \frac{\partial^2}{\partial r_{13}\partial r_{23}}\right] \tag{3.57}$$

The backward diffusion equation for three identical particles is (using equation (3.27) and (2.19))

$$\frac{\partial P}{\partial t} = L^{(3)} P \qquad : P = P\left(t, r_{ij}; a\right) \tag{3.58}$$

where P is the probability that a reaction has taken place by time t and a is the reaction (or encounter) distance of two particles.

The first point to make about the last equation is that there is, unfortunately, no analytic solution for it, at least when the diffusing particles can react. Clearly, the separation of variables method is not viable because the covariance terms mix the variable. The second point to make is that the IRT approximation ignores the L_p part of $L^{(3)}$, in some ways similar to the orbital approximation in electronic structure. We will be looking next at possible approximations to relax the above problem. It should be noted though that the joint probability density function for the squared distances is known (equation (3.23)).[144]

3.2.2.4.1. Perturbation

It is possible to consider a simpler version of the last equation. This is at very large times ($t \to \infty$ the steady state limit) when the probability function P is no longer time-dependent (the simulations shown in part 3.2.1). In this case, the left hand side of the last equation vanishes and so we have

$$L^{(3)}P = 0 \qquad : \; P = P_{\infty}\left(r_{ij}\,; a\right) \tag{3.59}.$$

It is convenient in this case to write the last equation in terms of the survival probability Ω, the probability that no encounter or reaction ever happens, where[6]

$$\Omega = 1 - P \tag{3.60}$$

and so

$$L^{(3)}\Omega = 0 \qquad : \; \Omega = \Omega_{\infty}\left(r_{ij}\,; a\right) \tag{3.61}.$$

As was discussed before, for the two particles case the reaction probability is given in equation (2.43) and because of the properties of erfc function, we have

$$W_{\infty}\left(r; a\right) = \lim_{t\uparrow\infty} W\left(t, r; a\right) = \frac{a}{r} \tag{3.62}.$$

The survival probability for the pair is given as follows

$$\Omega_{\text{pair}}\left(t, r; a\right) = 1 - W\left(t, r; a\right) \tag{3.63}.$$

At very large times we have

$$\Omega_{\infty,\text{pair}} = 1 - \frac{a}{r} \tag{3.64}.$$

Within the IRT approximation, the survival probability for the case of three particles is simply given as follows

$$\Omega_{\text{IRT}} = \left(1 - \frac{a}{r_{12}}\right)\left(1 - \frac{a}{r_{13}}\right)\left(1 - \frac{a}{r_{23}}\right) \tag{3.65}$$

where this equation is written for $t \to \infty$.

Since the difference between the RF model and the IRT method in the simulations shown in Figures 3.1-3.5 is generally small, the problem of finding the survival probability function Ω in equation (3.61) is hoped to be reduced to a perturbation problem where the perturbation is simply the L_p part of $L^{(3)}$. To discuss this, we write the $L^{(3)}$ operator as follows

$$L^{(3)} = L_{12} + L_{13} + L_{23} + \lambda L_p = L_0 + \lambda L_p \tag{3.66}$$

where λ is the parameter normally used in perturbation theories (it is set to the value of one at the end) and

$$L_0 = L_{12} + L_{13} + L_{23} \tag{3.67}.$$

We also write Ω as follows

$$\Omega = \Omega_{\mathrm{IRT}} + \lambda \Omega_p \tag{3.68}$$

where Ω_p is the perturbation part in Ω. Now if we use equation (3.61), we have

$$\left(L_0 + \lambda L_p\right)\left(\Omega_{\mathrm{IRT}} + \lambda \Omega_p\right) = 0 \tag{3.69},$$

and hence

$$L_0\Omega_{\mathrm{IRT}} + \lambda\left(L_0\Omega_p + L_p\Omega_{\mathrm{IRT}}\right) + \lambda^2 L_p\Omega_p = 0 \tag{3.70}.$$

If we consider the first order perturbation only, then the problem reduces to the following equation

$$L_0\Omega_p + L_p\Omega_{\mathrm{IRT}} = 0 \tag{3.71},$$

or more specifically

$$\begin{aligned}\frac{1}{r_{12}}\frac{\partial^2}{\partial r_{12}^2}\left(r_{12}\Omega_p\right) + \frac{1}{r_{13}}\frac{\partial^2}{\partial r_{13}^2}\left(r_{13}\Omega_p\right) + \frac{1}{r_{23}}\frac{\partial^2}{\partial r_{23}^2}\left(r_{23}\Omega_p\right) + \cos\theta_1\frac{\partial^2\Omega_{\mathrm{IRT}}}{\partial r_{12}\partial r_{13}} \\ + \cos\theta_2\frac{\partial^2\Omega_{\mathrm{IRT}}}{\partial r_{12}\partial r_{23}} + \cos\theta_3\frac{\partial^2\Omega_{\mathrm{IRT}}}{\partial r_{13}\partial r_{23}} = 0\end{aligned} \tag{3.72}$$

where we have used the expressions for L_0 and L_p and used the following notations (Figure 3.8)

$$\cos\left(\hat{\mathbf{r}_{ij}, \mathbf{r}_{ik}}\right) = \cos\theta_i \tag{3.73}.$$

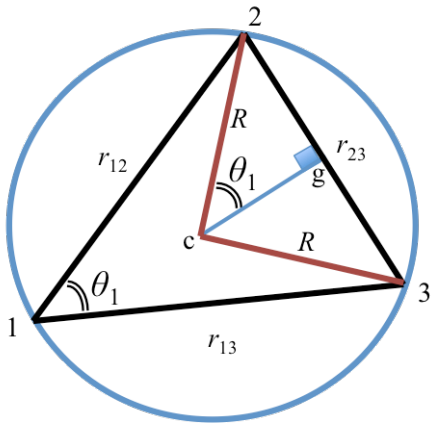


Figure 3.8. The geometry of the problem. R is the radius of the circle containing the triangle formed by the particles. The angle 213 (θ_1) is equal to half of the angle 2c3 because the first is an inscribed angle and the second is a central angle and they both share the same arc (23). The triangle 2c3 is isosceles because both of the length c-2 and c-3 are equal to R, the radius. Hence cg is a median, altitude and bisector at the same time and so the angle gc2 equals θ_1.

If we use equation (3.65) in equation (3.72), we have the following

$$\frac{1}{r_{12}}\frac{\partial^2}{\partial r_{12}^2}\left(r_{12}\,\Omega_p\right)+\frac{1}{r_{13}}\frac{\partial^2}{\partial r_{13}^2}\left(r_{13}\,\Omega_p\right)+\frac{1}{r_{23}}\frac{\partial^2}{\partial r_{23}^2}\left(r_{23}\,\Omega_p\right)= \\ -\frac{a^2}{r_{12}^2 r_{13}^2}\left(1-\frac{a}{r_{23}}\right)\cos\theta_1-\frac{a^2}{r_{12}^2 r_{23}^2}\left(1-\frac{a}{r_{13}}\right)\cos\theta_2-\frac{a^2}{r_{13}^2 r_{23}^2}\left(1-\frac{a}{r_{12}}\right)\cos\theta_3 \tag{3.74}.$$

Because of the "symmetrical" nature of the last equation (in each term on the right hand side two of the three distances appear similarly and the third is different, and on the left hand side each term contains the second derivative with regard to one of the distances), we might connect each term on the left hand side with a term on its right hand side and get the following three equations

$$\frac{1}{r_{12}}\frac{\partial^2}{\partial r_{12}^2}\left(r_{12}\,\Omega_p\right)=-\frac{a^2}{r_{13}^2 r_{23}^2}\left(1-\frac{a}{r_{12}}\right)\cos\theta_3+\varsigma \tag{3.75}$$

$$\frac{1}{r_{13}}\frac{\partial^2}{\partial r_{13}^2}\left(r_{13}\,\Omega_p\right)=-\frac{a^2}{r_{12}^2 r_{23}^2}\left(1-\frac{a}{r_{13}}\right)\cos\theta_2+\tau \tag{3.76}$$

$$\frac{1}{r_{23}}\frac{\partial^2}{\partial r_{23}^2}\left(r_{23}\,\Omega_p\right)=-\frac{a^2}{r_{12}^2 r_{13}^2}\left(1-\frac{a}{r_{23}}\right)\cos\theta_1+\upsilon \tag{3.77}$$

where the added coefficients ς, τ and υ satisfy the following

$$\varsigma+\tau+\upsilon=0 \tag{3.78}$$

so that when we sum the three equations (3.75)-(3.77) we get equation (3.74). It is important at this stage to introduce the following boundary condition that the survival probability Ω has to satisfy

$$r_{12}, r_{23} \text{ and } r_{13}\to\infty \;\Rightarrow\; \Omega\to 1 \tag{3.79},$$

i.e. when the particles are very far apart, their reaction probability becomes infinitely small. Now because of equation (3.65) we have

$$r_{12}, r_{23} \text{ and } r_{13}\to\infty \;\Rightarrow\; \Omega_{\mathrm{IRT}}\to 1 \tag{3.80}$$

which consequently requires that (equation (3.68))

$$r_{12}, r_{23} \text{ and } r_{13}\to\infty \;\Rightarrow\; \Omega_p\to 0 \tag{3.81}.$$

If we look at equations (3.75)-(3.77), it is straightforward to show that the separation coefficients ς, τ and υ are going to respectively lead to terms of r_{12}^2, r_{13}^2 and r_{23}^2 after evaluating the integrals. These terms respectively tend to infinity as the distances r_{12},

r_{13} and r_{23} tend to infinity. Hence because of the boundary condition of the last equation we have

$$\varsigma = \tau = \upsilon = 0 \tag{3.82}$$

and hence

$$\frac{1}{r_{12}}\frac{\partial^2}{\partial r_{12}^2}\left(r_{12}\,\Omega_p\right) = -\frac{a^2}{r_{13}^2 r_{23}^2}\left(1-\frac{a}{r_{12}}\right)\cos\theta_3 \tag{3.83}$$

$$\frac{1}{r_{13}}\frac{\partial^2}{\partial r_{13}^2}\left(r_{13}\,\Omega_p\right) = -\frac{a^2}{r_{12}^2 r_{23}^2}\left(1-\frac{a}{r_{13}}\right)\cos\theta_2 \tag{3.84}$$

$$\frac{1}{r_{23}}\frac{\partial^2}{\partial r_{23}^2}\left(r_{23}\,\Omega_p\right) = -\frac{a^2}{r_{12}^2 r_{13}^2}\left(1-\frac{a}{r_{23}}\right)\cos\theta_1 \tag{3.85}.$$

The last three equations cannot be integrated in general. This is because of the product $r_{13}r_{23}$ on the right hand side of the first one (for example) and also because of $\cos\theta_3$. One way around this might be to consider again Figure 3.8 and write A, the area of the triangle formed by the particles, in the following form

$$A = \frac{1}{2}r_{12}r_{13}\sin\theta_1 = \frac{1}{2}r_{12}r_{13}\frac{r_{23}}{2R} = \frac{r_{12}r_{13}r_{23}}{4R} \tag{3.86}$$

where R is the radius of the circle containing the triangle formed by the particles and is given as follows (Figure 3.8)

$$R = \frac{r_{ij}}{2\sin\theta_k} \tag{3.87}$$

where θ_k is the angle opposite to the distance r_{ij}. If we consider the case when the changes in r_{12}, r_{13} and r_{23} happen in such a way that the area A does not significantly change (for example, one of the three lengths shrinks slightly and the other two expand slightly but the product of the three does not change significantly), we write

$$A \approx const \tag{3.88}.$$

In this case equation (3.83) (similarly for equations (3.84) and (3.85)) would be integrated when it is written in the following form (using equation (3.86))

$$\frac{1}{r_{12}}\frac{\partial^2}{\partial r_{12}^2}\left(r_{12}\,\Omega_p\right) = -\frac{a^2 r_{12}^2}{16R^2A^2}\left(1-\frac{a}{r_{12}}\right)\cos\theta_3 \tag{3.89}$$

and so we have

$$r_{12}\,\Omega_p = -\frac{a^2}{16A^2}\iint \frac{r_{12}^3}{R^2}\left(1-\frac{a}{r_{12}}\right)\cos\theta_3\; dr_{12}dr_{12} \qquad (3.90).$$

Similar equations can be written for the cases of equations (3.84) and (3.85) as follows

$$r_{13}\,\Omega_p = -\frac{a^2}{16A^2}\iint \frac{r_{13}^3}{R^2}\left(1-\frac{a}{r_{13}}\right)\cos\theta_2\; dr_{13}dr_{13} \qquad (3.91)$$

$$r_{23}\,\Omega_p = -\frac{a^2}{16A^2}\iint \frac{r_{23}^3}{R^2}\left(1-\frac{a}{r_{23}}\right)\cos\theta_1\; dr_{23}dr_{23} \qquad (3.92).$$

We write the integral in equation (3.90) as

$$\iint \frac{r_{12}^3}{R^2}\left(1-\frac{a}{r_{12}}\right)\cos\theta_3\; dr_{12}dr_{12} = I\left(r_{12}\right)+\alpha\, r_{12}+\beta \qquad (3.93)$$

where α and β are the coefficients added when performing the integrals and (computing the integral explicitly will be discussed more shortly)

$$\frac{d^2 I\left(r_{12}\right)}{dr_{12}^2} = \frac{r_{12}^3}{R^2}\left(1-\frac{a}{r_{12}}\right)\cos\theta_3 \qquad (3.94)$$

or in general

$$\frac{d^2 I\left(r_{ij}\right)}{dr_{ij}^2} = \frac{r_{ij}^3}{R^2}\left(1-\frac{a}{r_{ij}}\right)\cos\theta_k \qquad (3.95)$$

where again θ_k is the angle opposite to the distance r_{ij}. Equation (3.90) then becomes as follows

$$\Omega_p = -\frac{a^2 I\left(r_{12}\right)}{16A^2 r_{12}}+\alpha+\frac{\beta}{r_{12}} \qquad (3.96).$$

However, we know that Ω_p depends explicitly on r_{13} because of equation (3.91) and hence if we choose the coefficient α (which is arbitrary at this stage) to be dependent on r_{13} then the last equation gives the following result (bearing in mind equation (3.88))

$$\frac{\partial^2}{\partial r_{13}^2}\left(r_{13}\,\Omega_p\right) = \frac{\partial^2}{\partial r_{13}^2}\left(r_{13}\,\alpha\right) \qquad (3.97)$$

and so because of equations (3.91) and (3.95) we have

$$\alpha = -\frac{a^2 I(r_{13})}{16A^2 r_{13}} + \gamma + \frac{\eta}{r_{13}} \tag{3.98}$$

where again γ and η are the coefficients added when performing the integrals. Hence, equation (3.96) becomes

$$\Omega_p = -\frac{a^2 I(r_{12})}{16A^2 r_{12}} - \frac{a^2 I(r_{13})}{16A^2 r_{13}} + \gamma + \frac{\beta}{r_{12}} + \frac{\eta}{r_{13}} \tag{3.99}.$$

Following the same argument with the third distance r_{23} where we use the coefficient γ and also make use of equations (3.91) and (3.95) we have

$$\gamma = -\frac{a^2 I(r_{23})}{16A^2 r_{23}} + \chi + \frac{\kappa}{r_{23}} \tag{3.100}$$

and so equation (3.99) finally becomes

$$\Omega_p = -\frac{a^2}{16A^2}\left[\frac{I(r_{12})}{r_{12}} + \frac{I(r_{13})}{r_{13}} + \frac{I(r_{23})}{r_{23}}\right] + \frac{\beta}{r_{12}} + \frac{\eta}{r_{13}} + \frac{\kappa}{r_{23}} + \chi \tag{3.101}.$$

Now the important question is how to determine the constants appearing in the last equation β, η, κ and χ. These coefficients are integration coefficients and hence they can be determined using the boundary conditions of the problem. We have already established the first boundary condition that Ω_p must satisfy (equation (3.81)). If we use this condition again and bear in mind that the area also becomes infinitely large when the distances r_{12}, r_{13} and r_{23} are infinitely large, we have

$$\chi = 0 \tag{3.102}.$$

This is because all of the terms in equation (3.101) vanish, when the distances r_{12}, r_{13} and r_{23} are infinitely large, except for χ. To determine the remaining coefficients, we consider the case when only two of the three distances (say r_{ik} and r_{jk} for example) tend to infinity. In this case the two particles separated by the distance r_{ij} will evolve as if the third particle is not there because it is infinitely far from them. In this case we have the following

$$\Omega = \Omega_{\mathrm{IRT}} = \left(1 - \frac{a}{r_{ij}}\right) \qquad : r_{ik}, r_{jk} \to \infty \tag{3.103}.$$

The last condition indicates that

$$\Omega_p = 0 \qquad : r_{ik}, r_{jk} \to \infty \tag{3.104}.$$

Applying this to equation (3.101), bearing in mind that the area A tends to infinity quickly when r_{ik} and r_{jk} tend to infinity and also using equation (3.102), we have

$$\beta = \eta = \kappa = 0 \tag{3.105}$$

and hence equation (3.101) becomes

$$\Omega_p = -\frac{a^2}{16A^2}\left[\frac{I\left(r_{12}\right)}{r_{12}} + \frac{I\left(r_{13}\right)}{r_{13}} + \frac{I\left(r_{23}\right)}{r_{23}}\right] \tag{3.106}.$$

Finally, we need to discuss $I\left(r_{ij}\right)$ of equation (3.95). We write (it is worth emphasising that we do not need to add coefficients when performing the integrals as we have already done that in equation (3.93) for example),

$$I\left(r_{ij}\right) = \iint \frac{r_{ij}^3}{R^2}\left(1 - \frac{a}{r_{ij}}\right)\cos\theta_k \, dr_{ij} \, dr_{ij} = \iint \frac{r_{ij}^3}{R^2}\cos\theta_k \, dr_{ij} \, dr_{ij} - a\iint \frac{r_{ij}^2}{R^2}\cos\theta_k \, dr_{ij} \, dr_{ij} \tag{3.107}.$$

The idea is that if we use equation (3.87) (the geometry of the problem in Figure 3.8), we have

$$r_{ij} = 2R\sin\theta_k \quad , \quad dr_{ij} = 2\left(R\cos\theta_k d\theta_k + \sin\theta_k dR\right) \tag{3.108}$$

and hence $I\left(r_{ij}\right)$ becomes

$$I\left(r_{ij}\right) = I\left(R,\theta_k\right) = 32\iint R\sin^3\theta_k \cos\theta_k \left(R\cos\theta_k d\theta_k + \sin\theta_k dR\right)^2 - 16a\iint \sin^2\theta_k \cos\theta_k \left(R\cos\theta_k d\theta_k + \sin\theta_k dR\right)^2 \tag{3.109}.$$

If we introduce the following notation

$$I_1\left(r_{ij}\right) = I_1\left(R,\theta_k\right) = 32\iint R\sin^3\theta_k \cos\theta_k \left(R\cos\theta_k d\theta_k + \sin\theta_k dR\right)^2 \tag{3.110}$$

and

$$I_2\left(r_{ij}\right) = I_2\left(R,\theta_k\right) = 16a\iint \sin^2\theta_k \cos\theta_k \left(R\cos\theta_k d\theta_k + \sin\theta_k dR\right)^2 \tag{3.111}$$

we then write

$$I\left(r_{ij}\right) = I\left(R,\theta_k\right) = I_1\left(R,\theta_k\right) - I_2\left(R,\theta_k\right) \tag{3.112}.$$

Obtaining the integrals I_1 and I_2 of the last equation is straightforward.[149,150] We start with I_1 where after performing the square on the right hand side we obtain a sum of three integrals, the first one contains ($d\theta_k \, d\theta_k$) as follows

$$I_{1,1} = 32\iint R^3 \sin^3\theta_k \cos^3\theta_k \, d\theta_k d\theta_k \tag{3.113}$$

which is a "standard" trigonometric integral and can be evaluated. The final answer is given as follows

$$I_{1,1} = -\frac{2R^3}{3}\sin 2\theta_k \left(1 + \frac{1}{6}\sin^2 2\theta_k\right) \tag{3.114}.$$

The second integral of I_1 contains ($dR\ dR$) and is given as follows

$$I_{1,2} = 32\iint R\sin^5\theta\cos\theta \, dR\, dR = \frac{16R^3}{3}\sin^5\theta\cos\theta \tag{3.115}.$$

The third integral of I_1 contains ($dR\ d\theta_k$) and is given as follows

$$I_{1,3} = 32\iint 2R^2 \sin^4\theta_k \cos^2\theta_k \, dR\, d\theta_k = \frac{64R^3}{3}\int \sin^4\theta_k \cos^2\theta_k \, d\theta_k \tag{3.116}$$

which is again a standard and can be evaluated. The final answer is given as follows

$$I_{1,3} = \frac{4R^3}{3}\left(\theta_k - \frac{1}{4}\sin 4\theta_k - \frac{1}{3}\sin^3 2\theta_k\right) \tag{3.117}.$$

Finally the integral I_1 is then the sum of the last three equations as follows

$$I_1\left(r_{ij}\right) = I_1\left(R, \theta_k\right) = I_{1,1} + I_{1,2} + I_{1,3} \tag{3.118}$$

Now we move to consider the integral I_2. Following the same treatment, the integral I_2 is also a sum of three integrals (after we calculate the square on the right hand side of equation (3.111)). The first of them $I_{2,1}$ is

$$I_{2,1} = 16a\iint R^2 \sin^2\theta_k \cos^3\theta_k \, d\theta_k \, d\theta_k \tag{3.119}$$

which is

$$I_{2,1} = \frac{16aR^2}{5}\cos\theta_k \left(-\frac{2}{3} - \frac{1}{9}\cos^2\theta_k + \frac{1}{5}\cos^4\theta_k\right) \tag{3.120}.$$

The second integral $I_{2,2}$ is

$$I_{2,2} = 16a\iint \sin^4\theta_k \cos\theta_k \, dR\, dR = 8aR^2 \sin^4\theta_k \cos\theta_k \tag{3.121}.$$

The last integral $I_{2,3}$ is

$$\begin{aligned} I_{2,3} &= 16a\iint 2R\sin^3\theta_k \cos^2\theta_k \, dR\, d\theta_k \\ &= 16aR^2 \int \sin^3\theta_k \cos^2\theta_k \, d\theta_k \end{aligned} \tag{3.122}$$

and hence

$$I_{2,3} = 16\,a\,R^2 \cos^3\theta_k \left(-\frac{1}{3} + \frac{1}{5}\cos^2\theta_k \right) \tag{3.123}.$$

The integral I_2 is then

$$I_2\left(r_{ij}\right) = I_2\left(R,\theta_k\right) = I_{2,1} + I_{2,2} + I_{2,3} \tag{3.124}.$$

The integral I of equation (3.95) can then be obtained using the last equation and equation (3.118) in equation (3.112).

Unfortunately, it turned out that calculating the value of Ω_p using equation (3.106) does not produce the desired results. For example, in the case of equilateral triangle whose edge is $10\sqrt{2}$ Å (Figure 3.3), the simulations indicate that the difference between the RF model and the IRT theory should be around 0.021 at 500 ps (the value may change slightly if the simulations run for a longer cut off time). However, the value of Ω_p is -0.0405. The negative sign might originate from the perturbation theory itself (equation (3.71) where the two terms are automatically of opposite signs). This might be overcome by considering the absolute value of Ω_p instead (perhaps this could be thought of in a similar way to quantum mechanics where only $|\psi|^2$ is physically meaningful). In that case, the value does not seem to be very unreasonable, particularly when considering the number of assumptions made to obtain equation (3.106). Similarly, if we consider the case of the isosceles triangle of Figure 3.4, the difference between the RF model and the IRT theory should be around 0.012 at 500 ps based on the simulations. The absolute value of Ω_p in that case is 0.0387.

3.2.2.4.2. Equilateral triangle

A special case arises when the three distances r_{12}, r_{13} and r_{23} are constrained to be equal. In this case, L_p in equation (3.57) becomes very simple as follows

$$L_p = \frac{3D'}{2}\frac{\partial^2}{\partial r^2} \tag{3.125}$$

where the three angles θ_k become equal to 60° ($\cos(60^\circ) = 0.5$), and

$$r_{12} = r_{13} = r_{23} = r \tag{3.126}.$$

The backward diffusion equation (equation (3.58)) becomes

$$\frac{\partial P}{\partial t} = 3D'\left(\frac{1}{r}\frac{\partial^2}{\partial r^2}(rP) + \frac{1}{2}\frac{\partial^2 P}{\partial r^2}\right) \tag{3.127}$$

or

$$\frac{\partial P}{\partial t} = \frac{9D'}{2}\left(\frac{\partial^2}{\partial r^2} + \frac{4}{3r}\frac{\partial}{\partial r}\right)P \tag{3.128}.$$

If we take the Laplace transform (equation (3.6)) of the last equation, we have

$$s\tilde{P} = \frac{9D'}{2}\left(\frac{\partial^2}{\partial r^2} + \frac{4}{3r}\frac{\partial}{\partial r}\right)\tilde{P} \quad : \tilde{P} = \tilde{P}(s,r) \tag{3.129}$$

where we used s here as the Laplace transform variable (instead of p in equation (3.6)) to avoid any confusion, and we have also assumed the following

$$t \to 0 \Rightarrow P \to 0 \tag{3.130},$$

i.e. it is very unlikely that a reaction takes place at zero time. Hence we have

$$r\frac{\partial^2 \tilde{P}}{\partial r^2} + \frac{4}{3}\frac{\partial \tilde{P}}{\partial r} - \frac{2s}{9D'}r\tilde{P} = 0 \tag{3.131}$$

which has the following general solution[151,152]

$$\tilde{P} = r^{-1/6}\left[c_1 I_{(1/6)}\left(r\sqrt{\frac{2s}{9D'}}\right) + c_2 K_{(1/6)}\left(r\sqrt{\frac{2s}{9D'}}\right)\right] \tag{3.132}$$

where I_ν and K_ν are the modified Bessel functions of order ν,[153] c_1 and c_2 are coefficients and they will be determined from the boundary conditions. We require that

$$r \to \infty \Rightarrow P \to 0 \tag{3.133}.$$

Because I_ν diverges to infinity when $r \to \infty$, it is essential that

$$c_1 = 0 \tag{3.134}$$

and so $\tilde{P}$ becomes

$$\tilde{P} = c_2\, r^{-1/6}\, K_{(1/6)}\left(r\sqrt{\frac{2s}{9D'}}\right) \tag{3.135}.$$

The coefficient c_2 is determined from the following boundary condition

$$r = a \Rightarrow P = 1 \Rightarrow \tilde{P} = \frac{1}{s} \tag{3.136}$$

which gives

$$c_2 = \frac{a^{1/6}}{s\,K_{(1/6)}\left(a\sqrt{\frac{2s}{9D'}}\right)} \tag{3.137}$$

and so $\tilde{P}$ finally becomes

$$\tilde{P} = \frac{1}{s}\left(\frac{a}{r}\right)^{1/6}\left(K_{(1/6)}\left(r\sqrt{\frac{2s}{9D'}}\right)\Big/ K_{(1/6)}\left(a\sqrt{\frac{2s}{9D'}}\right)\right) \tag{3.138}.$$

Now we need the inverse Laplace transform of the last function so that we obtain P, the probability that a reaction has occurred by time t. This unfortunately does not seem to be known.[154,155] A very similar case appears in the theory of heat conduction, where trying to get the inverse of the Laplace transform ended up with the following equation[152]

$$P = 1 + \frac{2}{\pi}\int_0^\infty e^{-k\,t\,u^2}\,\frac{J_\nu(ur)Y_\nu(ua) - Y_\nu(ur)J_\nu(ua)}{J_\nu^2(ua) + Y_\nu^2(ua)}\,\frac{du}{u} \tag{3.139}$$

where J_ν and Y_ν are Bessel functions of order ν, which is (1/6) in our case (it is zero in the cited reference), and k is a constant (in our case $k = 9D'/2$). Unfortunately, in the above equation we have an improper integral of the second kind as the integrand tends to infinity when $u = 0$.

It is possible to consider the simple version of equation (3.128) when $t \to \infty$ (the steady state limit) where we have

$$\frac{\partial P}{\partial t} = 0 \qquad : t \to \infty \tag{3.140}.$$

In this case equation (3.128) becomes

$$\frac{\partial^2 P_\infty}{\partial r^2} + \frac{4}{3r}\frac{\partial P_\infty}{\partial r} = 0 \tag{3.141}.$$

After we introduce the following function

$$f = \frac{\partial P_\infty}{\partial r} \tag{3.142},$$

we get

$$\frac{\partial f}{\partial r} + \frac{4}{3r} f = 0 \tag{3.143},$$

and hence

$$f = \frac{c}{r^{4/3}} \tag{3.144},$$

and so

$$P_{\infty} = \frac{-3c}{r^{1/3}} + m \tag{3.145}$$

where the coefficients c and m are determined from the boundary conditions above (equations (3.133) and (3.136)) to get the following result (this can also be obtained form equation (3.138) using the final value theorem of the Laplace transform)

$$P_{\infty} = \left(\frac{a}{r}\right)^{1/3} \tag{3.146}.$$

In order to compare this function with the RF model accurately, we need to run the simulations for longer times (so that the condition $t \to \infty$ is reasonably achieved). We run RF simulations for three equilateral triangles (the side lengths are $8\sqrt{2}$ Å, $9\sqrt{2}$ Å and $10\sqrt{2}$ Å) with a "cut off" time equal to 3000 ps. The results are summarized in table 3.1. In general, the calculated values of P_{∞} are in good agreement with the RF results (it is thought the agreement for the last value will improve if it runs longer than 3000 ps).[††] The simulations are shown in Figure 3.9.

Table 3.1. The probabilities of a reaction having taken place. The simulations are shown in Figure 3.9 and the values of P_{∞} are from equation (3.146).

Side length/Å	RF simulations at 3000 ps	IRT simulations at 3000 ps	P_{∞}
8√2	0.779(±0.003)	0.800(±0.003)	0.762
9√2	0.723(±0.003)	0.740(±0.003)	0.732
10√2	0.670(±0.003)	0.686(±0.003)	0.707

Unfortunately, it turned out the above agreement is not general. To show this we write the corresponding expression for P_{∞} using the IRT theory as follows (we use equations (3.60) and (3.65))

[††] It should be noted that the value of $|\Omega_p|$ of the last section decreases from 0.0599 when the side length is 8√2 Å to 0.0405 when the side length is 10√2 Å. The discrepancy between the RF and IRT simulations decreases in the same direction (Table 3.1 and Figure 3.9). It is therefore thought that when we have a case of different geometries, the value of $|\Omega_p|$ might generally be used to arbitrarily predict which case would give the better agreement between the RF and IRT simulations (only arbitrarily because it does not give the right values).

$$P_{\infty,\mathrm{IRT}} = 1 - \left(1 - \frac{a}{r}\right)^3 \tag{3.147}$$

where r, as before, is the edge of the equilateral triangle. Figure 3.10 shows the last function and the solution P_∞ above (equation (3.146)). P_∞ is an improvement only over a certain region (relatively small r/a) and not all the time. This is clearly because we constrained the three distances to be equal. To highlight this further, we have included the results of the last table on Figure 3.10, and also included results for larger values of side length (r = $12\sqrt{2}$, $18\sqrt{2}$ and $19\sqrt{2}$ Å). It should be noted that (as mentioned above) the agreement between the simulation results and the curves will improve (the red dots should be on the orange curve) if we choose a larger cut off time (because the curves correspond to $t \rightarrow \infty$). It should also be noted that the agreement between the RF model and the IRT method improves as r/a increases. This is because when r/a is large, each pair of particles will be far from the third particle, and as a result the pair will evolve "almost" independently from the third particle.

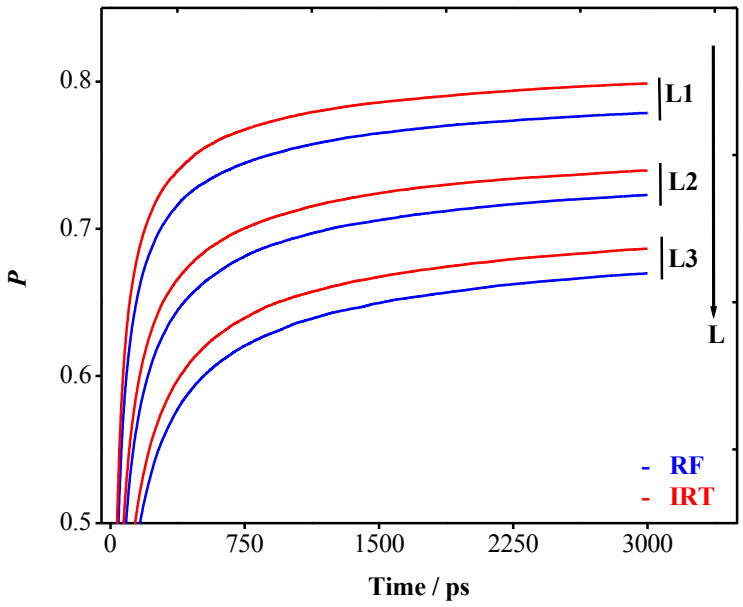


Figure 3.9. The RF and IRT simulations for three different equilateral triangles. L refers to the length of the side of the triangle. The values are L1 = 8√2, L2 = 9√2 and L3 = 10√2 Å.

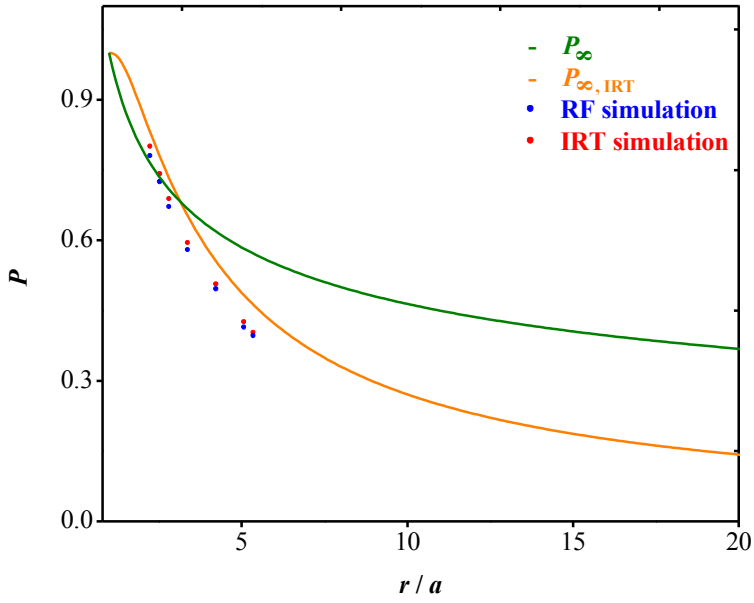


Figure 3.10. Comparing the solutions, P_∞ of equation (3.146) and $P_{\infty,\mathrm{IRT}}$ of equation (3.147). RF and IRT simulations at different values of r/a are also included.

3.2.3. Further simulations

As discussed above, the mathematics of the problem of three-body correlation seems to be intractable. However, it is always possible to investigate these correlations using computer simulation. Hence a specific simulation program was built, using the RF model described in chapter 2, to give the covariance coefficients of three random variables Q_{ij} describing the occurrence of the three possible reactions of three particles, each one of the random variables takes on the value zero if the corresponding pair reacts and takes on the value one if the pair does not. As before, the simulations start from a certain configuration (either a random of some sort or a specific geometry) and then the simulations continue exactly as described in chapter 2. The difference is that when a certain pair reacts, the program does not stop (since we are studying the case of three particles, the simulations normally stops if a reaction occurs) and move to the next realization, but it rather carries on simulating until a maximum cut-off time is reached. In this case, the simulations allow us to investigate what happens after a certain encounter (reaction) has taken place and see if there are other encounters of other particles at later times and hence the covariances of the random variables Q_{ij} are obtained.

The random variable Q_{ij} takes on the value of unity if the pair i and j do not react and the value of zero if they do and hence using Ω_{ij}, the marginal survival probability for a pair (equation (3.64)), we have

$$\Pr\left\{Q_{ij}=1\right\}=\Omega_{ij} \tag{3.148}$$

and

$$\Pr\left\{Q_{ij}=0\right\}=1-\Omega_{ij} \tag{3.149}.$$

The variables Q_{ij} have the following properties

$$E\left(Q_{ij}\right)=\Omega_{ij} \quad , \quad \sigma^2\left(Q_{ij}\right)=\Omega_{ij}\left(1-\Omega_{ij}\right) \tag{3.150}.$$

The covariance of two random variables Q_{ij} and Q_{jk} is

$$\sigma^2\left(Q_{ij},Q_{jk}\right)=E\left(Q_{ij}Q_{jk}\right)-E\left(Q_{ij}\right)E\left(Q_{jk}\right) \tag{3.151}$$

or

$$\sigma^2\left(Q_{ij},Q_{jk}\right)=E\left(Q_{ij}Q_{jk}\right)-\Omega_{ij}\Omega_{jk} \tag{3.152}$$

and so we have the following

$$\Pr\left\{Q_{ij}=1,Q_{jk}=1\right\}=E\left(Q_{ij}Q_{jk}\right) \tag{3.153}.$$

When considering the three random variables together, we have the combinations of values included in the following table (Table 3.2)

Table 3.2. The possible combinations of values of the three random variables.

Pr	P_{111}	P_{101}	P_{110}	P_{100}	P_{011}	P_{001}	P_{010}	P_{000}
Q_{12}	1	1	1	1	0	0	0	0
Q_{13}	1	1	0	0	1	1	0	0
Q_{23}	1	0	1	0	1	0	1	0

where we have used the following notation

$$P_{abc}=\Pr\left\{Q_{12}=a\,,Q_{13}=b\,,Q_{23}=c\right\} \tag{3.154}.$$

A set of equations is then written for the probabilities P_{abc} and if we solve the equations for the covariances, we get the following equation

$$\sigma^2\left(Q_{ij},Q_{jk}\right)=\Pr\left\{Q_{ij}=1,Q_{jk}=1,Q_{ik}=1\right\}+\Pr\left\{Q_{ij}=1,Q_{jk}=1,Q_{ik}=0\right\}-\Omega_{ij}\Omega_{jk} \quad (3.155).$$

The survival probabilities can be calculated once the initial separations of the particles are known (equation (3.64)). The simulations produce the probabilities P_{abc} and hence the covariances are obtained using the last equation.

The results for three particles whose initial coordinates are generated from a random distribution (Gaussian with mean zero and a standard deviation of $2a$) are

$$\sigma^2\left(Q_{12},Q_{13}\right)=0.145\,(\pm0.002)\quad,\quad\sigma^2\left(Q_{12},Q_{23}\right)=0.144\,(\pm0.002)$$
$$\sigma^2\left(Q_{13},Q_{23}\right)=0.145\,(\pm0.002) \quad (3.156)$$

and for the case of three particles initially fixed on a straight line of length $20\sqrt{3}$ Å where two particles are located on the two ends and one is in the middle (the one labelled 2)

$$\sigma^2\left(Q_{12},Q_{13}\right)=0.157\,(\pm0.002)\quad,\quad\sigma^2\left(Q_{12},Q_{23}\right)=0.123\,(\pm0.002)$$
$$\sigma^2\left(Q_{13},Q_{23}\right)=0.158\,(\pm0.002) \quad (3.157).$$

When we set the total length of the straight line to $16\sqrt{3}$ Å, the results become

$$\sigma^2\left(Q_{12},Q_{13}\right)=0.145\,(\pm0.002)\quad,\quad\sigma^2\left(Q_{12},Q_{23}\right)=0.092\,(\pm0.002)$$
$$\sigma^2\left(Q_{13},Q_{23}\right)=0.145\,(\pm0.002) \quad (3.158).$$

When the length of the straight line is $14\sqrt{3}$ Å we have

$$\sigma^2\left(Q_{12},Q_{13}\right)=0.134\,(\pm0.002)\quad,\quad\sigma^2\left(Q_{12},Q_{23}\right)=0.069\,(\pm0.002)$$
$$\sigma^2\left(Q_{13},Q_{23}\right)=0.132\,(\pm0.002) \quad (3.159).$$

The results when the particles are located initially on an equilateral triangle, whose edge is of length $10\sqrt{2}$ Å, are as follows

$$\sigma^2\left(Q_{12},Q_{13}\right)=0.126\,(\pm0.002)\quad,\quad\sigma^2\left(Q_{12},Q_{23}\right)=0.125\,(\pm0.002)$$
$$\sigma^2\left(Q_{13},Q_{23}\right)=0.124\,(\pm0.002) \quad (3.160).$$

Also the results for an equilateral triangle, whose edge is of length $9\sqrt{2}$ Å, are

$$\sigma^2\left(Q_{12},Q_{13}\right)=0.115\,(\pm0.002)\quad,\quad\sigma^2\left(Q_{12},Q_{23}\right)=0.114\,(\pm0.002)$$
$$\sigma^2\left(Q_{13},Q_{23}\right)=0.115\,(\pm0.002) \quad (3.161).$$

For an equilateral triangle, whose edge is of length $8\sqrt{2}$ Å we have

$$\sigma^2\left(Q_{12},Q_{13}\right)=0.100\ (\pm 0.002)\ ,\ \ \sigma^2\left(Q_{12},Q_{23}\right)=0.101\ (\pm 0.002)$$
$$\sigma^2\left(Q_{13},Q_{23}\right)=0.101\ (\pm 0.002) \qquad (3.162).$$

Hence the covariances decrease as the length of side of the triangle decreases. In other words (when we consider also the results for a straight line), the wider the particles are apart, the bigger the covariances are. To check this further, we looked at the correlation coefficients in the case of equilateral triangles and found that the "average" correlation coefficient (the average of the three possible correlation coefficients (we have included the average because the three coefficients are nearly equal anyways)) is 0.634 when the length is $2\sqrt{10}$, it is 0.531 when the length is $2\sqrt{9}$ and it is 0.432 when the length is $2\sqrt{8}$. This can be interpreted as follows: Firstly, the positive correlation coefficients indicate that if the first pair survives (or react since the two events complement one another), then it is likely that the second pair has the same fate (either survive or react). This is because if the first pair has, for example, reacted then that means the two particles have actually diffused toward each other until they reached a reactive configuration, and hence the second reaction is more likely to happen (because if the third particle approaches as the diffusion occurs, then it will be approaching two particles rather than just one). This effect becomes more important when the initial distances are large and hence the correlation coefficients (also the covariance) are large. When the distances are initially small, this effect becomes less important because the particles are already close to one another (hence the correlation coefficients are small).

When the particles form at the start a right triangle where the initial separations are as follows (in Å)

$$r_{12}=10\sqrt{2}\quad ,\quad r_{13}=10\sqrt{3}\quad ,\quad r_{23}=10 \qquad (3.163)$$

the results are

$$\sigma^2\left(Q_{12},Q_{13}\right)=0.141\ (\pm 0.002)\ ,\ \ \sigma^2\left(Q_{12},Q_{23}\right)=0.086\ (\pm 0.002)$$
$$\sigma^2\left(Q_{13},Q_{23}\right)=0.109\ (\pm 0.002) \qquad (3.164).$$

Finally, for an isosceles triangle where we have the following separations (in Å)

$$r_{12}=r_{13}=10\sqrt{3}\quad ,\quad r_{23}=20\sqrt{2} \qquad (3.165)$$

the results are

$$\sigma^2\left(Q_{12},Q_{13}\right)=0.130\ (\pm 0.002)\ ,\quad \sigma^2\left(Q_{12},Q_{23}\right)=0.158\ (\pm 0.002)$$
$$\sigma^2\left(Q_{13},Q_{23}\right)=0.158\ (\pm 0.002) \qquad (3.166).$$

3.3. Summary and conclusions

The problem of three-body correlations and their effects in radiation chemistry has rarely been addressed before.[144] This is because it is very challenging mathematically. The original aim of this chapter was to investigate whether there was a way to correct the IRT method for three body correlations. We have tried to investigate this in detail, and made some progress but unfortunately this has not resulted in clear conclusive results, nor in any results that can be included in the IRT program.

We have started this study using the only result currently available in the literature, the Clifford-Green theorem, for the case of three particles whose initial coordinates are generated from a Gaussian distribution.[144,145] The theorem gives the joint probability density function and moment generating function for the squared distances in the triangle. We have used these results to find the mean and variance of the squared distances and also the covariance of two squared distances. The last has not been calculated explicitly before, but the hope was that correlations of reaction times could be interpreted in terms of the correlations of the distances.

We have then presented simulations of the reaction probability for various initial triangle shapes. We have also included simulations where the particles are initially on a straight line and also for a random configuration. This indicated that the discrepancy between the IRT simulations and the RF simulations of the probability that a reaction takes place is generally small, especially for a random configuration. The reason for this is that in any realisation of a random configuration one of the distances will generally be smaller than the other two, and so the recombination of this pair will be more likely, so that the reaction times for the other pairs will not be important, and since the IRT method is based on the exact solution for a single pair it will be a good approximation. The same is seen for isosceles triangles with one short distance. The worst case for the IRT method is when all three distances are equal, as this maximises the correlation effects that are ignored in the independence approximation. Interestingly, in the linear configuration, where two distances are in

competition with each other and the third distance is larger, the IRT method for the total reaction is accurate, but this is due to cancellation of errors.

We have also formulated and attempted to analyse the exact backward diffusion equation for three diffusing particles. We have, for the first time, derived the explicit expression for the infinitesimal covariance of two diffusing distances in a multi-particle system.

We have looked at possible approximations to solve the backward diffusion equation. This included a perturbation treatment, which required a great deal of algebra. The method predicts a correction in the wrong direction and it is not very clear at the moment if this method can be, somehow, improved or if the absolute value can be used instead. We have also looked at another case when the particles are constrained to lie on an equilateral triangle. In this case it is possible to obtain an analytic solution for the Laplace transform of the probability that a reaction has taken place but, unfortunately, the inverse Laplace transform does not seem to be known. It is possible in this case to obtain an exact solution for the ultimate reaction probability, as the solution to the steady-state equation. This solution seems to be an improvement only over a certain region and not in general. However, it is the first-known solution that takes the correlation coefficients into account.

Finally, we have looked at simulated results for the correlations between the hit probabilities of pairs. In particular we have looked at how the correlation coefficients change depending on how far the particles are apart initially and the initial shape of the triangle. We have concluded that the wider the particles initially are apart, the larger the correlation coefficients are. But, unfortunately there seems to be no clear relationship between the correlations of the reaction probabilities and either the infinitesimal correlations in the backward equation or the long-time correlations from the Clifford-Green theorem. For the moment we can see no clear way to correcting the IRT method for these correlations.

Chapter 4

Scavenging and Recombination Kinetics I: Smoluchowski Theory[‡‡]

"Each piece, or part, of the whole of nature is always merely an approximation to the complete truth, or the complete truth so far as we know it. In fact, everything we know is only some kind of approximation, because we know that we do not know all the laws as yet. Therefore, things must be learned only to be unlearned again or, more likely, to be corrected…" ***Richard Feynman***

When trying to obtain an analytic solution for a given problem, the mathematics very often forces certain assumptions so that the problem can be relaxed. If a solution is eventually obtained, it will be exact for an "ideal" system where these assumptions are perfectly met. For practical systems that deviate from the ideal system, the solution may become inaccurate, and generally the greater the deviation from the ideal system, the greater the inaccuracy of the analytic solution. This has been found to be the case in Smoluchowski theory for the diffusion-controlled reactions.[14,16] This is very important because radical scavenging is a commonly used technique in radiation chemistry, and in many cases the scavenging reaction is effectively diffusion-controlled. In fact, for some species the competition between scavenging and recombination may be the only way to gain insight into their track kinetics.[6,12,13,75] In this chapter we will examine this in more detail.

[‡‡] **Acknowledgements and details**: N. Green has greatly helped in planning the recipe for the simulations described in section 4.2. Section 4.4 was proposed by E. Al-Samra.

4.1. Smoluchowski theory

As mentioned before, it is known that for a diffusion-controlled reaction the rate constant becomes a time-dependent quantity.[14, 156] This becomes particularly important in radiation-induced spur reactions because the effects that lead to the time dependence of the rate constant are the same as those that lead to the transient kinetics of spur recombination. Theoretical approaches have been developed to describe the chemical kinetics of such reactions.[6,10,101,129,157] Diffusion-controlled reactions also occur in many areas including polymerization and biochemistry.[15,158,159]

The expression for the time-dependent rate constant was first derived by M. Smoluchowski in a paper dated 1917.[16] Consider the reaction R+S in an inert continuum-like solvent, where the concentration of R is very low relative to the concentration of S. Under these conditions, a large distance (and many S molecules) separates two molecules of R and consequently the molecules of R behave independently of one another. Furthermore, C_S, the bulk concentration of S, does not change substantially as a result of the reaction R+S and can be considered constant throughout the experiment. If we denote the reaction distance as a, a diffusion-controlled reaction happens instantly when the distance between R and S is equal to a. The reaction reduces the local concentration of S, $C(r,t)$, around the central R particle relative to the concentration in the bulk, C_S. Assuming the spherical symmetry of the problem, where the molecule R occupies the centre of a sphere and is surrounded by molecules of S, the concentration of S will have the general profile shown in Figure 4.1 where we define the ratio ρ as follows[14,156,160]

$$\rho(r,t) = \frac{C(r,t)}{C_S} \tag{4.1}.$$

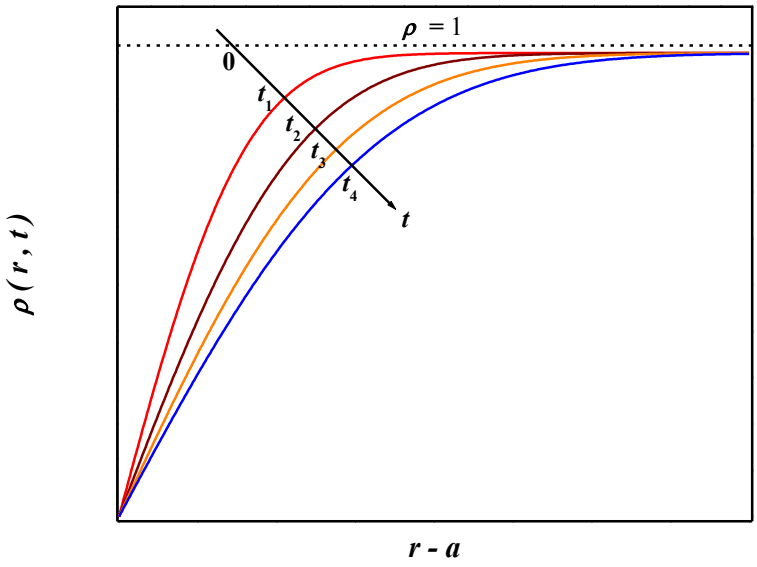


Figure 4.1. The concentration profile. This is taken at few times $t_1 < t_2 < t_3 < t_4$ after the introduction of the radical R. At short times (t_1), the disturbance in the concentration due to the reaction is rather localized around the original location of the radical R that has reacted. The reaction is fully diffusion controlled so the concentration (or the ratio ρ) drops to zero for $r = a$.[14,156]

The next step is to write the diffusion equation describing the change in the ratio given in the last equation and it is given as follows

$$\frac{\partial \rho}{\partial t} = D'\left(\frac{\partial^2}{\partial r^2} + \frac{2}{r}\frac{\partial}{\partial r}\right)\rho \tag{4.2}$$

where D' is the relative diffusion coefficient ($D' = D_S + D_R$ where D_S and D_R are the diffusion coefficients for S and R respectively). There is an implicit approximation at this stage: The assumption has been made that the diffusion of the S particles relative to R is independent, i.e. that S particles diffuse independently in the frame of reference of R. This assumption is only true if R is stationary. After taking the Laplace transform of the last equation with respect to time, and using the initial condition $\rho(0,r) = 1$ ($r > a$), it becomes an ordinary differential equation, which can be solved in the light of the following boundary conditions extracted from Figure 4.1

$$r = a \Rightarrow \rho = 0 \ , \ r \to \infty \Rightarrow \rho \to 1 \tag{4.3}.$$

After taking the inverse Laplace transform of the final result, we have

$$\rho\left(t, r\right) = 1 - \frac{a}{r}\operatorname{erfc}\left(\frac{r-a}{\sqrt{4D't}}\right) \tag{4.4}$$

where erfc is the complementary error function defined in equation (2.44). The current of S particles, denoted $I(a)$, is then given as follows

$$I(a)=\left[4\pi D' r^2 C_S \frac{\partial \rho(r,t)}{\partial r}\right]_{r=a} = 4\pi a D'\left(1+\frac{a}{\sqrt{\pi D' t}}\right)C_S \qquad (4.5).$$

The rate of the reaction R+S is

$$-\frac{dN}{dt} = I(a)N = k(t)C_S N \qquad (4.6)$$

where N is the number of R particles (concentration) and $k(t)$ is the Smoluchowski rate constant and given by

$$k(t) = 4\pi a D'\left(1+\frac{a}{\sqrt{\pi D' t}}\right) \qquad (4.7).$$

A common application for the above theory is the radical-scavenger reaction (R+S). The radicals are generated in an initial step (the interaction of the sample with radiation for example). A scavenger is added to compete with the recombination of the radicals, and with their reactions with other molecules present.[12,13] The question this chapter poses is whether the Smoluchowski rate constant, derived on the assumption that the radicals are isolated from one another, is also applicable to situations in which the radicals are generated close to one another, and there is a competition between scavenging and recombination. Since one of the main aims of scavenger experiments is to use this competition in order to extract information about the recombination kinetics, this is potentially an important question. The aim of this chapter is to investigate this question using computer simulations. Starting from a situation where the conditions perfectly meet the assumptions made to obtain equation (4.7), in order to test the simulation method, it then goes on to situations where the assumptions are not perfectly met by the conditions, specifically, when the radicals are generated relatively close to one another and cannot be considered isolated. In this case, the competition between the R+S reaction and R+R reaction becomes important. The results indicate that equation (4.4) should be corrected and this will be discussed in sections 4.3-4.5. In section 4.2, the details of the computer simulation method used here are discussed, and section 4.6 includes a summary and conclusions.

4.2. Details of the simulations

The computer program used here consists of two parts; one runs Monte Carlo Random Flight (RF) simulations for the purpose of comparison (denoted P1) and another hybrid one runs calculations in which the scavenging is based on the Smoluchowski theory, described above (denoted P2). The program accounts for three reaction schemes, scheme one (denoted S1) where the two reactions R+R and R+S are allowed, and scheme two (denoted S2) where we have the reaction R+S only. The third scheme (S3) has two types of radicals and will be discussed in detail later. As was discussed before, the RF simulations generate the diffusive trajectories of all the reacting particles involved using discrete time-step jumps (or flights) of normally distributed, random numbers, this is equivalent to exact sampling of the trajectory implied by the use of a diffusion equation. The method has been described in detail in chapter 2 and only certain aspects of it will be described here.

The P1 simulations are summarized in Figure 4.2. The radicals are introduced inside a cubic box. Their coordinates are generated randomly from a Gaussian distribution centred at the centre of the box with standard deviation of a tenth of the box edge (for some runs a different distribution was used and this will be discussed later). The cubic box divides space into two regions. Region (I) contains a certain number of scavengers (corresponds to C_S in equation (4.5)) uniformly distributed in this region (their coordinates are randomly generated from a uniform distribution). The box (region (I)) is repeated using a periodic boundary condition (that is the box with the scavengers but without the radicals) so that each scavenger in region (I) has images periodically repeated outside it; the region containing the images is region (II). The scavengers inside region (I) diffuse freely, and their images move similarly in region (II). If a scavenger in region (I) reaches the edge of the box and moves outside it, it gets removed and reintroduced from the opposite side of the box. This ensures that the number of scavengers inside the box does not drop as a result of the Brownian motion. The diffusive trajectories of the radicals are generated. If the distance between a radical and a scavenger (or an image of a scavenger) becomes equal to the corresponding reaction distance, then a scavenging reaction is counted. Thus the presence of the scavengers' images ensures that the radicals may continue to get scavenged if they diffuse away from the centre of the box and outside it. For the S1 scheme then, as the radicals diffuse, if the distance between two radicals becomes

equal to the corresponding reaction distance, a radical-radical reaction is counted. Because of the way the simulations are built, when considering the S2 scheme (especially for high number of radicals) each scavenging event eliminates the involved scavenger particle and all its images, this reduces the probability of scavenging outside the box. To reduce this effect, whenever a scavenging event occurs, a new scavenger particle is introduced in a random location in the box with its images outside. This effect becomes unimportant when considering the S1 scheme as fewer scavenging events occur due to the competition with the radical recombination. Note that the simulations with and without this replacement give upper and lower bounds on the true scavenging kinetics.

The P2 hybrid simulations are simple. Equation (4.7) is used to generate a scavenging time for each radical in the box using the inversion method for generating random numbers (the details of this are given in the appendix at the end of this chapter).[131] When the S1 scheme is considered, P2 uses the same initial coordinates and trajectories for the radicals as in P1 to simulate the radical-radical reactions, using a typical RF routine (and so the simulations are hybrid in this case where the scavenging is simulated through Smoluchowski theory and the recombination is simulated through the RF model). In this case, using the same trajectories and initial coordinates for the radicals in both P1 and P2 ensures a better comparison between the scavenging times calculated based on equation (4.7) and the scavenging times obtained from the Monte Carlo simulations in P1.

In the simulations, the reaction distance for the reaction R+S is equal $a = 5$ Å and so is the reaction distance for R+R reaction. The box edge is equal to 100 Å. The number of scavengers introduced in region (I) is 60 scavengers and it corresponds to a concentration of 6×10^{-5} particles/Å^3 (this corresponds to a concentration of about 0.1 M). The diffusion coefficients for R and S are assumed equal with a value of 1 Å^2.ps^{-1}. Although this diffusion coefficient is large compared with the typical values found in a spur, this has no consequence on the results, because in diffusion controlled reactions the diffusion coefficient is simply a scale factor for the time, for example the results shown here could equally well be interpreted with a diffusion coefficient 10 times smaller and with times 10 times larger. The other values (reaction distance, initial distances, scavenger concentrations) are all of the same magnitude as would be found in experiments.[6,18] The time step is considered constant with a value

of 1 ps, and we used the Bessel bridge condition (equation (2.40)). The typical number of realizations per run is 10^5 and for a small number of radicals (up to 4 radicals) is 10^6. Finally, it should be noted that the simulations make use of the Message Passing Interface (MPI) technique as discussed in chapter 2.

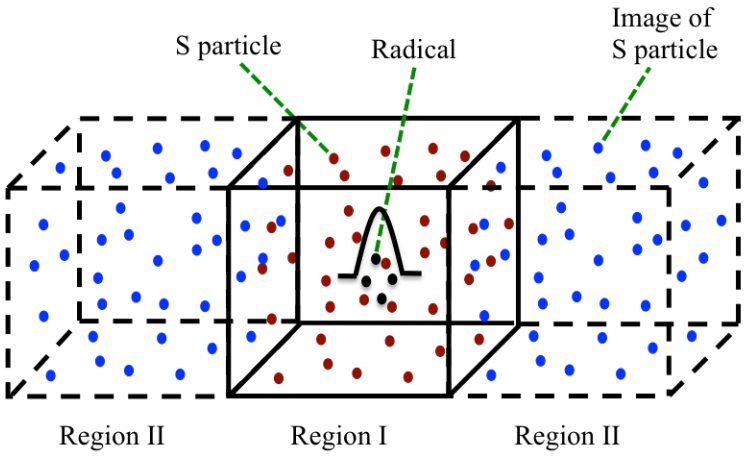


Figure 4.2. The simulation box and two of its images. Region I (the central box) contains the radicals (here their coordinates are generated from a Gaussian distribution) and scavenger particles. Region II contains the images of the scavenger particles. It should be noted that the central box has images in all directions and only two of them are shown above.

4.3. Results

The starting point is to test the above simulation method and check that it gives the expected results. This is done through introducing one radical into the box, matching the assumptions made to obtain equation (4.7). The outcome is shown in Figure 4.3 where the results of both simulations are identical within statistical variation.

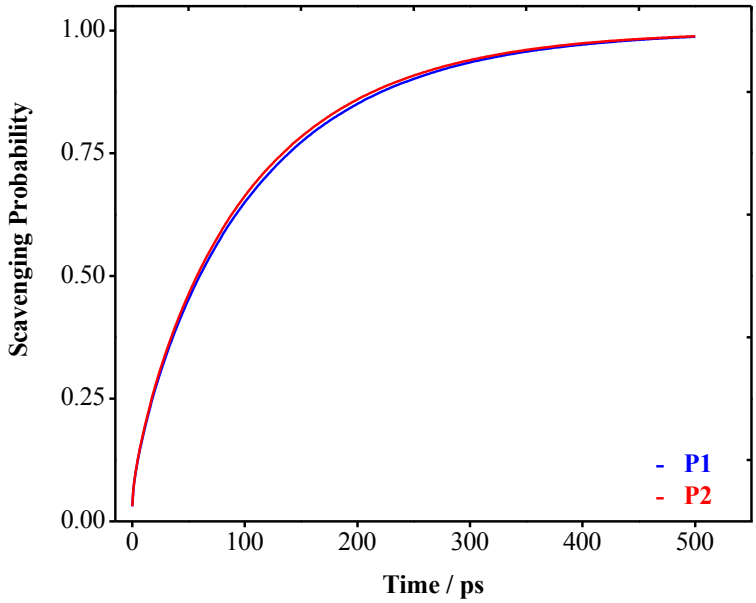


Figure 4.3. The simulations for 1 radical. Both simulations (P1 is the RF model and P2 is the simulations based on Smoluchowski theory) are in agreement with each other (the values at 500 ps are 0.988(±0.002) for P1 and 0.989(±0.002) for P2.

As more radicals are introduced into the box this agreement breaks down gradually. A selection of the simulations is shown in Figure 4.4 (we have run simulations for initial number of radicals $N_R = 1-12$), and a summary is in Table 4.1. The hybrid simulations based on Smoluchowski theory (P2) overestimate the scavenging probability and underestimate the recombination probability (Figure 4.5) relative to the RF simulations in P1. To discover whether or not this disagreement is because of the competition between scavenging and recombination, we also ran simulations where the recombination was turned off (the S2 scheme) and these results are shown in Figure 4.6. The P2 simulations are able to predict well the scavenging probability at long times (this is not technically difficult because the scavenging probability must approach one in that case) but it is clear that the time dependence is not in agreement with the P1 simulations. The observed discrepancy, which increases with N_R, is due to the assumptions (or approximations) made in the Smoluchowski theory and this will be discussed in the next section. However, it is clear that the Smoluchowski theory makes a systematic error when describing the scavenging of particles generated close to one another, irrespective of whether they can recombine,

and so this effect must be considered when modelling the scavenging of spurs, and even more importantly, high LET tracks.

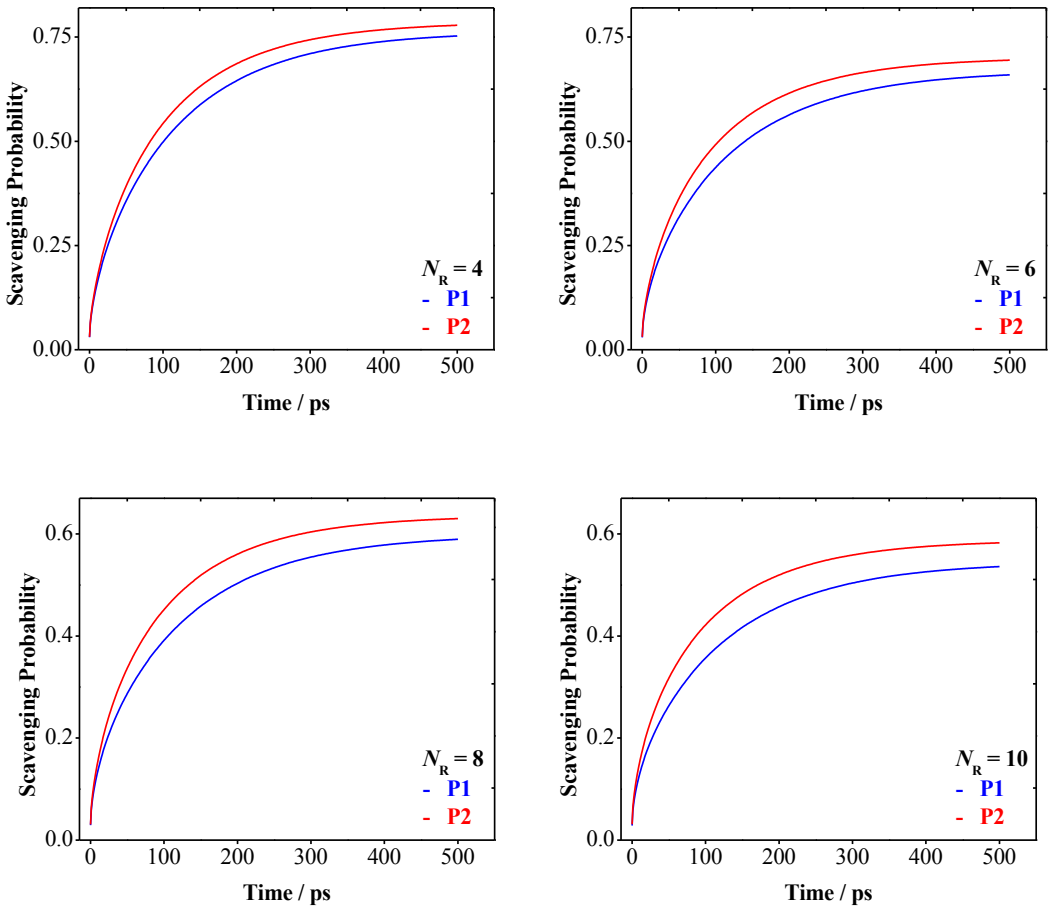


Figure 4.4. The scavenging probability for the S1 scheme. N_R is the number of radicals at zero time. The discrepancy between the P1 (RF) and P2 (hybrid) simulations increases as N_R increases.

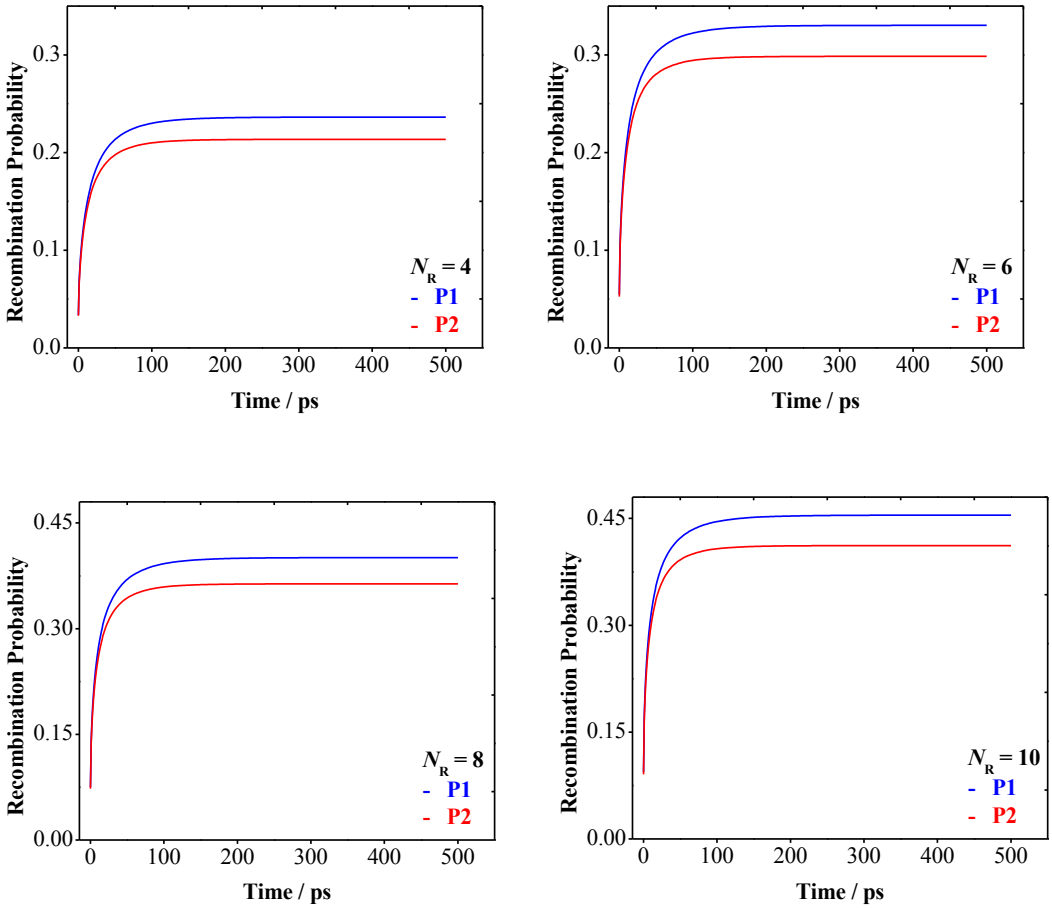


Figure 4.5. The recombination probability for the S1 scheme. N_R is the number of radicals at zero time. The discrepancy between the P1 (RF) and P2 (hybrid) simulations increases as N_R increases.

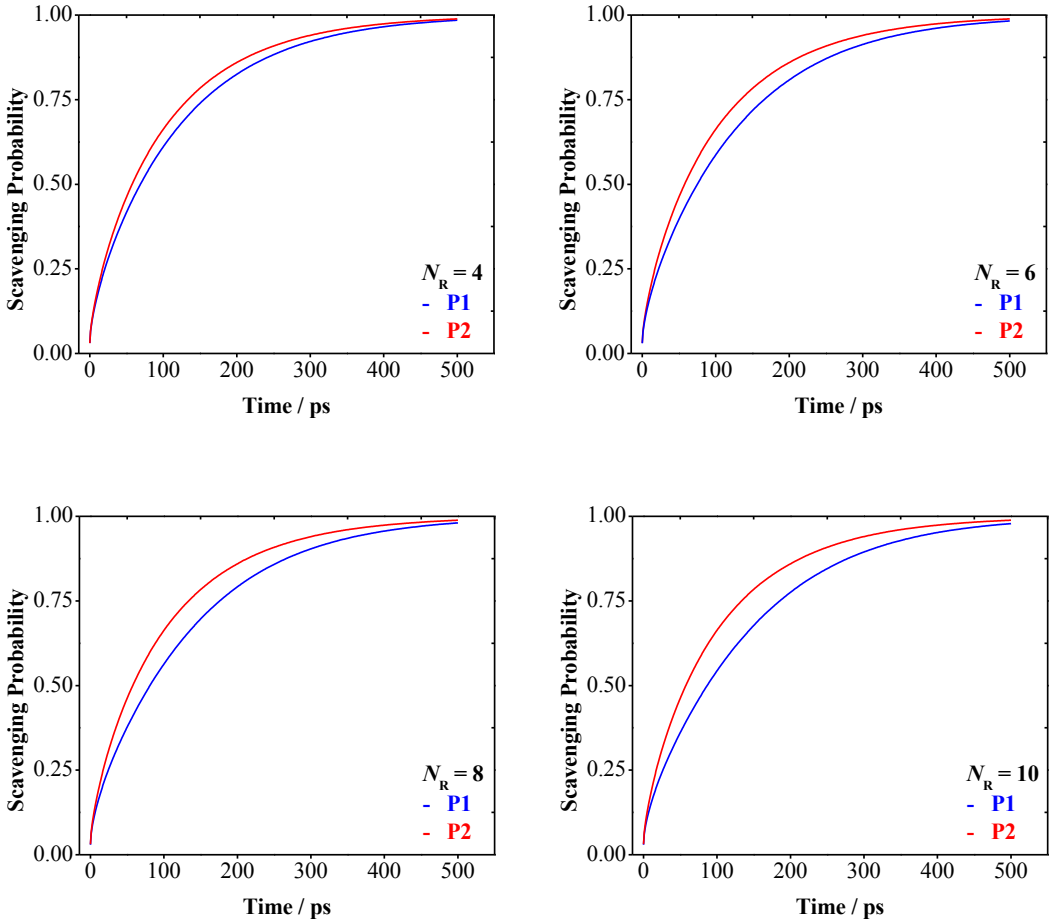


Figure 4.6. The scavenging probability for the S2 scheme. N_R is the number of radicals at zero time. The discrepancy between the P1 (RF) and P2 (hybrid) simulations increases as N_R increases.

Table 4.1. The results of the simulations. The numbers are the probability of the corresponding reaction at 500 ps. The statistical error in the numbers is ~ ±0.002. P1 refers to the RF simulations and P2 refers to the hybrid simulations based on Smoluchowski theory.

Simulations	P1			P2		
Reaction scheme	S1		S2	S1		S2
Reaction	R+S	R+R	R+S	R+S	R+R	R+S
N_R = 4	0.753	0.236	0.985	0.778	0.214	0.989
N_R = 6	0.658	0.330	0.983	0.694	0.299	0.989
N_R = 8	0.590	0.401	0.981	0.630	0.364	0.989
N_R = 10	0.536	0.455	0.979	0.583	0.412	0.989

4.4. Correction

In the Smoluchowski theory each radical is surrounded by its own concentration gradient of scavengers (this because the radicals are assumed to be very far from one another) and the scavenging rate is then calculated from the rate of diffusion down this concentration gradient. In a spur the problem is that the concentration gradients around each radical overlap and so the scavenger concentration around a radical is reduced, not only by the scavenging reaction of that radical but also by the reduction of the scavenger concentration caused by the presence of the other radicals. This may also result in the breakdown of the assumption of spherical symmetry. These factors explain the disagreement between the P1 and P2 simulations for the results presented in the last section. The obvious question is whether a simple correction can be included to take into account this "multi-radical correlation effect".

If we assume, as an approximation, that the spherical symmetry continues to hold in the case when we have more than one radical, then the multi-radical correlation effect described above can be explained as follows, choosing, for example, the curve taken at time t_2 in Figure 4.1. This curve is effectively for an isolated radical (Smoluchowski assumptions). Now if there are other radicals nearby, the local scavenger concentration (or the ratio ρ of equation (4.1)) is reduced further, i.e. at each value for $r - a$, the value of ρ will be smaller. This is schematically shown in Figure 4.7. A correction should then be added to equation (4.4) to include the multi-radical correlation effect. The expression for the ratio ρ is pretty simple (equation (4.4)). To reduce the value of ρ, the argument of the complementary error function should be reduced, thus we suggest a generic correction of the form

$$\rho(t,r) = 1 - \frac{a}{r}\operatorname{erfc}\left(\frac{r-a}{f(N_R)\sqrt{4D't}}\right) \tag{4.8}$$

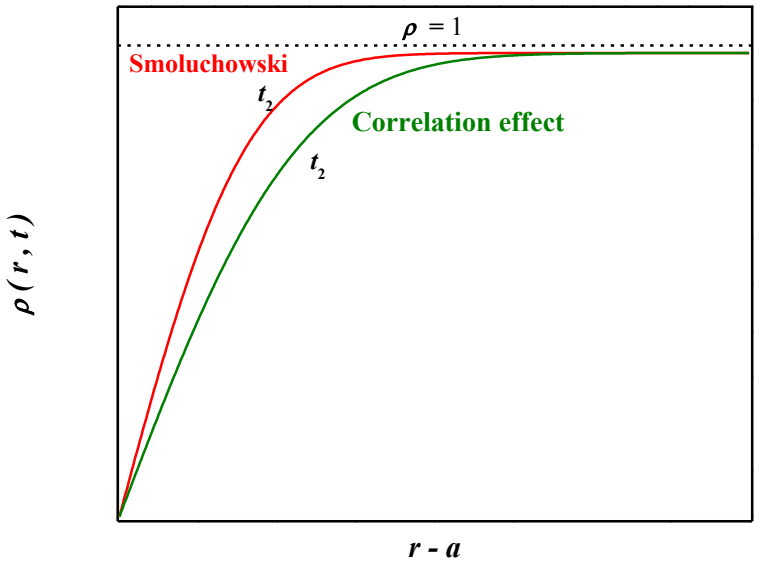


Figure 4.7. A schematic concentration profile illustrating the multi-radicals correlation effect. The red curve is taken from Figure 4.1 at time t_2 based on Smoluchowski theory. The green curve is how the profile should be if we consider the multi-radical correlation effect where the ratio ρ is supposed to rise to unity slower than expected based on Smoluchowski theory.

where N_R is the number of radicals at $t = 0$. The function f is the correction and it depends on N_R because the increase of the discrepancy with N_R (as shown in Figures 4.4-4.6) is the result of the superposition of more and more of these depletion zones. As the value of the function f increases, the value of the complementary error function increases and the value of ρ decreases. Now if we use the last equation rather than equation (4.4) in equation (4.5) and then follow equation (4.6), we eventually obtain the following corrected-rate constant

$$k(t) = 4\pi a D' \left(1 + \frac{a}{f(N_R)\sqrt{\pi D' t}} \right) \qquad (4.9).$$

Obtaining an analytic expression for the function f is difficult. However, we know that it satisfies the following condition

$$f(N_R) \geq 1 \qquad (4.10)$$

where the equality is for the case of one radical (where equation (4.9) becomes equation (4.7)) and then it increases as we introduce more radicals. It is not unreasonable to assume that each additional radical has the same effect on the concentration profile, giving a correction proportional to the number of additional radicals N_R as follows

$$f\left(N_{\mathrm{R}}\right)=1+\alpha\left(N_{\mathrm{R}}-1\right) \tag{4.11}.$$

The problem is now reduced to finding the value of the coefficient α in the last equation. If we use $\alpha=0.5$, we obtain

$$f\left(N_{\mathrm{R}}\right)=\frac{N_{\mathrm{R}}+1}{2} \tag{4.12}$$

and so we have $f\left(N_{\mathrm{R}}=1\right)=1$ as required. Furthermore, the last function satisfies that for the case of two radicals, its value is 1.5 which is in reasonable agreement with the value of $\sqrt{2}$ obtained based on the independent reaction time theory before (this will be discussed in more detail in chapter 5).[17] Now the use of equation (4.9) with the last equation in the P2 simulations (it is denoted C. P2) gives the results shown in Figures 4.8-4.10. In Figures 4.8 and 4.9 the simulations for the scheme S1 are shown where we also included the P2 simulations when equation (4.7) is used for a complete comparison. In Figure 4.10 the simulations for the scheme S2 are shown. As it is clear from these results, the above correction seems to be remarkably accurate. The results are summarized in Table 4.2.

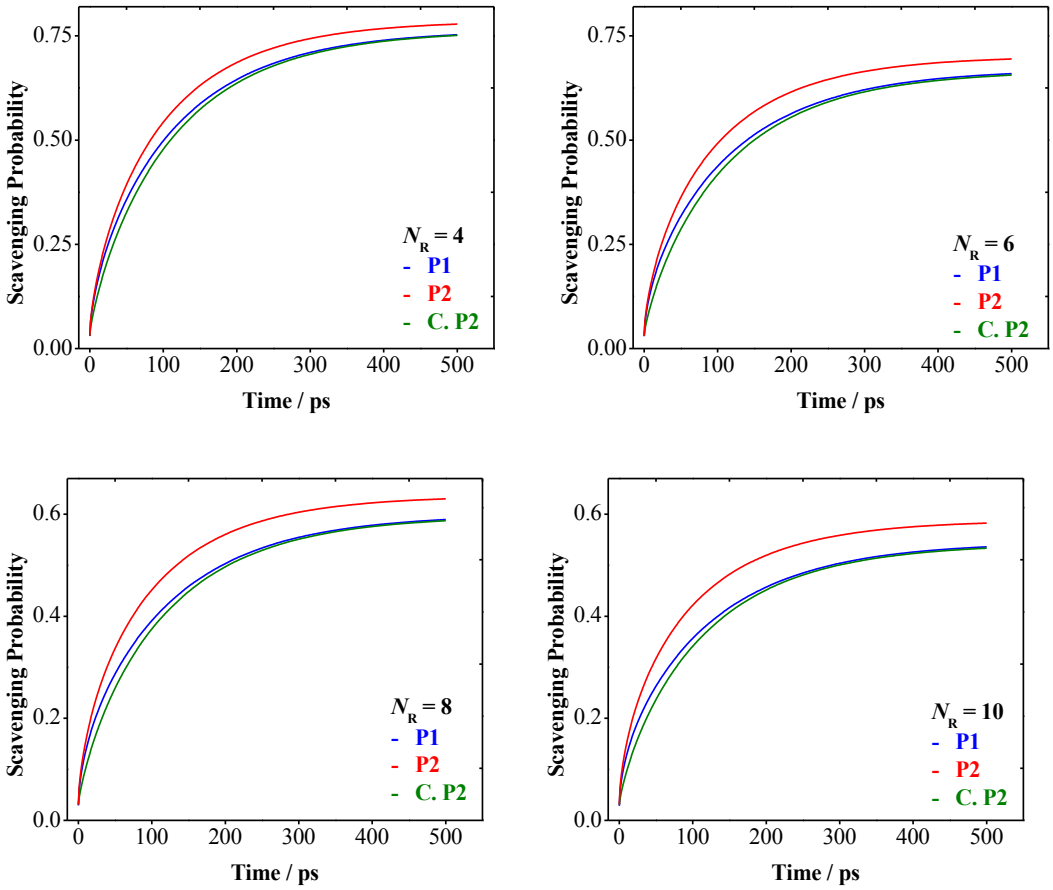


Figure 4.8. The scavenging probability in the S1 scheme. The random Flight is the simulations of P1. The P2 simulations are with the use of equation (4.7) and the C. P2 simulations are with the use of equation (4.9) with equation (4.12).

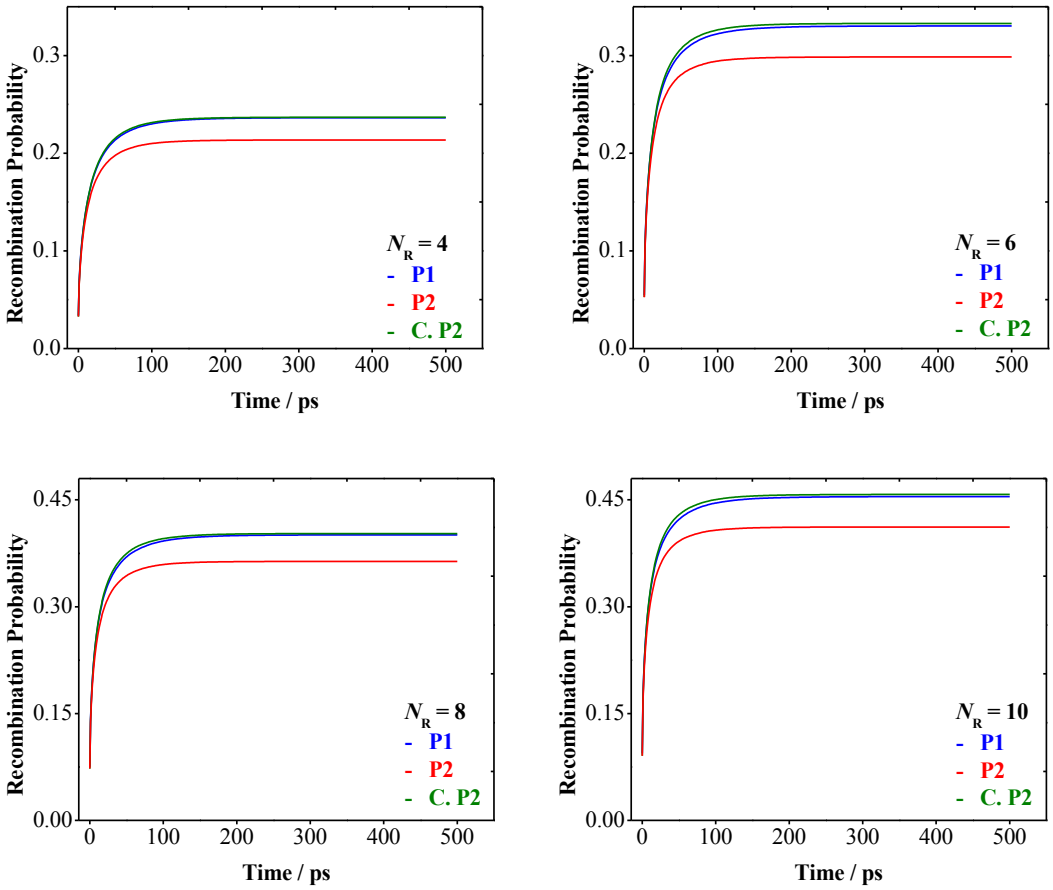


Figure 4.9. The recombination probability in the S1 scheme. The random Flight is the simulations of P1. The P2 simulations are with the use of equation (4.7) and the C. P2 simulations are with the use of equation (4.9) with equation (4.12).

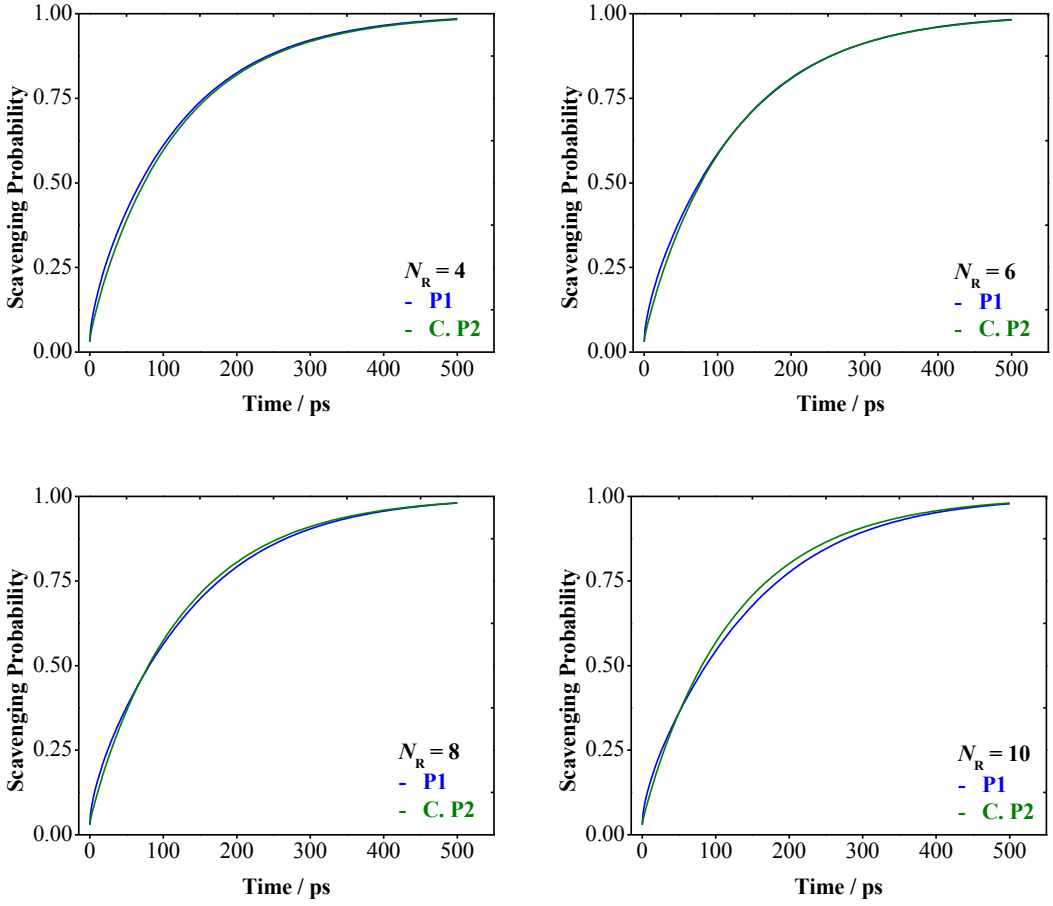


Figure 4.10. The scavenging probability in the S2 scheme. The random Flight is the simulations of P1. The C. P2 simulations are with the use of equation (4.9) with equation (4.12).

Table 4.2. The results of the simulations after including the correction. The numbers are the probability of the corresponding reaction at 500 ps. The statistical error in the numbers is ~ ±0.002. P1 refers to the RF simulations and C. P2 refers to the hybrid simulations when the proposed correction is included.

Simulations	P1			C. P2		
Reaction scheme	S1		S2	S1		S2
Reaction	R+S	R+R	R+S	R+S	R+R	R+S
N_R = 4	0.753	0.236	0.985	0.751	0.237	0.983
N_R = 6	0.658	0.330	0.983	0.656	0.333	0.981
N_R = 8	0.590	0.401	0.981	0.587	0.403	0.981
N_R = 10	0.536	0.455	0.979	0.533	0.458	0.980

4.5. More tests

4.5.1. Different distributions

All of the results that have been shown so far are for radicals whose initial coordinates generated randomly from a Gaussian distribution with mean zero and standard deviation of 10 Å. The simulation box shown in Figure 4.2 spans from −50 to +50 Å along each axis, thus over 99% of the radicals will have initial coordinates ranging between −30 and +30 Å along each axis. To test the above correction further we want to examine the effects of spreading the radicals wider so that they cover the entire simulation box. The reason for this is that we would expect competition effects caused by the overlap of concentration gradients to get smaller as the distribution gets wider. For this purpose the value of the standard deviation of the Gaussian is increased to 15 Å and the radicals coordinates will range in this case between −45 and +45 Å along each axes and the radicals will almost spread over the entire box. The results of this are shown in Figure 4.11 and Figure 4.12 for the case of 10 radicals. As the radicals spread widely, the recombination probability decreases relative to the one shown in Figure 4.9. The Smoluchowski method with the correction does not agree perfectly with the random flight simulations up to around 200 ps and then the two curves are almost on top of each other for the rest of the time. The Smoluchowski method using equation (4.7) shows good agreement with the random flight at short times, but agreement deteriorates very quickly and it clearly underestimates the recombination probability. These results might then be explained as follows: because we are using a relatively wide distribution, the radicals are relatively far from each other. Hence, for the first couple of scavenging events, the picture is rather similar to the Smoluchowski picture (isolated radicals surrounded by their own gradients of scavenger concentration) because these events take place at short times and the concentration gradients have not yet developed to a scale comparable to the interparticle distances. As more scavenging events occur, the scale of the concentration depletion extends further, the overlap of the gradients becomes more pronounced and the proposed correction becomes vital.

Another example for further testing is to use a uniform distribution. In this case, the radical coordinates are sampled from a uniform distribution (−30 to +30 Å) forming a small unit of homogenous radical solution. The corresponding scavenging

and recombination probabilities are shown in 4.13 and 4.14 respectively for the case of 10 radicals.

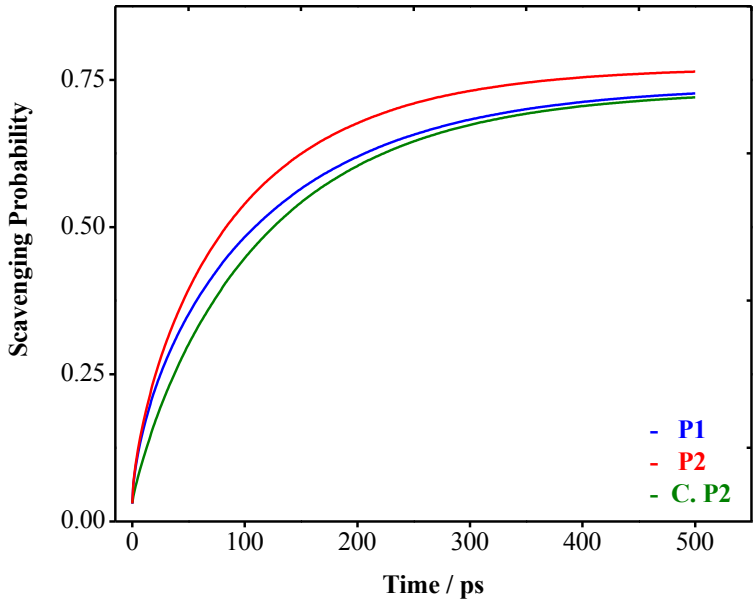


Figure 4.11. The scavenging probability in the S1 scheme. The initial distribution is Gaussian with a standard deviation of 15 Å. The notations are similar to those of Figure 4.8 and the number of radicals is 10. The values at 500 ps are 0.727(±0.002) for P1, 0.720(±0.002) for C. P2 and 0.764(±0.002) for P2.

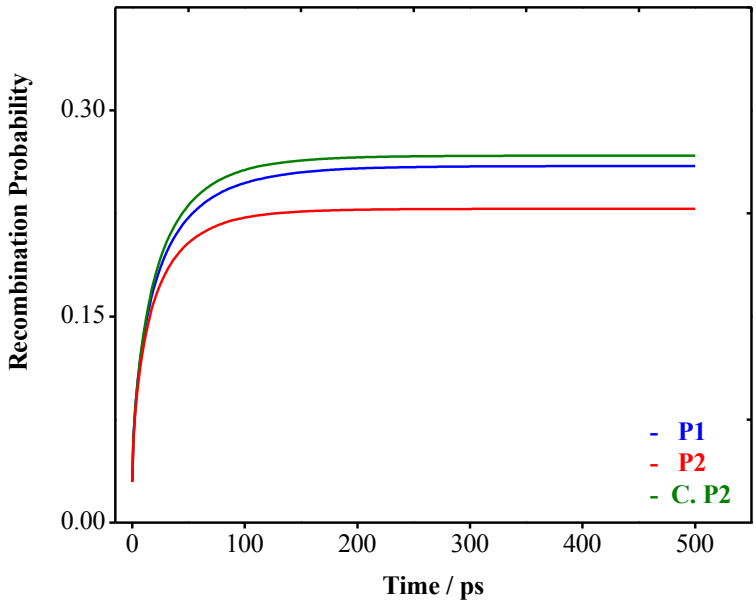


Figure 4.12. The recombination probability. The initial distribution is Gaussian with a standard deviation of 15 Å. The notations are similar to those of Figure 4.8 and the number of radicals is 10. The values at 500 ps are 0.259 (±0.002) for P1, 0.267(±0.002) for C. P2 and 0.228(±0.002) for P2.

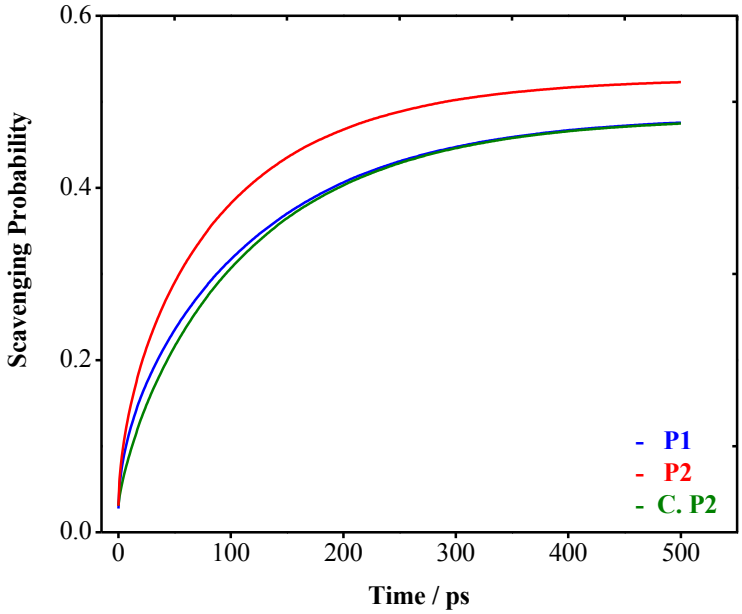


Figure 4.13. The scavenging probability in the S1 scheme. A uniform distribution is used to generate the coordinates of the radicals. The notations are similar to those of Figure 4.8 and the number of radicals is 10. The values at 500 ps are 0.476(±0.002) for P1, 0.475(±0.002) for C. P2 and 0.523 (±0.002) for P2.

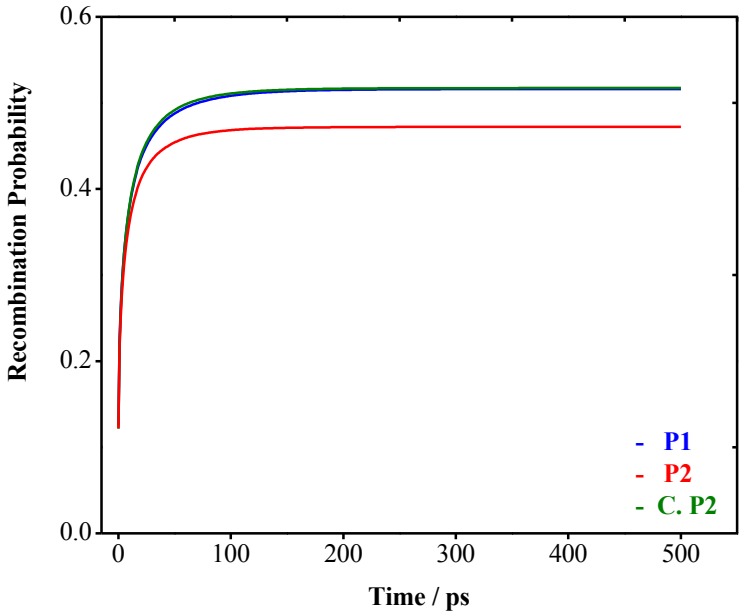


Figure 4.14. The recombination probability in the S1 scheme. A uniform distribution is used to generate the coordinates of the radicals. The notations are similar to those of Figure 4.8 and the number of radicals is 10. The values at 500 ps are 0.516(±0.002) for P1, 0.507(±0.002) for C. P2 and 0.472(±0.002) for P2.

4.5.2. The S3 scheme

So far, we have considered two simple schemes with only one type of radicals. In this section, we will consider an example where we introduce into the box two types of radicals A and B. We will consider the following possible reactions

$$\begin{aligned} A + A &\rightarrow A_2 \\ B + B &\rightarrow B_2 \\ A + B &\rightarrow AB \\ A + S &\rightarrow AS \end{aligned} \tag{4.13}$$

where only the radical A can be scavenged by S and all the reactions are assumed fully diffusion-controlled. All the particles are assumed to have the same diffusion coefficient and all the reaction distances are also the same (the same values used before). The scavenging probability is shown in Figure 4.15 and the probabilities of the other reactions are shown in Figure 4.16 where we have used three radicals of A and three radicals of B. The probability of the A+A reaction is the smallest because the reaction requires two A radicals while the other reactions of A (A+B and A+S) requires only one, and also because of the relatively high number of S particles, which makes A+S reaction the most likely one. The scavenging of an A has a large effect on the number of A+A pairs available for future recombination, for example, in the initial configuration there are 3 possible A+A pairs that can recombine, but the scavenging of just one A, reduces this to 1 pair, and if a second A is scavenged then no further A+A reaction is possible. Thus the A recombination reactions are very strongly affected by early scavenging and level off rapidly. The reaction probabilities in Figure 4.16 evolve differently in time. For A+B and A+A reactions, they rise very quickly (the first ~ 100 ps or so) and then they reach a steady limit. This is typical spur kinetics: as the radicals diffuse away from their initial configuration, they become further apart and it becomes less likely that two radicals will encounter (in particular, the main fate for the A particles in this case is the A+S reaction). Hence, most A+B and A+A reactions occur early on where the radicals are still relatively close to one another. Because the scavenger S is selective and does not react with B radicals, the probability of the reaction B+B evolves differently in time.

Finally, even for a low number of radicals (three in this example), the effects of the correction are still clear. When the correction is included, the results are in

much better agreement with the P1 simulations. This indicates that it is important to take the correction into account.

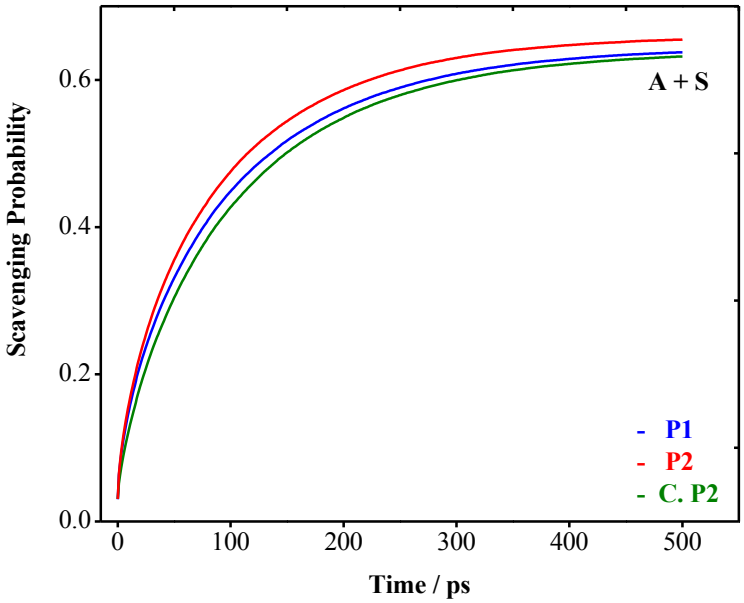


Figure 4.15. The scavenging probability in the S3 scheme. The values at 500 ps are 0.637(±0.002) for P1, 0.632(±0.002) for C. P2 and 0.655(±0.002) for P2.

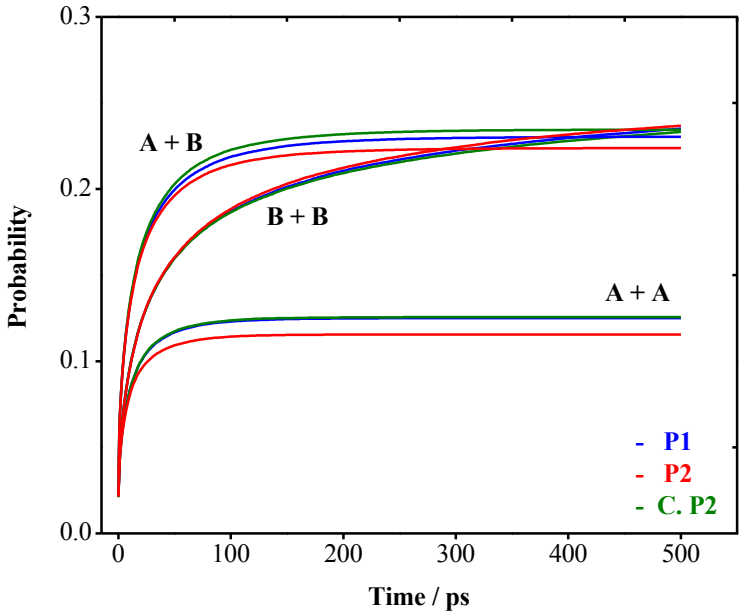


Figure 4.16. The radical-radial reaction probabilities in the S3 scheme. For A+A, the values at 500 ps are 0.125(±0.002) for P1, 0.126(±0.002) for C. P2 and 0.116(±0.002) for P2. For B+B, the values at 500 ps are 0.235(±0.002) for P1, 0.233(±0.002) for C. P2 and 0.237(±0.002) for P2. For A+B, the values at 500 ps are 0.230(±0.002) for P1, 0.235(±0.002) for C. P2 and 0.224(±0.002) for P2.

4.5.3. Different concentrations

So far we have considered one value of C_S, the scavenger concentration. In this section we will look at the effects of changing the concentration C_S. To discuss this we run simulations for $N_R = 6$ at different values for C_S (from 30 to 80 particles/10^6Å^3 in steps of 10). Examples of the results are shown in Figure 4.17 (scavenging probability for C_S = 80 particles/10^6Å^3) and Figure 4.18 (recombination probability for C_S = 80 particles/10^6Å^3). The results are summarized in Figures 4.19 and 4.20. In general, we see that when the proposed correction is included (C. P2), the agreement with the RF simulations (P1) is very good.

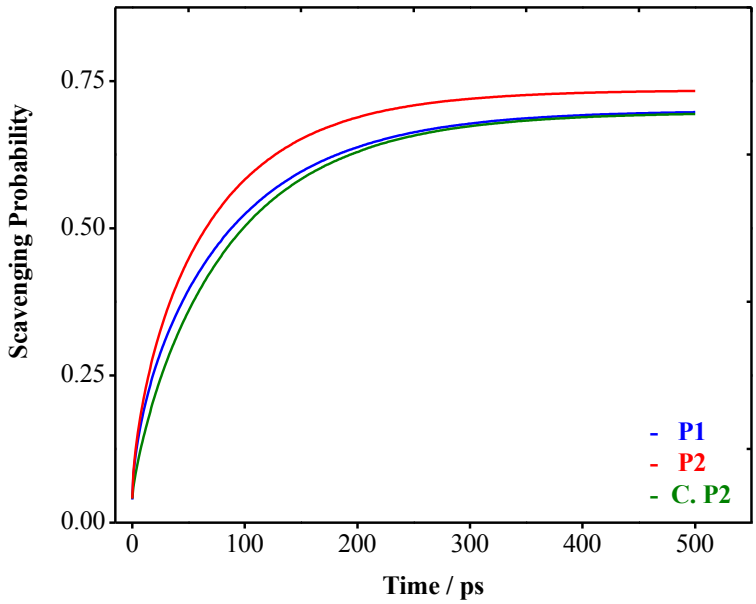


Figure 4.17. The scavenging probability for $N_R = 6$ in the S1 scheme and C_S = 80 particles/10^6Å^3.

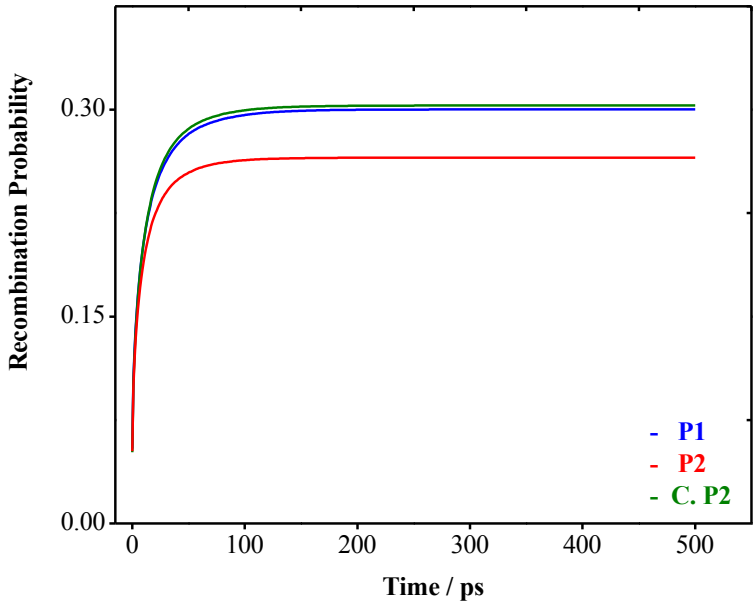


Figure 4.18. The recombination probability for $N_R = 6$ in the S1 scheme and $C_S = 80$ particles/10^6Å^3.

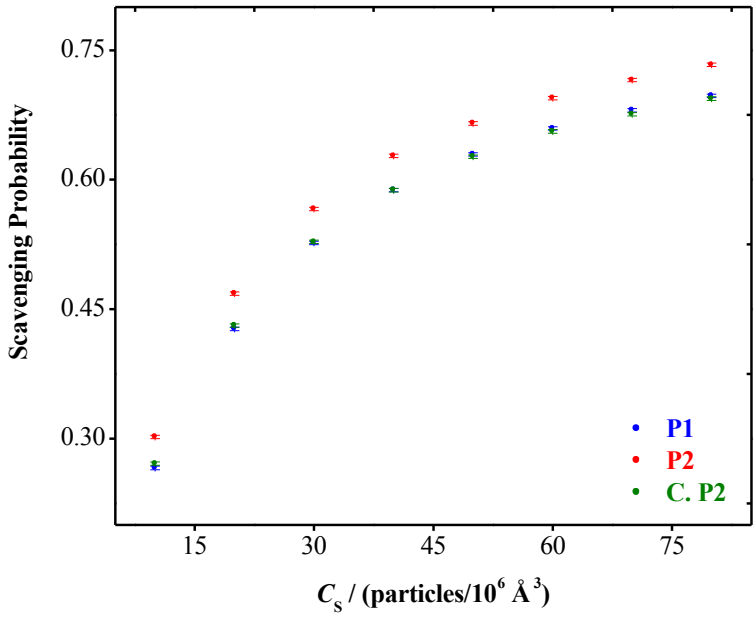


Figure 4.19. The effects of C_S on the scavenging probability in the S1 scheme. The values shown are the values at 500 ps. The number of radicals $N_R = 6$.

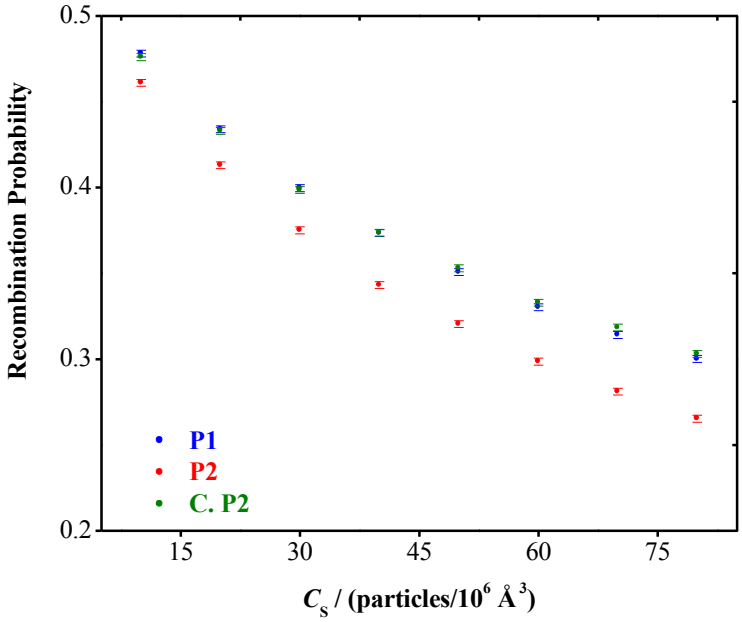


Figure 4.20. The effects of C_S on the recombination probability in the S1 scheme. The values shown are the values at 500 ps. The number of radicals $N_R = 6$.

4.6. Conclusions and future work

The rate coefficient for a fully diffusion-controlled reaction is time-dependent. Smoluchowski theory gives a formula for this dependence, under certain assumptions.[14,16] Practically, these assumptions are equivalent to having a case of an isolated radical and the problem is that in a radiation-generated spur a radical cannot normally be considered isolated from the other radicals in the spur. In this chapter we have proposed and tested a simple correction to the Smoluchowski rate constant (equation (4.9) with equation (4.12)) to include this multi-radical correlation effect and this correction seems to be a significant improvement under the conditions where the recombination and scavenging are in competition. In practice, this correction is going to be important in high LET tracks. Finally, it will be important to run more tests for this correction. The correction is expected to break down when the radical distribution is wide, but under these conditions the recombination is slow and there will be little competition between the recombination and the scavenging. It also seems that the approximation will break down at times short relative to the recombination time, when there will be little interference of the concentration gradients and the Smoluchowski theory will apply. It will also be interesting to see whether the IRT

method can reproduce or help rationalise these results, and this will be considered in the next chapters. Other future work will include cases of more than one spur, for example, and more importantly comparing the proposed correction with experimental data when possible. Since the uncorrected Smoluchowski theory works satisfactorily at short times future work might consider introducing a switching function into the correction so that the normal Smoluchowski theory operates at short times and switches smoothly to the corrected version on timescales where recombination can take place and the concentration gradients overlap.

4.7. Appendix

We will discuss here how to use the inversion method for generating random numbers to generate random scavenging times.[131] We will use the Smoluchowski rate constant given in equation (4.7) and also use the same notation as before. If we assume that the number of radicals at $t = 0$ is N_R and at time t is N, then the rate of the R+S reaction is

$$\frac{dN}{dt} = -k(t)C_S N = 4\pi a D' \left(1 + \frac{a}{\sqrt{\pi D' t}}\right) C_S N \tag{4.14}$$

which indicates that

$$\frac{N}{N_R} = e^{-C_S k_{D'}\left(t + 2a\sqrt{t/\pi D'}\right)} \qquad : \quad k_{D'} = 4\pi a D' \tag{4.15}.$$

The last ratio represents the fraction of radicals that have "survived" the R+S reaction and hence it can represent the time-dependent survival probability Ω, i.e. the probability that a radical will not react by time t. The reaction probability P is then

$$P = 1 - \Omega = 1 - e^{-C_S k_{D'}\left(t + 2a\sqrt{t/\pi D'}\right)} \tag{4.16}$$

which can be easily inverted so that we can express t as a function of P as follows

$$t = \left(\frac{-a}{\sqrt{\pi D'}} + \left(\frac{a}{\pi D'} - \frac{\ln(1-P)}{C_S k_{D'}} \right)^{1/2} \right)^2 \tag{4.17}.$$

Hence a scavenging time can be generated in the course of Monte Carlo simulations from the last equation if we replace P with a uniform random number between 0 and 1. It should be noted that when we use the proposed correction (equation (4.9) with equation (4.12)), the last equation becomes

$$t = \left(\frac{-a}{f\left(N_{\mathrm{R}}\right)\sqrt{\pi D'}} + \left(\frac{a}{\left(f\left(N_{\mathrm{R}}\right)\right)^2 \pi D'} - \frac{\ln\left(1-P\right)}{C_{\mathrm{S}} k_{D'}} \right)^{1/2} \right)^2 \tag{4.18}.$$

Finally, it should be noted that the last two equations do not include the possibility that $t = 0$, i.e. the radical will undergo a scavenging reaction immediately as it is introduced in contact with a scavenger particles. To take this into account (this approach is similar to that described in the Literature (reference 132 for example)), we assume that the number of scavengers M in the volume V follows a Poisson distribution as follows

$$\Pr\left\{M = m\right\} = \frac{\left(C_{\mathrm{S}} V\right)^m}{m!} e^{-C_{\mathrm{S}} V} \tag{4.19}.$$

The last equation will represent the zero-time survival probability Ω_0 if we set $V = 4\pi a^3/3$ and $m = 0$, and hence the zero-time reaction probability P_0 is

$$P_0 = 1 - \Omega_0 = 1 - e^{-4\pi a^3 C_{\mathrm{S}}/3} \tag{4.20}$$

which can be used in the simulation with a uniform random number between 0 and 1 to determine if the scavenging time is zero.

Chapter 5

Scavenging and Recombination Kinetics II: IRT Theory[§§]

"If you are receptive and humble, mathematics will lead you by the hand." ***Paul Dirac***

One of the strengths of the Independent Reaction Time (IRT) theory is that, in some cases, it can give an analytic solution to the problem of interest. This is because the independence approximation tends to substantially simplify the mathematics of the problem. For example, the time-dependent Smoluchowski rate constant (equation (4.7)) can be derived using the IRT method (this will be discussed in more detail shortly). Furthermore, when applied to a system of two closely spaced radicals in the presence of a scavenger, the IRT model predicts a correction to equation (4.7) (this will also be discussed in more detail shortly).[17] This poses some interesting questions. Can the correction proposed in the last chapter (equations (4.9) and (4.12)) be obtained or justified based on the IRT theory? Is there a way to build IRT simulations similar to those presented in the last chapter? Will the results of these simulations agree with the results of the last chapter? This chapter is intended to look into and answer the above questions.

[§§] **Acknowledgements and details**: The mathematics in sections 5.1 and 5.2 are in the literature (reference 17 and references therein, for example). The mathematics of the general case (section 5.3) was obtained by E. Al-Samra. The asymptotic treatment in equation (5.34) was inspired by N. Green (he originally proposed an asymptotic treatment for equation (5.25), and the idea is similar). N. Green also showed how to derive equation (5.47).

5.1. The Smoluchowski rate constant

As mentioned above, the Smoluchowski rate constant, given in equation (4.7), can actually be obtained using the IRT theory (the method is described in the literature).[17] The starting point is to consider the case of having one radical R and one scavenger S separated by a distance r. The survival probability for the pair is given in equation (3.63). If we assume that the particles are neutral and that their reaction distance is a, we can use equation (2.43) in equation (3.63) to obtain[6]

$$\Omega_{\text{pair}}\left(t,r;a\right)=1-\frac{a}{r}\text{erfc}\left(\frac{r-a}{\sqrt{4D't}}\right) \tag{5.1}$$

where D' is the relative diffusion coefficient and erfc is the complementary error function.

The next step is to consider the case where we have the radical R at the centre of a sphere of radius Q, and the single scavenger molecule S has a probability density that is spread uniformly inside that sphere. In that case, the survival probability will have the following known form[10,17,129,132,134]

$$\Omega_{\text{pair}}=\frac{1}{V}\int_a^Q\int_0^\pi\int_0^{2\pi}\left[1-\frac{a}{r}\text{erfc}\left(\frac{r-a}{\sqrt{4D't}}\right)\right]r^2\sin\theta\,dr\,d\theta\,d\varphi \tag{5.2}$$

where V is the volume of the sphere of radius Q and so we have

$$\Omega_{\text{pair}}=\frac{4\pi}{V}\int_a^Q\left[1-\frac{a}{r}\text{erfc}\left(\frac{r-a}{\sqrt{4D't}}\right)\right]r^2dr \tag{5.3}.$$

The last integral can be easily evaluated. A simple method is take the Laplace transforms, of both sides with respect to time, as follows[161]

$$\ell\left(\Omega_{\text{pair}}\right)=\frac{4\pi}{V}\int_a^Q\left(\frac{r^2}{p}-\frac{ar}{p}e^{-\left(r-a\right)\sqrt{p/D'}}\right)dr \tag{5.4}$$

where

$$\ell\left(\Omega_{\text{pair}}\right)=\int_0^\infty\Omega_{\text{pair}}\,e^{-pt}\,dt \tag{5.5}.$$

Calculating the integral of equation (5.4) is straightforward and we have

$$\ell\left(\Omega_{\text{pair}}\right)=\frac{4\pi}{pV}\left[\frac{Q^3}{3}-\frac{a^3}{3}-a\left(a\sqrt{\frac{D'}{p}}+\frac{D'}{p}\right)+a\left(Q\sqrt{\frac{D'}{p}}+\frac{D'}{p}\right)e^{-(Q-a)\sqrt{p/D'}}\right] \tag{5.6}$$

Taking the inverse Laplace transform of the last equation and ignoring the last term, because we are interested in the case where Q is infinitely large where the final term tends to zero exponentially, gives[154]

$$\Omega_{\text{pair}}=\frac{4\pi}{3V}\left(Q^3-a^3-6a^2\sqrt{\frac{D't}{\pi}}-3aD't\right) \tag{5.7}$$

The number of scavengers in the sphere of radius Q (which so far has been considered to be one) is an integer random variable N which follows a Poisson distribution, to a good approximation, as follows[17]

$$\Pr\left\{N=n\right\}=\frac{\left(C_{\text{S}}V\right)^n}{n!}e^{-C_{\text{S}}V} \tag{5.8}$$

where C_{S} is the concentration of S. Assuming that each radical-scavenger pair evolves independently, the survival probability is

$$\Omega=\sum_n\frac{\left(C_{\text{S}}V\right)^n}{n!}e^{-C_{\text{S}}V}\Omega_{\text{pair}}^n \tag{5.9}$$

and hence

$$\Omega=e^{\frac{-4\pi a^3C_{\text{S}}}{3}}\times e^{-4\pi aD'C_{\text{S}}\left(t+2a\sqrt{\frac{t}{\pi D'}}\right)} \tag{5.10}$$

The first term in the last equation represents the probability of surviving "zero-time" reaction, i.e. the probability that the radical does not overlap a scavenger in the initial configuration. The second term is the kinetics decay of the survival probability of the radical. If we use the well-known relationship between the time-dependent rate constant k and the survival probability Ω as follows[6,17]

$$k\left(t\right)=-\frac{1}{C_{\text{S}}}\frac{d\left(\ln\Omega\right)}{dt} \tag{5.11}$$

we obtain

$$k\left(t\right)=4\pi aD'\left(1+\frac{a}{\sqrt{\pi D't}}\right) \tag{5.12}$$

as required.

5.2. The predicted correction

As mentioned before, the IRT theory predicted a correction for the last equation when considering the scavenging reaction of two proximate radicals.[17] The interpretation of the predicted correction in that study was that the correction is for the first of the two scavenging events. Because of its importance, we will summarize it here. We will continue using the same notation as the last section. Consider the case of two radicals and one scavenger where the two distances R-S are equal (denoted r) and where the only possible reaction is R+S. Following the same method as the last section, the probability that no reaction has happened by time t (the probability that the two radicals have survived by a time t (Ω_{RR})) is

$$\Omega_{RR} = \frac{4\pi}{V}\int_a^Q \left[1-\frac{a}{r}\operatorname{erfc}\left(\frac{r-a}{\sqrt{4D't}}\right)\right]\left[1-\frac{a}{r}\operatorname{erfc}\left(\frac{r-a}{\sqrt{4D't}}\right)\right] r^2 dr \qquad (5.13)$$

where, as in the last section, Q is the radius of a sphere containing the system and V is the volume of that sphere. It should be noted that in the above-mentioned study (reference 17), different times were used in the complementary error functions (t and u). This is because that study was looking at few possibilities where one scavenger could react with more than one radical. In our case this is not important and we are only interested in the case where the scavenger reacts with only one radical and that is why we have used only one time t. The result of the last equation is (where again we are interested in the case of infinitely large Q, and keep terms of order $1/V$ because of the Poisson weighting to be applied in equation (5.16))[17]

$$\Omega_{RR} = 1-\frac{4\pi a^3}{3V}-\frac{8\pi aD't}{V}-\frac{8\pi a^2}{V}\sqrt{\frac{2D't}{\pi}} \qquad (5.14).$$

If we follow the same procedures of the last section where we assume that the number of scavengers in the volume V follows a Poisson distribution and that the pairs are independent, we have

$$\Omega = \sum_n \frac{\left(C_S V\right)^n}{n!} e^{-C_S V}\Omega_{RR}^n \qquad (5.15)$$

and so

$$\Omega = e^{-C_S V\left(1-\Omega_{RR}\right)} \tag{5.16}.$$

Now if we use equation (5.11) and realize that we have started from two radicals (hence we divide the answer by a factor of two), we have the following result[17]

$$k_c\left(t\right) = 4\pi a D'\left(1+\frac{a}{\sqrt{2\pi D' t}}\right) \tag{5.17}.$$

This result is important. In chapter 4, the correction factor f (equation (4.12)) suggested for the case of two radicals has the value of 1.5, which is in good agreement with the last equation, in which it has the value of $\sqrt{2}$.

5.3. General case

It is now interesting to see if the correction to the Smoluchowski rate coefficient (equations (4.9) and (4.12)) can be justified using the method of the last two sections, where we consider a system of N_R radicals. We will continue to use the same notations above and assume that only the reaction R+S can occur. If we start from one scavenger molecule S and consider that all the distances R-S are equal (denoted r as before), then for each R-S pair the survival probability Ω_{pair} is given in equation (5.1). The probability that all the radicals have survived by time t is given as follows

$$\Omega_{N_R} = \frac{4\pi}{V}\int_a^\infty \Omega_{pair}^{N_R} r^2\, dr = \frac{\eta}{V} \tag{5.18}$$

where

$$\eta = 4\pi\int_a^\infty \Omega_{pair}^{N_R} r^2\, dr \tag{5.19}.$$

If we assume that we have M scavenger particles in the spherical volume V (where, as before, we assumed that the radius of the spherical volume is infinitely large when writing the last two equations) and use the Poisson distribution (equation (5.8)), we have the following expression for the total survival probability Ω

$$\Omega = \sum_M \frac{\left(C_S V\right)^M}{M!} e^{-C_S V}\left(\frac{\eta}{V}\right)^M = e^{-C_S\left(V-\eta\right)} \tag{5.20}.$$

The time-dependent rate constant k is then given as follows

$$\frac{d\ln\Omega}{dt} = -k(t) N_{\mathrm{R}} C_{\mathrm{S}} \tag{5.21}$$

and hence

$$k(t) = -\frac{1}{N_{\mathrm{R}}}\frac{d\eta}{dt} = -\frac{4\pi}{N_{\mathrm{R}}}\frac{d}{dt}\int_a^\infty \Omega_{\mathrm{pair}}^{N_{\mathrm{R}}} r^2\, dr \tag{5.22}.$$

If we use equation (5.1), we obtain the following

$$k(t) = 4\pi a \int_a^\infty \frac{r-a}{\sqrt{4\pi D' t^3}} e^{-(r-a)^2/4D't} \left[1 - \frac{a}{r}\mathrm{erfc}\left(\frac{r-a}{\sqrt{4D't}}\right)\right]^{N_{\mathrm{R}}-1} r\, dr \tag{5.23}.$$

If we introduce the following two variables

$$x = \frac{r-a}{\sqrt{4D't}} \quad , \quad \alpha = \frac{a}{\sqrt{4D't}} \tag{5.24},$$

we can write equation (5.23) in the following simpler form

$$k(t) = 4\pi a D' \frac{4}{\sqrt{\pi}} \int_0^\infty x(x+\alpha) e^{-x^2} \left[1 - \frac{\alpha}{\alpha + x}\mathrm{erfc}(x)\right]^{N_{\mathrm{R}}-1} dx \tag{5.25}.$$

Unfortunately, this integral seems to be unknown in general.[149,150,162] However, it is useful to write it in the following form

$$\begin{aligned} k(t) = 4\pi a D' \frac{4}{\sqrt{\pi}} \Bigg\{ & \int_0^\infty x^2 e^{-x^2}\, dx + \alpha \int_0^\infty x\, e^{-x^2}\, dx - \\ & \alpha \int_0^\infty x\, e^{-x^2} \left[\sum_{m=1}^{N_R - 1} \frac{(N_R - 1)!}{(N_R - m - 1)!\, m!} \left(\frac{-\alpha}{\alpha + x}\right)^{m-1} \left(\mathrm{erfc}(x)\right)^m \right] dx \Bigg\} \end{aligned} \tag{5.167}.$$

The first two integrals are known and simple to evaluate.[162] They are respectively $\sqrt{\pi}/4$ and 1/2. Hence we have

$$k(t) = 4\pi a D' \left\{ 1 + \frac{4\alpha}{\sqrt{\pi}} \left(\frac{1}{2} - I_{N_R} \right) \right\} \tag{5.26}$$

where

$$I_{N_{\mathrm{R}}} = \int_0^\infty x\, e^{-x^2} \left[\sum_{m=1}^{N_{\mathrm{R}}-1} \frac{(N_R - 1)!}{(N_R - m - 1)!\, m!} \left(\frac{-\alpha}{\alpha + x}\right)^{m-1} \left(\mathrm{erfc}(x)\right)^m \right] dx \tag{5.27}$$

or

$$I_{N_R} = \sum_{m=1}^{N_R-1}\left\{\frac{(N_R-1)!}{(N_R-m-1)!m!}\int_0^{\infty}\left[x\left(\frac{-\alpha}{\alpha+x}\right)^{m-1}e^{-x^2}\left(\operatorname{erfc}(x)\right)^m dx\right]\right\} \qquad (5.28).$$

Now if we use the expression for the variable α in equation (5.26) we get

$$k(t) = 4\pi a D'\left\{1+\frac{a}{\sqrt{\pi D' t}}\left(1-2I_{N_R}\right)\right\} \qquad (5.29)$$

which explicitly points out, if we compare it with the Smoluchowski rate coefficient (equation (4.7)), that the time-dependent term (or the transient part) of the rate coefficient is always a function of N_R, the number of radicals at the start of the reaction , and that the steady-state rate constant is unaffected. It is worth noticing that the above equation includes the two cases (N_R = 1 and N_R = 2) discussed before. Simply equation (5.28) vanishes for N_R = 1 and for N_R = 2 we have the following known integral[162]

$$I_2 = \int_0^{\infty} x e^{-x^2}\operatorname{erfc}(x)\,dx = \frac{1}{2}\left(1-\frac{1}{\sqrt{2}}\right) \qquad (5.30)$$

which if used in the above expression for $k(t)$ gives equation (5.17).

However, it is possible to evaluate equation (5.28) numerically. To discuss this, we have set, for example, α = 5 (other values will be discussed shortly) and then varied N_R between 3 and 12. We then tried to find a function that produces a good fit. The following function

$$\psi(N_R) = c_1 + \frac{c_2}{N_R+1} \qquad (5.31)$$

gives the desired result as shown in Figure 5.1 where c_1 = 0.524 and c_2 = −1.206 with a determining coefficient of R^2 = 0.997, and hence we can write

$$I_{N_R} \approx \psi(N_R) = c_1 + \frac{c_2}{N_R+1} \qquad (5.32).$$

Now if we use the following approximate values $c_1 \approx 0.5$ and $c_2 \approx -1$ in the last equation and then put the result in equation (5.29), we get the correction proposed in the last chapter (equations (4.9) and (4.12)) and hence this justifies the choice for the correction. Finally, it is important to check whether or not the fitting described above changes as we change the value of α. The fitting for the case α = 15 (where c_1 = 0.4911 and c_2 = −1.079 with R^2 =0.999) is shown in Figure 5.2, and similarly when α

= 25 we have $c_1 = 0.4842$ and $c_2 = -1.053$ with $R^2 = 0.999$ (Figure 5.3). Hence, we can draw, in both cases, the same conclusion as we did in the case $\alpha = 5$ above, i.e. we use the following approximate values $c_1 \approx 0.5$ and $c_2 \approx -1$ in equation (5.32) and then put the result in equation (5.29) to get the correction proposed in the last chapter (equations (4.9) and (4.12)). The overall conclusion is that the results presented here justify the choice for the correction made in the last chapter.

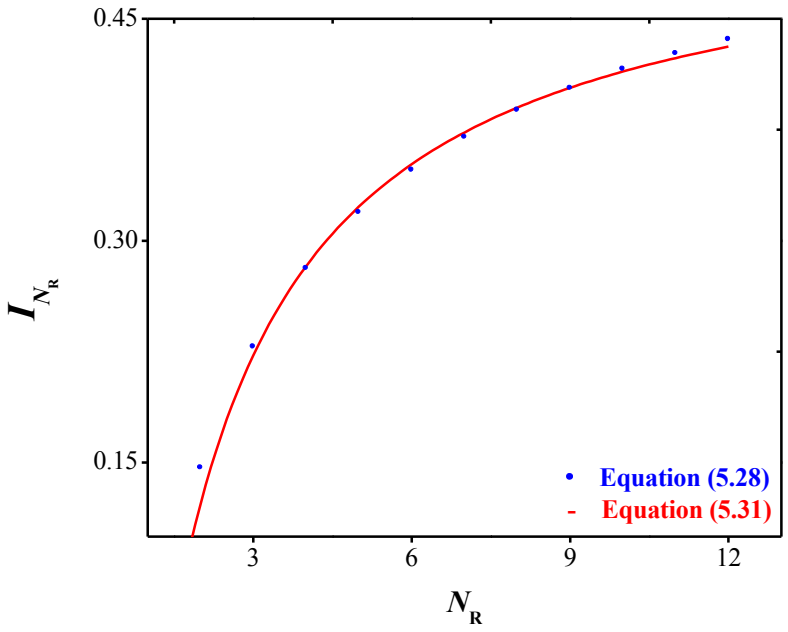


Figure 5.1. The fitting of equation (5.28) as a function of N_R. We used $\alpha = 5$. The determining coefficient $R^2 = 0.998$.

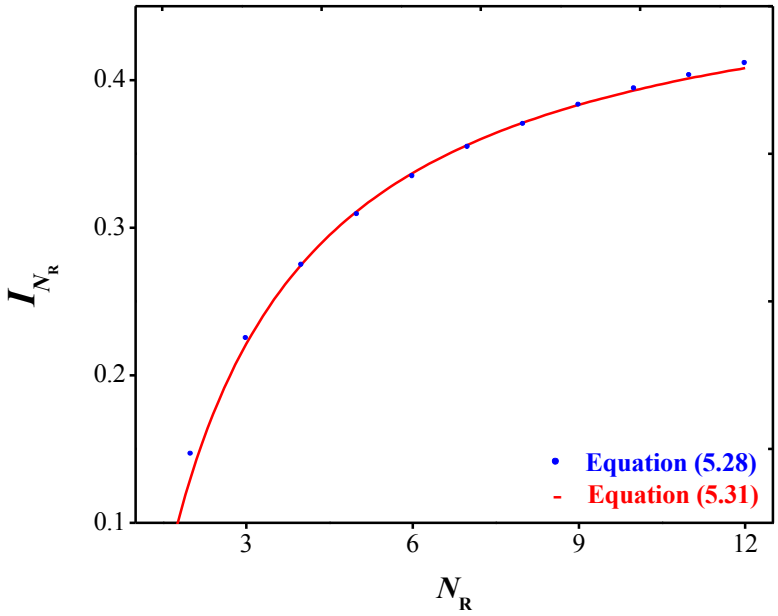


Figure 5.2. The fitting of equation (5.28) as a function of N_R. We used α = 15. The determining coefficient R^2 = 0.999.

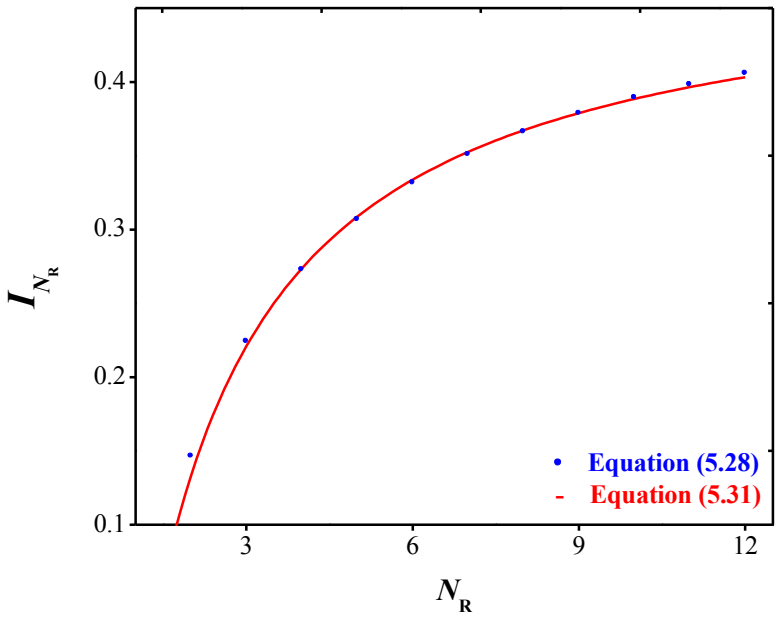


Figure 5.3. The fitting of equation (5.28) as a function of N_R. We used α = 25. The determining coefficient R^2 = 0.999.

There is a mathematical reason why the integral of equation (5.28) (or the equivalent equation (5.27)) does not vary much with the value of α, which will be discussed here. First, it should be noted that we are particularly interested in the

region where the time-dependent part of the rate constant is large (from equation (5.29), this corresponds to very small times $t \to 0$, and hence α is very large $\alpha \to \infty$). Otherwise the steady-state part (or the time-independent part) will dominate the rate constant (again equation (5.29)) and it will be difficult to obtain any information about (or in other words, resolve) the time-dependent part, which we are trying to examine. We now use equation (5.27) and write the integrand as follows

$$g_\alpha(x) = x e^{-x^2} \sum_{m=1}^{N_R-1} \frac{(N_R-1)!}{(N_R-m-1)!m!} \left(\frac{-\alpha}{\alpha+x}\right)^{m-1} \left(\text{erfc}(x)\right)^m \qquad (5.33).$$

This function is shown in Figure 5.4 for a few values of α where $N_R = 4$. The shape of the function does not change with α, and only the height of the peak changes slightly from one value to the other. Furthermore, the function decays to zero very quickly and hence the region of importance when considering the integral in equation (5.27) is when x is small (most of the area under the curve is between $x = 0$ and $x \approx 1$). Bearing this in mind and realizing that, as discussed above, that we are interested in the case of large α we write equation (5.27) in the following asymptotic form

$$I_{\substack{N_R \\ \alpha \uparrow \infty}} = \int_0^\infty x e^{-x^2} \left[\sum_{m=1}^{N_R-1} (-1)^{m-1} \frac{(N_R-1)!}{(N_R-m-1)!m!} \left(\text{erfc}(x)\right)^m \right] dx \qquad (5.34)$$

which indicates that the integral does not depend on α when it is large.

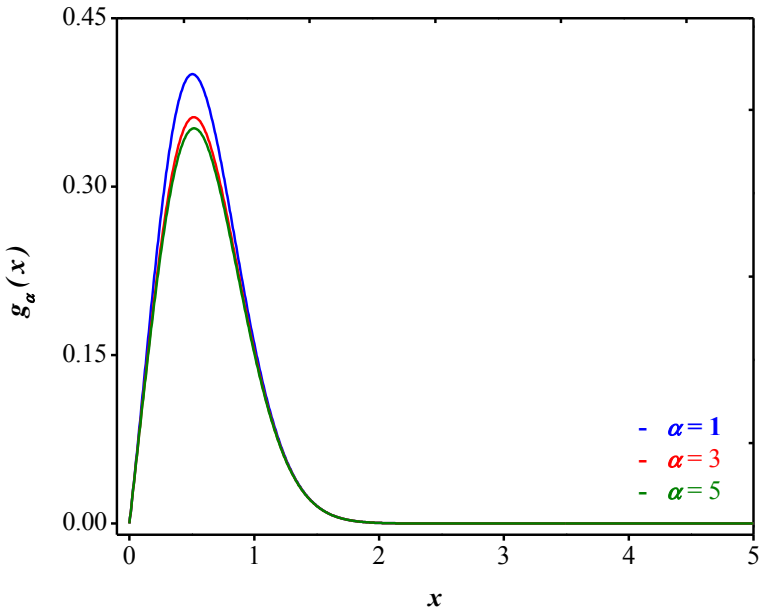


Figure 5.4. The integrand in equation (5.27). A few values of α are included. The peak is localized at small values of x and it drops to zero very quickly as x gets larger. The number of radicals, $N_R = 4$.

5.4. The simulation method

The difficulty in building up IRT simulations similar to those of the last chapter is the "images of scavengers" in region II in Figure 4.2. If the images of scavengers are ignored, the scavenging probability will be smaller than expected. Trying to include them makes the simulation program very complicated and we could not find a straightforward way to include them in that sense. As distances further and further away are considered, the simulation becomes rapidly more expensive for little gain because the reaction probabilities become much smaller and the effect on the short-term transient kinetics is negligible. The simplest way to overcome this difficulty is to assume spherical symmetry for the problem where we have two spheres that share the same centre. The small sphere is inscribed in the simulation box of Figure 4.2 (its radius b is half of the box edge) and contains the radicals as well as most of the real scavengers that are in the box (this is shown in Figure 5.5). The large sphere has a radius Q that is assumed to be infinitely large. Hence the volume between the two spheres contains the images of scavengers. The idea is to treat this region as "a continuum" region, calculate the probability that a radical gets scavenged by this continuum region and then incorporate that in the simulations.

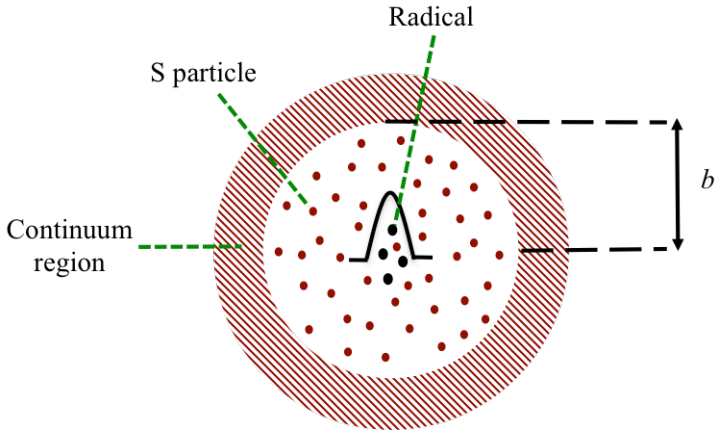


Figure 5.5. The plan for IRT simulations. The inner sphere contains the radicals and the scavenger molecules and the radius b is equal to half of the edge of the simulation box shown in Figure 4.2. The radius of the continuum region is infinitely large.

5.4.1. Scavenging probability with the continuum

Consider a radical R at some point *J* separated by a distance *z* from the center of a sphere with the radius *b*. Outside the sphere we have a scavenger S that is spread out with a radial distribution function *g* that satisfies the following

$$g(r)=\begin{cases}0 & : r<b\\ 1 & : b\le r\le Q\end{cases} \tag{5.35}$$

where *Q* is the radius of the large sphere (with a volume *V*) and as discussed above *Q* is very large. If we assume that the S particle has the polar spherical coordinate *r*, θ and φ, then the distance R-S is

$$q=\sqrt{r^2+z^2-2rz\cos\theta} \tag{5.36}.$$

The next step is consider the survival probability of the pair R-S which is as follows[10,17,129,132,134]

$$\Omega_{\text{pair}}=\frac{1}{V}\int_0^Q\int_0^\pi\int_0^{2\pi} g(r)\left[1-\frac{a}{q}\operatorname{erfc}\left(\frac{q-a}{\sqrt{4D't}}\right)\right] r^2\sin\theta\, dr\, d\theta\, d\varphi \tag{5.37}$$

where the distribution function *g* guarantees that the integral excludes the values between zero and *b* (this of course includes the reaction distance *a* since *b* is very large compared to *a*) and

$$V=4\pi\int_0^Q r^2\, g(r)\, dr=4\pi\int_b^Q r^2\, dr=\frac{4}{3}\pi\left(Q^3-b^3\right) \tag{5.38}$$

and so we have

$$\Omega_{\text{pair}}=\frac{2\pi}{V}\int_b^Q\int_0^\pi\left[1-\frac{a}{q}\operatorname{erfc}\left(\frac{q-a}{\sqrt{4D't}}\right)\right] r^2\sin\theta\, dr\, d\theta \tag{5.39}.$$

Applying the same procedures as in the last sections (the Poisson distribution and the independence of pairs), we have

$$\Omega=\sum_n\frac{\left(C_S V\right)^n}{n!}e^{-C_S V}\Omega_{\text{pair}}^n=e^{-C_S V}e^{C_S V\Omega_{\text{pair}}} \tag{5.40}.$$

A quantity of interest is the time-dependent rate constant of the scavenging with the continuum region and it can be obtained using equation (5.11) as follows[6,17]

$$k_b(t)=2\pi\frac{d}{dt}\int_b^Q\int_0^\pi\left[1-\frac{a}{q}\operatorname{erfc}\left(\frac{q-a}{\sqrt{4D't}}\right)\right] r^2\sin\theta\, dr\, d\theta \tag{5.41}.$$

Performing (*d/dt*) and then taking the Laplace transform of the result with respect to *t* give[161]

$$\ell\left(k_b(t)\right) = 2\pi \int_b^Q \int_0^\pi \frac{a}{q} e^{-(q-a)\sqrt{p/D'}} r^2 \sin\theta \, d\theta \, dr \tag{5.42}$$

where *p* is the Laplace transform variable. Now changing the variable using equation (5.36) gives

$$\ell\left(k_b(t)\right) = \frac{2\pi a}{z} \int_b^Q \int_{r-z}^{r+z} e^{-(q-a)\sqrt{p/D'}} r \, dq \, dr \tag{5.43}.$$

If we apply the limit where *Q* is infinitely large, we have

$$\ell\left(k_b(t)\right) = 4\pi a \frac{\sinh\left(z\sqrt{p/D'}\right)}{z\sqrt{p/D'}} \left(b\sqrt{\frac{D'}{p}} + \frac{D'}{p} \right) e^{-(b-a)\sqrt{p/D'}} \tag{5.44}.$$

It should be noted that for the special case when the radical R is at the center of the sphere ($z \to 0$) the last equation becomes

$$\ell\left(k_{b,z=0}(t)\right) = 4\pi a \left(b\sqrt{\frac{D'}{p}} + \frac{D'}{p} \right) e^{-(b-a)\sqrt{p/D'}} \tag{5.45}$$

which after taking the inverse of the Laplace transform gives[154]

$$k_{b,z=0}(t) = 4\pi a D' \left[\operatorname{erfc}\left(\frac{b-a}{\sqrt{4D't}} \right) + \frac{b}{\sqrt{\pi D' t}} e^{-(b-a)^2/4D't} \right] \tag{5.46}.$$

More importantly, taking the inverse of the Laplace transform of equation (5.44) (the general case) gives[154]

$$k_b(t) = \frac{2\pi a D'}{z} \left[(z+a)\operatorname{erfc}\left(\frac{b-z-a}{\sqrt{4D't}} \right) + (z-a)\operatorname{erfc}\left(\frac{b+z-a}{\sqrt{4D't}} \right) + \sqrt{\frac{4D't}{\pi}} \left(e^{-(b-z-a)^2/4D't} - e^{-(b+z-a)^2/4D't} \right) \right] \tag{5.47}.$$

If we use equation (5.11) again, we can write *H*, the probability of scavenging with the continuum, as follows[6,17]

$$H(t) = 1 - \Omega(t) = 1 - e^{-C_S \int_0^t k_b(t) dt} = 1 - e^{-C_S I(t)} \tag{5.48}$$

where

$$I(t)=\int_0^t k_b(t)\,dt=\frac{2\pi a}{z}\left(\chi+\delta+\varepsilon+\kappa\right) \tag{5.49}$$

where χ, δ, ε and κ are functions of time and given as follows

$$\chi=\left[bD't+\left[-D't+\frac{1}{3}\left(b+\frac{1}{2}(z+a)\right)\right](b-z-a)\right](b-z-a)\times\operatorname{erfc}\left(\frac{b-z-a}{\sqrt{4D't}}\right) \tag{5.50}$$

$$\delta=\left[-bD't+\left[D't+\frac{1}{3}\left(-b+\frac{1}{2}(z-a)\right)\right](b+z-a)\right](b+z-a)\times\operatorname{erfc}\left(\frac{b+z-a}{\sqrt{4D't}}\right) \tag{5.51}$$

$$\varepsilon=\frac{1}{3}\sqrt{\frac{D't}{\pi}}\left[4D't-(2b+z+a)(b-z-a)\right]e^{-(b-z-a)^2/4D't} \tag{5.52}$$

$$\kappa=\frac{1}{3}\sqrt{\frac{D't}{\pi}}\left[-4D't+(2b-z+a)(b+z-a)\right]e^{-(b+z-a)^2/4D't} \tag{5.53}.$$

Unfortunately, as it is clear from the above expression for the probability function $H(t)$, it can not be straightforwardly inverted (as was done in equation (3.1)) so that reaction times can be generated from it. Therefore, we have to look at other possibilities. Consider the probability density function $h(t)$ given as follows

$$h(t)=\frac{d}{dt}H(t)=C_S\,k_b(t)\,e^{-C_S\int_0^t k_b(t)\,dt}=C_S\,k_b(t)\,e^{-C_S\,I(t)} \tag{5.54}.$$

Fortunately, if we plot this function (Figure 5.6 shows the function for a few values of z where b = 50 Å, a = 5 Å, $C_S = 6\times10^{-5}$ particles/Å^3 and D' = 2 Å^2.ps^{-1} where these values are consistent with the values of the last chapter), it looks very similar to a gamma probability density function. After several attempts, the following function

$$\psi_{\alpha\beta\gamma}(t)=\frac{1}{\beta^\alpha\Gamma(\alpha)}(t-\gamma)^{\alpha-1}e^{-(t-\gamma)/\beta} \tag{5.55}$$

where Γ is the gamma function (equation (1.69)) was found to produce an excellent fit as shown in Figure 5.7 (the determining coefficient R^2 is 0.999). The only remaining step is to determine how the coefficients (α, β and γ) vary with the variable z. Fortunately, the three coefficients were found to follow second-order polynomial fits with z as follows

$$\lambda = \rho z^2 + \sigma z + \varsigma \tag{5.56}$$

where λ is α, β or γ. The fitting for α is shown in Figure 5.8 and for β and γ in Figures 5.9 and 5.10 respectively. The results of the fitting are summarized in Table 5.1. Now that all of this is resolved, we can use the appropriate gamma distribution to generate scavenging times with the continuum region. This will be described in more detail next as we discuss the simulation program.

Table 5.1. The fitting of α, β and γ as a function of z where the values of b, a and D' are respectively 50 Å, 5 Å and 2 Å^2.ps^{-1}. The scavengers concentration is $C_S = 6\times10^{-5}$ particles/Å^3.

	ρ	σ	ς	R^2
α	-9×10^{-4}	6.9×10^{-3}	2.612	0.999
β	0.02078	-0.1394	105.4	0.999
γ	-0.02066	-0.7044	46.21	0.999

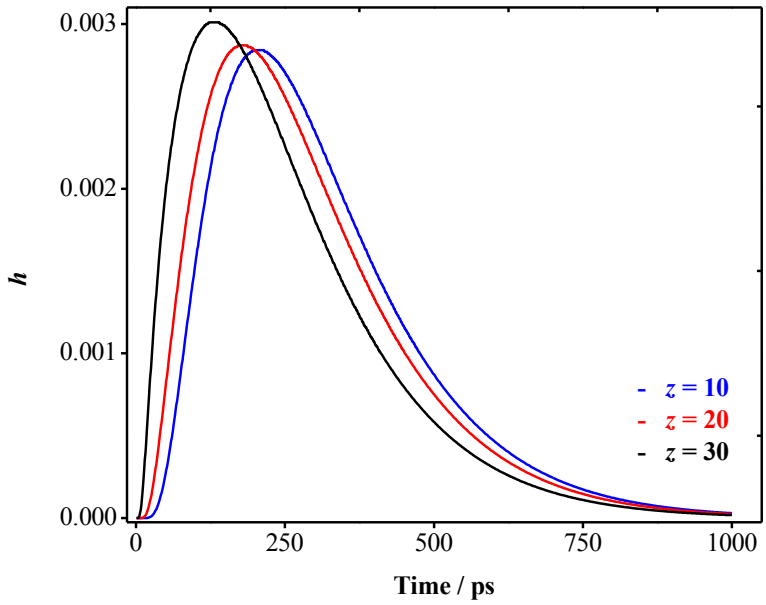


Figure 5.6. The probability density function for a few values of z (Å). We used b = 50 Å, a = 5 Å and D' = 2 Å^2.ps^{-1} where these values are consistent with the values of the last chapter.

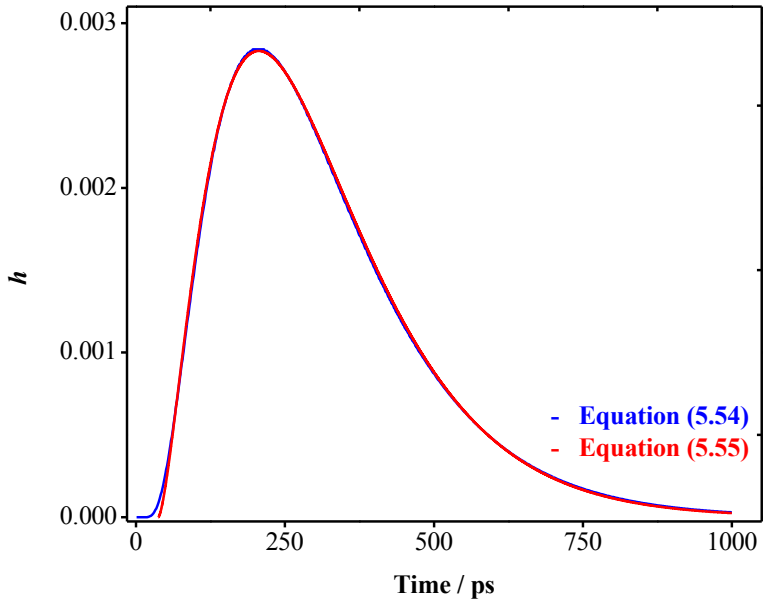


Figure 5.7. Fitting the probability density function (equation (5.54)), where z = 10 Å, to equation (5.55). This fitting produces values for α, β and γ of equation (5.55).

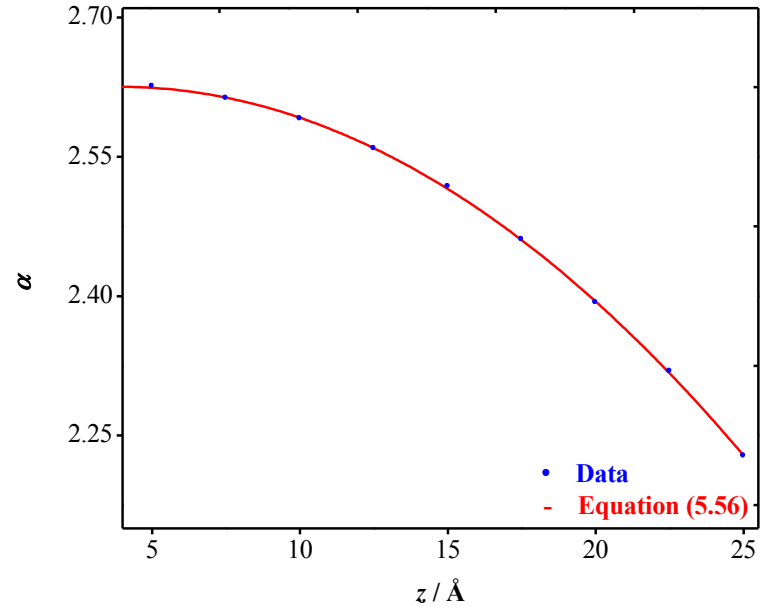


Figure 5.8. The fitting for α of equation (5.55) as a function of z. "Data" refers to the values of α obtained from fitting equation (5.54) to equation (5.55) (the example shown in the last Figure).

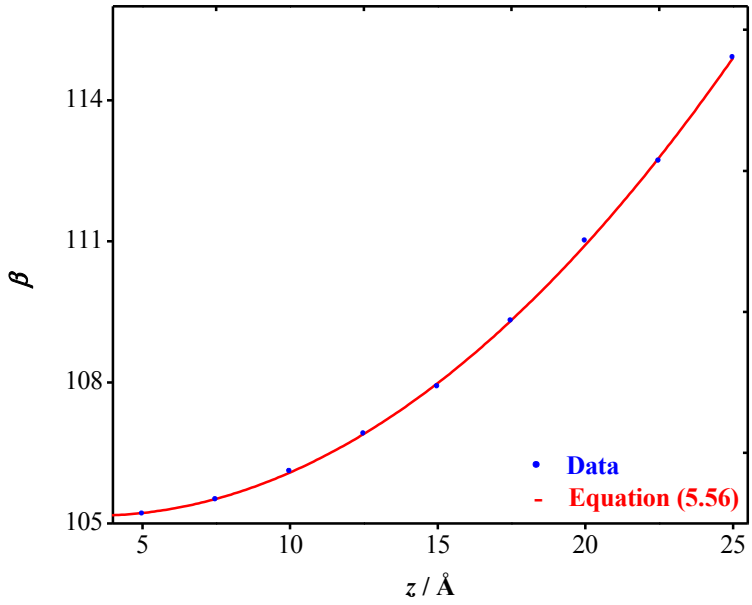


Figure 5.9. The fitting for β of equation (5.55) as a function of z. "Data" refers to the values of β obtained from fitting equation (5.54) to equation (5.55) (the example shown in Figure 5.7 above).

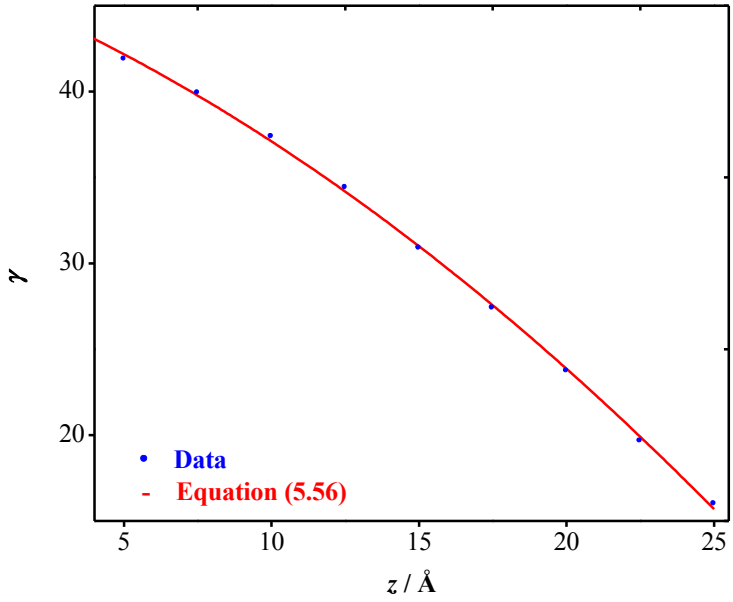


Figure 5.10. The fitting for γ of equation (5.55) as a function of z. "Data" refers to the values of γ obtained from fitting equation (5.54) to equation (5.55) (the example shown in Figure 5.7 above).

5.4.2. Details of the simulations

The simulation program that was described in the last chapter is extended to include a third part that runs IRT simulations and we will continue to use the same notations of

the last chapter and also the same parameters used there (diffusion coefficients and reaction distances etc.). Hence, the extended program consists of three parts. Part one (P1) runs the RF simulations with a periodic boundary condition as described before. Part two (denoted C. P2 as we will be focusing on the use of equations (4.9) and (4.12) rather than equation (4.7)) runs hybrid simulations as described in the last chapter. Part three (P3) runs IRT simulations.

The initial coordinates (for the radicals and the scavengers) used in P1 and P2 are passed on to P3. For the P3 simulations, the space is divided into two regions (as discussed above (Figure 5.5)). The first region, a sphere of a radius b and it is inscribed in the simulation box of Figure 4.2, contains particles (radicals and scavengers) and their reaction times are generated as was described in chapter 3 (equation (3.1) since the particles are neutral). This includes R+R and R+S reactions when the scheme one (S1) is considered and only the R+S reaction when the scheme two (S2) is considered. For each radical, explicit scavenging times are generated for the scavengers inside the inner sphere (equation (3.1)) and also a scavenging time with the continuum (the second region which is outside the sphere forming the first region) is generated. This is done using the values of Table 5.1 and equation (5.56) to obtain the values of α, β and γ which are then passed on to a routine to generate random reaction times based on equation (5.55) (the routine uses the standard C++ routine for generating random numbers from a gamma distribution). The reaction times are then put in order from small to large. At the end of each time step, the program checks if a reaction has occurred (this is limited of course to the particles that have survived so far) and makes the necessary changes (count a reaction and remove the particles that have reacted etc.) As before the typical number of realizations is 10^5 and for a small number of radicals (up to 4) we used 10^6.

5.4.3. Results

The results of the P3 simulations are generally in excellent agreement with the simulations presented in the last chapter for both S1 and S2 schemes. Samples of the results are shown in Figures 5.11-5.13 where the simulations for the P1 and C. P2 of the last chapter are also included for the purpose of comparison. The summary of the results is that the IRT method of simulations described above can be effectively used to describe the competition between scavenging and recombination reactions. The

results are summarized in Table 5.2. The IRT simulations (P3) are in good agreement with the simulations of the last chapter (P1 and C. P2). The key advantage of IRT simulation method described here is that it is time-efficient compared to the other methods of the last chapter, it also takes into account the important spatial correlations between particles close to one another without having to extend this to larger distances. The disadvantage is that it requires fitting processes as described in the last two sections.

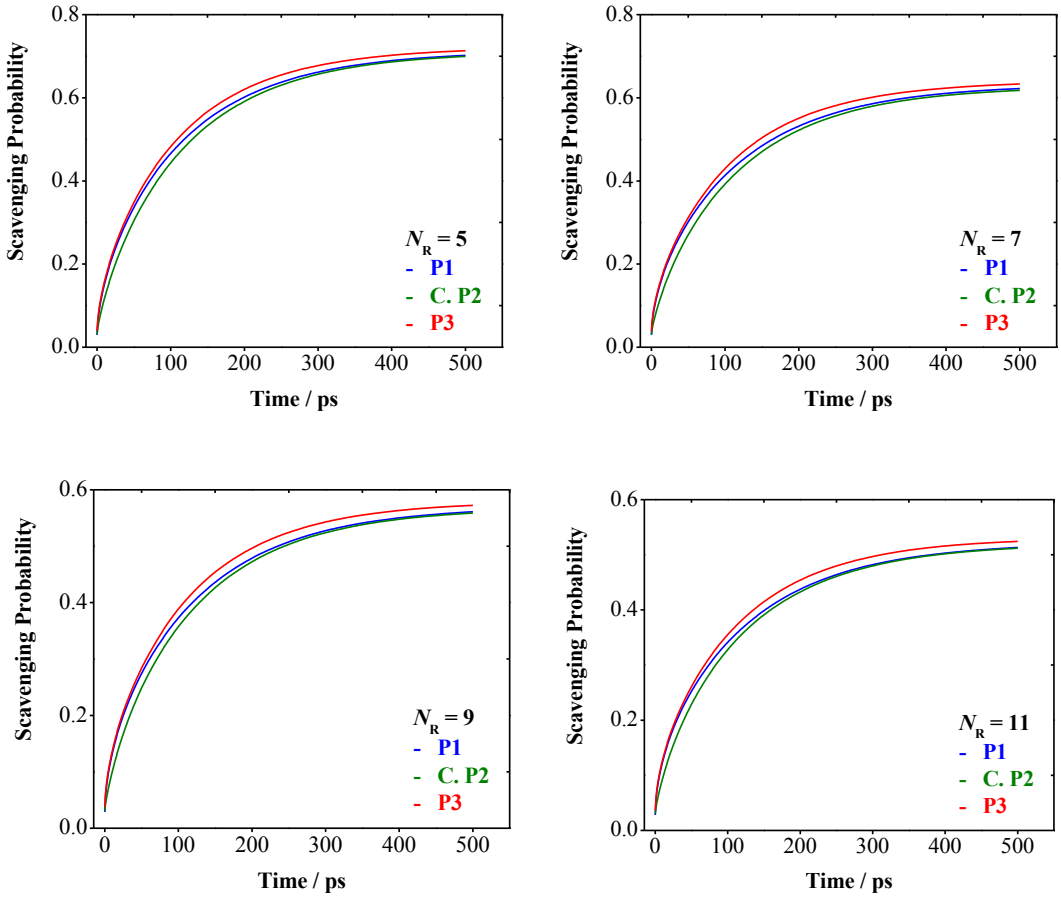


Figure 5.11. The scavenging probability in the S1 scheme. P1 and C. P2 are the simulations described in the last chapter. P3 refers to the IRT simulations described above.

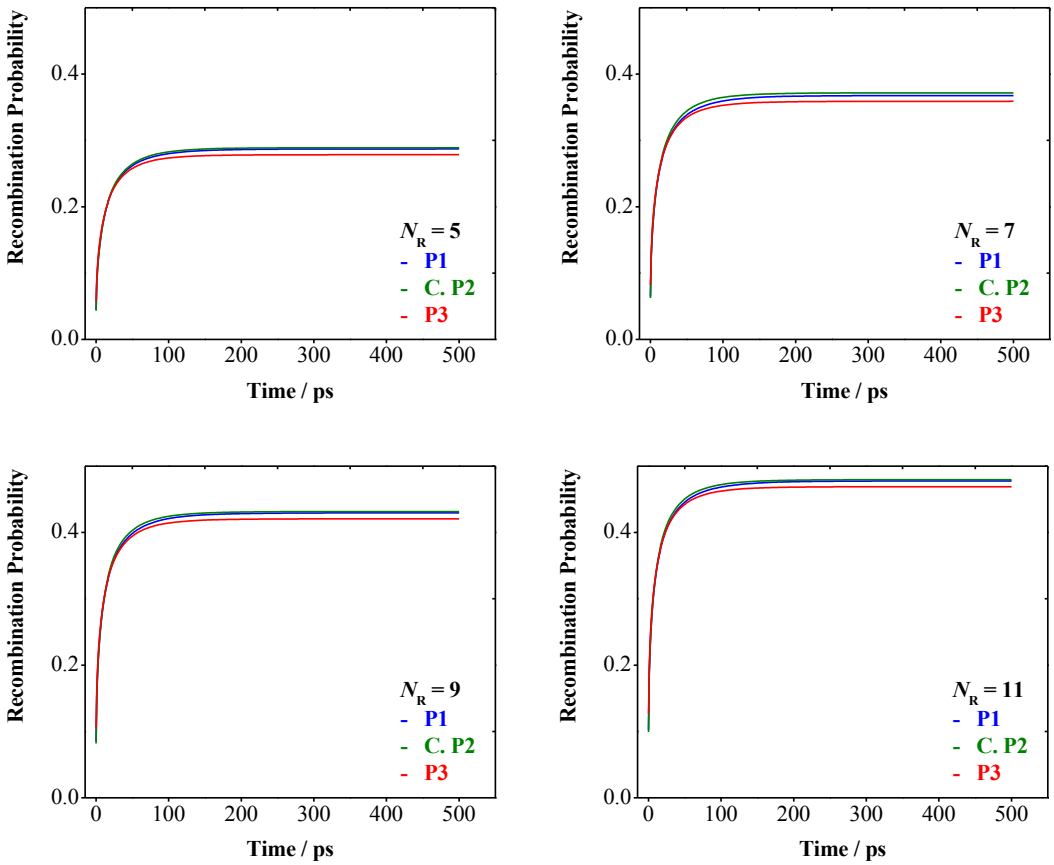


Figure 5.12. The recombination probability in the S1 scheme. P1 and C. P2 are the simulations described in the last chapter. P3 refers to the IRT simulations described above.

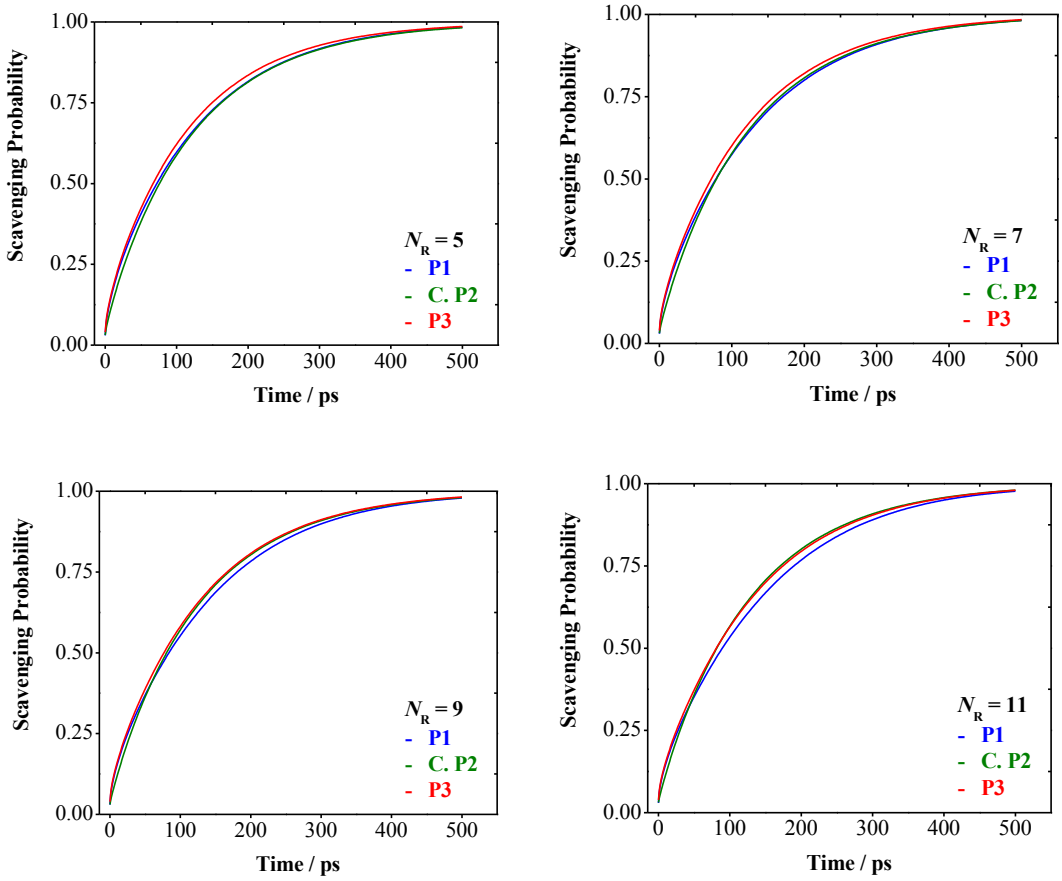


Figure 5.13. The scavenging probability in the S2 scheme. P1 and C. P2 are the simulations described in the last chapter. P3 refers to the IRT simulations described above.

Table 5.2. The results of the simulations. The numbers are the probability of the corresponding reaction at 500 ps. The statistical error in the numbers is ~ ±0.002. P1 refers to the RF simulations and C. P2 refers to the hybrid simulations when the correction proposed in the last chapter is included. P3 is the IRT simulations of this chapter.

Simulations	P1			C. P2			P3		
Reaction scheme	S1		S2	S1		S2	S1		S2
Reaction	R+S	R+R	R+S	R+S	R+R	R+S	R+S	R+R	R+S
N_R = 5	0.702	0.287	0.984	0.700	0.289	0.982	0.713	0.278	0.986
N_R = 7	0.622	0.368	0.982	0.618	0.372	0.981	0.633	0.359	0.984
N_R = 9	0.561	0.430	0.979	0.559	0.432	0.981	0.572	0.421	0.982
N_R = 11	0.513	0.478	0.977	0.512	0.480	0.980	0.524	0.469	0.980

5.4.4. Other coefficients

In the above simulations the radius b (the size of the spur), the encounter distance a and the relative diffusion coefficient D' were considered constant. This typically tends to be the case when considering an actual practical system. However, in this section we will discuss how the function h (equation (5.54)) changes with the reaction distance a and with the size of the spur b. We will show that it is always possible to fit the function h to equation (5.55) and find the coefficients α, β and γ in the same method discussed above. This may become important in certain cases. For example, when one (or more) of the coefficients (say a for example) is not precisely known and it is important to know how selecting a certain value may affect the overall results etc.

To discuss this, we have run calculations for a radical where z = 10 Å, b = 50 Å, $C_S = 6\times10^{-5}$ particles/Å^3 and $D' = 2$ Å^2.ps^{-1} and varied the encounter distance a (from 4 to 8.5 Å). We then repeated the fitting using equation (5.55) as in the previous sections (an example is shown in Figure 5.14 where the determining coefficient R^2 = 0.999). We then obtained the parameters α, β and γ of equation (5.55) using polynomial fit as before (equation (5.56) after replacing z with a). The results are shown in Figures 5.15, 5.16 and 5.17 and summarized in Table 5.3.

We have also run calculations where we varied the size of the spur b (between 35 and 55 Å) while keeping the other parameters constant (z = 10 Å, $C_S = 6\times10^{-5}$ particles/Å^3, a = 5 Å and $D' = 2$ Å^2.ps^{-1}). An example of this is shown in Figure 5.18. The fitting for α, β and γ of equation (5.55) was similar except for that we had to include an extra term when fitting β to improve the fit, i.e. we have used the following equation

$$\lambda = \tau b^3 + \rho b^2 + \sigma b + \varsigma \qquad (5.57).$$

The results of the fitting are shown in Figures 5.19, 5.20 and 5.21. A summary is presented in Table 5.4.

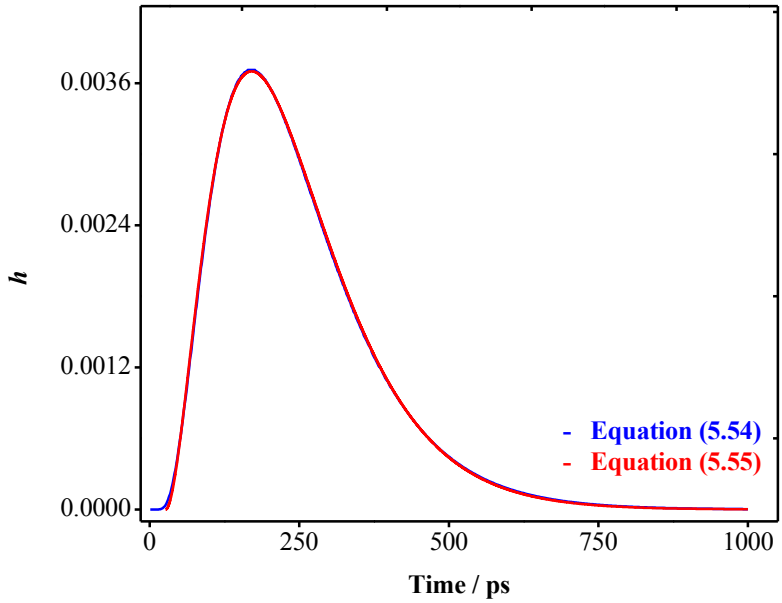


Figure 5.14. The fitting of equation (5.54) to equation (5.55) for a = 7 Å. The values for the other parameters are z = 10 Å, b = 50 Å, $C_S = 6\times10^{-5}$ particles/Å^3 and $D' = 2$ Å^2.ps^{-1}. This fitting produces values for α, β and γ of equation (5.55).

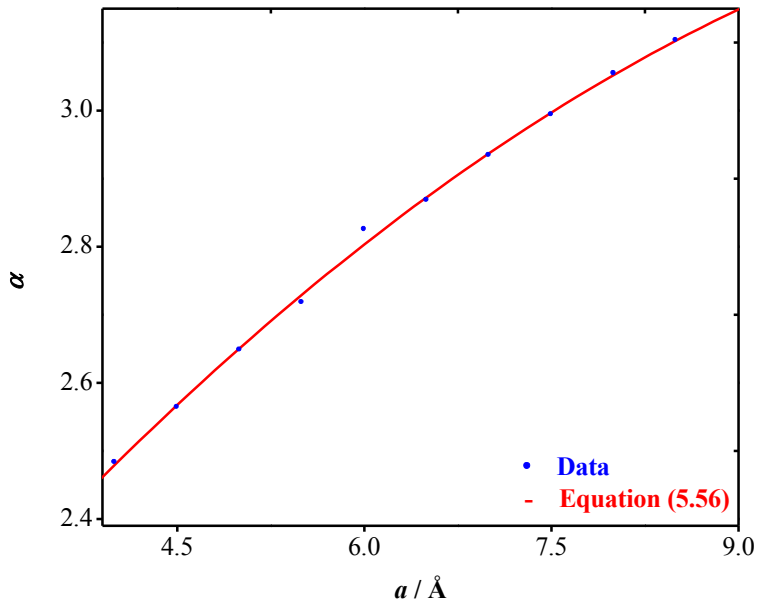


Figure 5.15. The fitting of α as a function of a. The values for the other parameters are z = 10 Å, b = 50 Å, $C_S = 6\times10^{-5}$ particles/Å^3 and $D' = 2$ Å^2.ps^{-1}. "Data" refers to the values of α obtained from fitting equation (5.54) to equation (5.55) (the example shown in the last Figure).

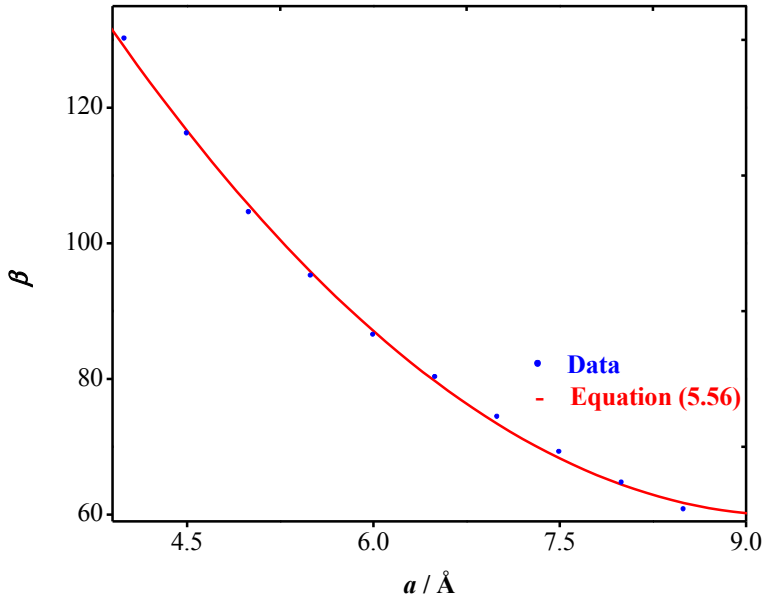


Figure 5.16. The fitting of β as a function of a. The values for the other parameters are z = 10 Å, b = 50 Å, $C_S = 6\times10^{-5}$ particles/Å^3 and $D' = 2$ Å^2.ps^{-1}. "Data" refers to the values of β obtained from fitting equation (5.54) to equation (5.55) (the example shown in Figure 5.14 above).

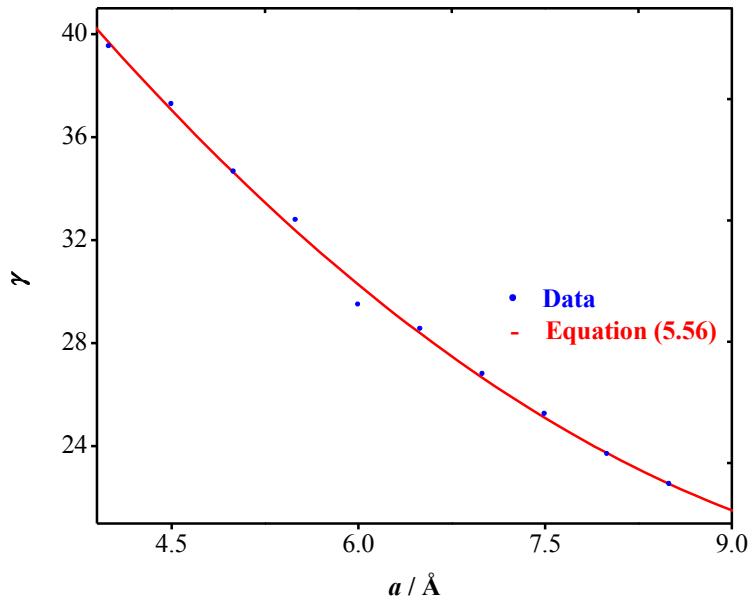


Figure 5.17. The fitting of γ as a function of a. The values for the other parameters are z = 10 Å, b = 50 Å, $C_S = 6\times10^{-5}$ particles/Å^3 and $D' = 2$ Å^2.ps^{-1}. "Data" refers to the values of γ obtained from fitting equation (5.54) to equation (5.55) (the example shown in Figure 5.14 above).

Table 5.3. The fitting of α, β and γ as a function of a where the values of b, z and D' are respectively 50 Å, 10 Å and 2 Å^2.ps^{-1}. The scavengers concentration is $C_S = 6\times10^{-5}$ particles/Å^3.

	ρ	σ	ς	R^2
α	-9.4×10^{-3}	0.2556	1.607	0.999
β	2.385	-44.73	269.6	0.999
γ	0.3539	-8.228	66.9	0.999

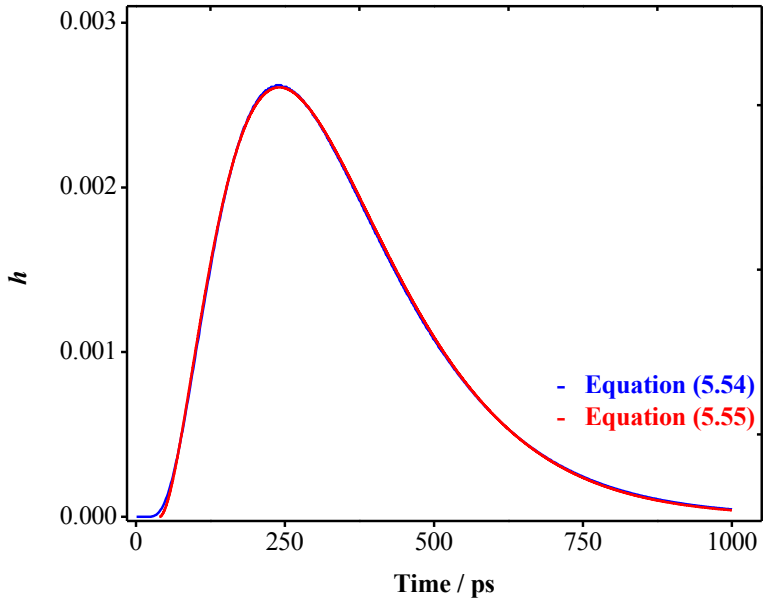


Figure 5.18. The fitting for b = 55 Å. The values for the other parameters are z = 10 Å, a = 5 Å, $C_S = 6\times10^{-5}$ particles/Å^3 and D' = 2 Å^2.ps^{-1}. Again this fitting produces values for α, β and γ of equation (5.55).

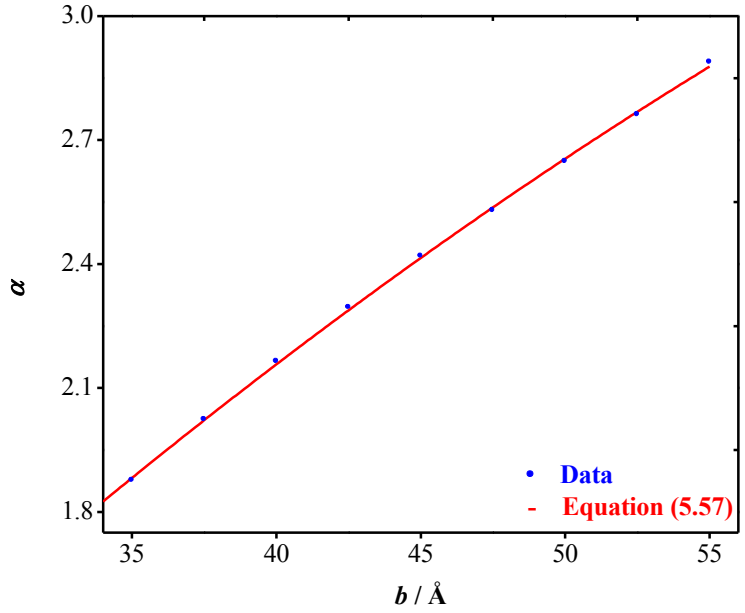


Figure 5.19. The fitting of α as a function of b. The values for the other parameters are z = 10 Å, a = 5 Å, $C_S = 6\times10^{-5}$ particles/Å^3 and $D' = 2$ Å^2.ps^{-1}. "Data" refers to the values of α obtained from fitting equation (5.54) to equation (5.55) (the example shown in the last Figure).

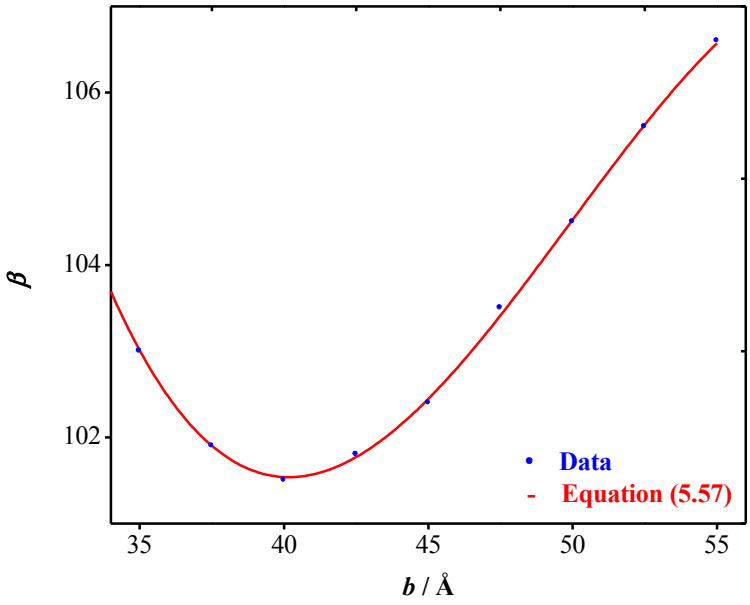


Figure 5.20. The fitting of β as a function of b. The values for the other parameters are z = 10 Å, a = 5 Å, $C_S = 6\times10^{-5}$ particles/Å^3 and $D' = 2$ Å^2.ps^{-1}. "Data" refers to the values of β obtained from fitting equation (5.54) to equation (5.55) (the example shown in Figure 5.18 above).

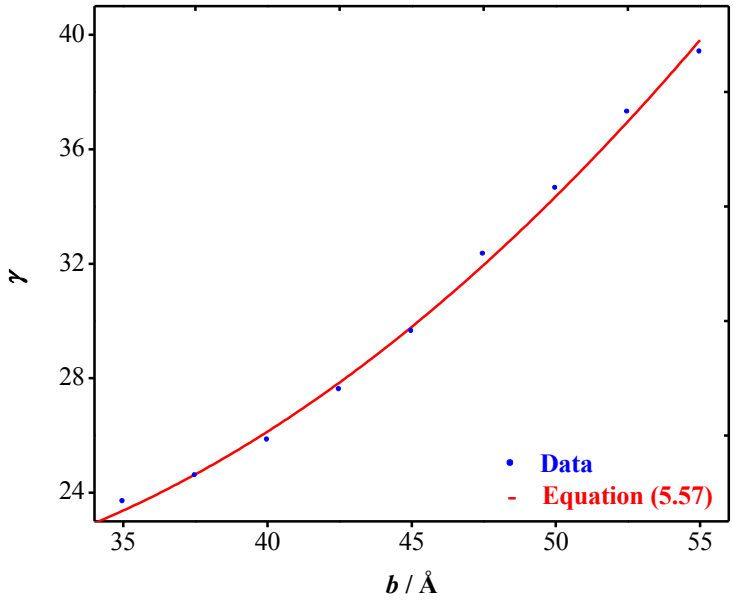


Figure 5.21. The fitting of γ as a function of b. The values for the other parameters are z = 10 Å, a = 5 Å, $C_S = 6\times10^{-5}$ particles/Å^3 and $D' = 2$ Å^2.ps^{-1}. "Data" refers to the values of γ obtained from fitting equation (5.54) to equation (5.55) (the example shown in Figure 5.18 above).

Table 5.4. The fitting of α, β and γ as a function of b where the values of a, z and D' are respectively 5 Å, 10 Å and 2 Å^2.ps^{-1}. The scavengers concentration is $C_S = 6\times10^{-5}$ particles/Å^3.

	τ	ρ	σ	ς	R^2
α	-	-3.5×10^{-4}	0.08099	-0.5271	0.999
β	-1.6×10^{-3}	0.2401	-11.52	280.9	0.999
γ	-	0.01804	-0.802	29.35	0.999

5.5. Conclusions

This chapter has shown how the IRT approximation can be used to derive the Smoluchowski theory, and how it can take account of correlations between the initial distances in principle to give corrections to the transient term in the Smoluchowski rate constant, generalising results previously obtained. Although this has only been possible for the limiting case for the first scavenging reaction where the radicals are initially at the same location, it is expected that it will also apply to systems where the radicals are close enough together for recombination to compete with scavenging. It is

also clear that the rate constant derived in this way from the IRT approximation is very similar to the empirical approximation proposed in chapter 4.

A new simulation method for scavenging in the IRT approximation has been introduced where the scavengers close to the spur are explicitly included and the scavengers further away are treated as a continuum. This should allow the IRT method to be used efficiently in such a way that the initial correlations between radical-scavenger distances are taken into account, and that it is no longer necessary to generate huge numbers of IRTs for scavengers far-off, most of which will be infinite. Unfortunately the method requires a fit of the density of the scavenging time in the outer region to a gamma distribution, but it has been shown that this fit is simple to obtain for reasonable choices of the parameters.

The IRT method realised in this way is in excellent agreement with both the Random flights method and the corrected Smoluchowski theory introduced in Chapter 4.

It remains to test whether the rate constant derived using the IRT method for the first reaction, which is affected only by competition effects, can also be used for subsequent scavenging reactions, where the local scavenger concentration has been depleted by earlier scavenging reactions. This is the subject of the next chapter.

Chapter 6

Scavenging and Recombination Kinetics III[***]

"Pure mathematics is, in its way, the poetry of logical ideas." ***Albert Einstein***

This chapter is meant to provide an overall summary of the results of the last two chapters and also discusses some of the points that were not discussed there. For example, since we are looking at the competition between scavenging and recombination using different approaches (so far we have used three methods; the Random Flight (RF) model, a hybrid model based on Smoluchowski theory and the Independent Reaction Time (IRT) method), but we have suggested a correction to the Smoluchowski rate constant which reflects the average environment. An obvious question is whether reactive depletion in a more classical model can give a similar correction, for example the prescribed diffusion model (pure deterministic approach[6,163]). And what information can be extracted from it (in fact most of the work done on the prescribed diffusion model was when we were trying to look for a justification for the empirical correction in equation (4.12))? Furthermore, the results presented in the last two chapters were in terms of "the reaction probability" but is it possible to extract numerical time-dependent rate constants from the simulations with reasonable precision? Also in reality, the scavenging of radicals happens discretely, i.e. radical-by-radical where two-successive scavenging events may be separated by a recombination event(s). So is there a detectable difference between the first scavenging event, the second scavenging event… and the n^{th} scavenging event, as

*** **Acknowledgements and details**: N. Green set up the coupled equations in the prescribed diffusion model (section 6.1). He suggested using the master equation in section 6.3. The general equations (6.29) and (6.44) were obtained by E. Al-Samra.

competition effects give way to depletion effects? This chapter will try to address the above questions in more detail. It should be noted that we will continue to use the same assumptions (fully diffusion-controlled reactions, neutral particles etc.) and the same coefficients (diffusion coefficients and reaction distances etc.) as in the last chapters.

6.1. Prescribed diffusion

The prescribed diffusion model is a deterministic treatment and is very well known.[6,130,163] It has also been used frequently to describe the chemistry in radiation spurs.[164,165,166] Briefly, the start is to write the set of coupled diffusion-reaction differential equations that describe the simultaneous evolution of the local spur concentrations as follows[167]

$$\frac{\partial C_i}{\partial t} = D_i \nabla^2 C_i - \sum_j k_{ij} C_i C_j + \sum_{l,m} k_{lm} C_l C_m \tag{6.1}$$

where C_n is the concentration of the species n, and depends on both space and time, D_i is the diffusion coefficient of i and k_{xy} is the rate constant of the reaction $x + y$. The first term in the last equation describes the change in C_i due to diffusion and the other two describe the change in C_i due to the chemical reactions. The last term only covers reactions in which species i is formed. The model assumes that the spatial distributions of the species start and remain Gaussian (spherical) i.e. the concentration of each species has the following form[168]

$$C(r,t) = N(t)\left(2\pi\sigma^2\right)^{-3/2} e^{-\frac{r^2}{2\sigma^2}} = N(t)g(r) \tag{6.2}$$

where N is the number of particles of the considered species and

$$g(r) = \left(2\pi\sigma^2\right)^{-3/2} e^{-\frac{r^2}{2\sigma^2}} \tag{6.3}.$$

The variance of the distribution is assumed to be a linear function of time as follows[169]

$$\sigma^2(t) = \sigma^2(t=0) + 2Dt \tag{6.4}$$

where D is the diffusion coefficient of the considered species. A numerical solution is then sought to the coupled diffusion-reaction differential equations and there are

codes to achieve this in the literature including the FACSIMILE model, which also allows the coupled diffusion-reaction differential equations to be solved without the Gaussian approximation above.[6]

To apply this to our reactions (R+S and R+R), we write the following equation

$$\frac{\partial C}{\partial t} = D_{\mathrm{R}} \nabla^2 C - 2k_{\mathrm{RR}} C^2 - k_{\mathrm{RS}} C_w C \tag{6.5}$$

where C is the radical concentration which corresponds to N radicals and D_{R} is the radical diffusion coefficient. k_{RR} is the rate constant for the recombination reaction (R+R) and k_{RS} is the rate constant for scavenging (R+S). C_w is the local (or effective) concentration of the scavenger particles and as it will be discussed shortly, it is different from C_{S} the concentration of the scavengers in the bulk, which is considered to be relatively large and constant (this is consistent with the assumptions of the last chapters). As before, the first term of the last equation is the diffusion term. The second term describes the change in the radical concentration due to the recombination reaction. The last term is the term that describes the change in the radical concentration due to the scavenging reaction. The only quantity that needs further discussion is C_w. Since the radicals are assumed to have a Gaussian distribution (equation (6.3)), their scavenging reaction will create "holes" in the scavenger concentration (locations where the scavengers are removed). If we denote the concentration of these holes as C_H, then in the prescribed diffusion approximation it will also have a Gaussian distribution that matches that of the radicals, i.e.

$$C_H(r,t) = H(t)g(r) \tag{6.6}$$

where g was given in equation (6.3) and H is the number of holes at time t. Hence the local concentration of scavengers C_w is going to be

$$C_w(r,t) = C_{\mathrm{S}} - C_H(r,t) \tag{6.7}.$$

The equation that couples with equation (6.5) is

$$\frac{\partial C_w}{\partial t} = D_{\mathrm{S}} \nabla^2 C_w - k_{\mathrm{RS}} C_w C \tag{6.8}$$

where D_{S} is the diffusion coefficient of S. If we use equation (6.7) and also if we consider that all particles have the same diffusion coefficient D, we have

$$\frac{\partial C_H}{\partial t} = D \nabla^2 C_H - k_{\mathrm{RS}} \left[C_{\mathrm{S}} - C_H(r,t) \right] C \tag{6.9}.$$

The treatment of the above problem is well known.[163–169] If we start with equation (6.5), use equation (6.7) and use the same convention about D as in the previous note, we have

$$\frac{\partial C}{\partial t} = D\nabla^2 C - 2k_{\mathrm{RR}} C^2 - k_{\mathrm{RS}}\left[C_{\mathrm{S}} - C_H(r,t)\right]C \qquad (6.10).$$

Now we use equation (6.2), integrate over the entire space and use the following three straightforward properties of equation (6.3)

$$\int_0^{\infty}\int_0^{\pi}\int_0^{2\pi} \nabla^2 g(r) r^2 \sin\theta\, dr\, d\theta\, d\varphi = 0 \qquad (6.11)$$

$$\int_0^{\infty}\int_0^{\pi}\int_0^{2\pi} g^2(r) r^2 \sin\theta\, dr\, d\theta\, d\varphi = \frac{1}{8\left(\pi\sigma^2\right)^{3/2}} \qquad (6.12)$$

$$\int_0^{\infty}\int_0^{\pi}\int_0^{2\pi} g(r) r^2 \sin\theta\, dr\, d\theta\, d\varphi = 1 \qquad (6.13)$$

to obtain the following equation for the number of radicals N, where H is the number of holes

$$\frac{dN}{dt} = -\frac{2k_{\mathrm{RR}}N^2}{8\left(\pi\sigma^2\right)^{3/2}} - k_{\mathrm{RS}}\left(1 - \frac{H}{8\left(\pi\sigma^2\right)^{3/2} C_{\mathrm{S}}}\right) N C_{\mathrm{S}} \qquad (6.14).$$

Similarly for equation (6.9) we have

$$\frac{dH}{dt} = k_{\mathrm{RS}}\left(1 - \frac{H}{8\left(\pi\sigma^2\right)^{3/2} C_{\mathrm{S}}}\right) N C_{\mathrm{S}} \qquad (6.15).$$

We want to find a solution to the last coupled differential equations and this was achieved using Matlab (we have used the standard routine for solving numerically a system of ordinary differential equations, ode45). It should be noted that the variance σ^2 is a linear function of time (equation (6.4)). Solutions were obtained for two cases. In the first one, we assumed that the rate constants k_{RR} and k_{RS} are time-independent and equal to the steady state limit as follows

$$k_{\mathrm{RR}} = k_{\mathrm{RS}} = 4\pi D' a \qquad (6.16)$$

where D' is the relative diffusion coefficient and a is the reaction distance. If we denote the number of radicals at $t = 0$ as N_{R}, then the numerical solutions for

different values of N_R (from 1 to 10) are shown in Figure 6.1. In the second case, we considered that k_{RR} and k_{RS} are time-dependent and equal to Smoluchowski rate constant (equation (4.7)). The solutions in this case are shown in Figure 6.2. The number of radicals in the system, N, decreases with time while the number of holes, H, increases with time.

A quantity of interest is the effective time-dependent scavenging rate constant, k. This can be obtained from equation (6.15) as follows

$$k(t) = k_{RS}\left(1 - \frac{H}{8\left(\pi\sigma^2\right)^{3/2} C_S}\right) \tag{6.17}.$$

For the solutions shown in Figure 6.1, k is shown in Figure 6.3. For the solutions shown in Figure 6.2, k is shown in Figure 6.4. Unfortunately, after considering the above, we could not spot anything that could directly justify equation (4.12). Indeed the prescribed diffusion method with a large number of particles leads to a negative transient in the scavenging rate constant (in other words the scavenging rate constant has a minimum as shown in Figures 6.3 and 6.4. This minimum reflects the depletion of scavengers in this model.), which is not in accord with the simulations presented in chapters 4 and 5.

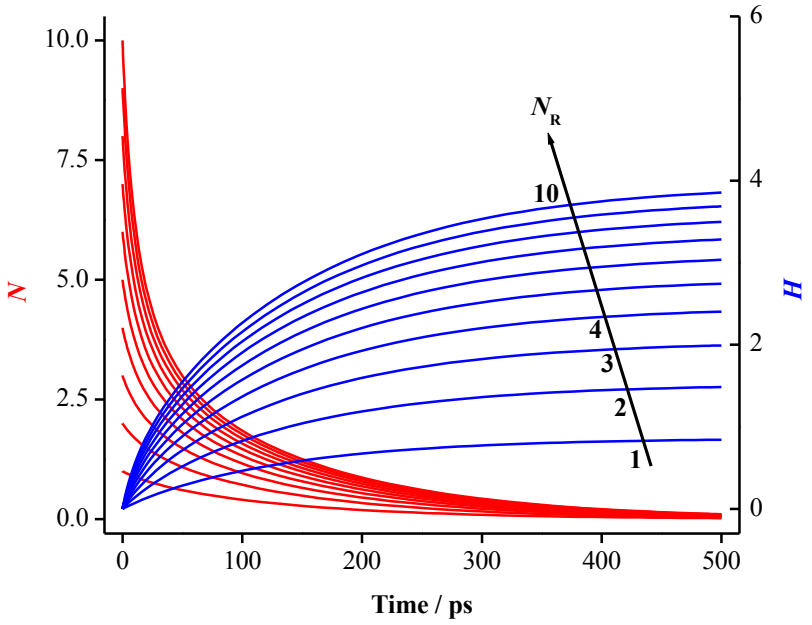


Figure 6.1. The numerical solutions for the coupled differential equations using time-independent rate constants. N_R is the initial number of radicals.

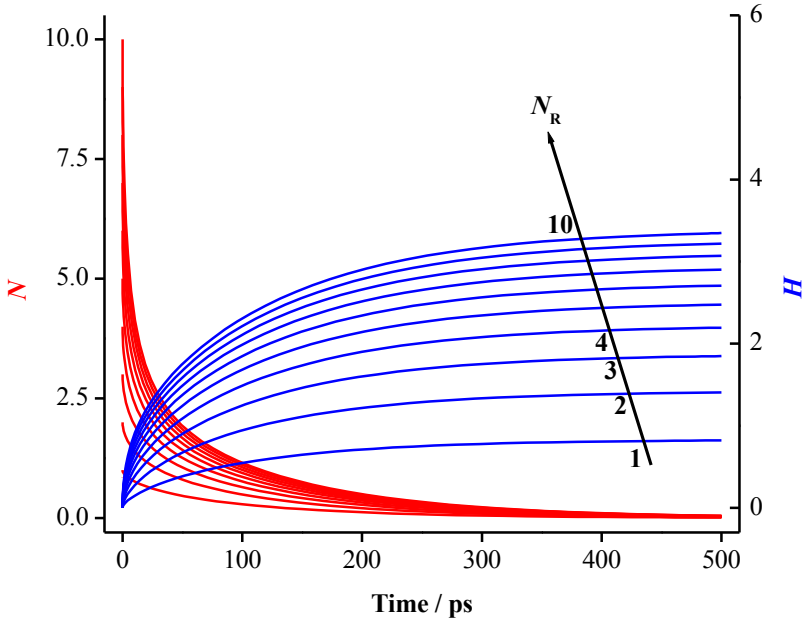


Figure 6.2. The numerical solutions for the coupled differential equations using time-dependent rate constants. N_R is the initial number of radicals.

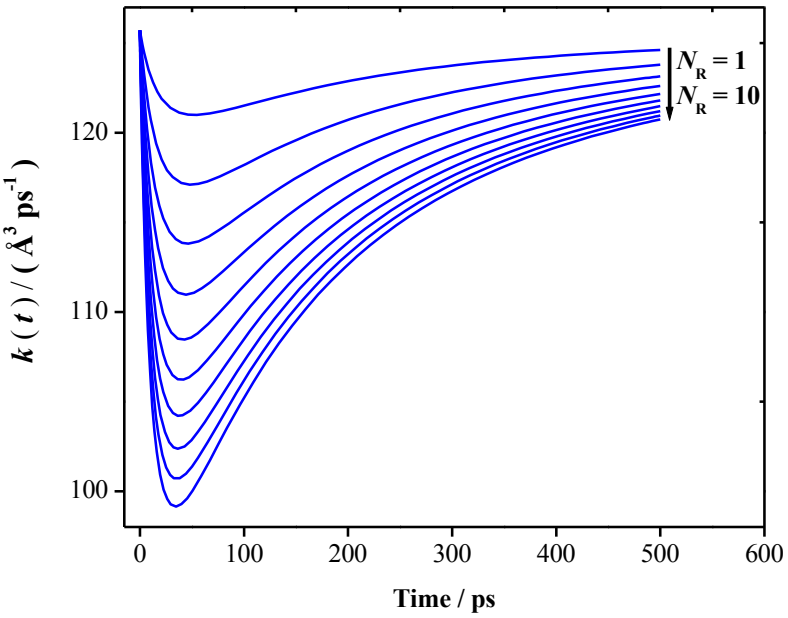


Figure 6.3. The effective time-dependent scavenging rate constant corresponds to the solutions of Figure 6.1.

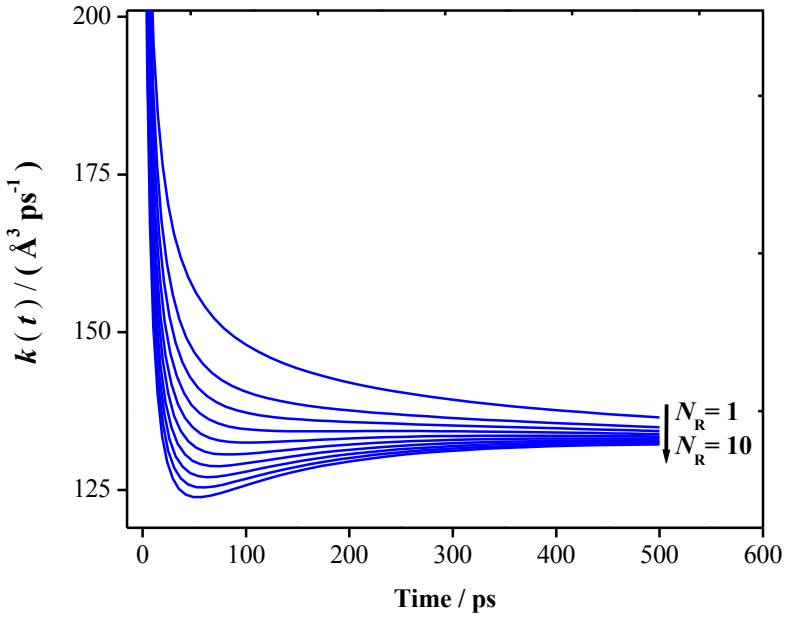


Figure 6.4. The effective time-dependent scavenging rate constant corresponds to the solutions of Figure 6.2.

6.2. Scavenging rate constant

As mentioned above, the results presented in the last chapters were in terms of the reaction probability, i.e. the probability that a particle will undergo a certain reaction (either scavenging or recombination). However, we are particularly interested in the time dependence of the scavenging rate constant and in this section we will discuss this further. If we denote the expectation number of radicals that have been scavenged as N_{RS}, then we have

$$\frac{dN_{RS}}{dt} = k(t) N C_S \tag{6.18}$$

where N is the expectation number of radicals at time t, i.e. the number of radicals that have survived and hence

$$k(t) = \frac{1}{N C_S} \frac{dN_{RS}}{dt} \tag{6.19}.$$

The right hand side of the above equation can be estimated from simulated results using the scavenging and recombination probabilities presented in chapters 4 and 5. At any time, N_{RS} can be estimated by multiplying the scavenging probability by N_R, the number of radicals at zero time. Similarly, the recombination probability can be scaled to give the expectation number of radicals that have recombined, N_{RR}. Hence N, the expectation number of radicals at time t, can be estimated from $N_R - N_{RR} - N_{RS}$. This equation can be used to generate a simulated scavenging rate constant from any type of simulation. The only problem is the estimation of the derivative from the data of the simulations, which are collected at discrete times. The statistical errors are much higher than for the cumulative reaction probabilities because of the relatively small numbers of reactions falling into a single time bin. Hence, we need to use a filtering or smoothing method to reduce this effect. We have selected the Savitzky-Golay filtering method (the generalized moving average) which is convenient to use and already available in Matlab. For example, the results of this are shown in Figure 6.5 for the case of one radical at the start (we denote the number of radicals at $t = 0$ as N_R), and in Figure 6.6 for the case of $N_R = 4$. All the methods predict well k for the simple case of a single radical. With regard to the case of 4 radicals, we notice first that the prescribed diffusion model passes through a minimum around 70 ps and then it starts to increase. This is clearly incorrect. We also notice that from around 200 ps onwards, the P1 (RF simulations) oscillates around an average of ~ 135 $Å^3.ps^{-1}$ and

the P3 (IRT simulations) oscillates around an average of ~ 140 $Å^3.ps^{-1}$ (the statistical errors will be discussed in detail shortly). This is expected because the IRT method tends to slightly overestimate the scavenging probability relative to the RF model (the results of the last chapter). The calculated Smoluchowski rate constant with the proposed correction (equations (4.9) and (4.12)) agrees well with the RF simulations.

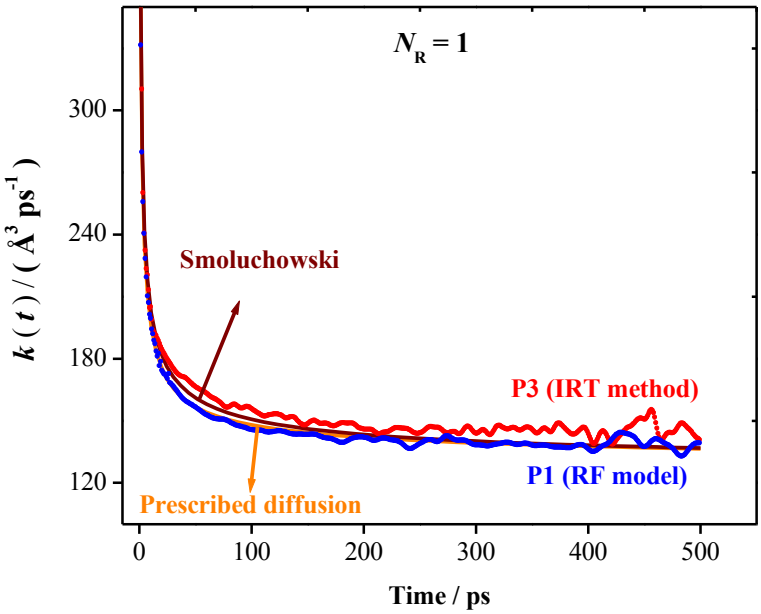


Figure 6.5. The time dependent rate constant for scavenging using different methods for one radical. P1 is the RF simulations with periodic boundary condition as discussed in chapter 4 and P3 is the IRT method simulations of chapter 5. We have also included the prescribed diffusion discussed above and the Smoluchowski rate constant calculated from equation (4.7). The data for the P1 and P3 curves were smoothed using the Savitzky-Golay method (the generalized moving average).

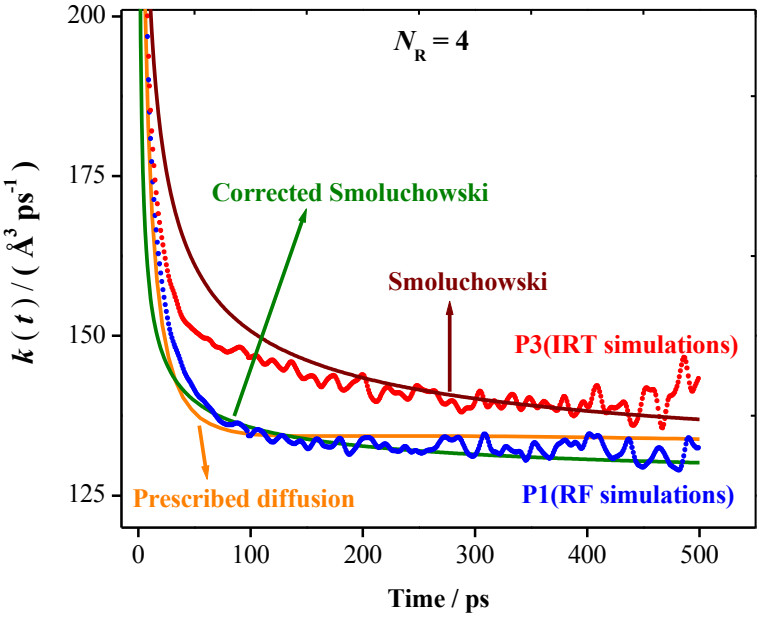


Figure 6.6. The time dependent rate constant for scavenging using different methods for four radicals. The notation are similar to those of Figure 6.5. The Smoluchowski rate constant is calculated from equation (4.7). The corrected Smoluchowski curve is calculate based on equations (4.9) and (4.12). The data for the P1 and P3 curves were smoothed using the Savitzky-Golay method (the generalized moving average).

6.3. Successive (ordered) scavenging events

As mentioned before, the scavenging events of radicals do not happen simultaneously. Hence, it is interesting to see how the system evolves event by event and also to see if there is a mathematical difference between the rate constants for successive (ordered) scavenging events. This requires a master equation treatment,[6,93,94,105] which will be discussed in detail in this section. We will start the discussion from the simple case of the S2 scheme of chapters 4 and 5 (where only the reaction R+S is allowed) and then we move on to discuss the S1 scheme (where we have the scavenging-recombination competition).

6.3.1. The S2 scheme (scavenging only)

This case is very simple because the only reaction allowed is scavenging. If we continue to use N_R as the number of radicals at the start of time, the number of radicals in the system at a given time t is an integer random variable N. The number

of radicals in the system decays by a step of one whenever a scavenging event occurs. This is summarised in the following equation

$$N_{\mathrm{R}} \xrightarrow{k_1} N_{\mathrm{R}}-1 \xrightarrow{k_2} \ldots N_{\mathrm{R}}-L+1 \xrightarrow{k_L} \ldots \xrightarrow{k_{N_{\mathrm{R}}}} 0 \tag{6.20}$$

where k_L is the rate constant of the L^{th} scavenging event. If we denote the probability that the L^{th} scavenging event has taken place as P_L, then the rate of the L^{th} scavenging event is as follows

$$\frac{dP_L}{dt} = \left(N_R - L + 1\right) k_L C_{\mathrm{S}} \Pr\left\{N = N_R - L + 1 \,\middle|\, N_{\mathrm{R}}\right\} \tag{6.21}$$

where C_{S} is the concentration of the scavengers. The probability P_L itself is given as follows

$$P_L = \Pr\left\{N = N_R - L\right\} + \Pr\left\{N = N_R - L - 1\right\} + \ldots + \Pr\left\{N = 0\right\} \tag{6.22}$$

where we have dropped the conditional probability indicator for convenience. The last equation is simply a statement that the L^{th} scavenging event has actually occurred if the number of radicals in the system is equal or less than $N_{\mathrm{R}} - L$. The last equation can be written as follows

$$P_L = \sum_{n=L}^{N_{\mathrm{R}}} \Pr\left\{N = N_{\mathrm{R}} - n\right\} \tag{6.23}$$

and hence for the $(L+1)^{\text{th}}$ scavenging event, we have

$$P_{L+1} = \sum_{n=L+1}^{N_{\mathrm{R}}} \Pr\left\{N = N_{\mathrm{R}} - n\right\} \tag{6.24}$$

and so we have

$$P_L - P_{L+1} = \Pr\left\{N = N_{\mathrm{R}} - L\right\} \quad : \; L = 1, 2, \ldots, N_{\mathrm{R}} - 1 \tag{6.25}.$$

Since L starts from the value of one, the last equation covers all the possibilities of the system except for the possibility that all radicals have survived by time t, i.e. $N = N_{\mathrm{R}}$ which has the following probability

$$1 - P_1 = \Pr\left\{N = N_{\mathrm{R}}\right\} \tag{6.26}$$

where P_1 is the probability that the first scavenging event has taken place. The reasoning behind the last equation is that the event $N = N_{\mathrm{R}}$ and the first scavenging event are complementary events. To generalize equation (6.25) so that it includes the last equation we introduce the following notation

$$P_0 = 1 \tag{6.27}$$

and hence equation (6.25) becomes

$$P_L - P_{L+1} = \Pr\left\{N = N_{\mathrm{R}} - L\right\} \quad : \; L = 0, 1, 2, ..., N_{\mathrm{R}} - 1 \tag{6.28}.$$

Combining the last equation with equation (6.21) gives the following general equation

$$\frac{dP_{L+1}}{dt} = \left(N_R - L\right) k_{L+1} C_{\mathrm{S}} \left(P_L - P_{L+1}\right) \quad : \; L = 0, 1, 2, ..., N_{\mathrm{R}} - 1 \tag{6.29}.$$

The simulation program of chapters 4 and 5 has been modified so that it produces the probabilities P_L, i.e. the probabilities of the successive scavenging events. The results of this are shown in Figure 6.7 for the case of four radicals at $t = 0$. All four probabilities approaches unity since there is no recombination reaction, but for the third and fourth scavenging events (noticeably the fourth) the probability approaches unity much slower.

The time-dependent rate constants can then be obtained easily using the last equation. However, the problem is that, in the case of four radicals, the first three scavenging events (particularly the first two) occur very quickly. Hence they reach the steady state very quickly and the time-derivative of the probabilities becomes zero (or almost zero). This complicates the calculations for the rate constants. The rate constants for the third and the fourth scavenging events are shown in Figure 6.8 (extracted from the P1 (RF) simulations). We have included the rate constants for the first and the second scavenging events over the range where the calculations were possible. The rate constant for the first scavenging event oscillates around ~129 $Å^3.ps^{-1}$ from 100 ps onwards (again the error will be discussed shortly). Similarly, for the rate coefficients of the second, third and fourth scavenging events, we have respectively the values ~131 $Å^3.ps^{-1}$, ~133 $Å^3.ps^{-1}$ and ~137 $Å^3.ps^{-1}$. It should be noted that we believe that the differences in the values are not very important and mainly due to the statistical error and the noise level (notice that the difference occurs mainly over the steady state region where all the four constants should be about equal). The main conclusion is that the simulated rate constants are all similar, and all close to the corrected Smoluchowski rate constant.

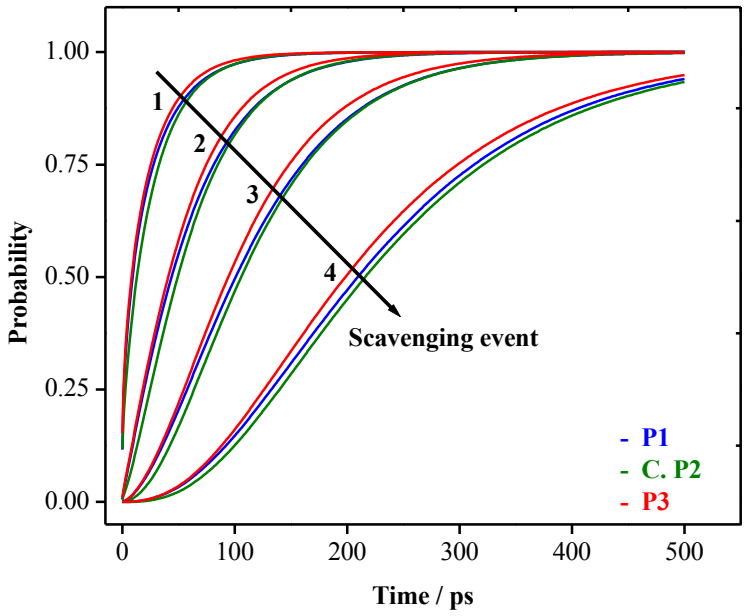


Figure 6.7. The probabilities for the successive scavenging events for the case of four radicals. P1 and C. P2 refer to the RF simulations and the hybrid simulations of chapter 4. P3 is the IRT simulations of chapter 5.

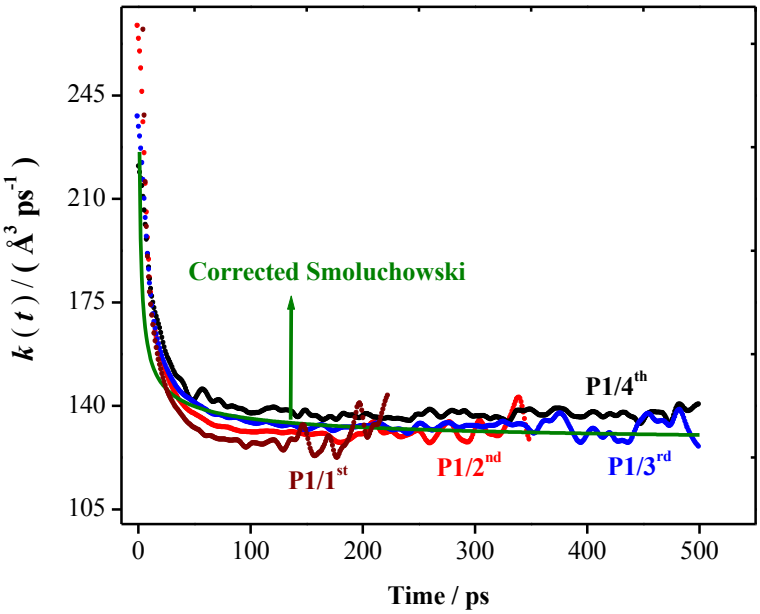


Figure 6.8. The time-dependent rate constants for the 3rd and 4th scavenging events in the case of four radicals. The rate constant for the 1st and 2nd scavenging events were partially included (when it is possible to calculate them). P1 refers to the RF simulations of chapter 4. The corrected Smoluchowski curve is calculated based on equations (4.9) and (4.12). The data were smoothed using the Savitzky-Golay method (the generalized moving average).

6.3.2. The S1 scheme

The situation in the S1 scheme (scavenging competing with recombination) is more complicated. This is because the system can reach a certain state through different routes. For example, consider the simplest possible case when we have two radicals at the start (we denote this N_R as before). If we denote the number of radicals in the system at some time t as N, then we see that the state $N = 0$ can be reached through two different routes. The first is through two scavenging events and the second is through a recombination event. If we denote a scavenging event as s and a recombination event as r, then we can chart the different stages of the system as shown in Figure 6.9.

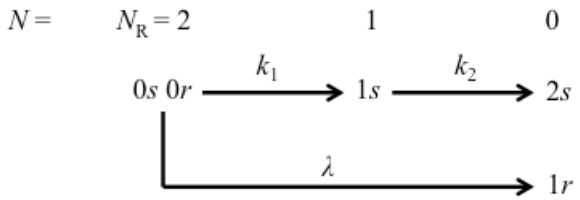


Figure 6.9. The possibilities in the S1 scheme for two radicals at the start.

We introduce now the following notation

$$P_{2s} = \Pr\left\{N = 0, 2s \,\middle|\, N_R = 2\right\} \tag{6.30}$$

to specify the probability that the number of radicals in the system is zero after two scavenging events have occurred. Similarly, we have the following

$$P_{1r} = \Pr\left\{N = 0, 1r \,\middle|\, N_R = 2\right\} \tag{6.31}$$

$$P_{1s} = \Pr\left\{N = 1, 1s \,\middle|\, N_R = 2\right\} \tag{6.32}$$

$$P_{0s\,0r} = P_0 = \Pr\left\{N = N_R\right\} \tag{6.33}.$$

The probability that the first scavenging event has taken place P_1 is

$$P_1 = P_{1s} + P_{2s} \tag{6.34}$$

and its rate of change is

$$\frac{dP_1}{dt} = 2k_1 P_0 C_S - k_2 P_{1s} C_S + k_2 P_{1s} C_S = 2k_1 P_0 C_S \tag{6.35}$$

where C_S is the scavenger concentration. Similarly, the probability of the second scavenging event P_2 is

$$P_2 = P_{2s} \tag{6.36}$$

and so we have

$$\frac{dP_2}{dt} = k_2 P_{1s} C_S \tag{6.37}.$$

The above example is very simple but the treatment gets complicated pretty quickly. For the case of three radicals at the start, the possibilities are shown in Figure 6.10.

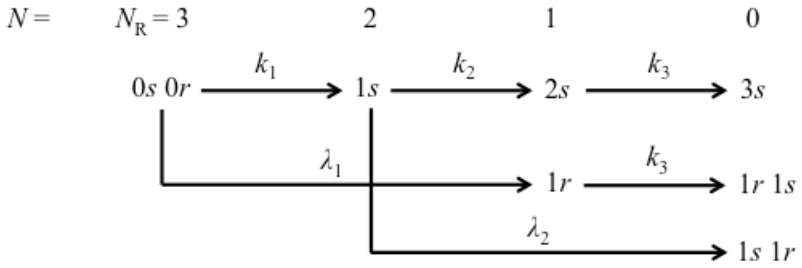


Figure 6.10. The possibilities in the S1 scheme for three radicals at the start. It should be noted that we have chosen to label the process according to the number of radicals present (two processes are labeled k_3 because they start from the state $N = 1$).

The probability of the first scavenging event P_1 is (using the same notations as before)

$$P_1 = P_{1s} + P_{2s} + P_{3s} + P_{1r\,1s} + P_{1s\,1r} = 1 - P_0 - P_{1r} \tag{6.38}$$

and the rate is

$$\frac{dP_1}{dt} = 3k_1 P_0 C_S + k_3 P_{1r} C_S \tag{6.39}.$$

Similarly, the probability of the second scavenging event P_2 is

$$P_2 = P_{2s} + P_{3s} \tag{6.40}$$

and so

$$\frac{dP_2}{dt} = 2k_2 P_{1s} C_S \tag{6.41}.$$

For the third scavenging event we have

$$P_3 = P_{3s} \tag{6.42}$$

and

$$\frac{dP_3}{dt} = k_3 P_{2s} C_S \tag{6.43}.$$

In general the rate of the L^{th} scavenging event, where we have N_R radical at the start, is given as follows

$$\frac{1}{C_{\mathrm{S}}}\frac{dP_L}{dt} = \left(N_{\mathrm{R}} - L + 1\right)k_L\, P_{(L-1)s} + \sum_{n=1}^{m_l}\left(N_{\mathrm{R}} - 2n - L + 1\right)k_{2n+L}\,\Pr\left\{L-1, n\right\} \tag{6.44}$$

where m_l is the integer part of $\left(N_{\mathrm{R}} - L\right)/2$ and hence the sum gives terms only when $N_{\mathrm{R}} \geq L + 2$. We have also used the following notation

$$\Pr\left\{u, v\right\} = \Pr\left\{N = N_{\mathrm{R}} - u - 2v, \xleftrightarrow{us\ vr} \middle| N_{\mathrm{R}}\right\} \tag{6.45},$$

i.e. the probability that we have N radicals in the system starting from N_{R} where we have had u scavenging events and v recombination events. The arrow is to indicate that the scavenging and recombination events can occur in any possible order. Hence the last equation is also a sum over all the possibilities that have u scavenging events and v recombination events in total. For example, for $u = v = 2$ we have

$$\Pr\left\{2, 2\right\} = P_{2s\,2r} + P_{2r\,2s} + P_{1s\,2r\,1s} + P_{1r\,2s\,1r} + P_{1r\,1s\,1r\,1s} + P_{1s\,1r\,1s\,1r} \tag{6.46}.$$

As an example of the above, we consider the case of four radicals at the start ($N_{\mathrm{R}} = 4$). The rate of the first scavenging event is given as follows (equation (6.44))

$$\frac{1}{C_{\mathrm{S}}}\frac{dP_1}{dt} = 4k_1P_0 + 2k_3P_{1r} \tag{6.47}.$$

Similarly, for the second scavenging event, we have

$$\frac{1}{C_{\mathrm{S}}}\frac{dP_2}{dt} = 3k_2P_{1s} + k_4\left(P_{1r\,1s} + P_{1s\,1r}\right) \tag{6.48}$$

and for the third

$$\frac{1}{C_{\mathrm{S}}}\frac{dP_3}{dt} = 2k_3P_{2s} \tag{6.49}.$$

For the fourth scavenging event, we have

$$\frac{1}{C_{\mathrm{S}}}\frac{dP_4}{dt} = 4k_4P_{3s} \tag{6.50}.$$

The probabilities of the scavenging events are shown in Figure 6.11. Because radical recombination is allowed, we see that the probabilities approach different limits at large times. If the first scavenging event occurs, the number of radicals in the system becomes three, which indicates that at least one more scavenging event must take

place at a later time. Similarly, if the third scavenging event takes place, there is one radical left in the system and the fourth scavenging event will occur at a later time.

Calculating the time-dependent rate coefficients for the first and the second scavenging events was found problematic. This is for two reasons. The first is that, as mentioned before, we need to evaluate the time derivative (the last four equations) and this is not simple when the events are very rapid (notice that the probability for the first scavenging event is horizontal for most of the time). The second reason is that the first two of the last four equations contain k_3 and k_4 (along with respectively k_1 and k_2) and this increased the noise level when trying to calculate k_1 and k_2. The rate coefficients for the third and fourth scavenging events are shown in Figure 6.12. The values k_3 and k_4 oscillate around ~132 $Å^3.ps^{-1}$ and ~131 $Å^3.ps^{-1}$ respectively from 100 ps onwards. However, once again, it is clear that the successive rate constants are similar and are in good agreement with the proposed correction to Smoluchowski theory.

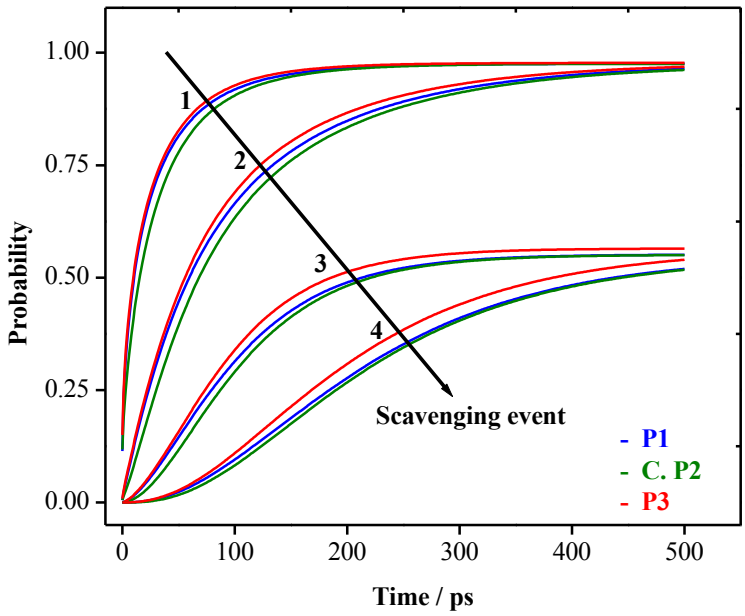


Figure 6.11. The probabilities for the successive scavenging events for the case of four radicals. P1 and C. P2 refer to the RF simulations and the hybrid simulations of chapter 4. P3 is the IRT simulations of chapter 5.

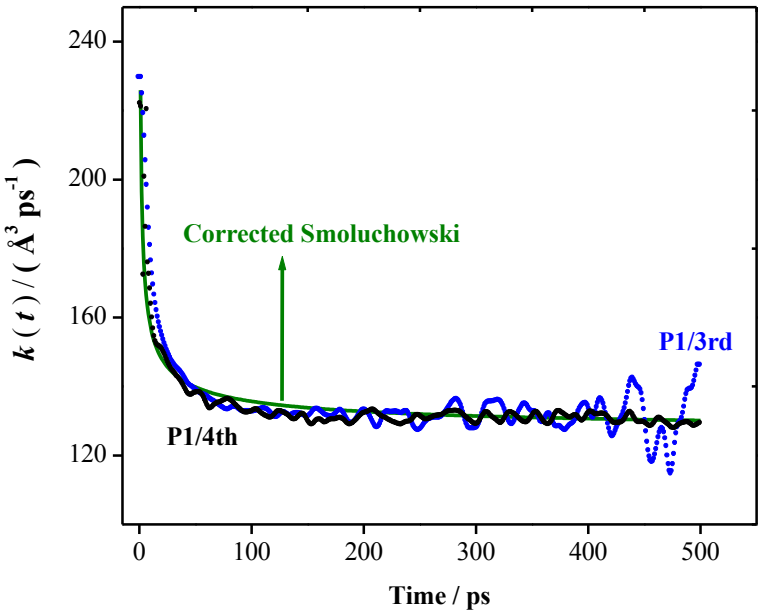


Figure 6.12. The time-dependent rate constants for the 3rd and 4th scavenging events in the case of four radicals. P1 refers to the RF simulations of chapter 4. The corrected Smoluchowski curve is calculate based on equations (4.9) and (4.12). The data were smoothed using the Savitzky-Golay method (the generalized moving average).

6.3.3. Statistical errors

We have not yet commented on the statistical error made when calculating the rate coefficients above. This is because calculating the error precisely has been found difficult due to the noise level. To discuss this, we show simulations for the case N_R = 3 (with the S1 scheme) using five different sequences of random numbers (the simulations are the P1 (RF model) simulations). The results of calculating k from the simulated kinetics (equation (6.19)) are in very good agreement with each other and they are shown in Figure 6.13. This indicates that the statistical error is small. For the first sequence of random numbers, the value of k oscillates around ~135 $Å^3.ps^{-1}$ from 100 ps onwards. For the other sequences, we similarly have the values ~134, ~133, ~133 and 134 $Å^3.ps^{-1}$. Hence, based on the previous values, we can estimate the error as ±2.0 $Å^3.ps^{-1}$.

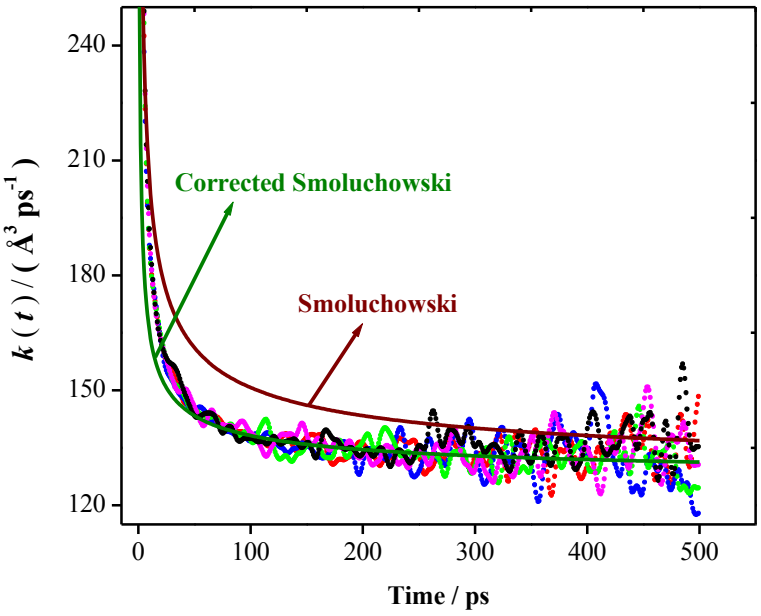


Figure 6.13. The time dependent rate constant for scavenging using different sequences of random numbers. The results from different sequences are in different colors. The number of radicals N_R = 3. The Smoluchowski rate constant is calculated from equation (4.7). The corrected Smoluchowski curve is calculate based on equations (4.9) and (4.12). The data were smoothed using the Savitzky-Golay method (the generalized moving average).

6.4. Summary and conclusions

As discussed before, in a radiation-induced spur the radicals are close together and it is necessary to take this into account when modelling the radiation chemical kinetics. The Smoluchowski theory requires a correction to include this multi-radicals effect. We have proposed a correction in chapter 4 and it seems to be very successful.

This chapter started from describing the prescribed diffusion model and applying it to the depletion of scavengers. The problem is that the effective rate constant in this model is physically unsound (it passes through a minimum and then starts to increase (Figures 6.3 and 6.4)).

In the current chapter we have presented the calculation of the scavenging rate constants from simulated kinetics. The results of this are consistent with the approximations formulated in the previous two chapters.

We have also presented a detailed master equation treatment to extract the rate constant of the successive scavenging events. We have applied this to the case of four radicals and presented the time-dependent probability of each scavenging event. It

seems that the four scavenging events have the same rate constant (Smoluchowski rate coefficient with the correction suggested in chapter 4). This indicates that the effects of competition on the first-rate constant and depletion on subsequent ones are essentially the same. Perhaps this is why the correction works: competition effects are dependent on the number of interfering concentration gradients and depletion effects on the number of scavengers removed. These are complementary.

Chapter 7

Reversible reaction[†††]

"All substances which tend to enter in combination act by reason of their affinity and their quantity. These truths are the basis of all chemical observation." ***Claude Louis Berthollet***

Historically, the first to consider that the products of a chemical reaction may react and produce the initial reactants was C. Berthollet in 1803.[170,171] Many have worked and developed this since then,[172] notably, P. Waage and C. Gulberg who jointly introduced the concept of chemical equilibrium in 1864,[173,174] and also J. Van't Hoff.[175]

Reversible reactions occur in radiation chemistry, for example[3,176,177]

$$OH + OH^- \leftrightarrows O^- + H_2O \tag{7.1}$$

and

$$Cl + Cl^- \leftrightarrows Cl_2^- \tag{7.2}$$

and also

$$OH + Cl^- \leftrightarrows HOCl^- \tag{7.3}.$$

It is possible sometimes to ignore the reversibility of the reaction (depending on the conditions). However, this cannot be done in general. Hence, it is very important to be able to model this kind of reaction in order to achieve a better understanding of the radiation-induced chemical effects in matter. Unfortunately, this is not very straightforward because (as discussed shortly) the reactions cannot be assumed fully diffusion- controlled. This chapter is meant to discuss this in more detail and develop methods for simulating reversible reactions. Before we start the discussion, it should

[†††] **Acknowledgements**: N. Green obtained the mathematics in sections 7.4.1.1–7.4.1.4.

be noted that we will concentrate on the reversible association-dissociation reaction, which has the following general form

$$A + B \leftrightarrows AB \tag{7.4}$$

We will start first with a general background on the effect of a radiation boundary condition. We then discuss how to modify the models (the RF and IRT models) so that they can be used to simulate a reaction with a radiation boundary condition. We then discuss the challenge in using the IRT method to model reversible reaction.

7.1. Radiation boundary condition (RBC)

As mentioned above, it is no longer possible to generally assume that the association reaction (or the direct reaction) is fully diffusion-controlled. This is because when a product particle (AB) undergoes the dissociation reaction (or the reversed reaction), the resulting two particles (A and B) are formed in contact (or in other words they are separated by their encounter radius a). This means that they would react instantly if the association reaction were fully diffusion-controlled. Hence, effectively the dissociation reaction would never take place.

One possible way to get around the above-mentioned problem is to continue to assume that the association reaction is fully diffusion-controlled but when an AB particle dissociates, A and B formed will not be in contact and they are pushed slightly further apart.[178] The problem with this method is that this distance is essentially arbitrary; the correct choice of distance depends on the reactivity of the pair because it determines the probability of recombination. Furthermore, the concern is that in a radiation spur (where all the reactants are relatively close to one another) pushing two particles away from each other may systematically alter the probability of other reactions. Hence, the formal (and reasonable) method to get around this is to assume that the association reaction occurs with a finite rate on encounter (in other words, it is partially diffusion-controlled and follows the RBC). The RBC has been described in many places.[14,134,137,156,179] The effect of applying the RBC can be better understood if we consider the following simple reaction

$$A + B \rightarrow AB \tag{7.5}$$

If we consider a particle A located at the origin of the coordinates, then the above reaction is going to reduce the local concentration of B, denoted C_B. The reaction rate

can then be obtained by considering R, the rate of diffusion of B molecules towards the origin of the coordinates through a sphere of radius r as follows

$$R = 4\pi r^2 D' \frac{\partial C_{\mathrm{B}}}{\partial r} \tag{7.6}$$

which is a consequence of Fick's first law where D' is the relative diffusion coefficient. Under the steady state condition (R is constant), the solution of the last equation is

$$C_{\mathrm{B}}(r) = \frac{\varsigma}{4\pi D'} - \frac{R}{4\pi D' r} \tag{7.7}$$

where the coefficient ς is determined by considering C_∞, the concentration of B in the bulk ($r \to \infty$) as follows

$$\varsigma = 4\pi D' C_\infty \tag{7.8}$$

and hence

$$C_B(r) = C_\infty - \frac{R}{4\pi D' r} \tag{7.9}.$$

The RBC specifies that the reaction occurs with a finite rate on encounter, i.e. the ratio ρ does not drop to zero as shown in Figure 4.1, as follows

$$R = k_a C_B(a) = k_a \left(C_\infty - \frac{R}{4\pi D' a} \right) \tag{7.10}$$

where k_a is the rate constant (this becomes infinitely large if the reaction fully diffusion-controlled) and so we have

$$R\left(\frac{1}{k_a} + \frac{1}{4\pi D' a} \right) = C_\infty \tag{7.11}.$$

The second order rate coefficient $k_{2\mathrm{nd}}$ under the steady state condition is

$$k_{2\mathrm{nd}} = \frac{R}{C_\infty} = \frac{k_a k_{D'}}{k_a + k_{D'}} \qquad : \quad k_{D'} = 4\pi D' a \tag{7.12}.$$

It should be noted that $k_{2\mathrm{nd}}$ is equal to $k_{D'}$, the steady state rate coefficient for a fully diffusion-controlled reaction (Smoluchowski boundary condition), when k_a is very large as follows

$$k_{2\mathrm{nd}} = \frac{k_a k_{D'}}{k_a} = k_{D'} \tag{7.13}.$$

Hence the effect of applying the RBC changes the rate coefficient of the reaction.

7.2. RF simulations with RBC

In consequence of the above discussion, we must treat the direct reaction (or the association reaction) as partially diffusion-controlled. It is therefore necessary to modify the RF model before we can apply it to a reaction that follows the RBC (in chapter 2 we considered only the fully diffusion-controlled reactions). This modification is described in detail in the literature,[6,18,122] and will be summarized here where we consider the reaction (7.5) as an example where there is no Coulombic influence on the reaction between A and B. Briefly, because encounter is the necessary (but in this case not sufficient because the reaction is partially diffusion-controlled) condition for two particles to react, we need to check at the end of each time step if an encounter has taken place (this is similar to what was described in chapter 2 and as discussed shortly this is done using equation (2.39) in particular). The key difference is that we need to consider what will happen if two particles meet (or encounter) and do not react. In this case, the particles will move away from one another (or in other words they will reflect from each other). This means that the positions of the particles need to be modified accordingly. The question is then how to determine the new positions after a reflection has taken place. To discuss this in more detail, we denote the vector position of the A particle $\mathbf{X}_A$ and the vector position of the B particle $\mathbf{X}_B$ at time t. Then we define the following two independent vectors

$$\mathbf{R} = \mathbf{X}_A - \mathbf{X}_B \tag{7.14}$$

$$\mathbf{S} = \frac{D_A \mathbf{X}_A + D_B \mathbf{X}_B}{D'} \quad : \quad D' = D_A + D_B \tag{7.15}$$

where D_i is the diffusion coefficient of i. Now after a sufficiently small time increment δt, the positions of the particles will become $\mathbf{X}_A+\delta\mathbf{X}_A$ and $\mathbf{X}_B+\delta\mathbf{X}_B$. Similarly after the time increment (or step), the vectors defined above will become $\mathbf{R}+\delta\mathbf{R}$ and $\mathbf{S}+\delta\mathbf{S}$. If the two particles have encountered and have not reacted, then we need to reflect them and that will change their position vectors $\mathbf{X}_A+\delta\mathbf{X}_A$ and $\mathbf{X}_B+\delta\mathbf{X}_B$ and the important question is how to specify these new positions. The method described in the literature (references 6, 18 and 122) indicates that the vector $\mathbf{S}+\delta\mathbf{S}$ does not actually change due to the reflection and only $\mathbf{R}+\delta\mathbf{R}$ does. Furthermore, the vector $\mathbf{R}+\delta\mathbf{R}$ can be divided into two components. The first one V_{par} is parallel to the vector $\mathbf{R}$ and the second one V_{per} is perpendicular to the vector $\mathbf{R}$. Now since we have

considered a sufficiently small time increment δt where $\mathbf{R}+\delta\mathbf{R}$ is actually not very much different from $\mathbf{R}$, then to first order the reflection only affects V_{par}, the component parallel to $\mathbf{R}$. The first order component of V_{per} depends on the magnitude of $\mathbf{R}$ and so the effect of $\delta\mathbf{R}$ is second order. Hence, in conclusion the problem is reduced to specifying what happens to the single variable V_{par} under a reflection.

Because it has been now established that the component that will be affected by reflection is V_{par}, there are mainly only two remaining points. The first one is how to determine whether or not an encounter has actually taken place. As mentioned briefly above, this is done using the probability function given in equation (2.39). The step is initially generated without taking into account the presence of the boundary, and so an encounter will take place if the distance of closest approach along the trajectories generated for this time step is less than the encounter distance. The function in equation (2.39) is used to calculate d_c, the distance of closest approach along the direction of $\mathbf{R}$ for the two relevant particles, using the standard inverse function method of random number generation.[131] First interpret equation (2.39) as the probability distribution of the distance of closest approach. Next invert the function for the corresponding distance

$$d_c = \frac{1}{2}\left[R + V_{\text{par}} - \left(\left(R - V_{\text{par}} \right)^2 - 4D'\delta t \ln W_{\text{Drift}} \right)^{1/2} \right] \tag{7.16}$$

where R is the length of $\mathbf{R}$ (it should be noted that the last equation simply results from equation (2.39) if we replace a, x and y by d_c, R, V_{par} respectively). In the course of the simulations, W_{Drift} will be replaced by a uniform random number between 0 and 1, and hence d_c can be generated, conditional on the interparticle distance at the start and end of the time step. If d_c is less than (or equal to) a, the reaction distance, then an encounter has occurred. As discussed above, an encounter may not result in a reaction and in this case a "reflection" takes place. The reflection affects only V_{par}. Hence, after a reflection, V_{par} is replaced by V_{ref}, the parallel component after reflection, which is calculated as follows[6,18,122]

$$V_{\text{ref}} = V_{\text{par}} + a - d_c \qquad : \; d_c \le a \tag{7.17}$$

where we have specified the condition for a reflection to take place, i.e. $d_c \le a$. This is an exact sample for Brownian motion with constant drift and so is acceptable as long as the time step is short.

The second (and final) point is how to incorporate the RBC into the simulation. The RBC is going to indicate whether or not an encounter results in a reaction. This requires that we solve the following forward diffusion equation for p, the reaction probability density function

$$\frac{\partial p}{\partial t} = D' \frac{\partial^2 p}{\partial y^2} - \mu \frac{\partial p}{\partial y} \quad : \; p = p\left(t, y \middle| y\left(t=0\right) = x\right) \tag{7.18}$$

under the following boundary conditions

$$\begin{aligned} p\left(t=0\right) &= \delta\left(y-x\right) \;,\; y \to \infty \;\Rightarrow p \to 0 \\ D' \left.\frac{\partial p}{\partial y}\right|_{y=a} &- \mu p\left(y=a\right) = v\, p\left(y=a\right) \end{aligned} \tag{7.19}$$

where a is the reaction distance (this has been done before (reference 18) and a similar case will be discussed in section 7.4 to come). The last condition is the RBC where v was specified in equation (3.10) and μ is the drift given as follows

$$\mu = \frac{2D'}{x} \tag{7.20}.$$

The final conclusion of the analysis is that the probability that the encounter that has taken place, when moving from a separation x to a separation y during a small time increment δt, results in a reaction is given as follows[18]

$$\Pr\left(x, y, \delta t\right) = 1 - \frac{1 - C_1 e^{C_2^2} \operatorname{erfc}\left(C_2\right)}{1 - C_3 e^{C_4^2} \operatorname{erfc}\left(C_4\right)} \tag{7.21}$$

where

$$C_1 = \frac{\mu + 2v}{2D'} \sqrt{\pi D' t} \tag{7.22}$$

$$C_2 = \frac{\mu + 2v}{2D'} \sqrt{D' t} + \frac{y + x - 2a}{\sqrt{4D' t}} \tag{7.23}$$

$$C_3 = \frac{\mu}{2D'} \sqrt{\pi D' t} \tag{7.24}$$

$$C_4 = \frac{\mu}{2D'} \sqrt{D' t} + \frac{y + x - 2a}{\sqrt{4D' t}} \tag{7.25}.$$

Now the final step is to summarize the above. The simulation starts from a certain configuration, which in a real track will usually be modelled as a random distribution of some kind, but for the purposes of testing approximations could be a

fixed geometry. The particles then take diffusive flights using the appropriate normally distributed random numbers as described in chapter 2. At the end of each time step, the vectors $\mathbf{R}+\delta\mathbf{R}$ and $\mathbf{S}+\delta\mathbf{S}$ are calculated (equations (7.14) and (7.15)) where $\mathbf{R}$ and $\mathbf{S}$ are the values of the vectors at the previous time step. The vector $\mathbf{R}+\delta\mathbf{R}$ is then divided into two components V_{par} parallel to $\mathbf{R}$ and V_{per} perpendicular to $\mathbf{R}$. The value of V_{par} (along with the value of R and a uniform random number between 0 and 1 in the place of W_{Drift}) is then used to calculate d_c, the distance of closest approach, from equation (7.16). If this distance is greater than a, the encounter distance, then there is no encounter and consequently no reaction and the simulation continues to the next step. If d_c is equal to (or smaller than) a, then an encounter has taken place and we need to evaluate the probability in equation (7.21) and compare it with a random number between 0 and 1 (it should be noted that $y = |\mathbf{R}+\delta\mathbf{R}|$ after we take V_{ref} into account (equation (7.17)) and $x = R$) to determine if the encounter results in a reaction. If there is a reaction, the relevant changes are made. If the encounter does not result in a reaction, then the particles reflect. The reflection does not affect $\mathbf{S}+\delta\mathbf{S}$ or V_{per} but only V_{par}. Following that, the values of V_{per} and V_{ref} (equation (7.17)) are put together to give the new $\mathbf{R}+\delta\mathbf{R}$. The new $\mathbf{R}+\delta\mathbf{R}$ vector and the unchanged vector $\mathbf{S}+\delta\mathbf{S}$ are then used to obtain the new vector positions of the two particles, which will be used in the next step. The simulation includes a number of new complications and Figure 7.1 shows a test against the analytic solution (equation (3.11)) for comparison. The RF simulation is in good agreement with the analytic solution, validating the simulation method for future use.

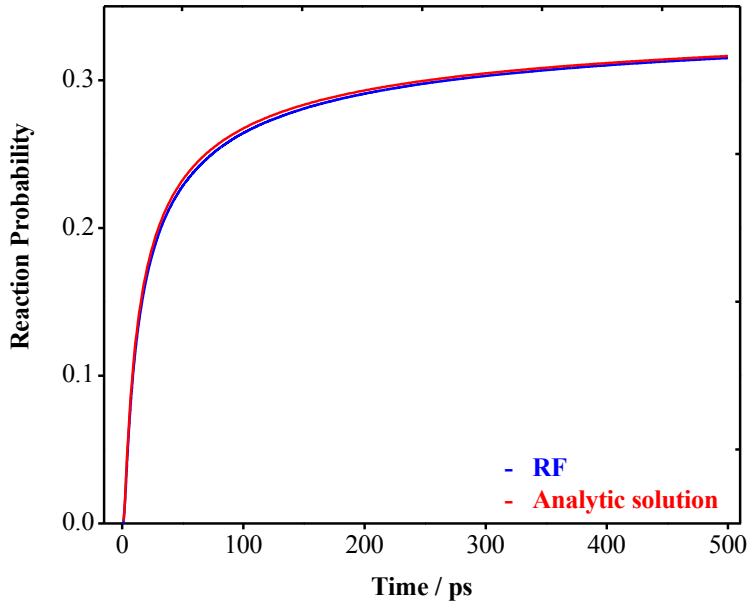


Figure 7.1. Example of the RF simulations. This is for two neutral particles separated by 10 Å initially. The analytic solution is equation (3.11). The values of the coefficients are a = 5 Å, D' = 2 Å^2.ps^{-1} and v = 1 Å.ps^{-1}. The minimum time step is 0.1 ps. The values at 500 ps are 0.315(±0.002) for the RF simulation and 0.316 for the analytic solution.

7.3. IRT simulations with RBC

We will continue with the simple example above (reaction (7.5)) where we assume that A and B are neutral for simplicity. In order to build IRT simulations with RBC we need to be able to generate a random reaction time where the RBC is taken into account. If we consider the pair A and B, then their random reaction time with RBC (denoted T) can be divided into two parts. The first part T_1 is the time necessary for the two particles to encounter for the first time. The second part T_2 is the time between the first encounter and the reaction (that is if a reaction eventually happens), and then the random reaction time for the relevant pair will be the sum of the two parts as follows:

$$T = T_1 + T_2 \qquad (7.26).$$

With regard to the first part T_1, the problem is straightforward for neutral particles. It is the reaction time for a fully diffusion-controlled reaction (or in other words we effectively have the Smoluchowski boundary condition) and can be obtained using equation (3.1) as before.

With regard to the second part T_2, the treatment is more challenging and requires the analysis of equation (3.11). This has been described in detail in the literature,[180] and will be briefly discussed here. It is helpful to first introduce the following

$$k_a = 4\pi a^2 v \quad , \quad k_{D'} = 4\pi a D' \tag{7.27}$$

where v is the reaction velocity, and so equation (3.11) is written for two neutral particles as follows[6,18,134]

$$W\left(t, r; a\right) = \frac{a}{r}\frac{k_a}{k_a + k_{D'}}\left[\operatorname{erfc}\left(\alpha\right) - e^{\beta\left(2\alpha+\beta\right)}\operatorname{erfc}\left(\alpha+\beta\right)\right] \tag{7.28}$$

where

$$\alpha = \frac{r-a}{\sqrt{4D't}} \quad , \quad \beta = \frac{\left(1+\delta^{-1}\right)}{a}\sqrt{D't} \quad , \quad \delta = \frac{D'}{v\,a} \tag{7.29}.$$

Now, since we are interested in T_2, we are looking at the two particles right at the end of the first stage, i.e. right at the time T_1 where the first encounter is taking place. In this case, the pair starts in contact ($r = a$), and hence the last equation reduces to

$$W\left(t, r=a\right) = \frac{k_a}{k_a + k_{D'}}\left[1 - e^{\beta^2}\operatorname{erfc}\left(\beta\right)\right] \tag{7.30}.$$

The basic idea to generate a reaction time from the last equation is to consider a random variable X whose probability distribution function F is

$$F_X\left(\beta\right) = \Pr\left\{X \le \beta\right\} = 1 - e^{\beta^2}\operatorname{erfc}\left(\beta\right) \tag{7.31}$$

and the probability density f is

$$f_X\left(\beta\right) = \frac{\partial F_X}{\partial \beta} = \frac{2}{\sqrt{\pi}} - 2\beta e^{\beta^2}\operatorname{erfc}\left(\beta\right) \tag{7.32}$$

which can be written in the following form[162,180]

$$f_X\left(\beta\right) = \frac{2}{\sqrt{\pi}} - 2\beta e^{\beta^2}\operatorname{erfc}\left(\beta\right) = \frac{1}{\sqrt{\pi}}\int_0^{\infty} y\, e^{-\beta y} e^{-y^4/4}\, dy \tag{7.33}.$$

If we introduce the following notation

$$f_Y\left(y\right) = \frac{1}{\sqrt{\pi}} e^{-y^2/4} \tag{7.34}$$

and

$$f_{X|Y}\left(\beta|y\right) = y\,e^{-\beta y} \tag{7.35},$$

equation (7.33) can be written as

$$f_X\left(\beta\right) = \int_0^\infty f_{X|Y}\left(\beta|y\right) f_Y\left(y\right) dy \tag{7.36}.$$

This matches the relationship between the marginal probability density of a random variable X and the joint probability density of the two random variables X and Y. More specifically we write

$$f_X\left(\beta\right) = \int_0^\infty f_{XY}\left(\beta, y\right) dy = \int_0^\infty f_{X|Y}\left(\beta|y\right) f_Y\left(y\right) dy \tag{7.37}$$

where f_{XY} is the joint probability density function of X and Y. Hence, the random variable X with the required density can be obtained by first generating a random variable Y to be the absolute value of a normal random variable with mean 0 and variance 2 and then generating X from an exponential distribution with mean $1/Y$. This can be accomplished as follows:[180]

- We generate a uniform random number between 0 and 1 denoted U_1.
- If U_1 is greater than $k_a/(k_a + k_{D'})$, then the reaction time is infinitely large, i.e. the reaction will not take place. If this is not the case, then we generate Y, a normally distributed random number with mean 0 and variance 2.
- We generate a new uniform random number between 0 and 1 denoted U_2. Then $X = -\left(\ln U_2\right)\big/\left|Y\right|$ is an exponentially distributed random variable with mean 1/Y.
- The required reaction time is $T_2 = \dfrac{D'X^2}{v^2}\left(\dfrac{k_a}{k_a + k_{D'}}\right)^2$.

Once T_1 and T_2 are known, the total reaction time T is then calculated from equation (7.26). Hence, the Monte Carlo IRT simulations proceed then as described before, the only difference is that for each pair we need to generate two times and sum them to obtain the random reaction time. This method is tested against the RF model in Figure 7.2. The IRT simulation is in very good agreement with the RF, and this therefore validates its use for future application.

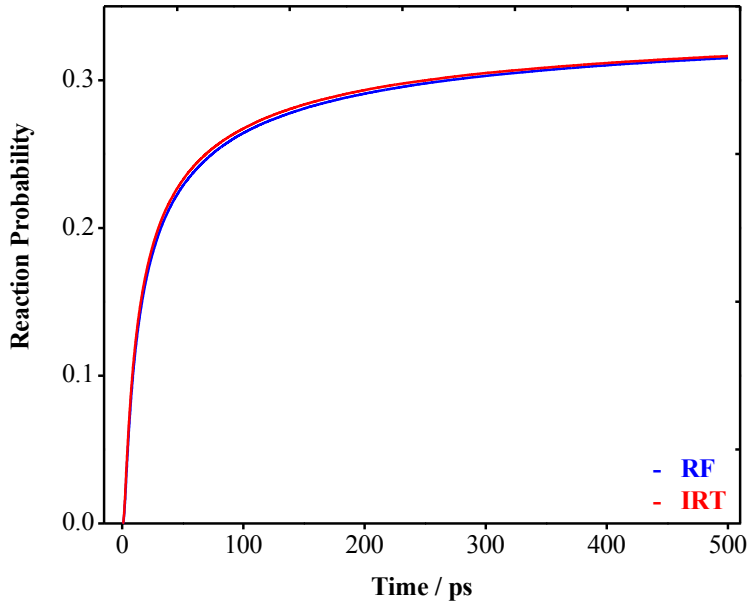


Figure 7.2. Example of the IRT simulations with RBC. This is for two neutral particles separated by 10 Å initially. The values of the coefficients are a = 5 Å, D' = 2 Å^2.ps^{-1} and v = 1 Å.ps^{-1}. The RF simulation is included for comparison. The minimum time step is 0.1 ps. The values at 500 ps are 0.316(±0.002) for the IRT simulation and 0.315(±0.002) for the RF simulation.

7.4. The IRT method and a reversible reaction

As discussed above, the first challenge that arises when trying to model a reversible reaction is that the forward reaction (equation (7.4)) obeys the radiation boundary condition and this is relatively more complicated to model. The second challenge is related to the IRT method in particular. As discussed before, in order to generate a random reaction time for a pair of particles (A and B in reaction (7.4)), we need to know exactly their separation distance. The IRT method tells when the pair is going to react but does not automatically give any information about where in space (i.e. coordinates) the resulting product is going to be once the reaction has taken place. Consequently, when the product particle (in our example AB) eventually dissociates and forms two new particles (A and B) in contact, there is no information available about where they are in space. Hence, we cannot actually generate reaction times for the new A and B with the pre-existing A and B particles because the corresponding distances are not known. Resolving this issue is technically very challenging.[19,120]

The logical method to deal with the above issue is to "diffuse" the A-B distances for the A and B particles in the system until the time when the AB product

re-dissociates (in a similar way to the RF model when diffusive motion for each particle is simulated), but this is actually complicated and requires extra caution. This is because we have already generated an IRT T, the reaction time for each pre-existing pair, which means that the distance A-B must evolve in such a way that at this "future" time T the pair will be in reactive configuration (i.e. they are separated by a, their encounter distance) and also that at some earlier time T_1 the pair will encounter for the first time. In other words, we need to "diffuse" the distance A-B conditional on the reaction time for the pair T and the first encounter time T_1, and where we also take the RBC into account. This requires solving the appropriate diffusion equations and will be discussed next (Bessel process with RBC). It should be noted that this is similar to "the first passage approach", and "the centre of diffusion" method for reactive products that has been described elsewhere.[19,120]

Before we move and consider Bessel process with RBC, it should be noted that the situation is actually much more complicated than what has been described above. This is because it seems (this is not yet fully resolved) that we need to effectively monitor how a complete "net" of distances evolve (or diffuse) in time, and not only the A-B distances. For example, if we consider **S** "the sort of diffusive centre of gravity"[6,18,122,181] vector given in equation (7.15) associated with a certain A-B pair, then it seems that we need to monitor the distances A-S and B-S for the all other A and B particles and so on. Similarly, it seems also that we need to monitor the distances A-AB and B-AB when there are AB (the product) particles in the sample. This makes developing a computer simulation program really challenging.

7.4.1. Bessel process with RBC

We have presented the definition of the Bessel process (or radial process) before (equation (2.27)). If we denote the probability density function that the pair of particles diffuses from a separation x to a separation y in time t as $p(t,x,y)$, we will be looking in this section at the differential equations of diffusion for p.

7.4.1.1. The backward and forward diffusion equations

The backward diffusion equation is written as follows (equation (2.16))

$$\frac{1}{D'}\frac{\partial p}{\partial t}=\frac{\partial^2 p}{\partial x^2}+\frac{2}{x}\frac{\partial p}{\partial x} \qquad : \; p=p\left(t,x,y\right) \tag{7.38}$$

where the drift (or infinitesimal mean) $\mu = 2D'/x$ and the infinitesimal variance $\sigma^2 = 2D'$. The forward diffusion equation is (equation (2.18))

$$\frac{1}{D'}\frac{\partial p}{\partial t}=\frac{\partial^2 p}{\partial y^2}-\frac{\partial}{\partial y}\left(\frac{2}{y}p\right) \qquad : \; p=p\left(t,x,y\right) \tag{7.39}$$

where the drift (or infinitesimal mean) is $2D'/y$ and the infinitesimal variance is $2D'$ (it should be noted that the difference between the last equation and equation (7.18) is that in the latter the drift μ was considered constant). The boundary conditions are similar to those of equation (7.19) and will be detailed here. The initial condition is that

$$p\left(t=0,x,y\right)=\delta\left(x-y\right)=\delta\left(y-x\right) \tag{7.40}.$$

We also require that

$$x\to\infty \text{ or } y\to\infty \Rightarrow p\left(t,x,y\right)\to 0 \tag{7.41}.$$

Furthermore, at the separation a, we have the RBC. For the backward diffusion equation we have

$$\left.\frac{\partial p}{\partial x}\right|_{x=a}=\frac{v}{D'}p\left(t,x=a,y\right) \tag{7.42}$$

and for the forward diffusion equation we have

$$\left(\frac{\partial p}{\partial y}-\frac{2}{y}p\right)_{y=a}=\frac{v}{D'}p\left(t,x,y=a\right) \tag{7.43}.$$

One of the standard techniques to deal with the above equations (either the backward or the forward) is to use the Laplace transform (equation (3.6)), which changes the differential equation from a partial differential equation to an ordinary one. For the backward equation (equation (7.38)) we have

$$\frac{1}{D'}\left(s\tilde{p}-\delta\left(x-y\right)\right)=\frac{\partial^2 \tilde{p}}{\partial x^2}+\frac{2}{x}\frac{\partial \tilde{p}}{\partial x} \tag{7.44}$$

where $\tilde{p}$ is the Laplace transform of p. Similarly for the forward equation we have

$$\frac{1}{D'}\left(s\tilde{p}-\delta\left(y-x\right)\right)=\frac{\partial^2 \tilde{p}}{\partial y^2}-\frac{\partial}{\partial y}\left(\frac{2}{y}\tilde{p}\right) \tag{7.45}.$$

The RBC boundary condition becomes for the backward diffusion equation (after the Laplace transform) as follows

$$\left.\frac{\partial \tilde{p}}{\partial x}\right|_{x=a} = \frac{v}{D'}\tilde{p}\left(t, x=a, y\right) \tag{7.46}$$

and for the forward diffusion equation, we have

$$\left(\frac{\partial \tilde{p}}{\partial y} - \frac{2}{y}\tilde{p}\right)_{y=a} = \frac{v}{D'}\tilde{p}\left(t, x, y=a\right) \tag{7.47}.$$

It is useful to introduce the following function q as follows

$$q = \frac{x}{y}\tilde{p} \tag{7.48}$$

which if used, equations (7.44) and (7.45) respectively become self-adjoint

$$-\frac{x}{D'y}\delta\left(x-y\right) = \frac{\partial^2 q}{\partial x^2} - \frac{s}{D'}q \tag{7.49}$$

and

$$-\frac{x}{D'y}\delta\left(y-x\right) = \frac{\partial^2 q}{\partial y^2} - \frac{s}{D'}q \tag{7.50}.$$

In this case the RBC becomes respectively

$$\left.\frac{\partial q}{\partial x}\right|_{x=a} = \left(\frac{v}{D'} + \frac{1}{a}\right)q\left(s, x=a, y\right) = \beta q\left(s, x=a, y\right) \qquad : \beta = \frac{v}{D'} + \frac{1}{a} \tag{7.51}$$

and

$$\left.\frac{\partial q}{\partial y}\right|_{y=a} = \left(\frac{v}{D'} + \frac{1}{a}\right)q\left(s, x, y=a\right) = \beta q\left(s, x, y=a\right) \tag{7.52}$$

and the function q is symmetric in x and y. It should be noted that the function q is continuous at the point $x = y$ but its derivative is not. This can be shown if we integrate equation (7.49) from y-ε to y+ε (or similarly equation (7.50) from x-ε to x+ε) and then take the limit $\varepsilon \to 0$ as follows

$$-\frac{1}{D'} = \lim_{\varepsilon \downarrow 0}\left\{\left.\frac{\partial q}{\partial x}\right|_{x=y+\varepsilon} - \left.\frac{\partial q}{\partial x}\right|_{x=y-\varepsilon}\right\} \tag{7.53}$$

and similarly for equation (7.50) have

$$-\frac{1}{D'} = \lim_{\varepsilon \downarrow 0}\left\{\left.\frac{\partial q}{\partial y}\right|_{y=x+\varepsilon} - \left.\frac{\partial q}{\partial y}\right|_{y=x-\varepsilon}\right\} \tag{7.54}.$$

We will discuss (for example) the case of the forward equation (equation (7.50)) but a similar discussion can be written for the case of the backward equation. The solution to equation (7.50) has the following general form

$$q = \varsigma e^{\gamma y} + \tau e^{-\gamma y} \quad : \ \gamma = \sqrt{s/D'} \tag{7.55}$$

but because there are two regions for the values of y ($x < y$ and $a \le y < x$), then the coefficients ς and τ will have different values over each region. For the region $x < y$, then we apply the condition in equation (7.41) to obtain the following

$$q = \tau_1 e^{-\gamma y} \quad : \ x < y \tag{7.56}.$$

For the region $a < y < x$, we use the RBC of equation (7.52) to get

$$(\beta + \gamma)\varsigma_2 e^{\gamma a} = (\beta - \gamma)\tau_2 e^{-\gamma a} \tag{7.57}$$

which indicates that

$$(\beta + \gamma)\varsigma_2 e^{\gamma a} = (\beta - \gamma)\tau_2 e^{-\gamma a} = \kappa \tag{7.58}$$

where κ is a constant. Hence, we have

$$q = \kappa\left(\frac{e^{\gamma(y-a)}}{\gamma - \beta} + \frac{e^{-\gamma(y-a)}}{\gamma + \beta}\right) \quad : \ a \le y < x \tag{7.59}.$$

The constants κ in the last equation and τ_1 in equation (7.56) can be obtained if we combine the continuity of q written as follows

$$\tau_1 e^{-\gamma x} = \kappa\left(\frac{e^{\gamma(x-a)}}{\gamma - \beta} + \frac{e^{-\gamma(x-a)}}{\gamma + \beta}\right) \tag{7.60}$$

and the discontinuity of the derivative (equation (7.54))

$$-\kappa\left(\frac{\gamma e^{\gamma(x-a)}}{\gamma - \beta} - \frac{\gamma e^{-\gamma(x-a)}}{\gamma + \beta}\right) - \tau_1 \gamma e^{-\gamma x} = -\frac{1}{D'} \tag{7.61}$$

to give

$$\tau_1 = \frac{1}{2\gamma D'}\left(e^{\gamma x} + \frac{\gamma - \beta}{\gamma + \beta} e^{-\gamma(x-2a)}\right) \tag{7.62}$$

and

$$\kappa = \frac{\gamma - \beta}{2\gamma D'} e^{-\gamma(x-a)} \tag{7.63}$$

and hence we can write

$$q=\begin{cases}\dfrac{1}{2\gamma D'}\left(e^{\gamma(y-x)}+\dfrac{\gamma-\beta}{\gamma+\beta}e^{-\gamma(y+x-2a)}\right) & :\ a\le y<x\\ \dfrac{1}{2\gamma D'}\left(e^{-\gamma(y-x)}+\dfrac{\gamma-\beta}{\gamma+\beta}e^{-\gamma(y+x-2a)}\right) & :\ y>x\end{cases} \tag{7.64}$$

or in general

$$q=\frac{1}{2\gamma D'}\left(e^{-\gamma|y-x|}+\frac{\gamma-\beta}{\gamma+\beta}e^{-\gamma(y+x-2a)}\right) \tag{7.65}.$$

Hence if we use equation (7.48), we obtain

$$\tilde{p}(s,x,y)=\frac{1}{2\gamma D'}\frac{y}{x}\left(e^{-\gamma|y-x|}+\frac{\gamma-\beta}{\gamma+\beta}e^{-\gamma(y+x-2a)}\right) \tag{7.66},$$

and the inverse Laplace transform is[154]

$$\begin{aligned}p(t,x,y)=\frac{y}{x\sqrt{4\pi D't}}\Bigg\{&e^{-(y-x)^2/4D't}+\\ &e^{-(y+x-2a)^2/4D't}\left(1-\beta\sqrt{4\pi D't}\ \mathrm{eerc}\left(\beta\sqrt{D't}+\frac{y+x-2a}{\sqrt{4D't}}\right)\right)\Bigg\}\end{aligned} \tag{7.67}$$

where we have used the following notation

$$\mathrm{eerc}(x)=e^{x^2}\mathrm{erfc}(x) \tag{7.68}.$$

For the special case when $x = a$ (the particles start in contact), we have

$$\begin{aligned}p(t,x=a,y)=\frac{y\,e^{-(y-a)^2/4D't}}{a\sqrt{\pi D't}}\Bigg[&1-\beta\sqrt{\pi D't}\times\\ &\mathrm{eerc}\left(\beta\sqrt{D't}+\frac{y-a}{\sqrt{4D't}}\right)\Bigg]\end{aligned} \tag{7.69}.$$

Similarly for the special case when $y = a$ (the particles end up in contact), we have

$$\begin{aligned}p(t,x,y=a)=\frac{a\,e^{-(x-a)^2/4D't}}{x\sqrt{\pi D't}}\Bigg[&1-\beta\sqrt{\pi D't}\times\\ &\mathrm{eerc}\left(\beta\sqrt{D't}+\frac{x-a}{\sqrt{4D't}}\right)\Bigg]\end{aligned} \tag{7.70}.$$

Finally when $x = y = a$ (the particles start in contact and end up in contact), we have

$$p(t,x=a,y=a)=\frac{1}{\sqrt{\pi D't}}\left(1-\beta\sqrt{\pi D't}\ \mathrm{eerc}\left(\beta\sqrt{D't}\right)\right) \tag{7.71}.$$

7.4.1.2. The survival probability

The probability that the pair will survive Ω can be obtained from

$$\Omega(t,x)=\int_a^\infty p(t,x,y)\,dy \tag{7.72}.$$

If we take the Laplace transform, we have

$$\tilde{\Omega}(s,x)=\int_a^\infty \tilde{p}(s,x,y)\,dy \tag{7.73}$$

where $\tilde{\Omega}$ is the Laplace transform of Ω. $\tilde{p}$, the Laplace transform of p, is already available (equation (7.66)) and hence

$$\tilde{\Omega}(s,x)=\frac{1}{2\gamma D'x}\left[\int_a^x y\,e^{\gamma(y-x)}\,dy+\int_x^\infty y\,e^{-\gamma(y-x)}\,dy+\frac{\gamma-\beta}{\gamma+\beta}\int_0^\infty y\,e^{-\gamma(y+x-2a)}\,dy\right] \tag{7.74}$$

where β and γ were defined in equations (7.51) and (7.55) respectively. The last equation gives[149,150]

$$\tilde{\Omega}(s,x)=\frac{1}{s}\left[1-\frac{\beta a-1}{(\gamma+\beta)x}e^{-\gamma(x-a)}\right] \tag{7.75}.$$

If we take the inverse of the Laplace transform, we obtain[154]

$$\Omega(t,x)=\left[1-\frac{a}{x}\frac{v}{\beta D'}\left(\operatorname{erfc}\left(\frac{x-a}{\sqrt{4D't}}\right)-e^{-(x-a)^2/4D't}\operatorname{eerc}\left(\beta\sqrt{D't}+\frac{x-a}{\sqrt{4D't}}\right)\right)\right] \tag{7.76}$$

where eerc was defined in equation (7.68). For the special case $x = a$, we have the following simple equation

$$\Omega(t,x=a)=1-\frac{v}{\beta D'}\left(1-\operatorname{eerc}\left(\beta\sqrt{D't}\right)\right) \tag{7.77}.$$

Finally, it should be noted that the same result can be obtained if we solve the following backward diffusion equation for Ω

$$\frac{1}{D'}\frac{\partial\Omega}{\partial t}=\frac{\partial^2\Omega}{\partial x^2}+\frac{2}{x}\frac{\partial\Omega}{\partial x}\qquad :\ \Omega=\Omega(t,x) \tag{7.78}$$

with the following boundary conditions

$$\Omega\left(t=0,x\right)=1 \quad , \quad \lim_{x\uparrow\infty}\Omega=1$$
$$\left.\frac{\partial\Omega}{\partial x}\right|_{x=a}=\frac{v}{D'}\Omega\left(t,x=a\right) \tag{7.79}.$$

7.4.1.3. The reaction probability

The reaction probability W can be obtained from the survival probability as follows

$$W\left(t,x\right)=1-\Omega\left(t,x\right)=\frac{a}{x}\frac{v}{\beta D'}\left(\operatorname{erfc}\left(\frac{x-a}{\sqrt{4D't}}\right)+ e^{-\left(x-a\right)^2/4D't}\operatorname{eerc}\left(\beta\sqrt{D't}+\frac{x-a}{\sqrt{4D't}}\right)\right) \tag{7.80}$$

where eerc is given in equation (7.68). Hence, the probability density function for the reaction time is

$$w\left(t,x\right)=\frac{\partial W}{\partial t}=\frac{a}{x}\frac{v}{\sqrt{\pi D't}}e^{-\left(x-a\right)^2/4D't}\left[1-\beta\sqrt{\pi D't}\times \operatorname{eerc}\left(\beta\sqrt{D't}+\frac{x-a}{\sqrt{4D't}}\right)\right] \tag{7.81}.$$

For $x = a$ we have

$$w\left(t,x=a\right)=\frac{v}{\sqrt{\pi D't}}\left(1-\beta\sqrt{\pi D't}\,\operatorname{eerc}\left(\beta\sqrt{D't}\right)\right) \tag{7.82}.$$

7.4.1.4. Interpolation conditional on a reaction time

As mentioned before, we are interested in how the separation of the two particles y evolves given that the reaction takes place at some time T. Hence we define p^*, the probability density function of the separation y at time t given that a reaction will take place at time T, as follows (the particles start in contact $x = a$ and then they diffuse away to a separation of y. Following that they diffuse to a separation of a at time T and react)

$$p^*\left(t,T,y\right)=\frac{p\left(t,x=a,y\right)w\left(T-t,y\right)}{w\left(T,x=a\right)} \tag{7.83}.$$

Using the results above (equations (7.69), (7.81) and (7.82)), we have

$$p^*(t,T,y)=\frac{e^{-(y-a)^2 T/4D't(T-t)}}{\sqrt{\pi D't(T-t)/T}}\times$$
$$\left[1-\beta\sqrt{\pi D'(T-t)}\,\mathrm{eerc}\left(\beta\sqrt{D'(T-t)}+\frac{y-a}{\sqrt{4D'(T-t)}}\right)\right]\times \qquad (7.84)$$
$$\frac{1-\beta\sqrt{\pi D't}\,\mathrm{eerc}\left(\beta\sqrt{D't}+\frac{y-a}{\sqrt{4D't}}\right)}{1-\beta\sqrt{\pi D'T}\,\mathrm{eerc}\left(\beta\sqrt{D'T}\right)}$$

where β, γ and eerc were defined in equations (7.51), (7.55) and (7.68) respectively. It should be noted that the last equation is symmetrical between t and T-t. This type of diffusion, where the initial and final points are the same and the point is not visited in between is called a meander, and will always exhibit this time symmetry.

7.4.2. Practical considerations

Equation (7.84) specifies how the separation distance of a pair y evolves in time, given that the pair reacts at some time T. The key question now is how to apply this function in a practical simulation method. Answering this question is technically very difficult because p^* is a multi-variable function and has a very complicated formula. Clearly, we need to be able to generate random numbers (so that we can "diffuse" y) from the probability density function p^* and this does not seem to be easy due to the above-mentioned reasons.

In order to relax this, the first step is to characterize p^* and investigate its general properties. Examples are presented in Figure 7.3 where we set a = 5 Å, D' = 2 Å^2.ps^{-1} and v = 1 Å.ps^{-1}. We have chosen the reaction time T = 10 ps to be constant and changed the time variable t from 1 to 9 ps. The function shows a symmetrical property with regard to t as, for example, the curves for t = 1 and t = 9 ps are identical, as can be seen from the symmetry of the function between t and $T - t$ (as mentioned above, this type of diffusion process is known as a meander). Due to the shape of the function, it is hoped that a reasonable fit can be obtained. We tried first to fit it to a Gaussian but that did not seem to give the desired result. It seems that a reasonable fit can be obtained using a gamma probability density function as follows

(we have listed the results of the fitting of this section in the appendix at the end of this chapter)

$$\psi_{\kappa\lambda}(y) = \frac{1}{\lambda^{\kappa}\Gamma(\kappa)}\, y^{\kappa-1}\, e^{-y/\lambda} \tag{7.85}$$

where Γ is the gamma function (equation (1.69)). Examples of this are shown in Figures 7.4 and 7.5. We have included two examples to show that the fitting can sometimes be good (Figure 7.4 where the determining coefficient $R^2 = 0.999$) and can be reasonable at other times (Figure 7.5 where $R^2 = 0.995$).

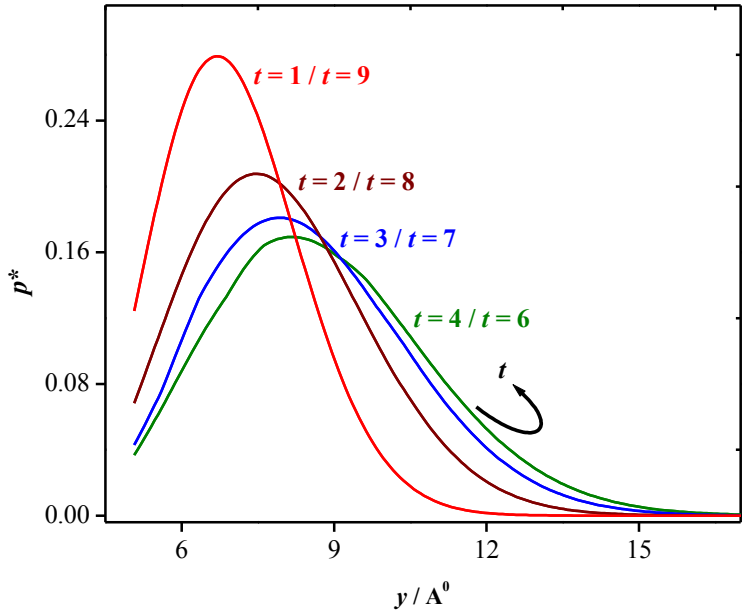


Figure 7.3. Examples of the function p^*. The values of the coefficients used when calculating p^* are a = 5 Å, D' = 2 Å^2.ps^{-1} and v = 1 Å.ps^{-1}. The reaction time T = 10 ps and t is varied between 1 and 9 ps.

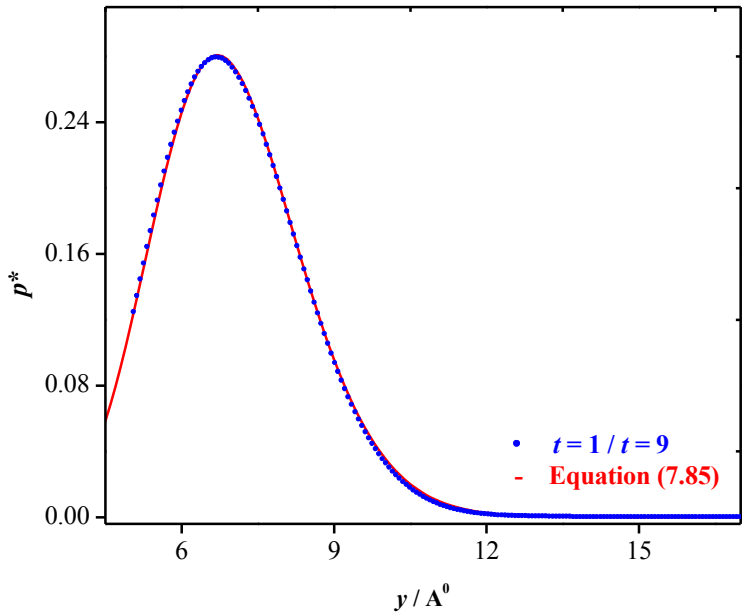


Figure 7.4. Example of the fitting. t = 1 / t = 9 are the curves from Figure 7.3. The values of the coefficients used when calculating p^* are a = 5 Å, D' = 2 Å^2.ps^{-1} and v = 1 Å.ps^{-1}. The reaction time T = 10 ps and t = 1 and 9 ps. This fitting produces values for κ and λ of equation (7.85).

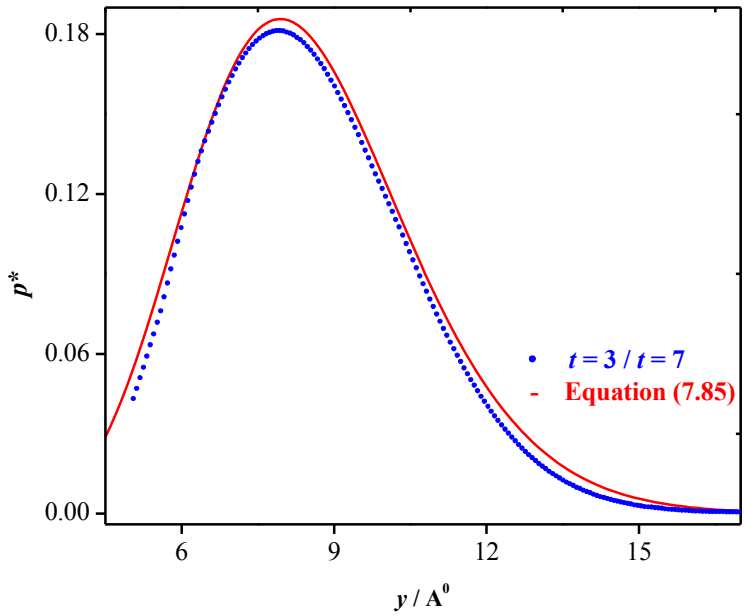


Figure 7.5. Example of the fitting. t = 3 / t = 7 are the curves from Figure 7.3. The values of the coefficients used when calculating p^* are a = 5 Å, D' = 2 Å^2.ps^{-1} and v = 1 Å.ps^{-1}. The reaction time T = 10 ps and t = 3 and 7 ps. This fitting produces values for κ and λ of equation (7.85).

It is interesting to see how the coefficients in the last equation (κ and λ) change with t. It turned out that they follow, reasonably, the following equation (again the results are available in the appendix at the end of the chapter)

$$\varphi = \frac{\rho}{\left[t\left(T-t\right)\right]^{\chi}} \tag{7.86}$$

where φ can be either κ or λ, and T is the reaction time (in this example T = 10 ps). The coefficients ρ and χ are determined from the fitting. The fitting is shown in Figure 7.6 for κ (where R^2 = 0.995) and Figure 7.7 for λ (where R^2 = 0.999).

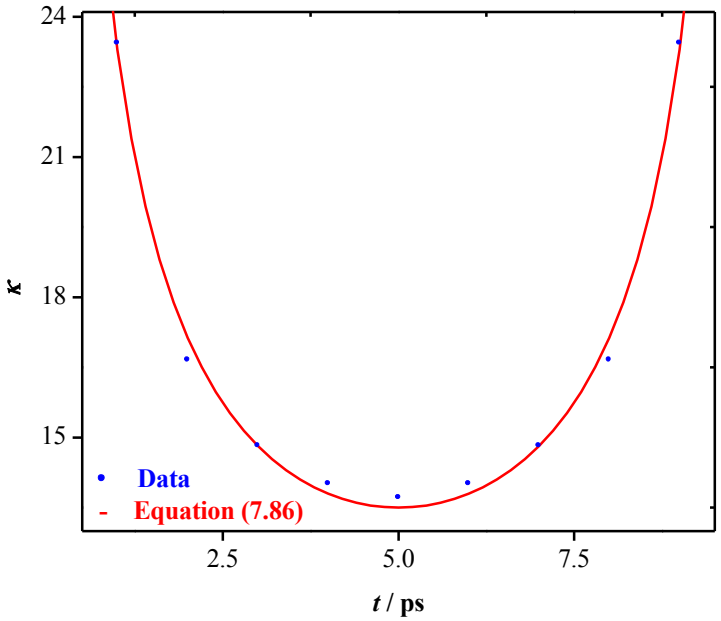


Figure 7.6. The fitting of the coefficient κ of equation (7.85) as a function of t. "Data" refers to the values of κ obtained from fitting processes (Figures 7.4-7.5 for example). The values of the coefficients used when calculating p^* are a = 5 Å, D' = 2 Å^2.ps^{-1} and v = 1 Å.ps^{-1}. The reaction time T = 10 ps. This fitting produces values for ρ and χ of equation (7.86).

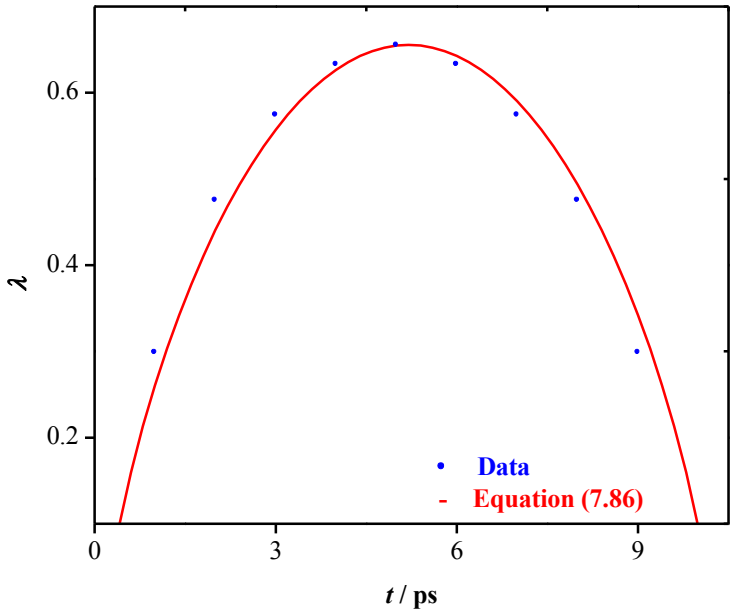


Figure 7.7. The fitting of the coefficient λ of equation (7.85) as a function of t. "Data" refers to the values of λ obtained from fitting processes (Figures 7.4-7.5 for example). The values of the coefficients used when calculating p^* are a = 5 Å, D' = 2 Å^2.ps^{-1} and v = 1 Å.ps^{-1}. The reaction time T = 10 ps. This fitting produces values for ρ and χ of equation (7.86).

It is now interesting to see how the coefficients in the last function (ρ and χ) depend on the reaction time T (this is interesting because, as discussed in more detail shortly, if ρ and χ systematically depend on T, then we can "approximately" solve the problem and generate random numbers from p^*). To discuss this, we have run calculations between T = 10 to T = 500 ps in steps of 10 ps. At each value for T, we have several values of t. At each value of t, we repeat the fitting process described above, i.e. we use equation (7.85) first to fit p^* and then we use equation (7.86) to fit the coefficients κ and λ of equation (7.85). After that we collect the obtained values of ρ and χ (it should be noted that there are two sets of values for each one. The first corresponds to κ, and the second corresponds to λ of equation (7.85)). It turned out that the values of ρ and χ can be reasonably fitted to the following equation (the results are listed in the appendix at the end of the chapter)

$$\varsigma = \alpha_1 T^{\alpha_2} + \alpha_3 \tag{7.87}$$

where ς can be either ρ or χ, T is the reaction time and α_i is a coefficient. The fittings for ρ and χ of κ of equation (7.85) are shown respectively in Figures 7.8 and 7.9.

Similarly, the fittings for ρ and χ of λ of equation (7.85) are shown respectively in Figures 7.10 and 7.11.

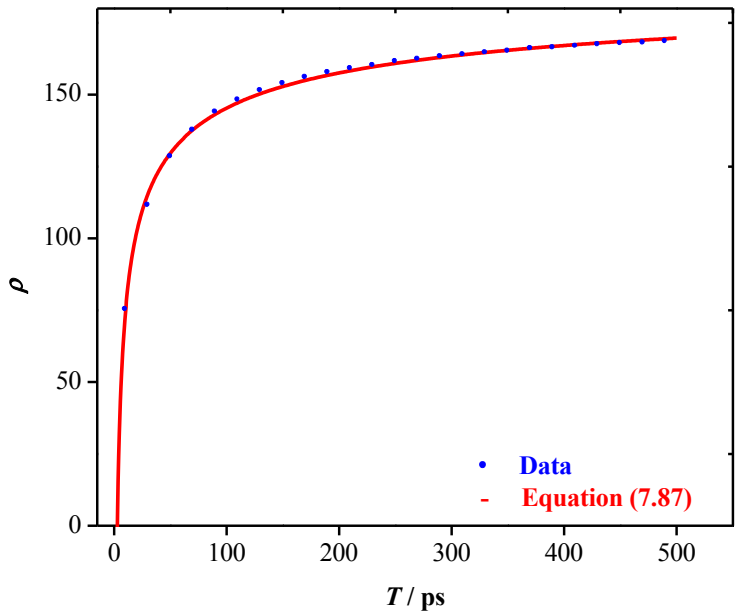


Figure 7.8. The fitting of the coefficient ρ of equation (7.86) for κ of equation (7.85) as a function of T, the reaction time. "Data" refers to the values of ρ obtained from fitting processes (Figure 7.6 for example). The values of the coefficients used when calculating p^* are a = 5 Å, D' = 2 Å^2.ps^{-1} and v = 1 Å.ps^{-1}. This fitting produces values for the coefficients α_i of equation (7.87).

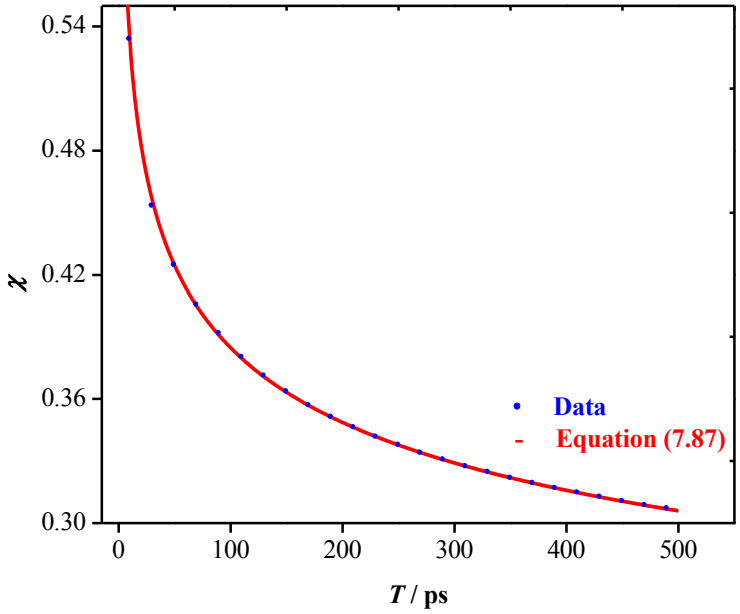


Figure 7.9. The fitting of the coefficient χ of equation (7.86) for κ of equation (7.85) as a function of T, the reaction time. "Data" refers to the values of χ obtained from fitting processes (Figure 7.6 for example). The values of the coefficients used when calculating p^* are a = 5 Å, D' = 2 Å^2.ps^{-1} and v = 1 Å.ps^{-1}. This fitting produces values for the coefficients α_i of equation (7.87).

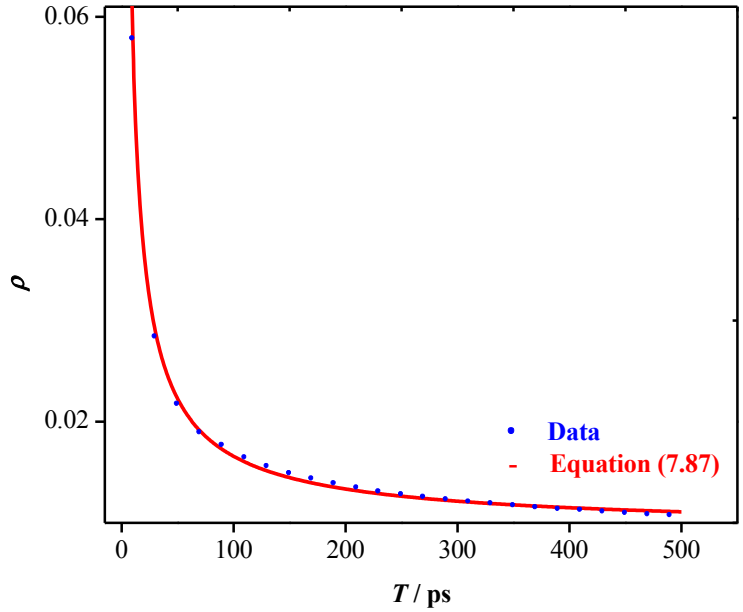


Figure 7.10. The fitting of the coefficient ρ of equation (7.86) for λ of equation (7.85) as a function of T, the reaction time. "Data" refers to the values of ρ obtained from fitting processes (Figure 7.7 for example). The values of the coefficients used when calculating p^* are a = 5 Å, D' = 2 Å^2.ps^{-1} and v = 1 Å.ps^{-1}. The fitting produces values for the coefficients α_i of equation (7.87).

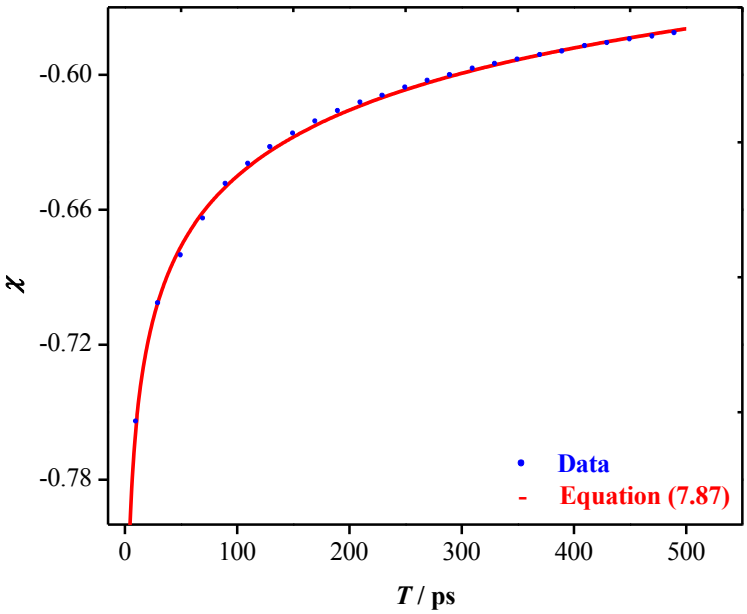


Figure 7.11. The fitting of the coefficient χ of equation (7.86) for λ of equation (7.85) as a function of T, the reaction time. "Data" refers to the values of χ obtained from fitting processes (Figure 7.7 for example). The values of the coefficients used when calculating p^* are a = 5 Å, D' = 2 Å^2.ps^{-1} and v = 1 Å.ps^{-1}. The fitting produces values for the coefficients α_i of equation (7.87).

The above results can be used to "approximately" generate random numbers from p^* (it is worth stressing that this is only an approximation since the fitting was not perfect all of the time (Figure 7.5)). The key idea is that when the reaction time of the pair T is known (this typically generated very early in the course of IRT simulations), then equation (7.87) can be used to produce values for ρ and χ of equation (7.86). These values are then used in equation (7.86), at any given time t during the simulations, to calculate the values of κ and λ which then can be used in equation (7.85) and hence the random numbers will be generated from equation (7.85) (and this is straightforward) instead of using directly p^*. To demonstrate this, let us suppose, for example, that we are considering a pair whose reaction time T = 100 ps and we are looking at t = 81 ps. Then we use T in equation (7.87) along with the values in Table 7.3 in the appendix to calculate ρ and χ for the coefficient κ first (respectively 145.338 and 0.385) and second for the coefficient λ (respectively 0.0166 and -0.645). After that the calculated values are put together with the value of t in equation (7.86) to obtain the values for κ first and then for λ (respectively 8.616 and 1.887). These values are then used to generate random y from equation (7.85), which is straightforward. As mentioned above, this is only an approximation (Figure 7.12 shows the difference between actual p^* and the curve that will be used to generate the random number from).

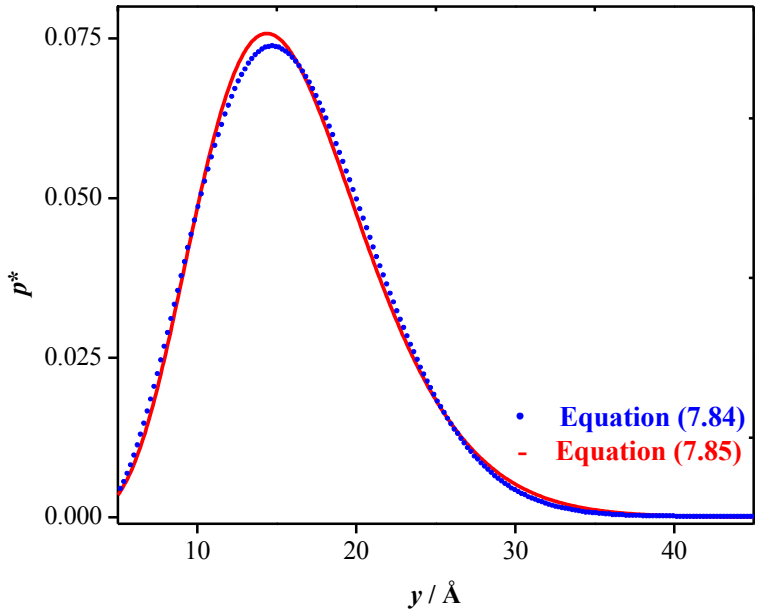


Figure 7.12. Example of using the proposed approximation. The approximation is to use the red curve (the gamma density function obtained from the fitting parameters in the appendix at the end of this chapter) instead of the blue curve, p^*. The values of the coefficients used when calculating p^* are $a = 5$ Å, $D' = 2$ Å^2.ps^{-1} and $v = 1$ Å.ps^{-1}.

7.5. Summary and future work

The problem of modelling reversible reaction is very challenging. The work presented in this chapter is incomplete and it needs to be considered further in a future work.

In this chapter, we have summarized the effects of RBC, and how the RF model and the IRT method can be used to model a partially diffusion-controlled reaction. We have also presented the solution for the diffusion equations for a Bessel process with RBC. The main new result in this chapter, which will be necessary for the IRT simulation of a reversible reaction, is an expression for the probability density function of the interparticle distance of a pair, conditional on a given reaction time in the future, and have proposed an approximate method to generate random numbers from it through a two-step fitting process. More work needs to be done before a complete model can be realised, but this has solved one of the harder problems on the way.

7.6. Appendix

Table 7.1. The fitting using equation (7.85). T is the reaction time.

T / ps	t / ps	κ	λ	R^2
10	1	23.44	0.2987	0.999
	2	16.66	0.4753	0.998
	3	14.83	0.5741	0.995
	4	14.02	0.6327	0.992
	5	13.72	0.6552	0.991
	6	14.02	0.6327	0.992
	7	14.83	0.5741	0.995
	8	16.66	0.4753	0.998
	9	23.44	0.2987	0.999
30	1	24.54	0.2915	0.999
	4	13.13	0.7483	0.999
	7	11.14	1.004	0.999
	10	10.29	1.169	0.999
	13	9.979	1.249	0.999
	16	9.939	1.26	0.998
	19	10.15	1.203	0.999
	22	10.73	1.073	0.999
	25	12.39	0.8371	0.999
	28	17.04	0.4867	0.999
50	1	24.78	0.2899	0.999
	6	11.55	0.9662	0.999
	11	9.725	1.355	0.999
	16	9.108	1.579	0.998
	21	8.845	1.696	0.998
	26	8.79	1.723	0.998
	31	8.922	1.66	0.998
	36	9.297	1.503	0.998
	41	10.17	1.227	0.999
	46	13.11	0.7644	0.999

T / ps	t / ps	κ	λ	R^2
70	1	24.89	0.2891	0.998
	8	10.38	1.186	0.999
	15	8.997	1.648	0.998
	22	8.47	1.925	0.998
	29	8.244	2.072	0.998
	36	8.192	2.109	0.998
	43	8.287	2.042	0.998
	50	8.578	1.86	0.998
	64	11.49	0.9847	0.999
90	1	24.96	0.2886	0.998
	10	9.754	1.369	0.999
	19	8.524	1.908	0.999
	28	8.057	2.23	0.998
	37	7.858	2.402	0.998
	46	7.811	2.448	0.998
	55	7.889	2.375	0.998
	64	8.133	2.173	0.998
	73	8.693	1.811	0.998
	82	10.34	1.203	0.999
110	1	25	0.2884	0.998
	12	9.303	1.537	0.999
	23	8.186	2.145	0.998
	34	7.766	2.507	0.998
	45	7.588	2.7	0.998
	56	7.54	2.755	0.998
	67	7.608	2.676	0.998
	78	7.819	2.455	0.998
	89	8.31	2.056	0.998
	100	9.723	1.385	0.999

T / ps	t / ps	κ	λ	R^2
130	1	25.04	0.288	0.998
	14	8.954	1.694	0.999
	27	7.93	2.364	0.998
	40	7.547	2.761	0.998
	53	7.381	2.976	0.998
	66	7.336	3.037	0.998
	79	7.397	2.953	0.998
	92	7.587	2.714	0.999
	105	8.024	2.282	0.998
	118	9.275	1.553	0.999
150	1	25.06	0.2879	0.998
	16	8.678	1.841	0.999
	31	7.726	2.569	0.998
	46	7.371	3	0.998
	61	7.22	3.231	0.998
	76	7.176	3.3	0.997
	91	7.23	3.211	0.998
	106	7.404	2.955	0.998
	121	7.804	2.491	0.998
170	1	25.08	0.2877	0.998
	18	8.453	1.98	0.999
	35	7.562	2.761	0.998
	52	7.228	3.224	0.998
	69	7.087	3.472	0.997
	86	7.048	3.546	0.997
	103	7.098	3.452	0.997
	120	7.257	3.181	0.998
	137	7.624	2.689	0.998
	154	8.659	1.855	0.999

T / ps	t / ps	κ	λ	R^2
190	1	25.1	0.2876	0.998
	20	8.266	2.111	0.999
	39	7.422	2.944	0.998
	58	7.112	3.435	0.997
	77	6.977	3.699	0.997
	96	6.94	3.778	0.997
	115	6.986	3.681	0.997
	134	7.132	3.395	0.998
	153	7.476	2.875	0.998
	172	8.436	1.994	0.999
210	1	25.11	0.2875	0.998
	22	8.105	2.238	0.999
	43	7.308	3.117	0.998
	64	7.012	3.636	0.997
	85	6.881	3.917	0.997
	106	6.847	4.001	0.997
	127	6.889	3.9	0.997
	148	7.03	3.598	0.997
	169	7.35	3.053	0.998
	190	8.251	2.125	0.999
230	1	25.12	0.2874	0.998
	24	7.964	2.359	0.998
	47	7.205	3.284	0.998
	70	6.921	3.831	0.997
	93	6.798	4.126	0.997
	116	6.764	4.215	0.997
	139	6.802	4.111	0.997
	162	6.94	3.793	0.997
	185	7.245	3.221	0.998

T / ps	t / ps	κ	λ	R^2
250	1	25.14	0.2873	0.998
	26	7.843	2.475	0.998
	51	7.116	3.444	0.998
	76	6.849	4.013	0.997
	101	6.728	4.324	0.997
	126	6.696	4.418	0.997
	151	6.734	4.308	0.997
	176	6.863	3.979	0.997
	201	7.151	3.384	0.998
	226	7.951	2.372	0.998
270	1	25.15	0.2871	0.998
	28	7.735	2.588	0.998
	55	7.039	3.598	0.998
	82	6.782	4.191	0.997
	109	6.663	4.518	0.997
	136	6.633	4.614	0.997
	163	6.673	4.498	0.997
	190	6.793	4.158	0.997
	217	7.065	3.542	0.998
	244	7.832	2.488	0.998
290	1	25.16	0.2871	0.998
	30	7.638	2.697	0.998
	59	6.969	3.746	0.997
	88	6.72	4.364	0.997
	117	6.608	4.702	0.997
	146	6.58	4.802	0.997
	175	6.613	4.687	0.997
	204	6.731	4.332	0.997
	233	6.993	3.692	0.998
	262	7.725	2.6	0.998

T / ps	t / ps	κ	λ	R^2
310	1	25.17	0.287	0.998
	32	7.55	2.803	0.998
	63	6.907	3.891	0.997
	94	6.666	4.53	0.997
	125	6.561	4.878	0.997
	156	6.531	4.985	0.996
	187	6.567	4.861	0.997
	218	6.676	4.499	0.997
	249	6.93	3.836	0.997
330	1	25.18	0.2869	0.998
	34	7.474	2.905	0.998
	67	6.849	4.03	0.997
	100	6.618	4.692	0.997
	133	6.515	5.052	0.997
	166	6.488	5.161	0.996
	199	6.519	5.037	0.997
	232	6.623	4.664	0.997
	265	6.868	3.98	0.997
	298	7.544	2.814	0.998
350	1	25.18	0.2869	0.998
	36	7.399	3.006	0.998
	71	6.796	4.167	0.997
	106	6.572	4.849	0.997
	141	6.472	5.221	0.996
	176	6.444	5.335	0.996
	211	6.477	5.206	0.996
	246	6.579	4.821	0.997
	281	6.819	4.114	0.997
	316	7.466	2.916	0.998

T / ps	t / ps	κ	λ	R^2
370	1	25.2	0.2868	0.998
	38	7.334	3.102	0.998
	75	6.747	4.301	0.997
	112	6.529	5.004	0.997
	149	6.434	5.384	0.996
	186	6.41	5.501	0.996
	223	6.438	5.371	0.996
	260	6.537	4.975	0.997
	297	6.768	4.249	0.997
	334	7.399	3.014	0.998
390	1	25.2	0.2868	0.998
	40	7.275	3.197	0.998
	79	6.707	4.427	0.997
	118	6.495	5.15	0.997
	157	6.403	5.541	0.996
	196	6.367	5.671	0.996
	235	6.402	5.532	0.996
	274	6.5	5.123	0.997
	313	6.725	4.378	0.997
410	1	25.21	0.2867	0.998
	42	7.215	3.292	0.998
	83	6.664	4.554	0.997
	124	6.457	5.296	0.997
	165	6.368	5.699	0.996
	206	6.343	5.823	0.996
	247	6.367	5.689	0.996
	288	6.464	5.269	0.997
	329	6.68	4.508	0.997
	370	7.268	3.208	0.998

T / ps	t / ps	κ	λ	R^2
430	1	25.22	0.2865	0.998
	44	7.167	3.38	0.998
	87	6.628	4.676	0.997
	130	6.426	5.437	0.996
	173	6.338	5.851	0.996
	216	6.312	5.98	0.996
	259	6.342	5.837	0.996
	302	6.43	5.412	0.997
	345	6.643	4.629	0.997
	388	7.214	3.3	0.998
450	1	25.23	0.2865	0.998
	46	7.118	3.469	0.998
	91	6.591	4.798	0.997
	136	6.397	5.576	0.996
	181	6.308	6.001	0.996
	226	6.283	6.134	0.996
	271	6.315	5.985	0.996
	316	6.404	5.549	0.996
	361	6.608	4.75	0.997
	406	7.161	3.391	0.998

T / ps	t / ps	κ	λ	R^2
	1	25.22	0.2865	0.998
	48	7.075	3.555	0.998
	95	6.562	4.913	0.997
	142	6.37	5.709	0.996
	189	6.279	6.149	0.996
470	236	6.26	6.279	0.996
	283	6.285	6.134	0.996
	330	6.37	5.69	0.996
	377	6.57	4.872	0.997
	424	7.114	3.479	0.998
	469	25.22	0.2865	0.998
	1	25.24	0.2864	0.998
	50	7.036	3.639	0.998
	99	6.527	5.032	0.997
	148	6.342	5.845	0.996
	197	6.26	6.287	0.996
490	246	6.235	6.426	0.996
	295	6.262	6.275	0.996
	344	6.346	5.82	0.996
	393	6.541	4.987	0.997
	442	7.07	3.565	0.998
	489	25.24	0.2864	0.998

Table 7.2. The fitting using equation (7.86).

T / ps	ρ_κ	χ_κ	R^2	ρ_λ	χ_λ	R^2
10	75.29	0.5339	0.995	0.05782	-0.7543	0.999
30	111.5	0.4532	0.995	0.02836	-0.7017	0.999
50	128.4	0.4246	0.995	0.02171	-0.6805	0.999
70	137.7	0.4054	0.995	0.01891	-0.664	0.999
90	144	0.3917	0.995	0.01765	-0.6487	0.999
110	148.2	0.3803	0.995	0.01644	-0.6398	0.999
130	151.5	0.3712	0.995	0.01556	-0.6324	0.999
150	153.9	0.3635	0.995	0.01488	-0.6263	0.999
170	156	0.3569	0.995	0.01433	-0.621	0.999
190	157.7	0.3512	0.995	0.01388	-0.6163	0.999
210	159.1	0.3461	0.996	0.01345	-0.6125	0.999
230	160.3	0.3416	0.996	0.01305	-0.6094	0.999
250	161.5	0.3376	0.996	0.01279	-0.6059	0.999
270	162.4	0.3339	0.996	0.01253	-0.6029	0.999
290	163.3	0.3305	0.996	0.01227	-0.6004	0.999
310	164	0.3273	0.996	0.01209	-0.5975	0.999
330	164.7	0.3245	0.996	0.01189	-0.5953	0.999
350	165.2	0.3217	0.996	0.01169	-0.5933	0.999
370	166	0.3193	0.996	0.01151	-0.5914	0.999
390	166.3	0.3169	0.996	0.01133	-0.5898	0.999
410	166.9	0.3147	0.996	0.01126	-0.5874	0.999
430	167.4	0.3126	0.996	0.01109	-0.5861	0.999
450	167.8	0.3106	0.996	0.01096	-0.5845	0.999
470	168	0.3086	0.996	0.01082	-0.5832	0.999
490	168.5	0.3069	0.996	0.01072	-0.5817	0.999

Table 7.3. The fitting using equation (7.87).

	α_1	α_2	α_3	R^2
ρ_κ	-290.4	-0.3595	200.8	0.997
χ_κ	0.746	-0.1387	-0.009112	0.999
ρ_λ	0.3137	-0.8099	0.009048	0.999
χ_λ	-0.7528	-0.08611	-0.1387	0.999

Chapter 8

Summary and Conclusions

This work has investigated in some detail theoretical problems relevant to radiation chemistry and has aimed to develop stochastic methods for the purpose of modelling radiation chemical kinetics in liquids. These problems are challenging mathematically, and for some of them it has not yet been possible to realize conclusive results.

In chapter 2 we have described how the Message Passing Interface can be successfully included in the algorithms used to simulate radiation chemical kinetics. This has been found helpful because it substantially increases the computational efficiency of the programs and has permitted the writing of hybrid simulation programs in which the same system is simulated by more than one method simultaneously and with the same initial conditions. These hybrid programs have been used in the remainder of the thesis.

In chapter 3 we have investigated the challenging problem of three-body correlation in the hope of finding a way of building this into the Independent Reaction Times (IRT) method. We have not been able to reach a final conclusion for the problem but have made clear progress. We have obtained the expression for the infinitesimal covariance of two diffusion distances (section 3.2.2.3) and hence formulated the backward diffusion equation of the problem of three-body diffusion. It quickly became clear that even the steady-state problem of calculating the probability that there is no reaction in a three-body system was extremely demanding. Possible approximations have been suggested: notably and attempt to use perturbation theory with the IRT solution as a starting point, and a solution in which the distances are constrained to be equal, however, neither of these seems to have proved useful. Several simulations of the problem have been presented, both of the time dependence and of correlations between which combinations of pair react. All of this will be useful in future studies for this problem.

In chapter 4 we showed by simulation that Smoluchowski theory overestimates the scavenging rate when the radicals are produced close to one another. We also proposed a very simple correction for Smoluchowski theory for diffusion-limited reactions (section 4.4). The correction takes into account the multi-radical correlation effect and has been found to be a significant improvement to the theory. This correction will be important when studying the competition of scavenging and recombination in high LET (Linear Energy Transfer) tracks where the radicals are close to one another and can no longer be considered isolated (Smoluchowski picture).

Chapter 5 shows that the IRT method is also in good agreement with the Random Flight (RF) simulations. We have also formulated a theoretical justification for the correction proposed in chapter 4 based on the IRT approximation (section 5.3). This implies that the origin of the effect has its roots in the initial configuration of the system, and not in correlations that may develop during the evolution of the spur. As part of this investigation a model was devised in which scavengers in the vicinity of the spur are treated explicitly and IRT times are generated for them, but scavengers further away are treated as a continuum. This method has the potential to be very useful in future track simulations, but at present the time for reaction with the other region has to be generated by a parametric method, and it has been shown how these parameters can be found in general. However, it would be very useful to see if there are any conditions where an analytical approach could be used here, avoiding the problems of fitting parameters.

In chapter 6 we have showed how a multi-radical system evolves event by event using the master equation (sections 6.3.1-6.3.2), which enables us to extract rate constants for the ordered (successive) scavenging reactions from the simulations. These simulated rate constants for successive reactions are statistically indistinguishable from one another, and are very close to the corrected Smoluchowski rate constant proposed in chapter 4. However, they are very hard to obtain because of the large statistical fluctuations, and further work would be helpful to optimise the efficiency of these estimates.

Chapter 7 is about the problem of reversible reaction in radiation chemistry. The key result of chapter 7 is the solution for the diffusion equations for a Bessel process with Radiation Boundary Condition (RBC) which consequently gives the

probability density function of the interparticle distance of a pair, conditional on a their reaction time and the generation of these distances using a parametric method.

Bibliography

[1] A. Mozumder, Fundamentals of Radiation Chemistry (Academic Press, San Diego 1999).

[2] A. Chatterjee, Interaction of Ionizing Radiation with Matter. In Farhataziz and M. A. J. Rodgers (eds.), Radiation Chemistry Principles and Applications (VCH Publishers, Inc. New York 1987).

[3] G. V. Buxton, An Overview of The Radiation Chemistry of Liquids. In M. Spotheim-Maurizot, M. Mostafavi, T. Douki and J. Belloni (eds.), Radiation Chemistry from Basics to Applications (EDP Sciences, France 2008).

[4] S. Karlin and H. M. Taylor, A First Course in Stochastic Processes (Academic Press, San Diego 1975).

[5] H. M. Taylor and S. Karlin, An Introduction to Stochastic Modelling, 3rd edition (Academic Press, San Diego 1998).

[6] S. M. Pimblott and N. J. B. Green, Recent Advances in the Kinetics of Radiolytic Processes. In R. G. Compton and G. Hancock (eds.), Research in Chemical Kinetics, Vol. 3 (Elsevier Science BV., Amsterdam 1995).

[7] N. J. B. Green, M. J. Pilling, S. M. Pimblott and P. Clifford, J. Phys. Chem. 93 (1989) 8025.

[8] P. S. Pacheco, An Introduction to Parallel Programming (Elsevier, Inc. Amsterdam 2011).

[9] M. Kupferschmid, Classical Fortran (Marcel Dekker, Inc. New York 2002).

[10] N. J. B. Green, M. J. Pilling, S. M. Pimblott and P. Clifford, J. Phys. Chem. 91 (1987) 4417.

[11] N. J. B. Green, M. J. Pilling, S. M. Pimblott and P. Clifford, J. Phys. Chem. 94 (1990) 251.

[12] K. Enomoto, J. A. LaVerne and S. M. Pimblott, J. Phys. Chem. A, 110 (2006) 4124.

[13] J. A. LaVerne, K. Enomoto and M. S. Araos, Radiat. Phys. Chem. 76 (2007) 1272-1274.

[14] S. A. Rice, Diffusion-Limited Reactions. In C. H. Bamford, C. F. H. Tipper and R. G. Compton (eds.), Comprehensive Chemical Kinetics, Vol. 25 (Elsevier Science Publishers B. V., Amsterdam 1985).

[15] B. U. Felderhof and J. M. Deutch, J. Chem. Phys. 64, 11 (1976) 4551.

[16] M. Smoluchowski, Z. Phys. Chem. 92 (1917) 129.

[17] V. M. Bluett and N. J. B. Green, J. Phys. Chem. A, 110 (2006) 6112.

[18] N. J. B. Green and S. M. Pimblott, J. Phys. Chem. 96 (1992) 9338.

[19] P. Clifford, N. J. B. Green, M. J. Oldfield, M. J. Pilling and S. M. Pimblott, J. Chem. Soc. Faruday Truns. I, 82 (1986) 2673.

[20] J. Bentley and D. Meisel, Radiation Chemistry: from The Early Days to The Next Millennium. In C. D. Jonah and B. S. M. Rao (eds.), Radiation Chemistry Present Status and Future Trends (Elsevier Science B. V., Amsterdam 2001).

[21] A. Mozumder , J. Phys. Chem. Lett. 2 (2011) 2994.

[22] C. D. Jonah, An Incomplete History of Radiation Chemistry. In J. F. Wishart and B. S. M. Rao (eds.), Recent Trends in Radiation Chemistry (World Scientific Publishing Co. Pte. Ltd. New Jersey 2010).

[23] H. Becquerel, Compt. Rend. 133 (1901) 709.

[24] W. Roentgen, Nature, 53 (1896) 274.

[25] W. Roentgen, Ann. Physik. 64 (1898) 1, 12, 18.

[26] P. Curie and A-L Debierne, Compt. Rend. 132 (1901) 770.

[27] W. J. Ramsay, J. Chem. Soc. 91 (1907) 931.

[28] M. Burton, J. Phys. Colloid Chem. 51 (1947) 611.

[29] A. Mozumder and J. L. Magee, Int. J. Radiat. Phys. Chem. 7 (1975) 83.

[30] E. Alizadeh and L. Sanche, Chem. Rev. 112 (2012) 5578.

[31] W. Friedland, M. Dingfelder, P. Kundrat and P. Jacob, Mutation Research, 711 (2011) 28.

[32] P. Rajesh, J.A. LaVerne and S. M. Pimblott, J. Nucl. Mater. 361 (2007) 10.

[33] A. R. Brown, C. Boothman, S. M. Pimblott and J. R. Lloyd Appl. Environ. Microbiol. 81, 12 (2015) 4014.

[34] J. Konya and N. M. Nagy, Nuclear and Radiochemistry (Elsevier Inc. Amsterdam 2012).

[35] P. Agnes et al. Phys. Lett. B, 743 (2015) 456.

[36] I. L. Plante, A. Filali-Mouhim and J-P. Jay-Gerin, Radiat. Phys. Chem. 72 (2005) 173.

[37] N. J. B. Green, C. E. Bolton and R. D. Spencer-Smith, Radiat. Environ. Biophys. 38 (1999) 221.

[38] N. J. B. Green and S. M. Pimblott, Res. Chem. Intermed. 27 (2001) 529.

[39] H. Kudoh and Y. Katsumura, Ion-beam Radiation Chemistry. In C. D. Jonah and B. S. M. Rao (eds.), Radiation Chemistry Present Status and Future Trends (Elsevier Science B. V., Amsterdam 2001).

[40] E. J. Williams, Proc. R. Soc. A, 139, 837 (1933) 163.

[41] E. B. Podgorsak, Radiation Physics for Medical Physicists, 2nd edition (Springer 2010).

[42] G. Choppin, J. O. Liljenzin, J. Rydberg and C. Ekberg, Radiochemistry and Nuclear Chemistry, 4th edition (Elsevier 2013).

[43] A. Mozumder, Interaction of Fast Charged Particles with Matter. In A. Mozumder and Y. Hatano (eds.), Charged Particle and Photon Interactions With Matter (Marcel Dekker Inc. New York 2004).

[44] B. J. McParland, Nuclear Medicine Radiation Dosimetry (Springer, Heidelberg 2010).

[45] P. Atkins and R. Friedman, Molecular Quantum Mechanics, 3rd edition (Oxford University Press, Oxford 2005).

[46] D. Emfietzoglou, I. Abril, R. Garcia-Molina, I. D. Petsalakis, H. Nikjoo, I. Kyriakou and A. Pathak, Nucl. Instr. and Meht. in Phys. Res. B, 266 (2008) 1154.

[47] P. Sigmund, Particle Pentration and Radiation Effects (Springer, Berlin 2006).

[48] H. Nikjoo, D. Emfietzoglou, R. Watanabe and Shuzo Uehara, Rad. Phys. & Chem. 77 (2008) 1270.

[49] J. D. Bjorken and S. D. Drell, Relativistic Quantum Mechanics (McGraw-Hill, Inc. New York 1964).

[50] W. Greiner, Relativistic Quantum Mechanics, 3rd edition (Springer, Berlin 2000).

[51] U. Fano, Annu. Rev. Nucl. Sci. 13 (1963) 1.

[52] N. Bohr, Philos. Mag. 25 (2013) 10.

[53] N. Bohr, Kgl. Dan. Vied. Selskab. Math.-Fys. Medd, 18 (1948) 9.

[54] H. A. Bethe, Ann. Physik. 5 (1930) 325.

[55] H. A. Bethe, Z. Physik. 76 (1932) 293.

[56] H. A. Bethe, Ann. Physik. 24 (1933) 273.

[57] M. Inokuti, Rev. Mod. Phys. 43, 3 (1971) 297-347.

[58] J. M. Fernandez-Varea, F. Salvat, M. Dingfelder and D. Liljequist, Nucl. Instr. and Meth. in Phys. Res. B, 229 (2005) 187.

[59] N. Sathish, I. Kyriakou, D. Emfietzoglou and A. P. Pathak, Nucl. Instr. and Meth. in Phys. Res. B, 268 (2010) 1723.

[60] D. Emfietzoglou, I. Abril, R. Garcia-Molina and H. Nikjoo, Int. J. Rad. Biol. 88 (2012) 22.

[61] H. Hayashi and Y. Udagawa, Generalized Oscillator Strength Distribution of Liquid Water. In Y. Hatano, Y. Katsumura and A. Mozumder (eds.), Charged Particle and Photon Interactions with Matter (CRC Press, Taylor & Francis Group, Boca Raton 2011).

[62] N. J. Carron, An introduction to the passage of energetic particles through matter (CRC Press, Taylor & Francis Group, Boca Raton 2007).

[63] O. Chibani, Med. Phys. 29 (2002) 2374.

[64] F. Salvat, J. M. Fernandez-Varea, J. Sempau and J Mazurier, Radiat Environ Biophys 38 (1999) 15.

[65] S. M. Pimblott and A. Mozumder, Modeling of Physicochemical and Chemical Processes in the Interactions of Fast Charged Particles with Matter. In A. Mozumder and Y. Hatano (eds.), Charged Particle and Photon Interactions With Matter (Marcel Dekker Inc. New York 2004).

[66] H. Nikjoo, S. Uehara, W. E. Wilson, M. Hoshi and D. T. Goodhead, Int. J. Radiat. Biol. 73, 4 (1998) 355.

[67] H. Nikjoo, S. Uehara, D. Emfietzoglou and F.A. Cucinotta, Radiat. Meas. 41 (2006) 1052.

[68] C. Bousis, D. Emfietzoglou, P. Hadjidoukas and H. Nikjoo, Phys. Med. Biol. 53 (2008) 3739.

[69] S. Incerti, A. Ivanchenko, M. Karamitros, A. Mantero, P. Moretto, H. N. Tran, B. Mascialino, M. A. Bernal, Z. Francis and C. Villagrasa, G. Baldacchino, P. Guèye, R. Capra, P. Nieminen and C. Zacharatou, Med. Phys. 37 (2010) 4692.

[70] B. G. Ershov, A.V. Gordeev, Radiat. Phys. Chem. 77 (2008) 928.

[71] G. V. Buxton, The Radiation Chemistry of Liquid Water: Principles and Applications. In A. Mozumder and Y. Hatano (eds.), Charged Particle and Photon Interactions With Matter (Marcel Dekker Inc. New York 2004).

[72] M. S. Kreipl, W. Friedland and H. G. Paretzke, Radiat. Environ. Biophys. 48 (2009) 11.

[73] S. M. Pimblott and J. A. LaVerne, J. Phys. Chem. A, 101 (1997) 5828.

[74] J. A. LaVerne, I. Stefanic´ and S. M. Pimblott, J. Phys. Chem. A, 109 (2005) 9393.

[75] S. Yamashita, M. Taguchi, G. Baldacchino and Y. Katsumura, Radiation Chemistry of Liquid Water with Heavy Ions: Steady-State and Pulse Radiolysis Studies. In Y. Hatano, Y. Katsumura and A. Mozumder (eds.), Charged Particle and Photon Interactions with Matter (CRC Press, Taylor & Francis Group, Boca Raton 2011).

[76] J. A. LaVerne, Radiat. Res. 153, 5 (2000) 487.

[77] J. Meesungnoen and J-P. Jay-Gerin, J. Phys. Chem. A, 109 (2005) 6406.

[78] V. D. Waele, I. Lampre and M. Mostafavi, Time-Resolved Study on Nonhomogeneous Chemistry Induced by Ionizing Radiation with Low Linear Energy Transfer in Water and Polar Solvents at Room Temperature. In Y. Hatano, Y. Katsumura and A. Mozumder (eds.), Charged Particle and Photon Interactions with Matter (CRC Press, Taylor & Francis Group, Boca Raton 2011).

[79] N. V. Klassen, Primary Products in Radiation Chemistry. In Farhataziz and M. A. J. Rodgers (eds.), Radiation Chemistry Principles and Applications (VCH Publishers, Inc. New York 1987).

[80] J. A. LaVerne, Radiation Chemical Effects of Heavy Ions. In A. Mozumder and Y. Hatano (eds.), Charged Particle and Photon Interactions With Matter (Marcel Dekker Inc. New York 2004).

[81] J. Meesungnoen and J-P. Jay-Gerin, Radiation Chemistry of Liquid Water with Heavy Ions: Monte Carlo Simulation Studies. In Y. Hatano, Y. Katsumura and A. Mozumder (eds.), Charged Particle and Photon Interactions with Matter (CRC Press, Taylor & Francis Group, Boca Raton 2011).

[82] G. Baldacchino, Radiat. Phys. Chem. 77 (2008) 1218.

[83] J. A. LaVerne, I. Stefanic and S. M. Pimblott, J. Phys. Chem. A, 109, 42 (2005) 9393.

[84] G. Baldacchino and Y. Katsumura, Chemical Processes in Heavy Ion Tracks. In J. F. Wishart and B. S. M. Rao (eds.), Recent Trends in Radiation Chemistry (World Scientific Publishing Co. Pte. Ltd. New Jersey 2010).

[85] B. Pastina and J. A. LaVerne, J. Phys. Chem. A, 105 (2001) 9316.

[86] N. J. B. Green and R. Harris, Chem. Phys. Lett. 198, 1, 2 (1992) 81.

[87] A. Hiroki, S. M. Pimblott and J. A. LaVerne, J. Phys. Chem. A, 106 (2002) 9352.

[88] M. H. Parajon, P. Rajesh, T. Mu, S. M. Pimblott and J. A. LaVerne, Radiat. Phys. Chem. 77 (2008) 1203.

[89] J. E. Turner, R. N. Hamm, H. A. Wright, R. H. Ritchie, J. L. Magee, A. Chatterjee and W. E. Bolch, Radiat. Phys. Chem. 32, 3 (1988) 503.

[90] G. V. Buxton, C. L. Greenstock, W. P. Helman and A. B. Ross, J. Phys. Chem. 17, 2 (1988) 513.

[91] P. Atkins and J. de Paula, Atkins' Physical Chemistry, 10th edition (Oxford University Press, Oxford 2006).

[92] P. Clifford, N. J. B. Green and M. J. Pilling, J. R. Statist. Soc. B, 43, 3 (1987) 266.

[93] D. A. McQuarrie, J. Chem. Phys. 38, 2 (1963) 433.

[94] D. A. McQuarrie, C. J. Jachimowski and M. E. Russell, J. Chem. Phys. 40, 10 (1964) 2914.

[95] D. A. McQuarrie, J. Appl. Prob. 4 (1967) 413.

[96] D. T. Gillespie, Physica A, 408 (1992) 404.

[97] M. W. Chevalier and H. El-Samad, J. Chem. Phys. 141 (2014) 214108.

[98] E. Kreyszig, Advanced Engineering Mathematics, 10th edition (John Wiley & Sons, Inc. USA 2011).

[99] P. Clifford, N. J. B. Green, M. J. Pilling, S. M. Pimblott and W. G. Burns, Radiat. Phys. Chem., 30, 2 (1987) 125.

[100] S. M. Pimblott, C. Alexander, N. J. B. Green and W. G. Burns, J. Chem. Soc. Faraday Trans. 88, 7 (1992) 925.

[101] P. Clifford, N. J. B. Green and M. J. Pilling, J. Phys. Chem. 86 (1982) 1318.

[102] I. Plante, Radiat. Environ, Biophys. 50 (2011) 389.

[103] K. B. Athreya and S. N. Lahiri, Measure Theory and Probability Theory (Springer 2006).

[104] D. Henderson and P. Plaschko, Stochastic Differential Equation in Science and Engineering (World Scientific Publishing Co. Pte. Ltd. 2006).

[105] N. G. Van Kampen, Stochastic Processes in Physics and Chemistry, 3rd edition (Elsevier 2007).

[106] S. Karlin and H. M. Taylor, A Second Course in Stochastic Processes (Academic Press, New York 1981).

[107] N. Ikeda and S. Watanabe, Stochastic Differential Equations and Diffusion Processes (Kodansha LTD. 1981).

[108] R. Brown, Pogg. Annalen, 14 (1828) 294.

[109] A. Einstein, Ann. Physik, 17 (1905) 549.

[110] M. Smoluchowski, Ann. Physik, 2, 1 (1906) 576.

[111] P. Langevin, Comptes Rendus Acad. Sci. 146 (1908) 530.

[112] N. Wiener, J. Math. Phys. 2 (1923) 131.

[113] R. Durrett, Probability Theory and Examples, 3rd edition (Thomson, Brooks/Cole 2005).

[114] L. Arnold, Stochastic Differential Equations (John Wiley & Sons, Inc. 1974).

[115] S. Chandrasekhar, Rev. Mod. Phys. 15,1 (1943) 1.

[116] C. E. Bolton, N. J. B. Green and S. M. Pimblott, Chem. Phys. Lett. 221 (1994) 175.

[117] W. Rumelin, SIAM J. Numer. Anal. 19 (1982) 604.

[118] G. N. Milshtein, Theory Probab. Its Appl. (Engl. Transl.), 23 (1982) 396.

[119] S. M. Pimblott, J. Chem. Soc. Faraday Trans. 89 (1993) 3533.

[120] A. Agarwal, D.Phil Thesis (Univeristy of Oxford, 2011/Springer Theses-Recognizing Outstanding PhD Research, 2014).

[121] P. Clifford and N. J. B. Green, Molec. Phys. 57, 1 (1986) 123.

[122] N. J. B. Green, Molec. Phys. 65, 6 (1988) 1399.

[123] R. H. Bisseling, Parallel Scientific Computation (Oxford University Press 2004).

[124] W. Gropp, E. Lusk and Rajeev Thakur, Using MPI-2 (Massachusetts Institute of Technology 1999).

[125] V. K. Decyk, D. E. Dauger and P. R. Kokelaar, Phys. Scripta, T84 (2000) 85.

[126] L. Russell, A. Buijs and G. Jonkmans, Ann. Nucl. Energy, 71 (2014) 451.

[127] S. Garashchuk, J. Jakowski, L. Wang and B. G. Sumpter, J. Chem. Theory Comput. 9 (2013) 5221.

[128] W. M. Bartczak and A. Hummel, J. Chern. Phys. 87, 9 (1987) 5222.

[129] P. Clifford, N. J. B. Green and M. J. Pilling, J. Phys. Chem. 86 (1982) 1322.

[130] N. J. B. Green, M. J. Oldfield, M. J. Pilling and S. M. Pimblott, J. Chem. Soc. Faraday Trans. I, 82 (1986) 2673.

[131] L. Devroye, Non-Uniform Random Variate Generation (Springer-Verlag, New York 1986).

[132] S. M. Pimblott, M. J. Pilling and N. J. B. Green, Radiat. Phys. Chem. 37, 3 (1991) 377.

[133] N. J. B. Green, M. J. Pilling and P. Clifford, Molec. Phys. 67, 5 (1989) 1085.

[134] N. J. B. Green and S. M. Pimblott, J. Phys. Chem. 93 (1989) 5462.

[135] W. Feller, An Introduction to Probability Theory and its Applications, Vol. 2 (John Wiley & Sons, Inc. NewYork 1971).

[136] P. Clifford, N. J. B. Green and M. Pilling, J. Chem. Phys. Lett. 91 (1982) 101.

[137] H. Sano and M. Tachiya, J. Chem. Phys. 71 (1979) 1276.

[138] V. M. Bluett and N. J. B. Green, J. Phys. Chem. A, 110 (2006) 4738.

[139] D. G. Kendall, Adv. Appl. Probab. 9, 3 (1977) 428.

[140] F. G. Ball, I. L. Dryden, M. Golalizadeh, Methodol. Comput. Appl. Probab. 10 (2008) 1, and their references therein.

[141] D. G. Kendall, J. Appl. Prob. 28, 1 (1991) 225.

[142] H. Le and D. G. Kendall, Ann. Stat. 21, 3 (1993) 1225.

[143] W. S. Kendall, Adv. Appl. Probab. 30, 2 (1998) 317.

[144] P. Clifford and N. J. B. Green, Math. Proc. Camb. Phil. Soc. 97 (1985)
515, and their references therein.

[145] W. S. Kendall, Adv. Appl. Probab. 20 (1988) 775.

[146] J. M. Harris, J. L. Hirst and M. J. Mossinghoff, Combinatorics And Graph Theory, 2nd edition (Springer, New York 2008).

[147] J. A. Bondy and U. S. R. Murty, Graph Theory with Applications (Elsevier Science Publications Co., Inc. New York 1976).

[148] N. J. B. Green and R. D. Spencer-Smith, J. Phys. Chem. 100 (1996) 13561.

[149] H. B. Dwright, Tables of Integrals and Other Mathematical Data, 4th edition (The Macmillan Company, New York 1968).

[150] A. P. Prudnikov, Y. A. Brychkov and O. I. Marichev, Integrals and Series Vol. 1 (Gordon and Breach Science Publishers, New York 1992).

[151] A. D. Polyanin and V. F. Zaitsev, Handbook of Exact Solutions for Ordinary Differential Equations, 2nd edition (Chapman & Hall/CRC, Boca Raton 2003).

[152] H. S. Carslaw and J. C. Jaeger, Conduction of Heat in Solids, 2nd editoin (Clarendon Press, Oxford 1986).

[153] H. A. Antosiewicz, Bessel Functions of Fractional Order. In Handbook of Mathematical Functions, 9th edition, M. Abramowitz and I. A. Stegun (eds.) (Dover Publications, Inc. New York 1972).

[154] A. P. Prudnikov, Y. A. Brychkov and O. I. Marichev, Integrals and Series Vol. 5 (Gordon and Breach Science Publishers, New York 1992).

[155] G. E. Roberts and H. Kaufman, Table of Laplace Transforms (W. B. Saunders Company, London 1966).

[156] A. Hummel, Kinetics in Radiation Chemistry. In Farhataziz and M. A. J. Rodgers (eds.), Radiation Chemistry Principles and Applications (VCH Publishers, Inc. New York 1987).

[157] P. Clifford, N. J. B. Green and M. J. Pilling, J. Phys. Chem., 89 (1985) 925.

[158] R. Zwanzig and A. Szabo, Biophys. J., 60 (1991) 671.

[159] P. H. Richter and M. Eigen, Biophys. Chem. 2(1974) 255.

[160] F. C. Collins and G. E. Kimball, Journal of Colloid Science, 4, 4 (1949) 425.

[161] A. P. Prudnikov, Y. A. Brychkov and O. I. Marichev, Integrals and Series Vol. 4 (Gordon and Breach Science Publishers, New York 1992).

[162] A. P. Prudnikov, Y. A. Brychkov and O. I. Marichev, Integrals and Series Vol. 2 (Gordon and Breach Science Publishers, New York 1992).

[163] N. J. B. Green, M. Pillin, P. Clifford and W. Burn, J. Chem. Soc. Faraday Trans. I, 80 (1984) 1313.

[164] S. M. Pimblott and J. A. LaVerne , J. Phys. Chem. 96 (1992) 8904.

[165] S. M. Pimblott and J. A. LaVerne, J. Phys. Chem. 98 (1994) 6136.

[166] J. A. LaVerne, S. M. Pimblott and L. Wojnarovits J. Phys. Chem. A, 101 (1997) 1628.

[167] H. A. Schwarz, J. Phys. Chem. 73 (1969) 1929.

[168] W. G. Burns, H. E. Sims and J A. B. Goodall, Radiat. Phys. Chem. 23 (1984) 143.

[169] W. G. Burns and A. R. Curtis, J. Phys. Chem. 76 (1972) 3008.

[170] C. L. Berthollet, *Essai de statique chimique*, vol. 1, (1803) 555.

[171] H. M. Leicester, H. S. Klickstein, A Source Book in Chemistry, 1400-1900 (Oxford University Press, London 1968).

[172] S. Califano, Pathways to Modern Chemical Physics (Springer-Verlag, Berlin 2012).

[173] P. Waago and C. M. Guldherg, Forhondiinger: Vidmskobs-SeIsknbet *i* Chrlslionia (1864) 35.

[174] P. Waage and C. M. Gulberg (H. I. Abrash, Translator), J. Chem. Educ. 63, 12 (1986) 1044.

[175] J. H. van't Hoff, Die Grenzebene ein Beitrag zur Kenntniss Esterbildung. Chem Ber, 10 (1877) 669.

[176] G. V. Buxton, Radiation Chemistry of the Liquid State: (1) Water and Homogenous Aqueous Solutions. In Farhataziz and M. A. J. Rodgers (eds.), Radiation Chemistry Principles and Applications (VCH Publishers, Inc. New York 1987).

[177] P. Bouniol, Water Radiolysis in Cement-Based Materials. In M. Spotheim-Maurizot, M. Mostafavi, T. Douki and J. Belloni (eds), Radiation Chemistry from Basics to Applications (EDP Sciences, France 2008).

[178] R. M. Noyes, Prog. React. Kinet. 1 (1961) 129.

[179] N. J. B. Green, R. D. Spencer-Smith and A. G. Rickerby, J. Chem. Phys. 212 (1996) 99.

[180] V. M. Bluett and N. J. B. Green, J. Phys. Chem. A, 110 (2006) 4738.

[181] C. E. Bolton, N. J. B. Green and R. Harris, J. Phys. Chem. A, 102 (1998) 730.